LIFE MODERN NEC

Qualità dell'aria, la risposta degli ecosistemi

Report on the results of the implementation and test at the project sites

LIFE MODERn(NEC) - ACTION B3

September 2025

Life MODERn(NEC)

2025

Report on the results of the implementation and test at the project sites

LIFE MODERn(NEC) - ACTION B3
September 2025

Deliverable
Action B3

September, 2025

Author contribution

TerraData environmetrics (coordinating partner): Giorgio Brunialti, Luisa Frati, Francesca Giorgolo, Marco Calderisi.

CUFAA, Ufficio Progetti, Convenzioni, Educazione Ambientale: Giancarlo Papitto, Cristiana Cocciufa, Domenico Di Martino.

CREA, Centro di Ricerca Foreste e Legno: Giada Bertini, Maurizio Piovosi, Valerio Moretti, Tiziano Sorgi, Luca Marchino.

CNR, Istituto di Ricerca sulle Acque (IRSA): Aldo Marchetto, Michela Rogora, Giulia Cesarini, Angela Boggero, Simona Musazzi, Silvia Zaupa, Riccardo Fornaroli

CNR, Istituto per il Rilevamento Elettromagnetico dell'Ambiente (IREA): Alessandro Oggioni, Daniela Stroppiana, Lorenzo Parigi.

CNR, Istituto di Ricerca sugli Ecosistemi Terrestri (IRET): Elena Paoletti, Barbara Baesso Moura, Elena Marra, Yasutomo Hoshika, Flavia Sicuriello, Paolo Colangelo, Serena Carloni, Silvia Pioli, Emanuela Solano, Giorgia Castiello, Leonardo Latilla, Bruno De Cinti.

Università degli Studi di Firenze, Dipartimento di Scienze della Terra: Stefano Carnicelli, Guia Cecchini.

Università degli Studi di Firenze, Dipartimento di Scienze e Tecnologie Agro-Alimentari, Ambientali e Forestali (DAGRI): Filippo Bussotti, Martina Pollastrini, Davide Bettini, Enrico Cenni.

ENEA, Laboratorio Inquinamento Atmosferico: Ettore Petralia, Antonio Piersanti, Alessandra De Marco, Teresa La Torretta, Milena Stracquadanio.

Università degli Studi di Camerino, Scuola di Bioscienze e Medicina Veterinaria: Roberto Canullo, Stefano Chelli, Marco Cervellini, Giandiego Campetella.

How to cite this document: Brunialti G., Frati L., Giorgolo F. (edited by), 2025. Report on the results of the implementation and test at the project sites. LIFE MODERn(NEC) - ACTION B3 Deliverable, September 2025, pp. 133.

Contents

Abstract

This report presents the results of the implementation and tests conducted at the sites of the LIFE MODERn(NEC) project - Action B3. The main objective of Action B3 is to study the direct (pollution) and indirect (climate change) relationships between indicators and stress factors. The document includes a detailed description of the monitoring sites, the data collected, and the principles of database interoperability. Results related to forest and freshwater ecosystems are also presented, with an integrated analysis of indicators and stress factors. Finally, the report discusses the preliminary results of the replicability study, which aims to multiply the impact of the project beyond its duration and outside the national partnership, involving other EU Member States committed to the NEC Directive.

1. Introduction

The goal of Action B.3 is to implement and test current and newly proposed indicators at existing monitoring sites and new ones, selected in Action B.2 (Selection of a new set of indicators for the study of atmospheric pollution impacts on ecosystems). Field surveys/monitoring activities have been carried out according to the protocols revised and established in Actions A.2 and B.2, and involved 3 groups of indicators: biological responses, ecosystem chemical parameters and meteorological data.

This action aims to assess whether the new and revised indicators can provide more comprehensive information on air pollution ecosystem impacts, and whether their routine use within the NEC network is sustainable. Therefore, it is necessary to obtain a comprehensive dataset of the functional components of forest and freshwater ecosystems, which are potentially affected by air pollution, and of the fluxes of pollutants and nutrients within these ecosystems. The full set of NECD indicators, including current ones, have been tested in an integrated manner.

Specific activity of Action B.3:

1. Implementing current indicator surveys in the new monitoring sites, while testing the revisions and updates defined in Action A.2.

2. Testing the new indicators proposed through Action B.2, with surveys in the existing and new monitoring sites.

3. Studying direct (pollution) or indirect (e.g. climate change) relationships among indicators and stressors.

This report covers the third activity of the Action presenting the project's findings on forest and freshwater ecosystems, including an integrated analysis of indicators and stress factors.

1.1 Monitoring sites

1.1.1 Forest sites

The project includes 10 forest sites (Table 1.1.1, Fig. 1.1.1): 4 Mountainous Beech Forests (ABR1, CAL1, PIE1, VEN1); 1 Mountainous Conifer Forest (BOL1); 3 Boadleaved Deciduous Forests (EMI1, LAZ1, VEN2) and 2 Broadleaved Evergreen Forests (SAR1, TOS2).

Table 1.1.1. Information on the 10 forest sites of the LIFE MODERn NEC Project. Forest type: MBF: Mountainous Beech Forest, MCF: Mountainous Conifer Forest, BDF: Boadleaved Deciduous Forest, BEF: Broadleaved Evergreen Forest. Forest Management: HF: High Forest, SC: Stored Coppice, TC: Transitory Crop. Main Tree species: FS: Fagus sylvatica, PA: Picea abies, MB: Mixed Broadleaved, QC: Quercus cerris, QI: Quercus ilex.

Site	Locality	Biogeographic region	Main tree species	Forest Type	Forest Management	Altitude	Zone	E (UTM WGS84)	N (UTM WGS84)
ABR1	Selva Piana	Alpine	FS	MBF	HF	1500	33t	382924.4	4633806
BOL1	Renon	Alpine	PA	MCF	HF	1740	32t	686516.9	5162237
CAL1	Piano Limina	Mediterranean	FS	MBF	HF	1100	33t	602974.3	4253877
EMI1	Carrega	Continental	MB	BDF	SC	200	32t	595326.7	4952366
LAZ1	Monte Rufeno	Mediterranean	QC	BDF	SC	690	32t	737293.8	4745037
PIE1	Val Sessera	Alpine	FS	MBF	TC	1150	32t	427360.2	5059133
SAR1	Marganai	Mediterranean	QI	BEF	SC	700	32t	462853.3	4355583
TOS2	Cala Violina	Mediterranean	QI	BEF	SC	30	32t	645074.5	4747909
VEN1	Cansiglio	Alpine	FS	MBF	HF	1100	33t	270438.8	5104688
VEN2	Bosco Fontana	Continental	MB	BDF	HF	60	32t	636309.5	5006726

Figure 1.1.1. Map with the distribution of the 10 forest sites.

1.1.2 Freshwater sites

The project includes 10 freshwater sites (Table 1.1.2; Fig. 1.1.2): 8 lakes (7 mountain lakes and 1 lowland lake) and 2 streams (1 mountain stream and 1 lowland river). Sites in mountain areas are representative of different parts of the Alps and of the Apennines. Considering the main descriptors to identify broad river and lake typology in Europe according to the WFD (Solheim et al., 2019), 8 sites are highland (> 800 m) and 2 lowland (< 200 m); geology is mostly siliceous (alkalinity < 1 meq L^{-1}, Ca < 20 mg L^{-1}); the two rivers are permanent and representative of the small (<100 km^2) and medium (100-10.000 km^2) categories according to catchment size; the lakes are mostly very small (<0.5 km^2 as lake area), with only one small-large lake (0.5-100 km^2). Lakes are all deeper than 3 m (category "shallow and deep") and only the deepest lake shows a stratification period and is monomictic experiencing a single full overturn in late winter. The other lakes are likely continuously or discontinuously polymictic. Further information on the selected sites and their characteristics, including catchment land cover and sensitivity to atmospheric pollution, have been presented in the final report of Action B1- Site selection.

Table 1.1.2. Main characteristics of the 10 freshwater sites of the LIFE MODERn NEC project.

Site	Acronym	Type	Lat. N	Long. E	Altitude (m a.s.l.)	Catchment area (km2)	Lake area/River length (ha/km)	Lake max depth (m)
PAIONE Inf.	PAI	Lake	46.169	8.188	2002	1.26	0.68	13.5
PAIONE Sup.	PAS	Lake	46.175	8.190	2269	0.50	0.86	11
GRANDE	GRA	Lake	46.001	8.078	2269	0.90	0.69	6
GELATO	GEL	Lake	46.249	8.441	2418	0.15	0.65	7
MERGOZZO	MER	Lake	45.954	8.458	194	10.4	183	70
DRES	DRE	Lake	45.411	7.223	2087	2.92	2.6	7.4
MARMOTTE	MAR	Lake	46.439	10.674	2704	0.89	2.1	6.5
SCURO	SCU	Lake	44.382	10.045	1507	2.5	1.2	10.4
BUSCAGNA	BUS	River	46.315	8.258	1646	26	8	
CANNOBINO	CAN	River	46.068	8.693	193	110	25	

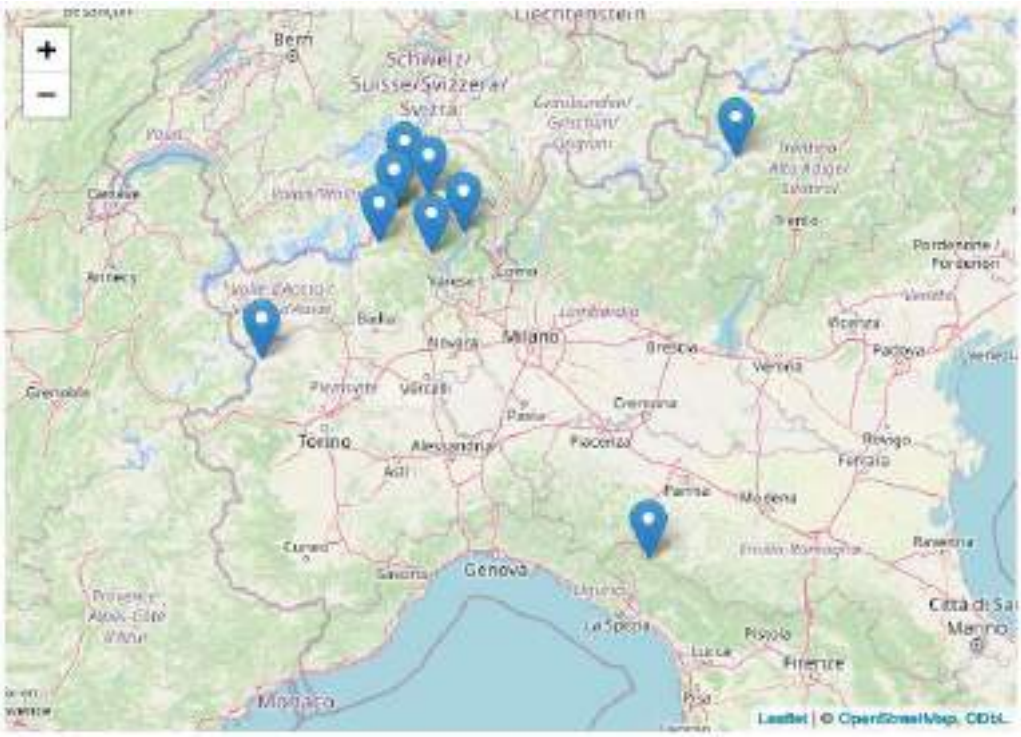

Figure 1.1.2. Map with the distribution of the 10 freshwater sites.

2. Database and interoperability

Within the project a data infrastructure was organized following the FAIR principles (Findability, Accessibility, Interoperability, and Reusability). An analysis was carried out of the state of interoperability of the data and of the level of adherence to the data management practices of the ICP Forests and ICP Water network, to verify possible higher interoperability paths.

2.1 The FAIR principles and the importance of their application

In an increasingly data-driven world, ensuring that research outputs—especially datasets—are easy to find, access, integrate, and reuse is essential. This is where interoperability and the FAIR principles come into play. These principles serve as guidelines for data management and stewardship that aim to maximize the value of data for both humans and machines. Interoperability, in particular, lies at the core of enabling diverse systems, tools, and communities to work together effectively and exchange data without loss of meaning or function.

The FAIR principles were introduced to address critical gaps in research data management. According to the GO FAIR initiative (https://www.gofair.foundation), these principles are not just about open data, but about well-prepared data that can be reliably interpreted and used by others, including machines. Let's break down the individual principles and explore the tools and practices that can help researchers and institutions implement them.

1. Findable

Data and metadata must first be discoverable, or in other words, they should be easy to locate by humans and machines. This requires the use of persistent identifiers (PIDs, such as URIs, Handles or DOIs), rich metadata, and registration in searchable repositories. Technologies such as metadata standards (e.g., Dublin Core or ISO 19115 schema) and platforms like CKAN or GeoNetwork enable the findability of datasets. XML, JSON-LD or schema.org annotations are also widely used to enhance discoverability on the web.

2. Accessible

Once found, data should be retrievable using standardized and open communication protocols (e.g., HTTP, FTP, OAI-PMH), and metadata should remain accessible even if the data themselves are no longer available. Access conditions, including authentication or licensing requirements, should be

clearly described. Tools such as APIs, data portals, and metadata harvesters play a key role here. Semantic web technologies like SPARQL endpoints allow structured access to data in machine-readable formats.

3. Interoperable

For data to be interoperable, it must use standardized vocabularies, formats, and ontologies. This ensures that data from different sources can be integrated and interpreted without ambiguity. Implementing interoperability often involves using Linked Data principles, SKOS (Simple Knowledge Organization System), RDF (Resource Description Framework), and OWL (Web Ontology Language). Controlled vocabularies and domain ontologies (e.g., EnvThes, AGROVOC, ENVO) facilitate semantic consistency. Tools such as Protégé for ontology development and triple stores like Apache Jena Fuseki or GraphDB are often employed to publish and query interoperable datasets.

4. Reusable

Data should be richly described with accurate metadata, usage licenses, and clear provenance to enable reuse in new contexts. To achieve this, standards such as PROV-O (Provenance Ontology) and best practices in metadata documentation are critical. Repositories that support versioning and detailed data citation practices also enhance reusability. FAIRsharing.org is a useful resource for discovering domain-specific standards and repositories.

Implementing the FAIR principles is not merely a technical exercise but a cultural shift. It requires collaboration between data producers, software developers, librarians, domain experts, and data stewards. Moreover, it involves adopting tools and practices that support openness, transparency, and machine-actionability.

From a practical standpoint, researchers can start their FAIR journey by using version-controlled data repositories (e.g., GitHub with Zenodo integration), writing comprehensive metadata using standards like ISO 19115 or DCAT, and selecting interoperable file formats such as CSV, NetCDF, or GeoJSON. Programming languages such as Python and R offer libraries for data wrangling, semantic annotation, and interfacing with APIs and SPARQL endpoints, making them powerful allies in achieving FAIRness.

In conclusion, moving toward interoperable and FAIR ecosystems is essential to enhance collaboration, reproducibility, and innovation across scientific domains. By embracing FAIR-aligned tools and workflows, research communities can unlock the full potential of their data, fostering a more integrated and transparent scientific environment.

2.2 Practices to make data FAIR in the project

To ensure that data are Findable, Accessible, Interoperable, and Reusable (FAIR), a combination of conceptual guidelines and practical tools must be adopted throughout the data lifecycle.

This involves applying a consistent framework for data description, storage, and publication that supports discovery, interoperability, and reuse across domains.

The Figure 2.2.1 summarizes a set of core FAIR-enabling practices that should be implemented when designing and managing datasets. These practices include the assignment of persistent identifiers, the use of standardized vocabularies and metadata schemas, the adoption of open and interoperable formats, and the provision of clear licensing and provenance information. Together, these measures ensure that data can be easily located, accessed, integrated with other resources, and reused within and beyond their original context.

Figure 2.2.1. Key practices to ensure data FAIRness. Core actions supporting the Findable, Accessible, Interoperable, and Reusable (FAIR) principles.

To operationalize these principles, several software platforms and repositories can be used, such as CKAN (https://ckan.org), Zenodo (https://zenodo.org), Figshare (https://figshare.com), OpenAIRE

(https://www.openaire.eu), PANGAEA (https://www.pangaea.de), and GeoNode (https://geonode.org).

GeoNode enables integrated management of both spatial and non-spatial data, offering functionalities for uploading, describing, and sharing datasets through standardized metadata profiles. It supports the assignment of unique identifiers (UUIDs) and DOIs, provides access control mechanisms, and manages usage licenses and permissions.

A GeoNode instance is hosted by CNR-IREA to support project activities, ensuring compliance with the FAIR principles and promoting transparent and sustainable data management.

2.3 Implementation of FAIR Principles in the Life MODERn NEC Data Portal

To ensure that data generated within the LIFE MODERn NEC project are Findable, Accessible, Interoperable, and Reusable (FAIR), a dedicated web portal has been developed and deployed at https://salmon.irea.cnr.it/. The portal is based on GeoNode, an open-source platform that enables the management, publication, and sharing of spatial and non-spatial datasets, while automatically associating rich metadata and licensing information with each resource.

The Life MODERn NEC Data Portal (Figure 2.3.1) hosts all datasets produced within the project and provides a unified environment for data discovery, visualization, and controlled access. Each dataset is associated with a CC-BY-SA license, assigned an explicit ownership, and is visible to non-registered users. However, downloads are restricted to users belonging to the MODERn NEC group to ensure proper management of project-related data.

Currently uploaded datasets include chlorophyll fluorescence, foliar analysis, forest growth, lichens, meteorological data, ozone, and soil solution, while additional datasets such as air quality visibility, animal biodiversity, depositions, phenology, and defoliation are in the process of being uploaded. User accounts have been created for data providers, granting them secure access to their respective resources.

Figure 2.3.1. Life MODERn NEC Data Portal homepage (https://salmon.irea.cnr.it/).

The architecture of the Life MODERn NEC Data Portal was designed to fully implement the FAIR principles — ensuring that every dataset is Findable, Accessible, Interoperable, and Reusable.

Both conceptual guidelines and technical solutions have been adopted to make the data lifecycle transparent, traceable, and sustainable over time.

Findability - Each dataset is automatically assigned a globally unique and persistent identifier (UUID).

Rich and standardized metadata are generated to describe the dataset content, structure, and provenance.

This enables the resources to be indexed, searched, and discovered directly through the GeoNode interface or via catalog services.

Accessibility - All datasets and metadata are published using open and standardized communication protocols (OGC, CSW, WMS, WFS), ensuring that information is machine-readable and interoperable.

Metadata remain permanently accessible even when the corresponding dataset is temporarily unavailable, maintaining full data traceability.

Interoperability - The portal supports multiple open data formats, including CSV, Excel, GeoJSON, PNG, zipped Shapefile, and GML (2.0 and 3.1.1).

Metadata comply with widely adopted community standards such as Dublin Core, ISO 19115, and Atom, enabling seamless integration of data into other repositories, analytical tools, and information systems.

Reusability - Each dataset is enriched with detailed metadata covering attributes, measurement units, methodologies, and provenance.

All resources are released under a Creative Commons BY-SA license, promoting transparent data reuse, citation, and long-term preservation in line with community and FAIR standards.

An additional feature of the portal is the Dashboard functionality, which enables the interactive visualization and comparison of datasets through customizable plots, time series, and spatial views. These dashboards provide an intuitive interface for exploring long-term trends, relationships between variables, and site-specific monitoring results, thus enhancing both the interpretability and shareability of project data. Figure 2.3.2 shows an example of such dashboards implemented within GeoNode, where meteorological and biological datasets can be dynamically combined and visualized.

Figure 2.3.2. Example of interactive data visualization through the GeoNode Dashboard interface.

Through this implementation, the Life MODERn NEC data infrastructure achieves an effective balance between data openness and controlled access, ensuring compliance with the FAIR principles while providing tools for data management, visualization, and long-term preservation.

3. Data processing

The main objective of this activity is to perform a data screening to discriminate the impacts of air pollution on reactive components of ecosystems from those pressures related to different environmental factors (i.e., forest management, climate change).

The dataset collected during the project has been refined and processed to ensure its suitability for data analyses.

As expected by the project, a multivariate approach was adopted with a double in-depth analysis: i)

descriptive multivariate statistics for each indicator; and, where possible, ii) a comprehensive integrated elaboration by means of multiple linear regression models.

See Annex B3.1 for detailed procedures and results.

Data characterization – A thorough screening of the set of data was performed to explore their completeness and to obtain a clear framework of their distribution both from the spatial (number of represented sites) and framework of their distribution both from the spatial (number of represented sites) and the temporal (number of yearly surveys) point of view.

3.1 Conceptual scheme

Figure 3.1.1 reports a simplified conceptual scheme grouping the variables enlisted in the previous paragraphs into two main categories:

i. drivers, that is the predictive variables which can influence the ecological indicators considered in the project.
ii. ecosystem responses, that is all the environmental variables (ecological indicators) which can be affected by the environmental predictors. It is possible to hypothesize potential

relationships between drivers and ecosystem responses, with a positive or negative effect to be assessed by further data processing. This is only a simplified scheme since it is possible that correlative relationships exist also among the indicators grouped within the ecosystem responses or within the drivers. For example, crown conditions may affect light availability for plants and epiphytic lichens, with an influence in their species composition, or water chemistry may influence macroinvertebrate communities.

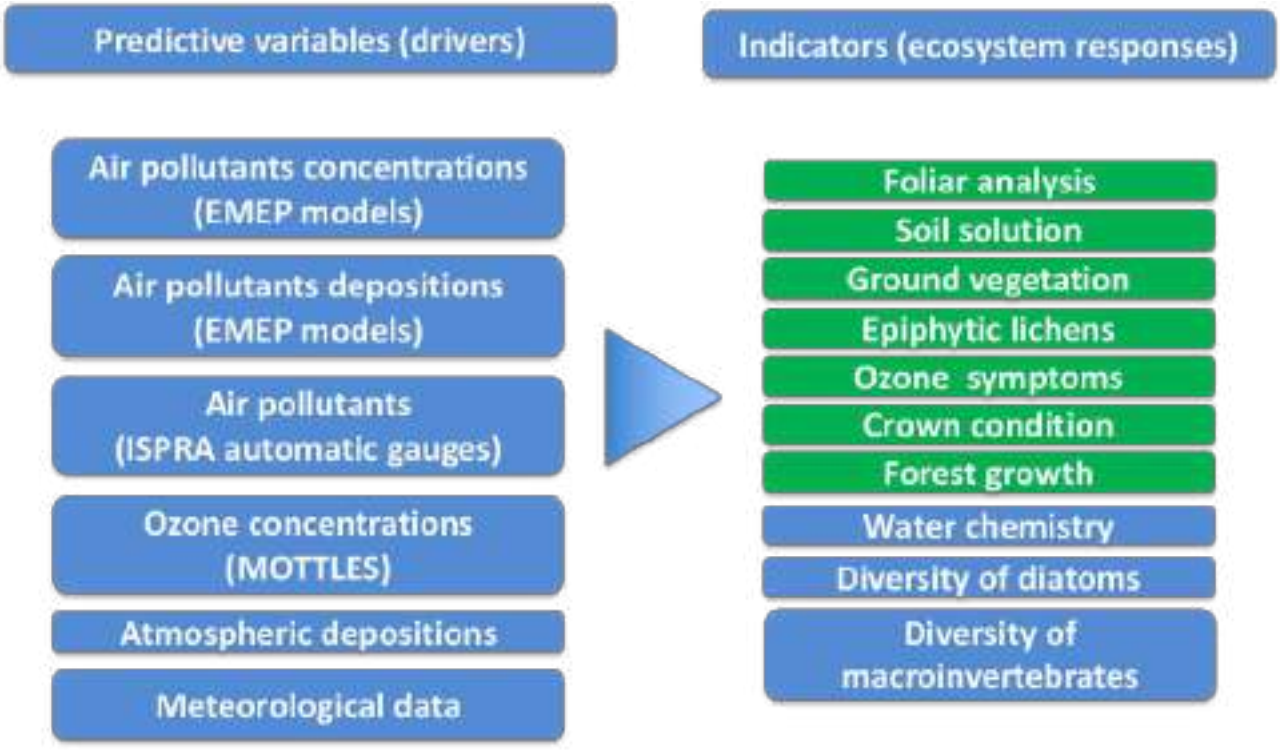

Figure 3.1.1. Simplified conceptual scheme grouping the variables in drivers and ecosystem responses.

3.2 Selection of the most suitable data processing procedure

Starting from the type, structure and completeness of the available data, the following univariate and multivariate analyses were adopted.

i) Considering each indicator individually (both driver and response), we studied the temporal trends of each variable, we obtained the correlation matrix between couples of variables, and we performed a Principal Component Analysis (PCA). In particular, PCA was used as explorative unsupervised multivariate analysis to study the relationships among variables within each indicator.

ii) Once this first exploratory survey was carried out, multiple linear regression models (MLRM) were adopted to obtain an overall picture of the relationships among drivers and ecosystem responses. In particular, Generalized Linear Models (GLM) were adopted to explore the relationship among the response and predictive variables in order to find out the best predictors explaining its variability. We have used a combined approach of multiple linear regression models to study the multicollinearity among variables, and GLM to explain response variable distribution in relation to predictive variables.

3.3 Univariate and multivariate analysis

This section reports a detailed analysis of the distribution of each indicator belonging to the three groups: air pollutants, forests and freshwaters. In particular, the following results are reported for each indicator, deriving from univariate and multivariate analyses:

- exploratory charts with the temporal distribution of each variable, to provide useful information for identifying any trend along the explored data series.
- Pie charts. They have been used for variables with a categorization in score values (percentage levels of defoliation and ozone symptoms).
- Correlation matrix between the variables for each forest and freshwater site. The variables were correlated in pairs in order to identify positive or negative relationships. This preliminary study on the correlation among variables is important for the further regressive model settings to avoid multicollinearity and to select only those variables not too correlated with the others.
- Principal Component Analysis (PCA) results: score plots of the PCA ordination were provided based on several categorical variables (year, site, altitude, tree species, forest type and forest management). For quantitative variables, the length of overlaid vectors is proportional to Pearson R^2 with the axis.
- Non-Metric Multidimensional Scaling (NMDS).

All the analyses have been carried out by means of the software R (R Core Team 2025). See Annex B3.1 for detailed procedures and results.

The main results are commented in the following paragraphs.

4. Forest ecosystems: results

This chapter summarizes the results from the forest sites, with each paragraph detailing the descriptive statistics for each indicator.

4.1 Air quality and visibility

4.1.1 Dataset

Table 4.1.1 provides an overview of the dataset. Air quality data (ozone concentrations, 5 variables) cover 6 years (2018-2023) in 5 forest sites of the project. Visibility data (16 variables) cover 2 sites with measures in the periods 2021-2022 (Lago Monaci) and 2023-2024 (Vincheto di Celarda). The analysis focus only on the results obtained at Lago Monaci, showing a more complete dataset.

Table 4.1.1. Overview of the available dataset.

	Air quality and visibility
Sites (2)	• Lago Monaci • Vincheto di Celarda
Variables (16)	• RH_avg (%) • NO2 (ppb) • PM10 (µg m^{-3}) • PM2.5 (µg m^{-3}) • EC (µgC m^{-3}) • OC (µgC m^{-3}) • Al (µg m^{-3}) • Si (µg m^{-3}) • Ca (µg m^{-3}) • Ti (µg m^{-3}) • Fe (µg m^{-3}) • NO3- (µg m^{-3}) • SO42- (µg m^{-3}) • NH4+ (µg m^{-3}) • SS Cl- (µg m^{-3}) • B_{ext}
Time period	Lago Monaci: form 2021-04-03 to 2022-05-04 Vincheto di Celarda: from 2023-05-19 to 2024-05-27
	Ozone concentrations

Forest sites (5)	• ABR1 (Selva Piana) • EMI1 (Carrega) • LAZ1 (Monte Rufeno) • PIE1 (Val Sessera) • VEN1 (Cansiglio)
Variables (5)	• O3_Annual mean (ppb) • O3_Growing season mean (ppb) • AOT40 (ppm h) • POD0 (mmol m-2) • POD1 (mmol m-2)
Years (6)	From 2018 to 2023

4.1.2 Results and discussion

Air quality and visibility

Figure 4.1.1 presents the trends of the air quality variables at the Lago Monaci site over the measurement period from April 3, 2021, to May 4, 2022.

The graph indicates two peaks in PM_{10} and $PM_{2.5}$ levels in the periods of June-July 2021 and February-April 2022. The first peak appears to be associated with elevated concentrations of terrigenous elements (Al, Ti, Si, Fe, and Ca), while the second peak is linked to increased levels of nitrogen compounds (NH_4^+, NO_2^-, and NO_3^-).

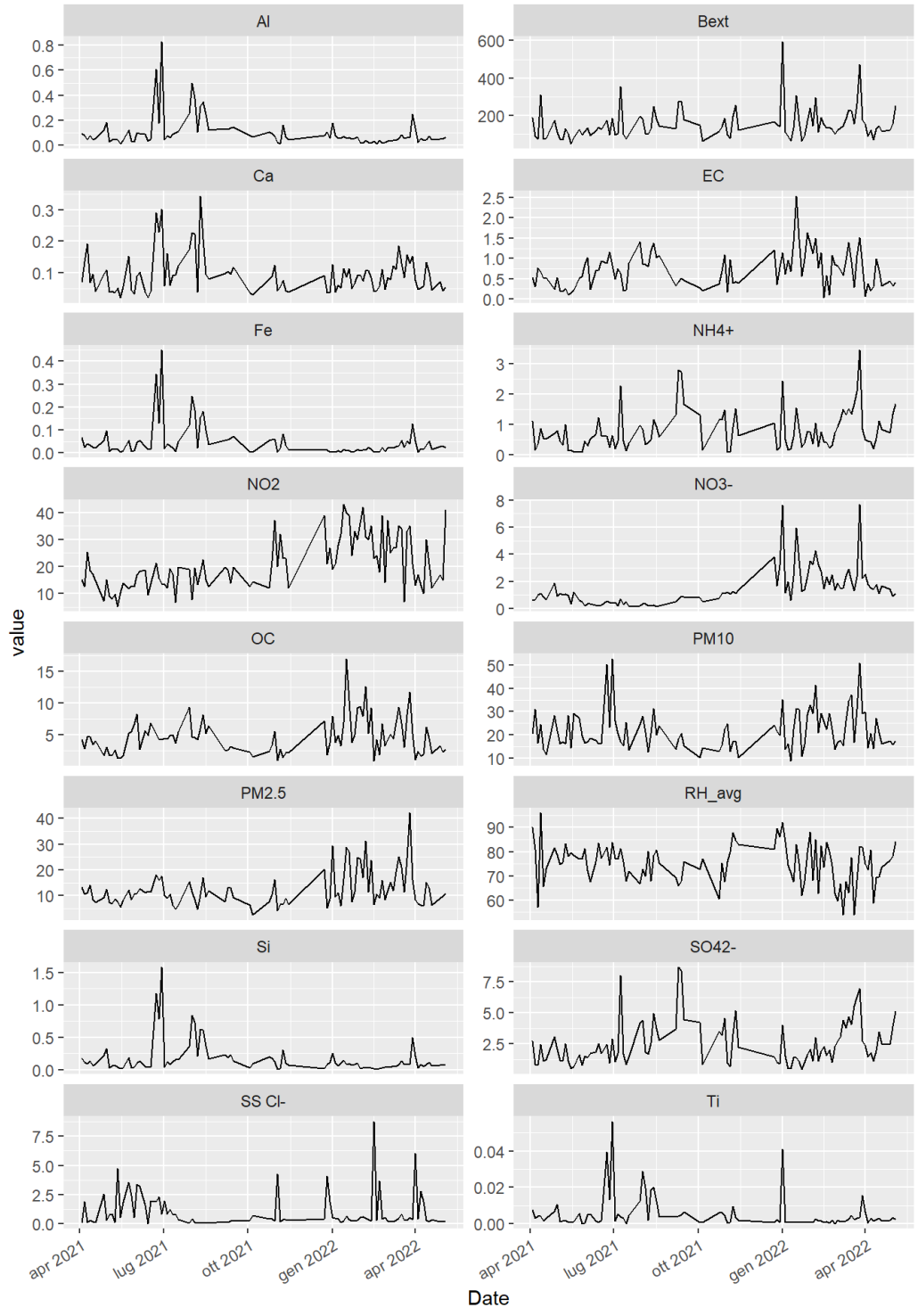

Figure 4.1.1. Trends of the 16 air quality variables at the Lago Monaci site over the measurement period.

Since data were collected over different year periods (03-04 to 29-12 for 2021, 01-01 to 04-05 for 2022), we considered also the trends between quarters (Figures 4.1.2 and 4.1.3). The first quarter of 2022 shows a peak of PM_{10} and $PM_{2.5}$, which is associated with the highest concentrations of nitrogen oxides (Fig. 4.3), while the peak of terrigenous elements measured in air samples occurs in the third quarter of 2021 (Fig. 4.4).

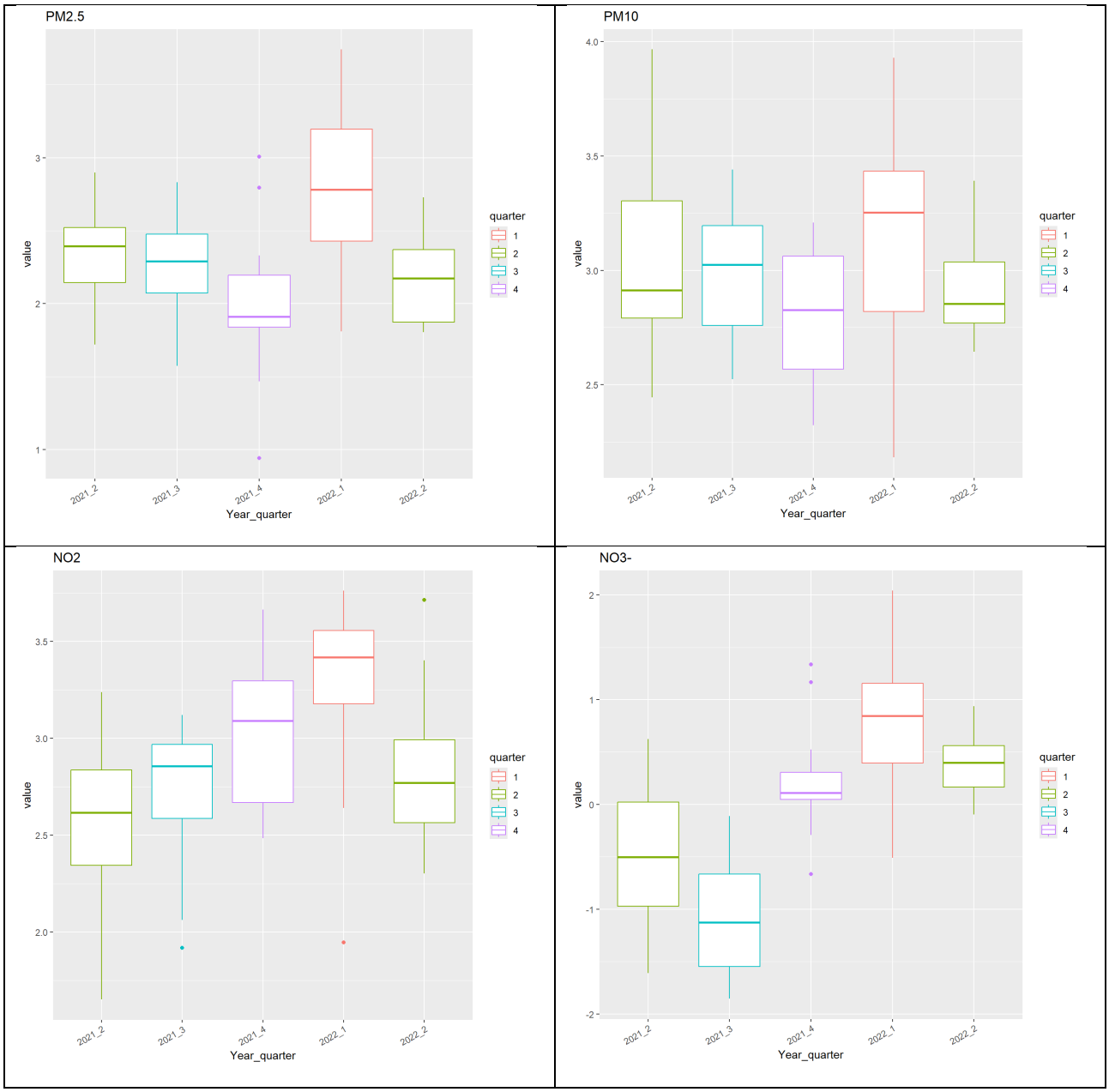

Figure 4.1.2. Boxplots showing the distribution of PM2.5, PM10, NO_2 and NO_3^- between quarters over the measuring period at the Lago Monaci site.

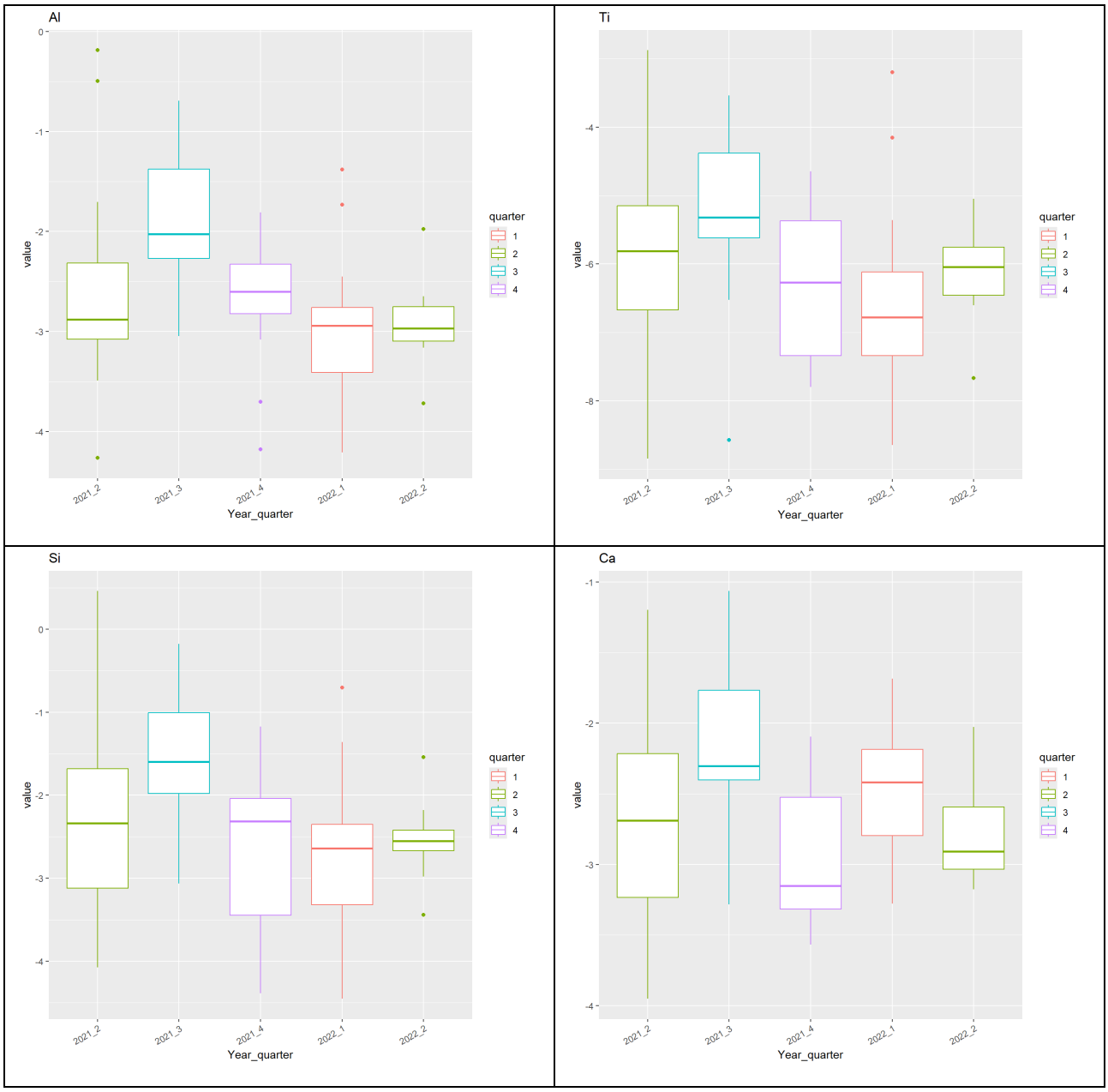

Figure 4.1.3. Boxplots showing the distribution of Al, Ti, Si and Ca between quarters over the measuring period at the Lago Monaci site.

The highest correlations between the variables (Pearson's correlation; Figure 4.1.4) are observed among the terrigenous elements (Ca, Fe, Ti, Si, Al; r > 0.6) as well as NH_4^+ and SO_4^{2-} (0.87). The B_{ext} index, associated with air visibility, shows a higher correlation (>0.6) with $PM_{2.5}$, NH_4^+, and SO_4^{2-}.

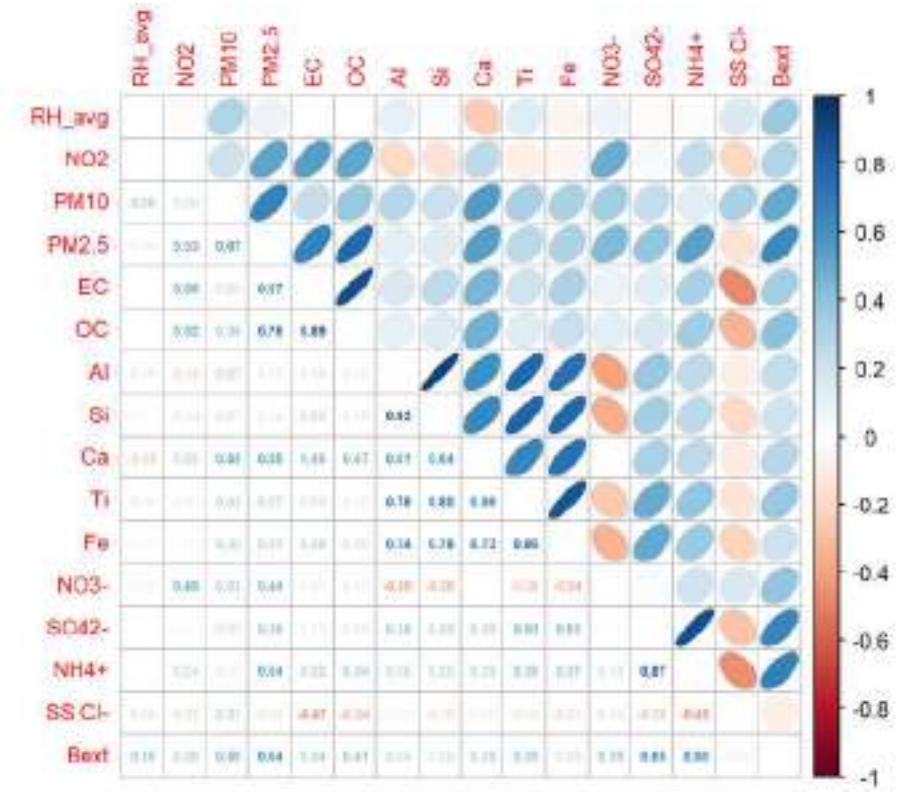

Figure 4.1.4. Pearson's correlation among variables over the measurement period at the Lago Monaci site.

The PCA confirms the trends and Pearson's correlations (Figure 4.1.5): terrigenous elements (Ca, Fe, Ti, Si, Al) correlate with each other and with negative PC1 and PC2 values. Nitrogen compounds align with positive PC2 values, along with PM_{10} and $PM_{2.5}$. B_{ext} strongly correlates with PM and nitrogen compounds. SS Cl- is clearly distinct from other parameters.

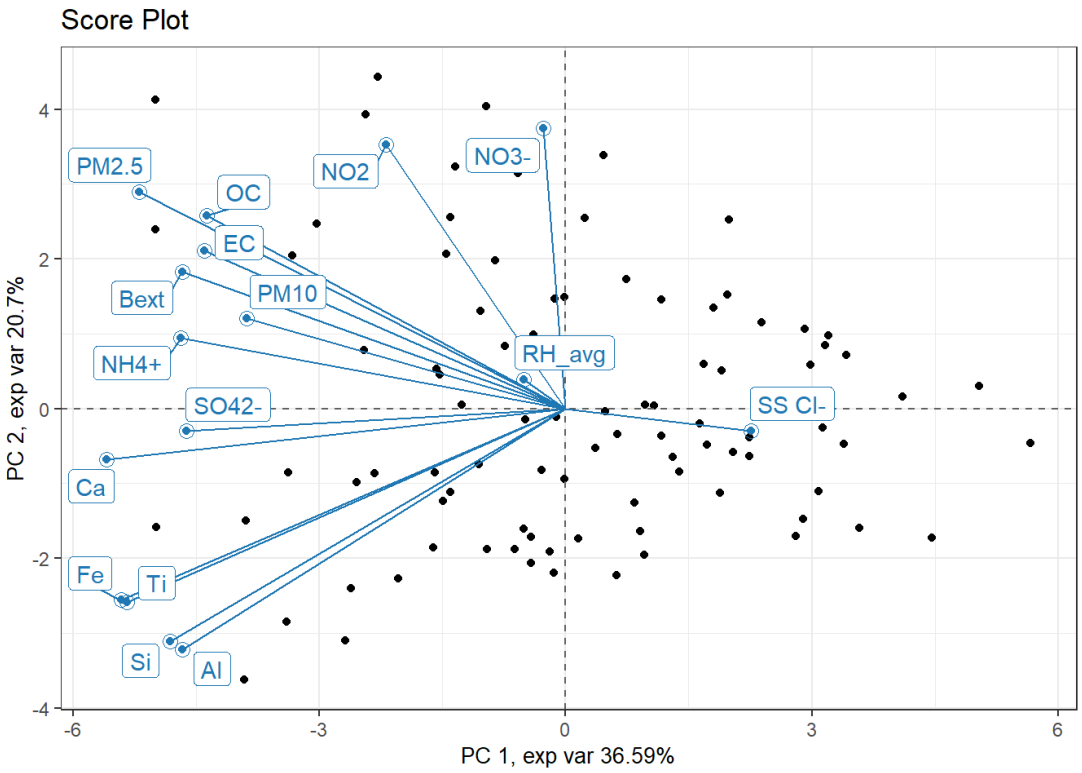

Figure 4.1.5. Results of the PCA on autoscaled data.

Ozone concentrations

Figure 4.1.6 illustrates the trends of the five ozone variables at the forest sites over a 6-year period.

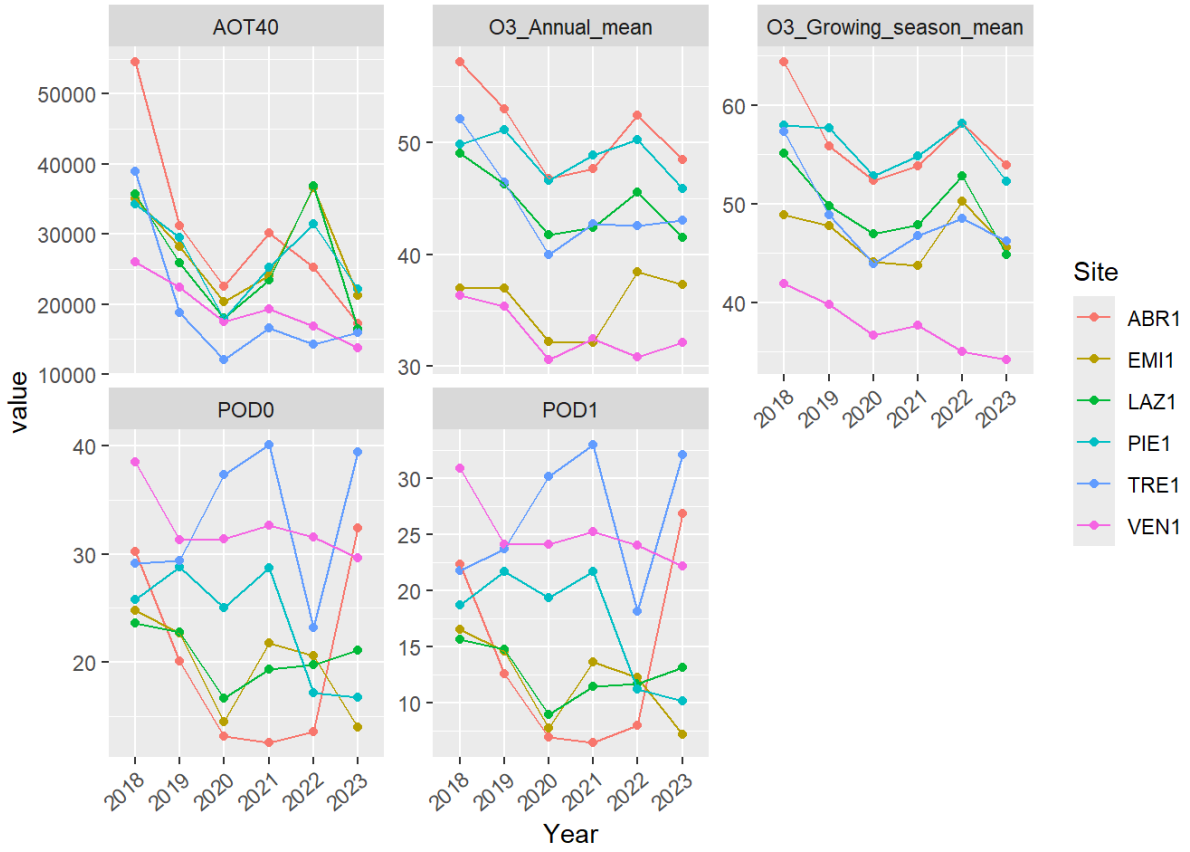

Figure 4.1.6. Trends of the 5 ozone variables at the forest sites over a 6-year period.

The correlation among variables has been analyzed for each forest site over the years using Pearson's correlation method. Figure 4.1.7 illustrates the results obtained for LAZ1. AOT40, POD0 and POD1 are positively correlated with O_3 concentrations. AOT40 is highly correlated to the average ozone concentration during the growing season.

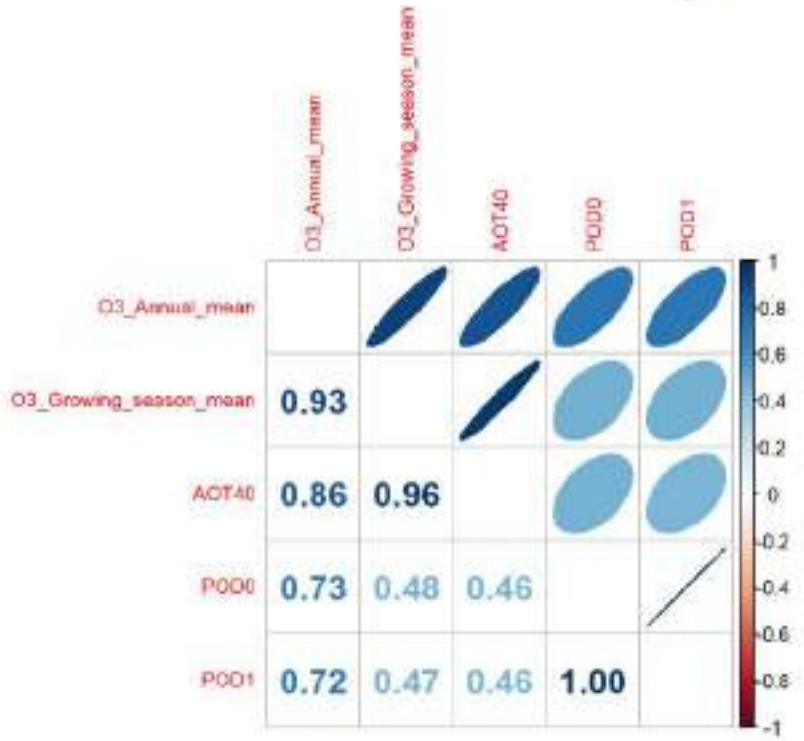

Figure 4.1.7. Pearson's correlation among variables over the years at the forest site LAZ1.

The results of the Principal Component Analysis (PCA) show that the POD1 and POD0 variables are uncorrelated to the others; PC1 explains the variability between Sites but not between Main tree species (Figure 4.1.8).

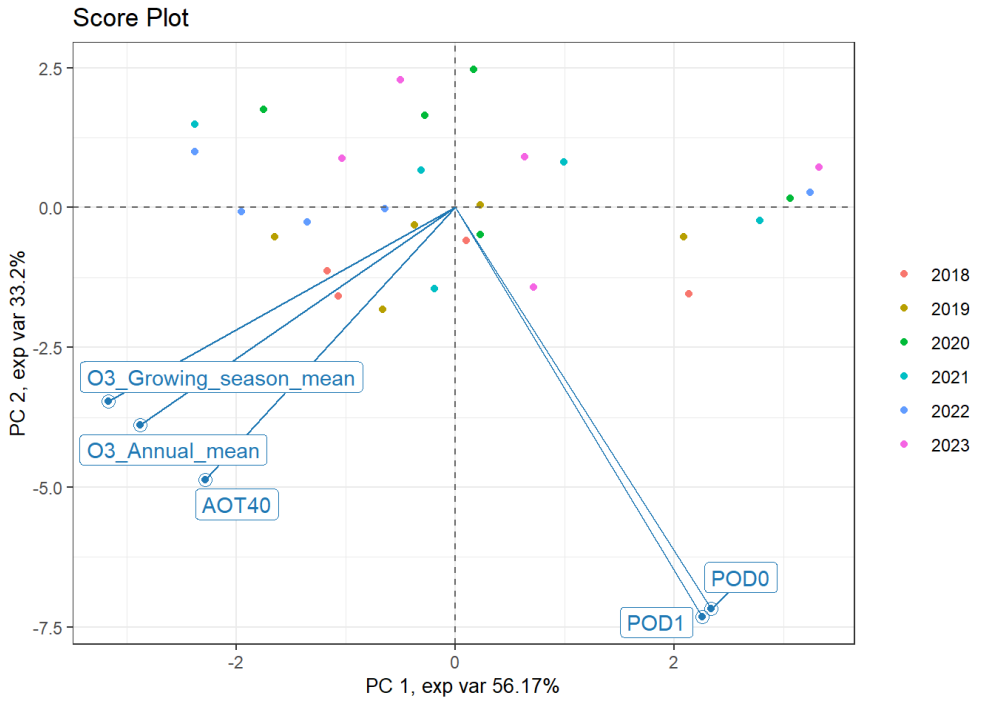

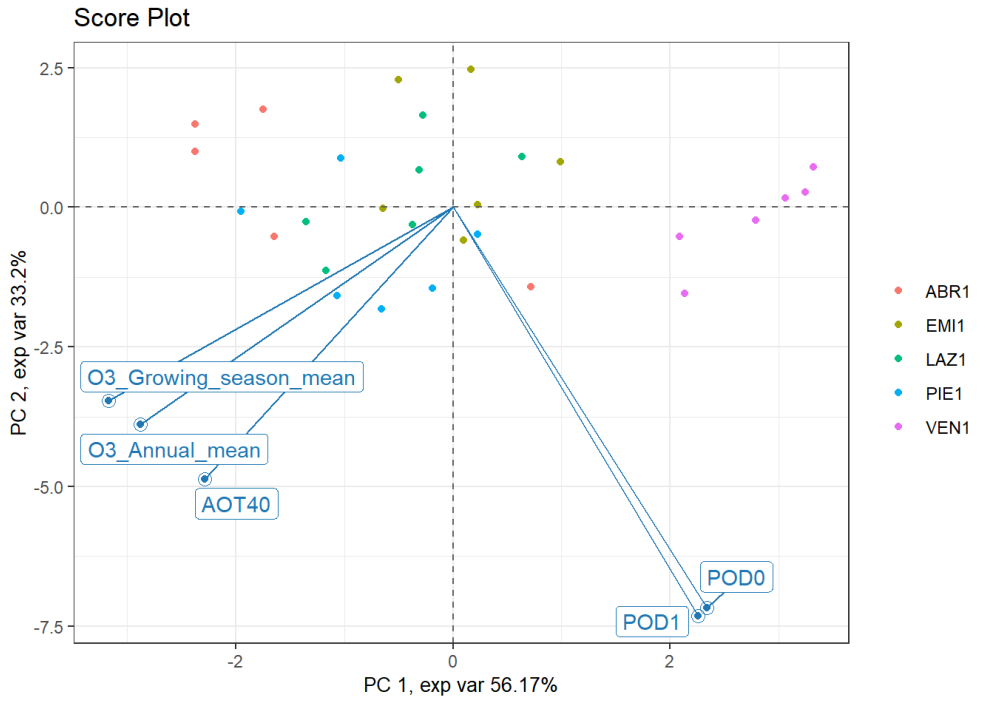

Figure 4.1.8. Results of the PCA on autoscaled data (→ continues).

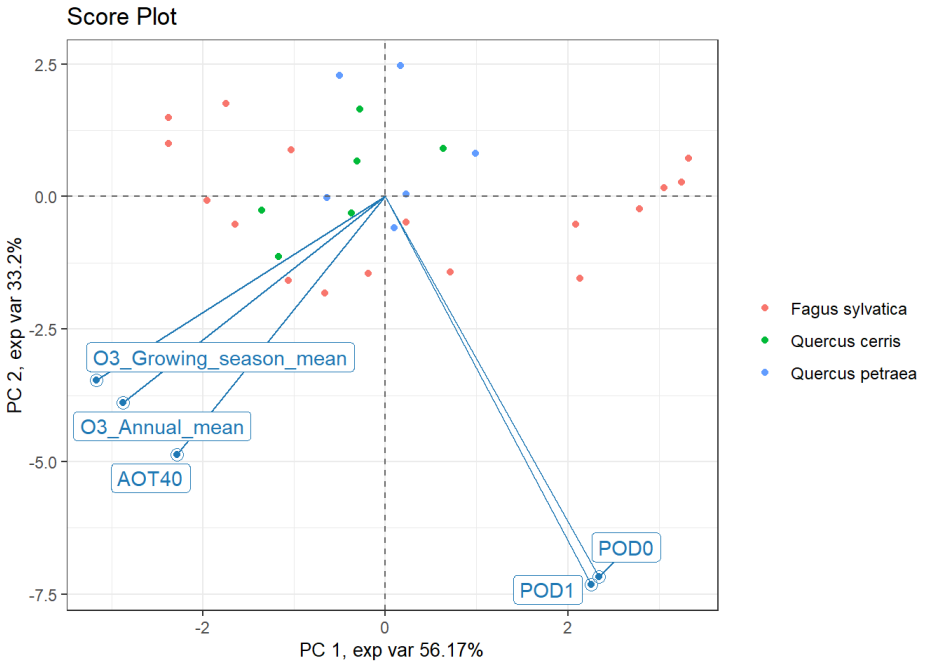

Figure 4.1.8. Results of the PCA on autoscaled data.

The results obtained for the 5 forest sites were compared using non-parametric Kruskal Wallis test and the post-hoc Wilcoxon rank sum test (Figure 4.1.9). Four variables significantly differ among the forest sites, with VEN1 showing the lower values of ozone concentrations (both annual mean and growing season) and the higher values of POD0 and POD1.

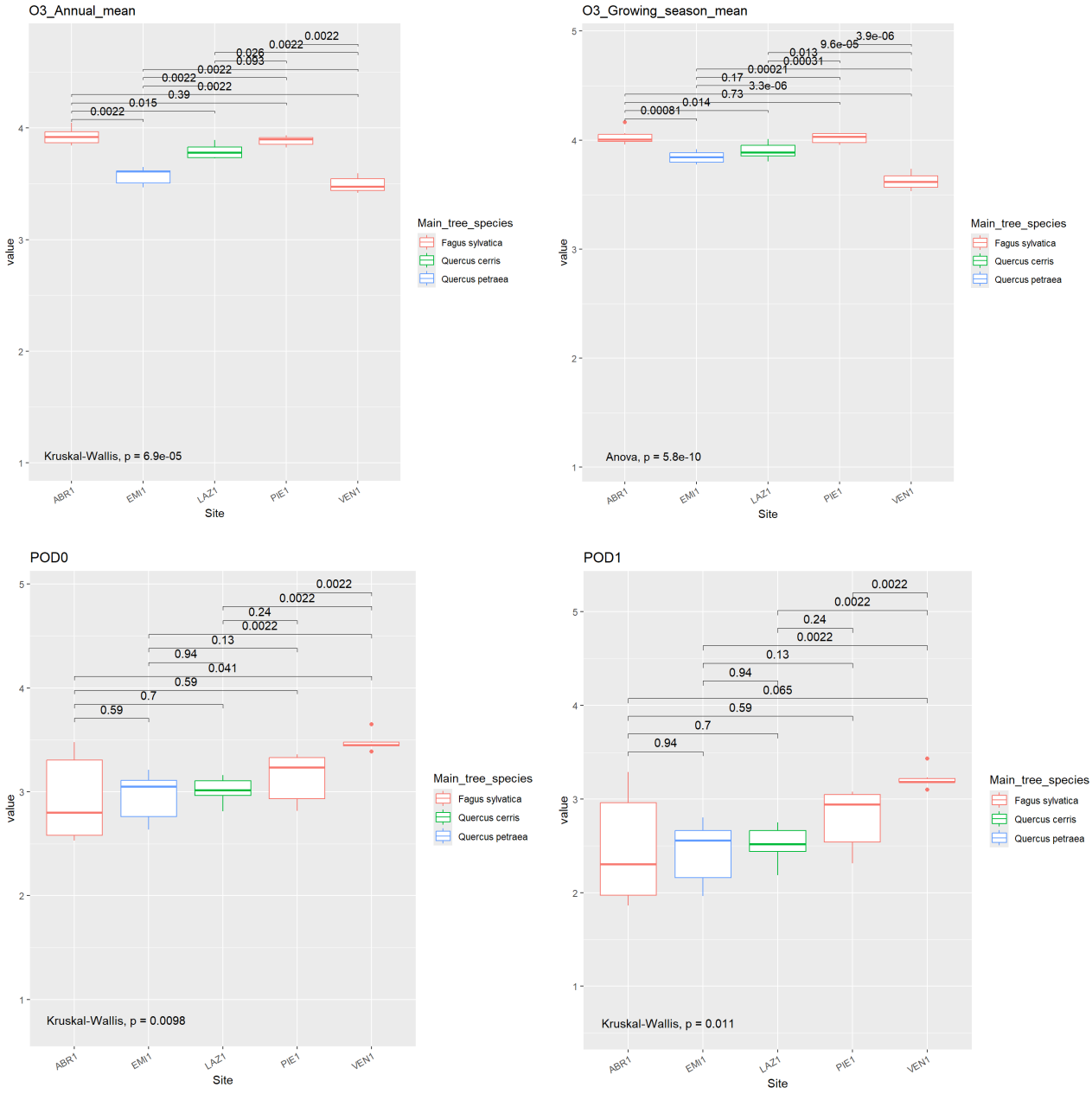

Figure 4.1.9. Boxplots with the results of the non-parametric Kruskal Wallis test and the post-hoc Wilcoxon rank sum test.

4.2 Meteorology

4.2.1 Dataset

Table 4.2.1 provides an overview of the dataset. Meteorological data cover 25 years (2000-2024) in the 10 forest sites of the project. Ten key variables have been considered for this analysis.

Table 4.2.1. Overview of the available dataset.

Forest sites (10)	• ABR1 (Selva Piana) • BOL1 (Renon) • CAL1 (Piano Limina) • EMI1 (Carrega) • LAZ1 (Monte Rufeno) • PIE1 (Val Sessera) • SAR1 (Marganai) • TOS2 (Cala Violina) • VEN1 (Cansiglio) • VEN2 (Bosco Fontana)
Variables (10)	• AT_Max: Average of the Maximum Temperatures • AT_Min: Average of the Minimum Temperatures • AT_Med: Average of the Mean Temperatures • PR_Sum: Total Rainfall • PR_Veg: Total Rainfall during the Vegetative Period (01/06 - 31/08) • RH_Med: Average of the Mean Relative Humidity • ST_Med: Average of the Mean Soil Temperatures • SR_Med: Average the Mean Solar Radiation • WS_Med: Average of the Mean Wind Speeds • WS_Max: Average of the Maximum Wind Speeds
Years (25)	From 2000 to 2024

4.2.2 Results and discussion

Figure 4.2.1 illustrates the trends of the 10 meteorological variables at the forest sites over a 25-year period, with point sizes proportional to the number of observations used in each aggregation. Figure 4.2.2 shows the distribution of precipitation variables (PR_Veg: Total Rainfall during the Vegetative Period (01/06 - 31/08); PR_Sum: Total Rainfall) in the 25-years' time span.

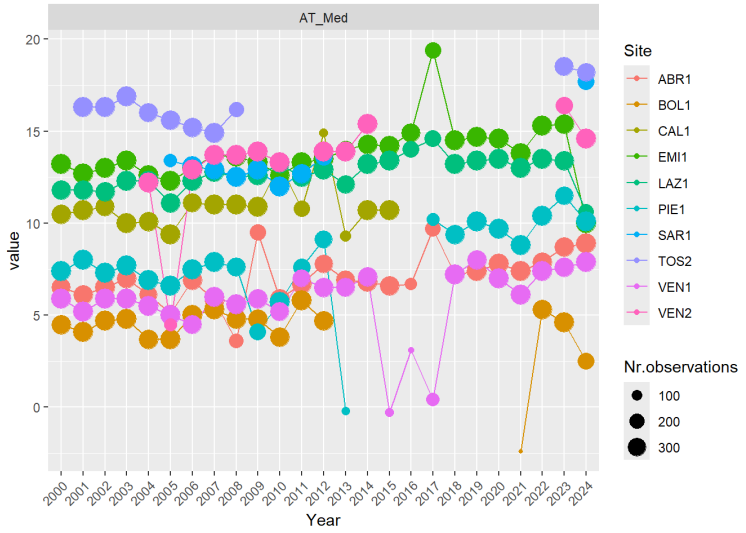

Figure 4.2.1. Trends of the meteorological variables at the forest sites over a 25-year period, with point sizes proportional to the number of observations used in each aggregation (→ continues).

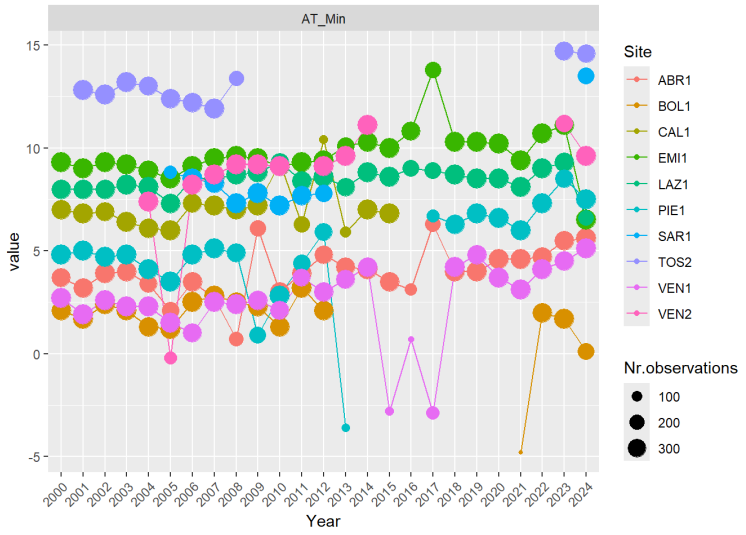

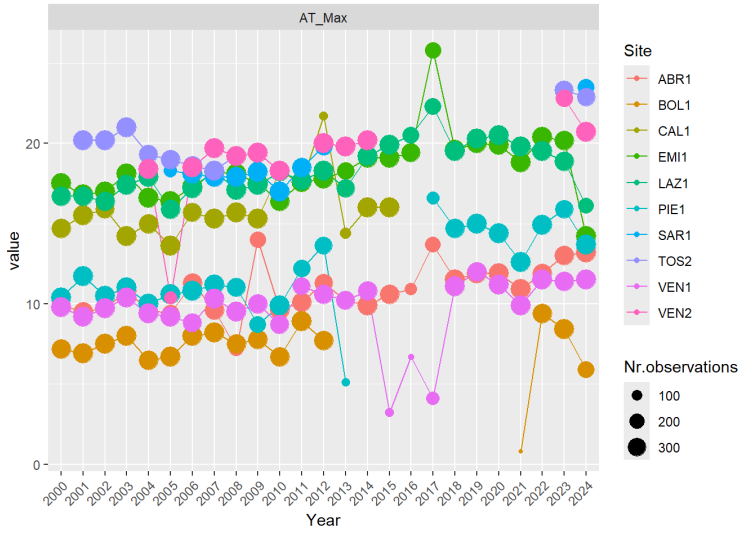

Figure 4.2.1. Trends of the meteorological variables at the forest sites over a 25-year period, with point sizes proportional to the number of observations used in each aggregation (→ continues).

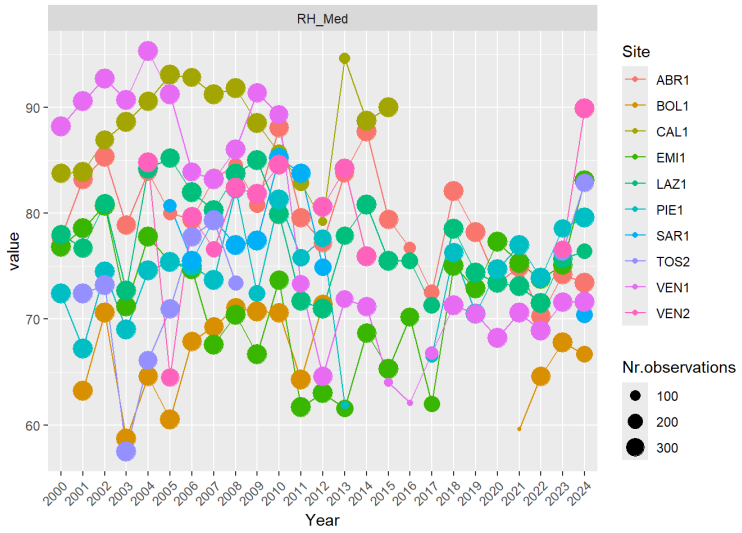

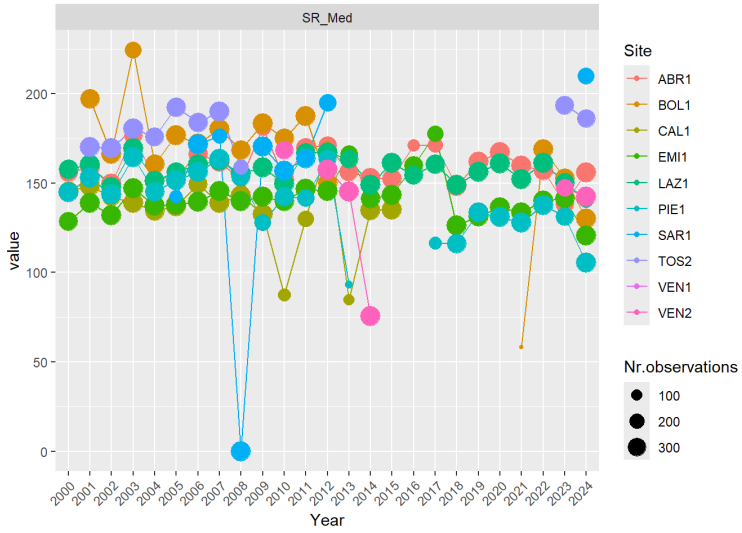

Figure 4.2.1. Trends of the meteorological variables at the forest sites over a 25-year period, with point sizes proportional to the number of observations used in each aggregation (→ continues).

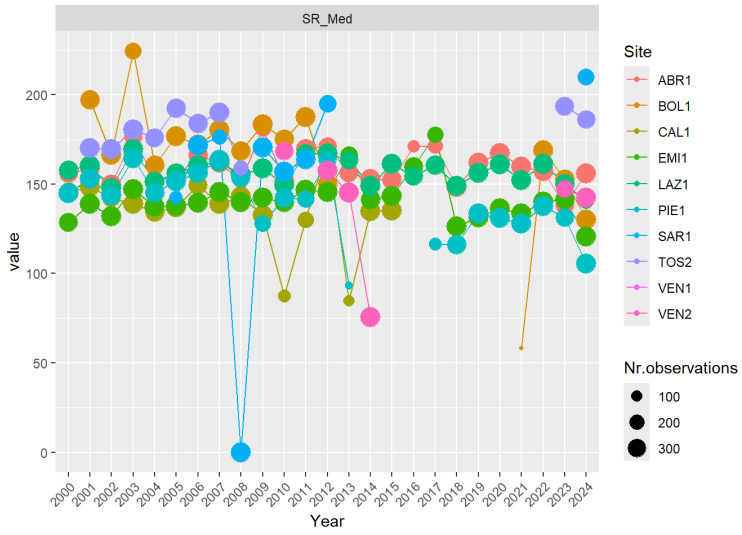

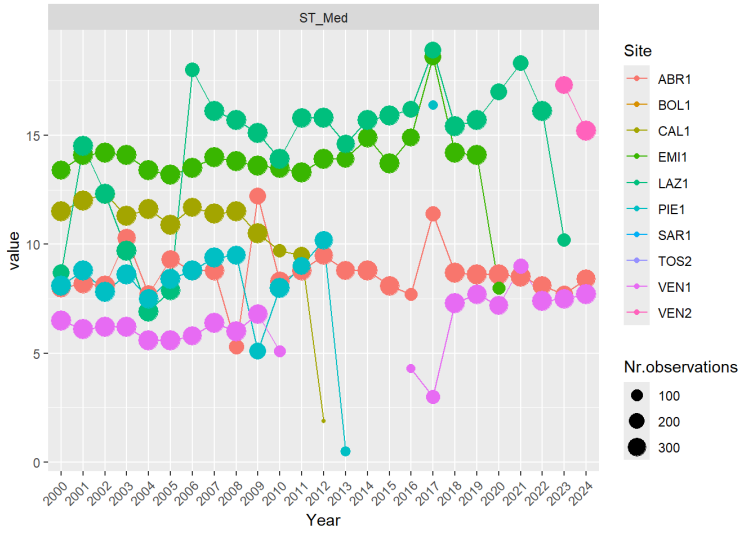

Figure 4.2.1. Trends of the meteorological variables at the forest sites over a 25-year period, with point sizes proportional to the number of observations used in each aggregation (→ continues).

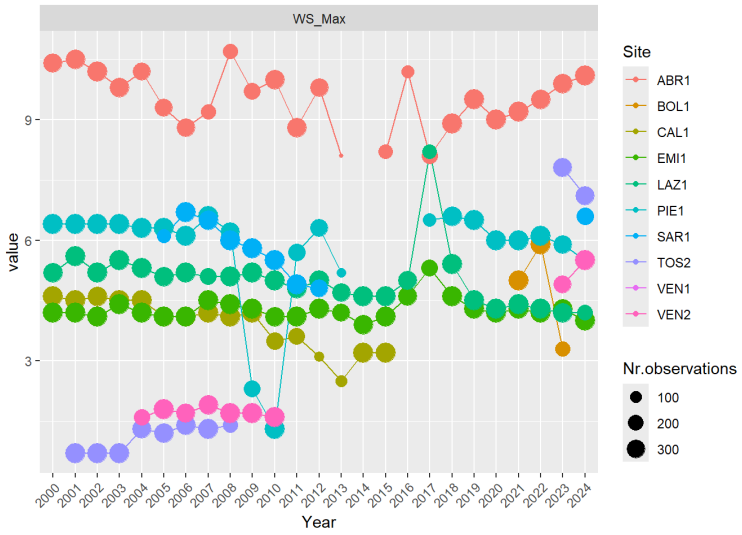

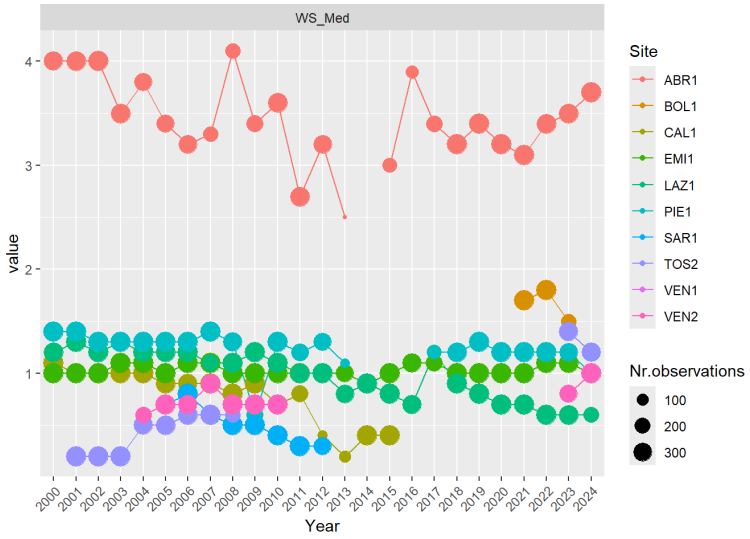

Figure 4.2.1. Trends of the meteorological variables at the forest sites over a 25-year period, with point sizes proportional to the number of observations used in each aggregation.

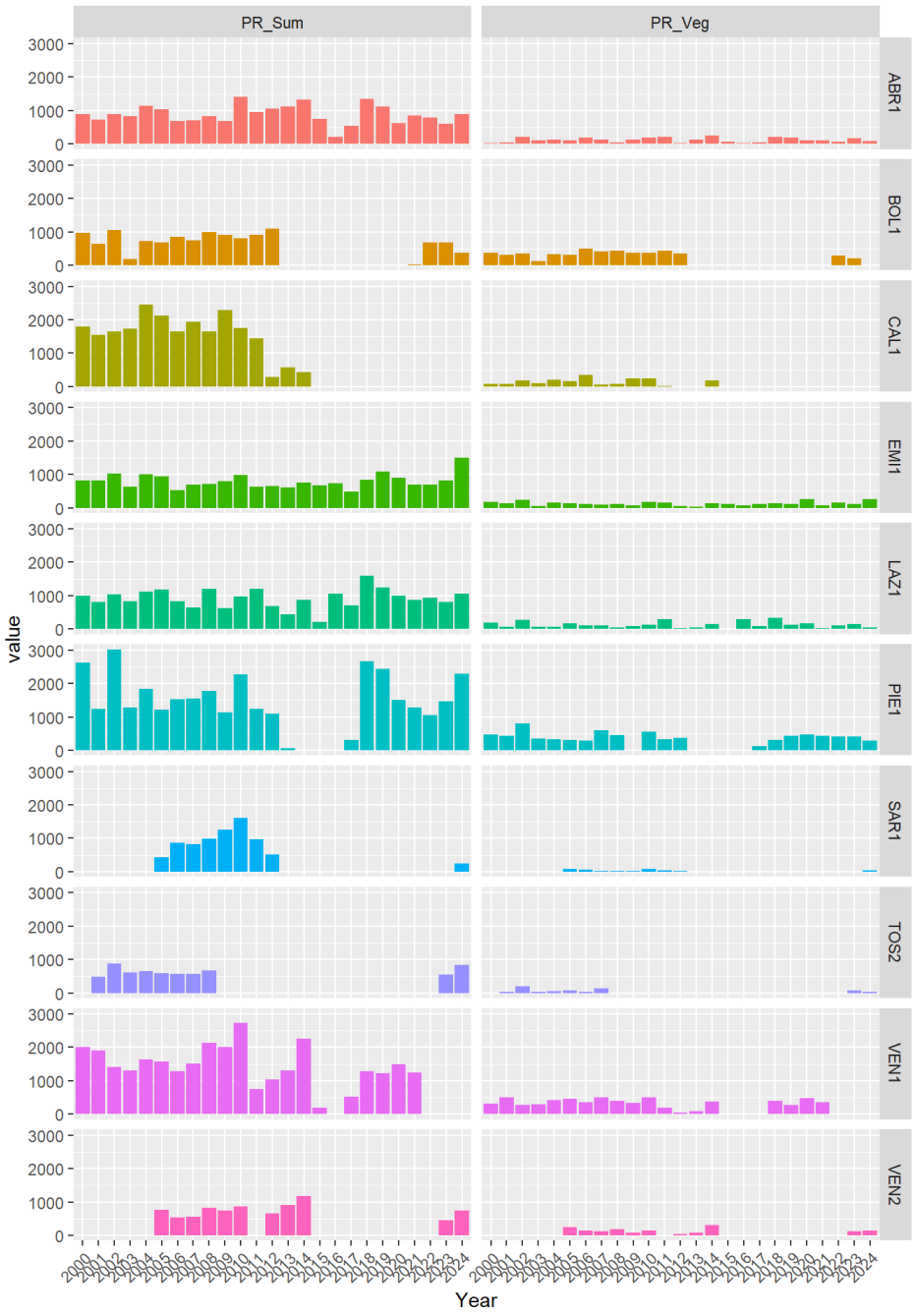

Figure 4.2.2 Trends of the precipitation variables at the forest sites over a 25-year period.

The correlation among variables has been studied for each forest site over the years (Pearson's correlation). Figure 4.2.3 provides an example of the results obtained for EMI1.

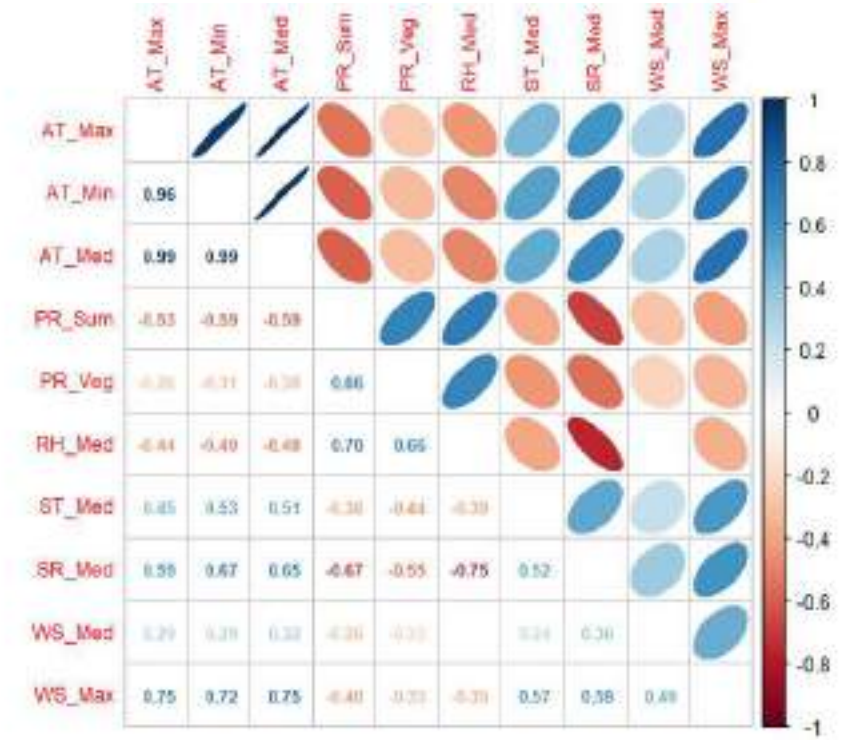

Figure 4.2.3. Pearson's correlation among variables over the years at the forest site EMI1.

The distribution of the variables in the four forest types is given in the boxplots of Figure 4.2.4.

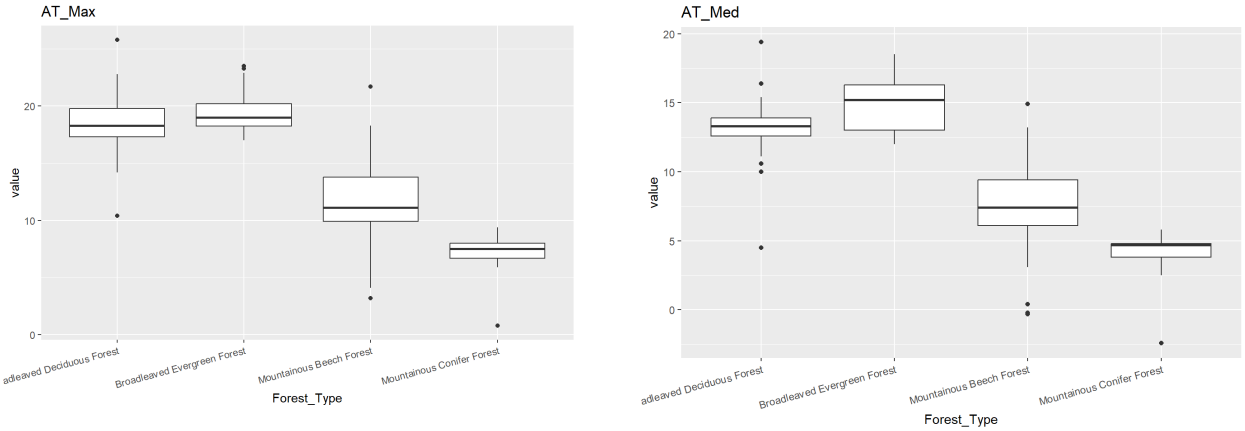

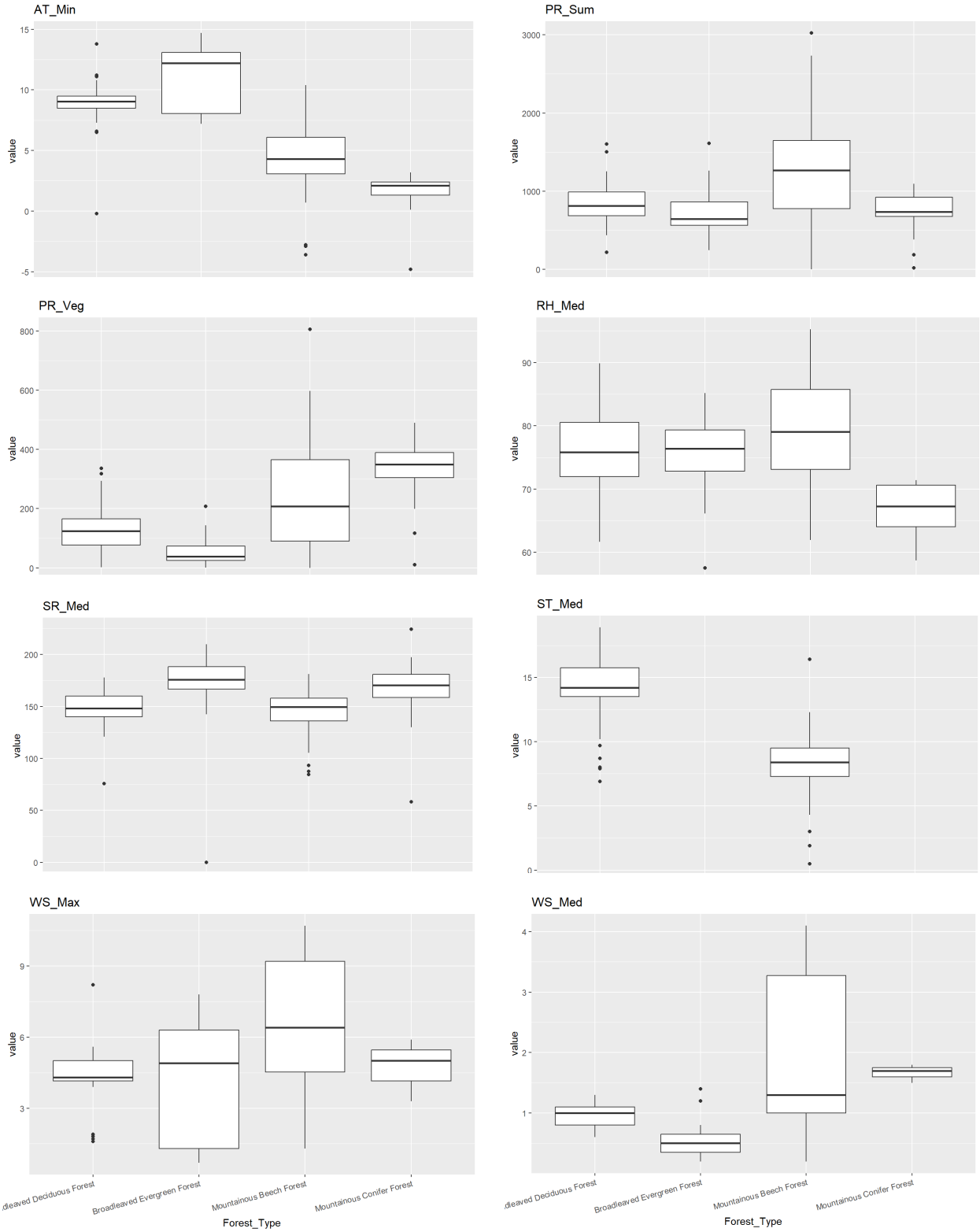

Figure 4.2.4. Boxplots showing the distribution of the meteorological parameters in the four forest types.

Main climate trends

This section aims to further explore the results presented above by showing the main trends observed along the time series (2000-2024) at the forest sites.

Figure 4.2.5 highlights the typical seasonal climate patterns for each site. Temperatures rise in spring, peak between July and August, and then drop in autumn and winter. The data confirms the more or less rapid increase in temperatures from 2000 to 2024 (Figure 4.2.6).

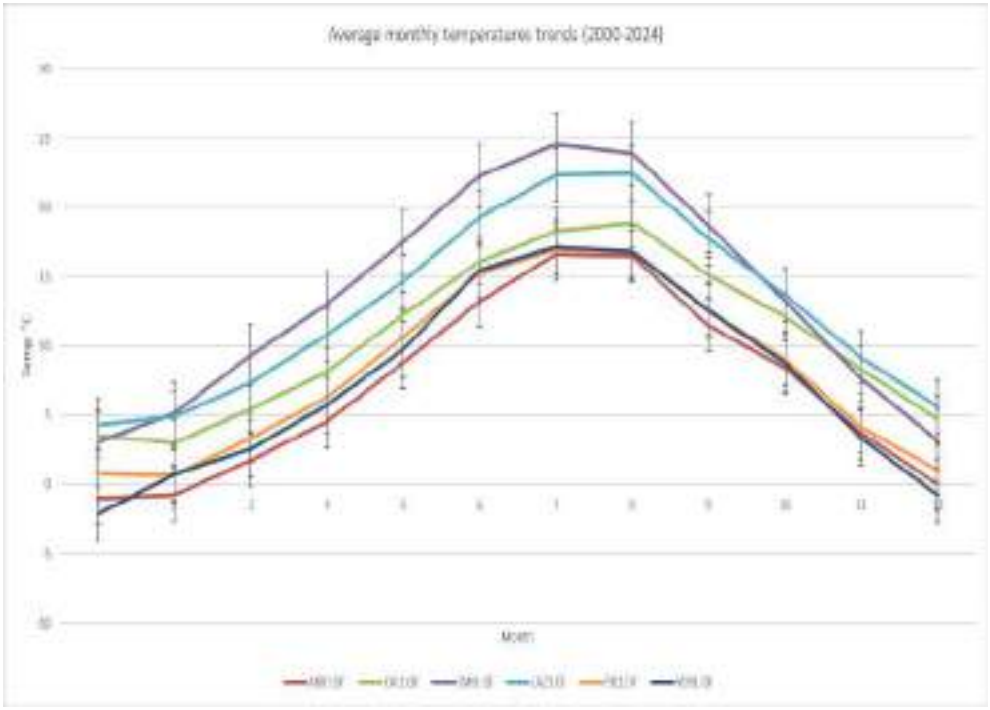

Figure 4.2.5. Trends in the average monthly temperatures recorded over the period 2000-2024.

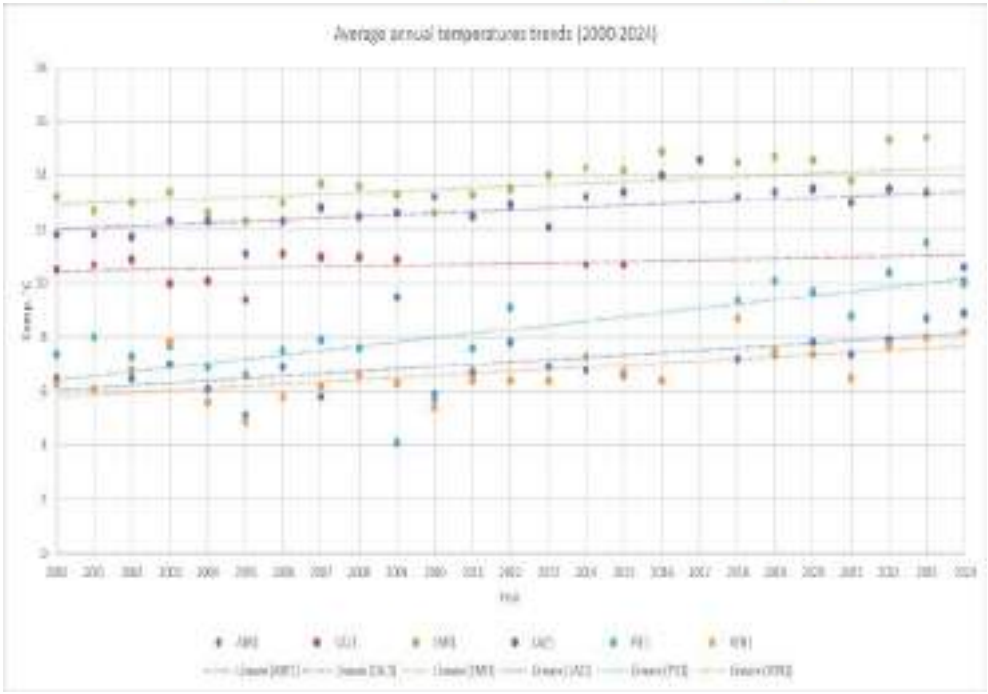

Figure 4.2.6. Trends in the average annual temperatures recorded over the period 2000-2024.

The diagrams in the following figures facilitate the visual identification of aridity periods, defined as times when the temperature curve is above the precipitation curve. At the ABR1 forest site, the period of aridity spans from June to August, observed exclusively at the 'in the plot' (ITP) station. Conversely, at the CAL1 site, aridity is evident in both the 'open field' (OFD) and the ITP datasets (Figures 4.2.7 and 4.2.8).

The period of aridity affects both recording stations (ITP and OFD) in EMI1 and LAZ1 forest sites; however this effect is higher in EMI1 (Figures 4.2.9 and 4.2.10).

For the PIE1 and VEN1 sites, conditions differ markedly. The graphs consistently show precipitation surpassing temperature, indicating no summer drought and confirming an 'Alpine' climate, unlike Central and Southern Italy sites (Figures 4.2.11 and 4.2.12).

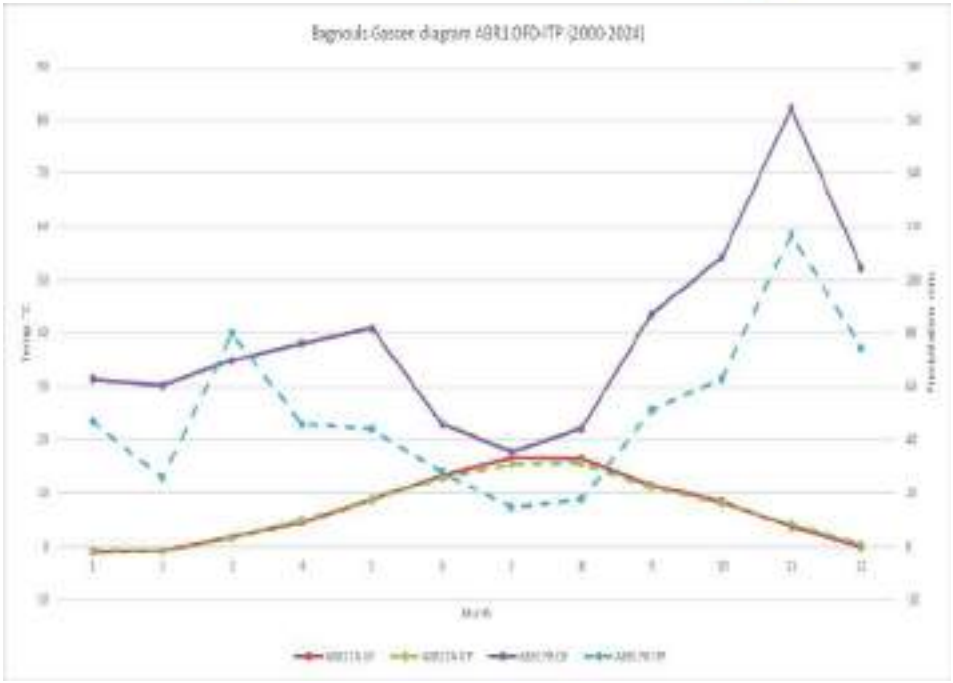

Figure 4.2.7. Bagnouls Gassen diagram showing temperatures and precipitations recorded over the period 2000-2024 at the ABR1 forest site (ITP: in the plot recording station; OFD: open field recording station).

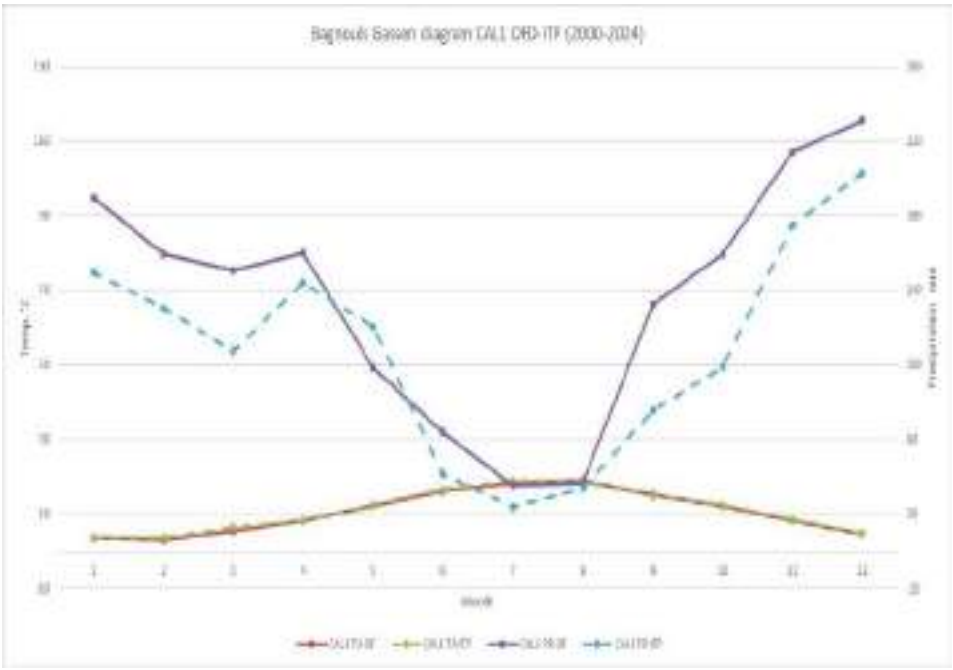

Figure 4.2.8. Bagnouls Gassen diagram showing temperatures and precipitations recorded over the period 2000-2024 at the CAL1 forest site (ITP: in the plot recording station; OFD: open field recording station).

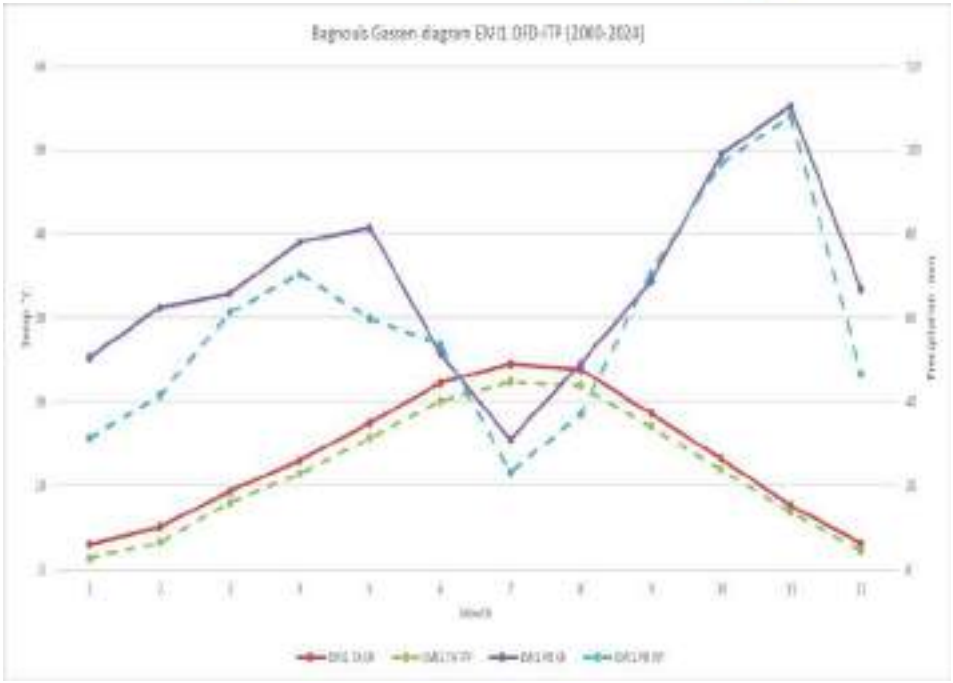

Figure 4.2.9. Bagnouls Gassen diagram showing temperatures and precipitations recorded over the period 2000-2024 at the EMI1 forest site (ITP: in the plot recording station; OFD: open field recording station).

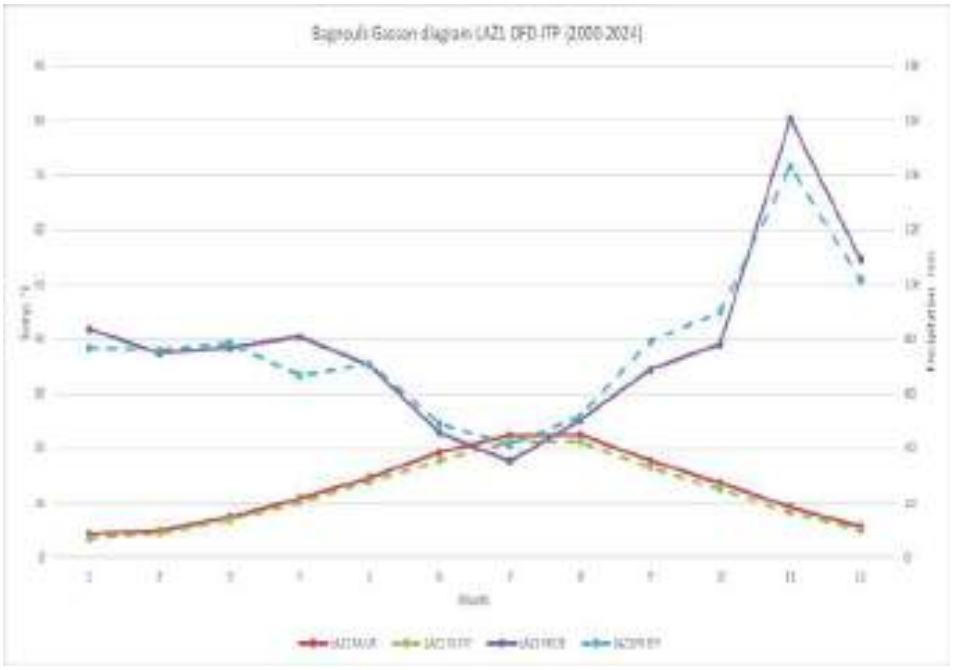

Figure 4.2.10. Bagnouls Gassen diagram showing temperatures and precipitations recorded over the period 2000-2024 at the LAZ1 forest site (ITP: in the plot recording station; OFD: open field recording station).

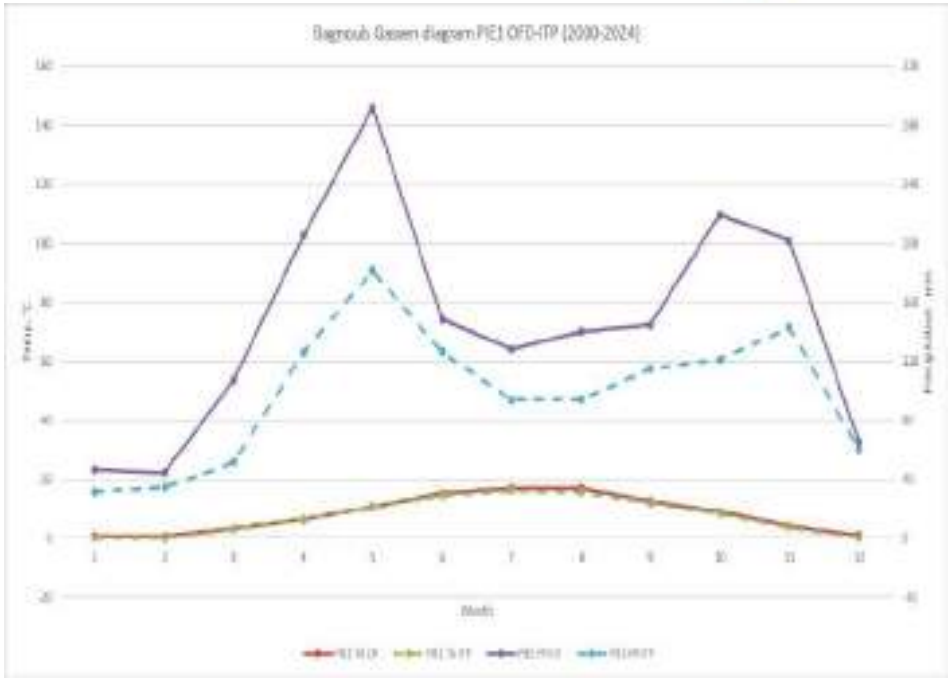

Figure 4.2.11. Bagnouls Gassen diagram showing temperatures and precipitations recorded over the period 2000-2024 at the PIE1 forest site (ITP: in the plot recording station; OFD: open field recording station).

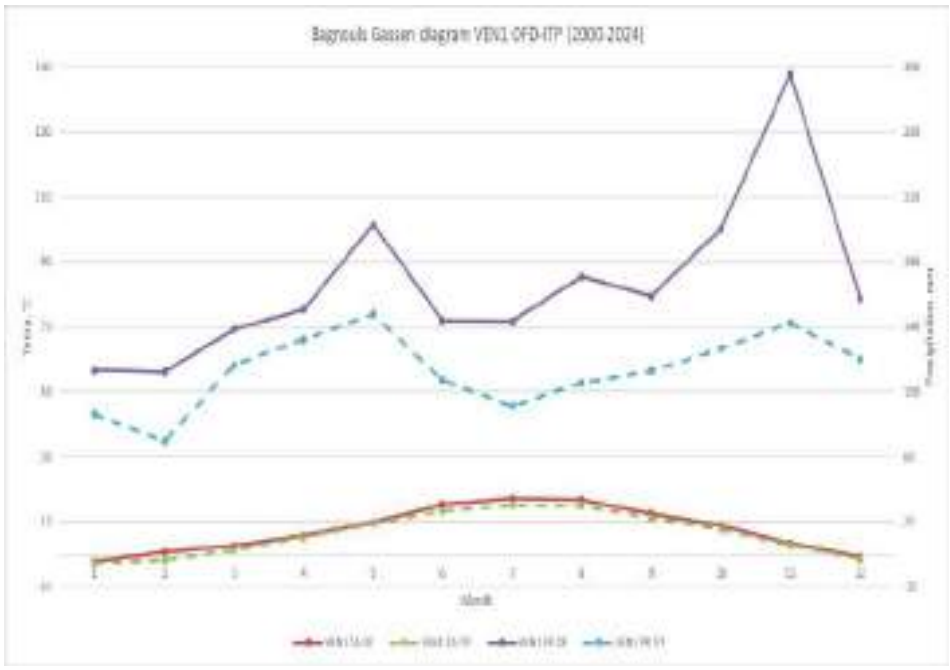

Figure 4.2.12. Bagnouls Gassen diagram showing temperatures and precipitations recorded over the period 2000-2024 at the VEN1 forest site (ITP: in the plot recording station; OFD: open field recording station).

Precipitation trends at the forest sites are evaluated using two complementary graphical representations: one depicting seasonal averages (Figure 4.2.13) and the other illustrating annual trends (Figure 4.2.14). The second graph shows that most sites have a slight decrease in total precipitation, with notable annual variability. VEN1 displays the most pronounced decrease, whereas PIE1 and EMI1 present marginally positive trends, although they are not significant.

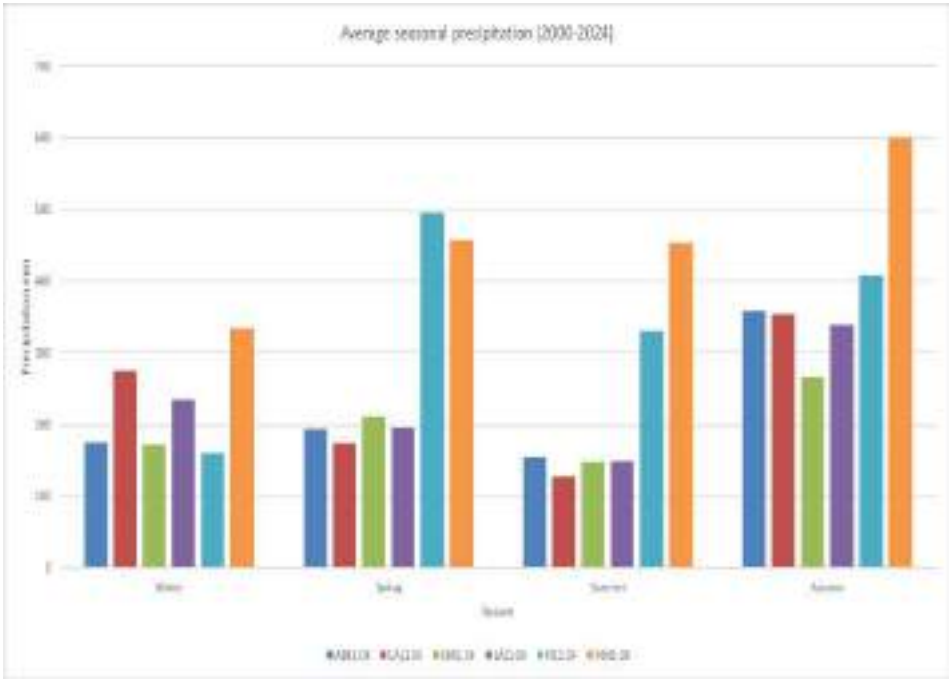

Figure 4.2.13. Trends of the seasonal average precipitations recorded at the forest site over the period 2000-2024.

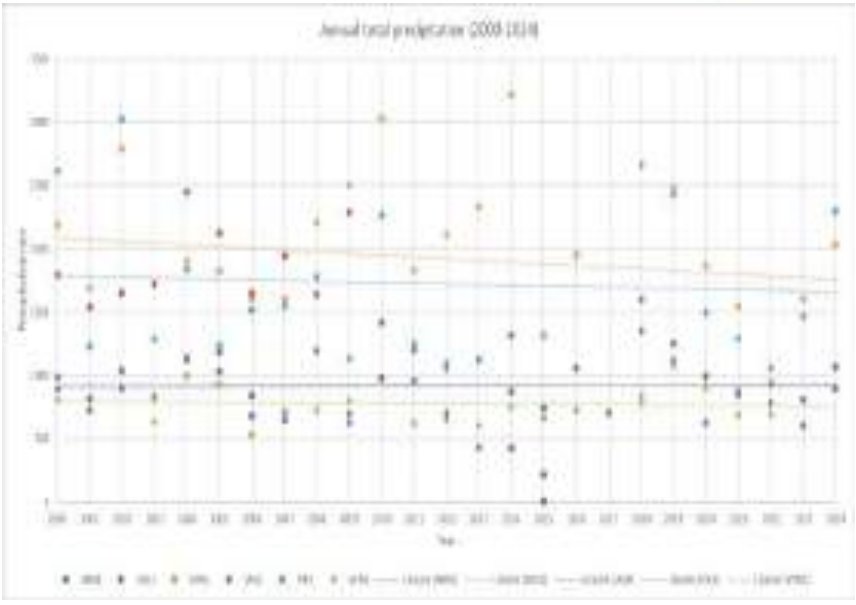

Figure 4.2.14. Trends of the annual precipitations recorded at the forest site over the period 2000-2024.

Detailed data on seasonal precipitation trends were obtained by considering the cumulative total for each year from 2000 to 2024 across all four seasons (Figures 4.2.15-4.2.18). Winter typically experiences higher precipitation in the northern regions, with EMI1 and VEN1 recording the largest amounts, especially in 2013 and 2014 (Figure 4.2.15). For spring, precipitation levels are elevated in VEN1 and PIE1, with notable peaks occurring in years such as 2002 and 2013 (Figure 4.2.16).

The summer precipitation graph indicates a sharp decline across all regions, especially in LAZ1 and CAL1, confirming the drought periods previously identified in the Bagnouls-Gaussen diagrams (Figure 4.2.17). Autumn is identified as the season with the highest overall precipitation, featuring notable peaks at the VEN1 site in 2010 and 2014. Seasonal analysis indicates not only a reduction in total precipitation, as previously discussed, but also an increasing concentration of rainfall over shorter periods, which may reflect changes related to climate change patterns (Figure 4.2.18).

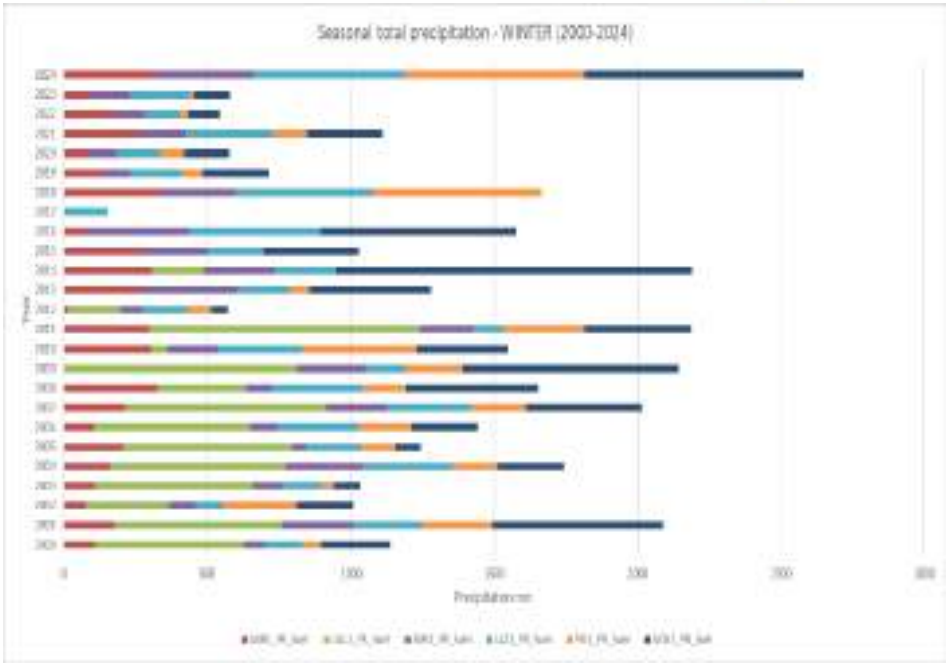

Figure 4.2.15. Cumulative total precipitations recorded during winter at the forest site over the period 2000-2024.

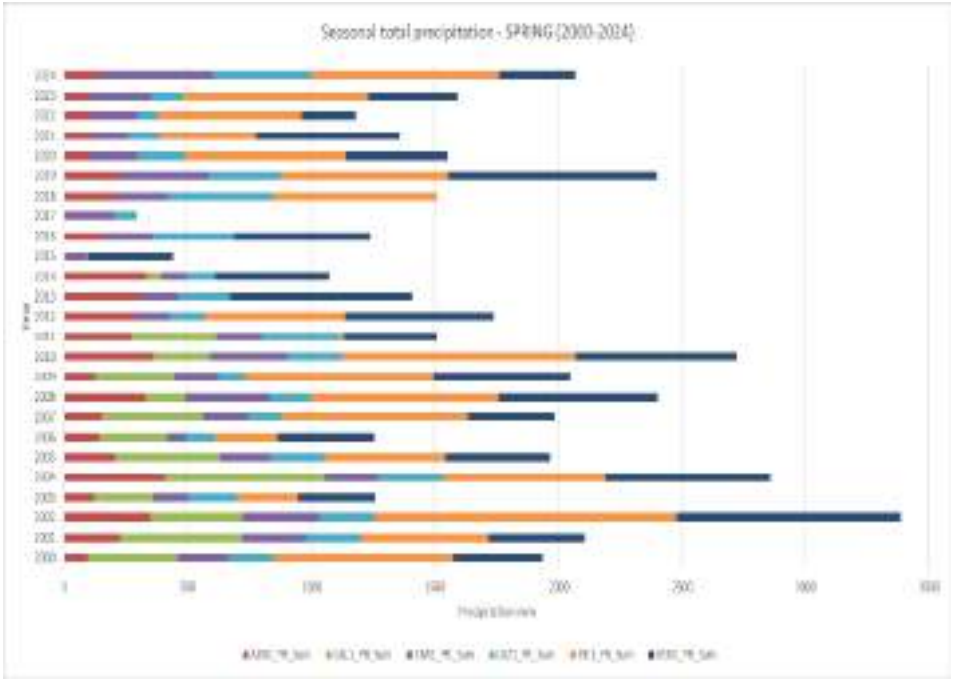

Figure 4.2.16. Cumulative total precipitations recorded during spring at the forest site over the period 2000-2024.

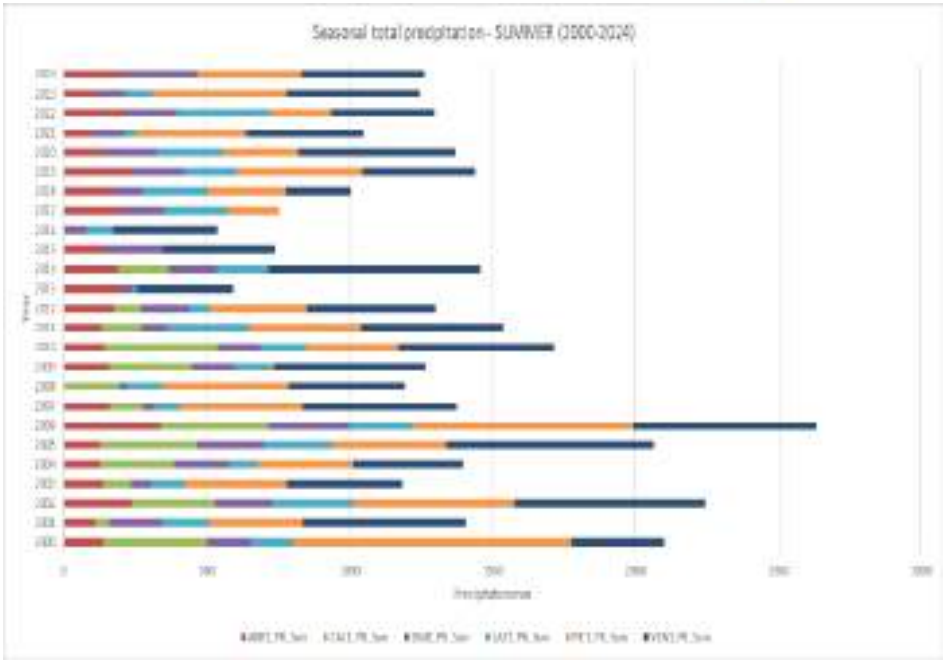

Figure 4.2.17. Cumulative total precipitations recorded during summer at the forest site over the period 2000-2024.

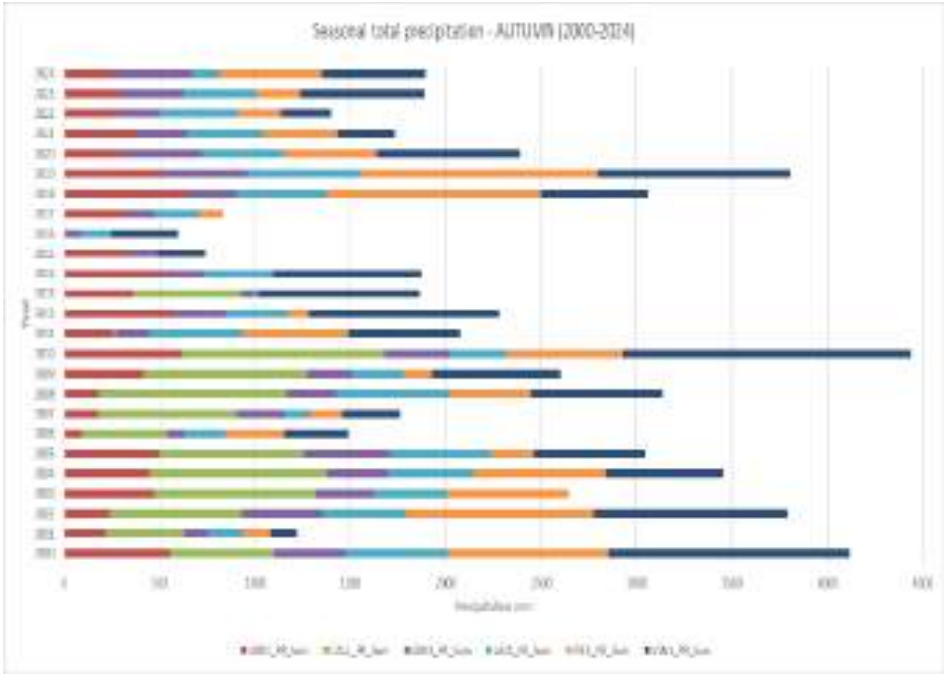

Figure 4.2.18. Cumulative total precipitations recorded during autumn at the forest site over the period 2000-2024.

The wind rose map diagram illustrates the predominant wind direction and intensity observed at the forest sites (Figure 4.2.19). Notable variations are evident among the different locations. ABR1 mainly experiences southerly winds, while CAL1 northwesterly, EMI1 southwesterly, and LAZ1 has winds spread from south to east. PIE1 is dominated by southeast winds. The monthly average graph highlights a notable distinction: ABR1 consistently achieves wind speeds of 4 m/s, never falling below 3 m/s, while the other sites range between 0.5 and 1.5 m/s, with increased gusts recorded during the spring months (Figure 4.2.20).

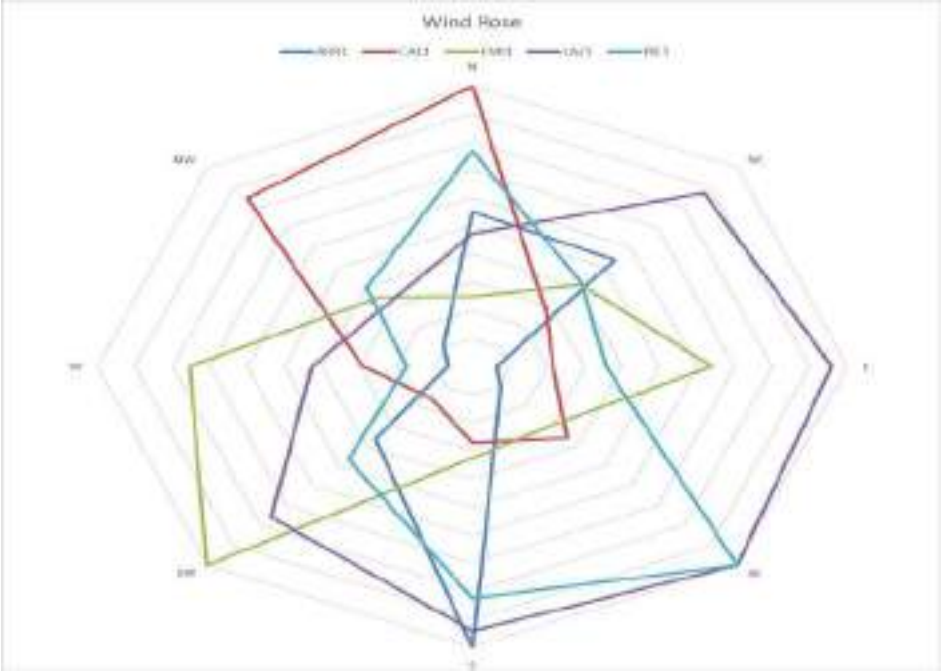

Figure 4.2.19. Trends of the annual precipitations recorded at the forest site over the period 2000-2024.

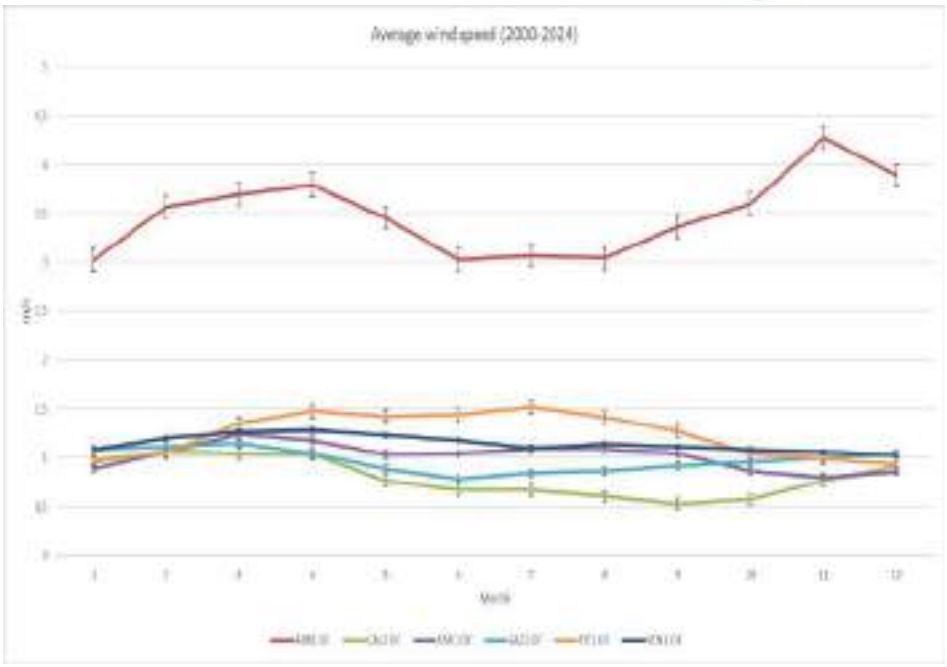

Figure 4.2.20. Trends of the annual precipitations recorded at the forest site over the period 2000-2024.

4.3 Atmospheric depositions

4.3.1 Dataset

Table 4.3.1 provides an overview of the dataset. The data on atmospheric depositions cover 4 years (2021, 2022, 2023 and 2024) in the 10 forest sites of the project. Ten key variables have been considered for this analysis.

Table 4.3.1. Overview of the available dataset.

Forest sites (8)	• ABR1 (Selva Piana) • BOL1 (Renon) • CAL1 (Piano Limina) • EMI1 (Carrega) • LAZ1 (Monte Rufeno) • PIE1 (Val Sessera) • VEN1 (Cansiglio) • VEN2 (Bosco Fontana)

Variables (12)	• Depo_alkalinity • Depo_Ca • Depo_Cl • Depo_DOC • Depo_H • Depo_K • Depo_Mg • Depo_N_NH4 • Depo_N_NO3 • Depo_N_total • Depo_Na • Depo_S_SO4
Years (4)	2021, 2022, 2023 and 2024

4.3.2 Results and discussion

Figure 4.3.1 illustrates the trends of the 12 deposition variables at the forest sites over a 4-year period in the open-field and troughfall samples.

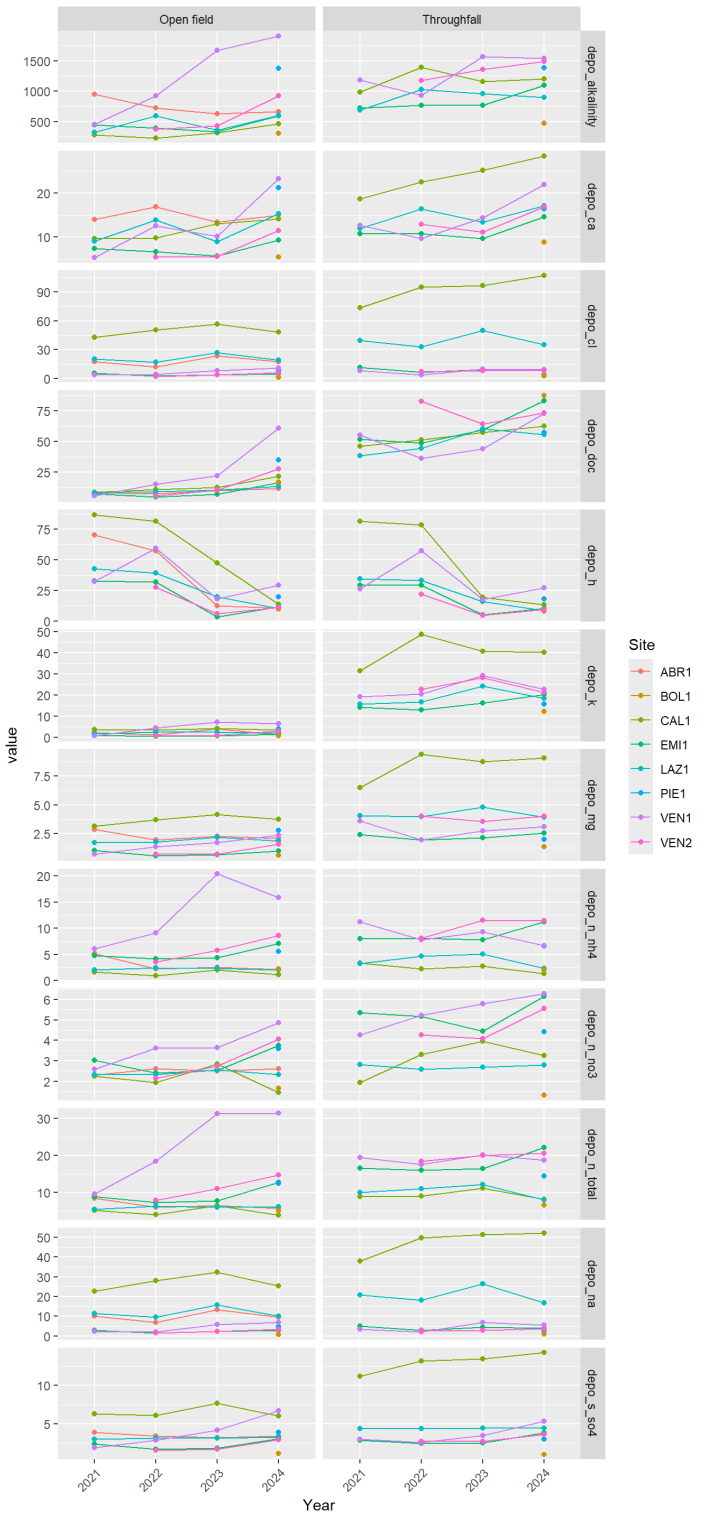

Figure 4.3.1. Trends of the deposition variables at the forest sites over a 4-year period.

At each forest site, the distribution of the variables has been studied, separating the *Throughfall* from the *Open field* values. Figure 4.16 provides an example of the results obtained for VEN1 (Fig. 4.3.2).

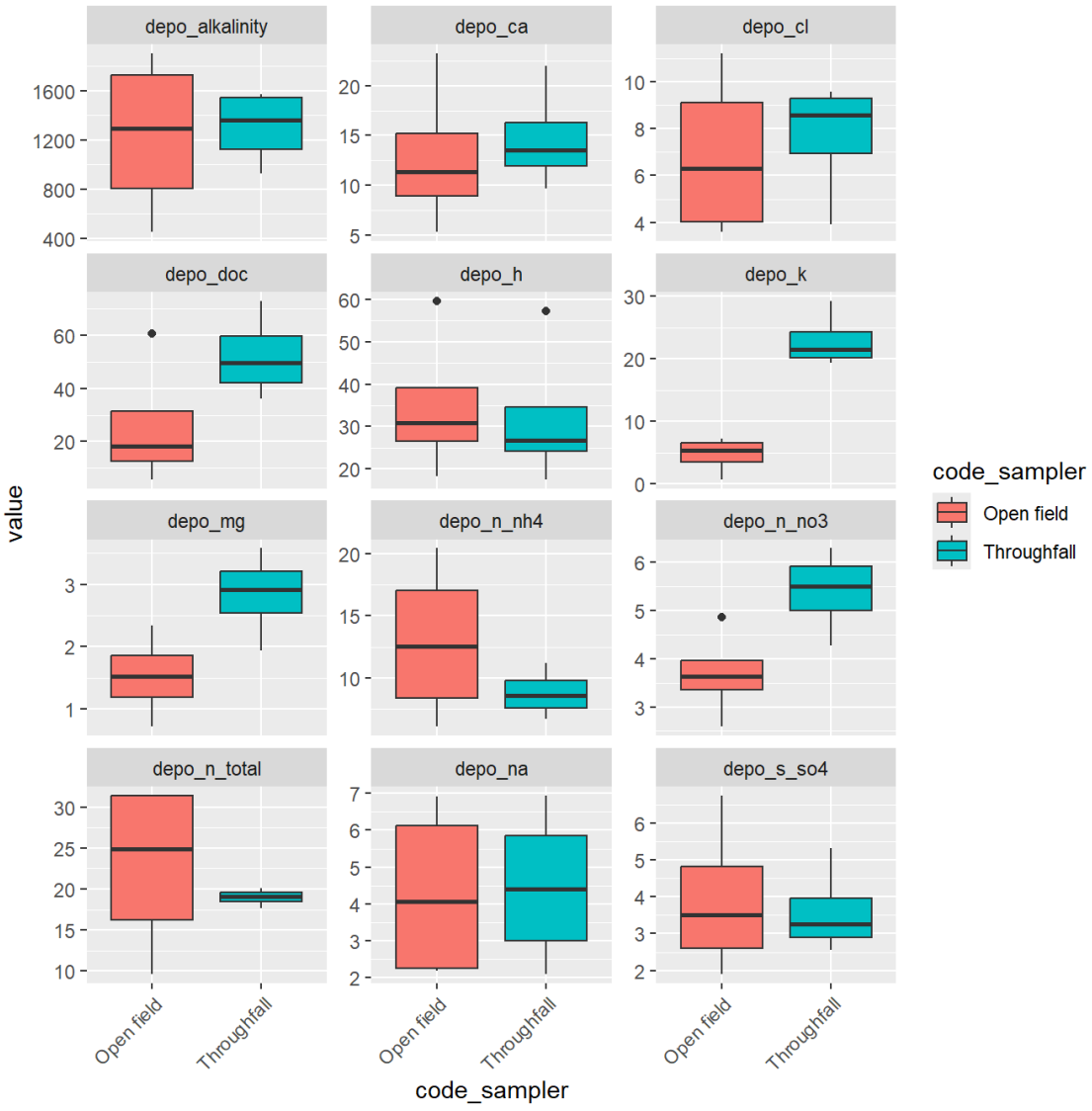

Figure 4.3.2. Boxplots showing the distribution of the variables, separating the Throughfall from the Open field value at the forest site VEN1.

Below, for each forest site, the correlation matrix between the values recorded over the years of the various parameters is shown, separating the *Throughfall* from the *Open field* values. Due to the

skewed distribution, deposition values were log-transformed before proceeding with the analysis. Figures 4.3.3 and 4.3.4 provide an example of the results obtained for CAL1 (*Throughfall*) and VEN1 (*Open field*), respectively.

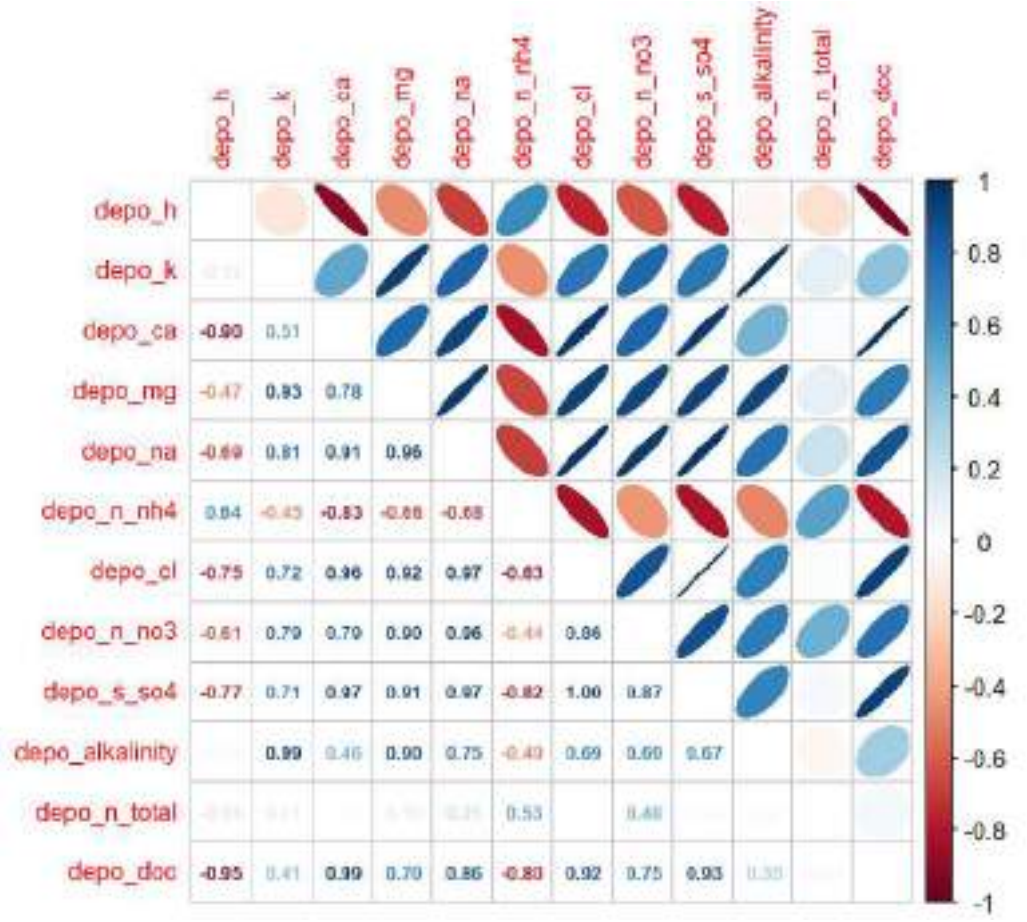

Figure 4.3.3. Pearson's correlation among Throughfall deposition variables at the forest site CAL1.

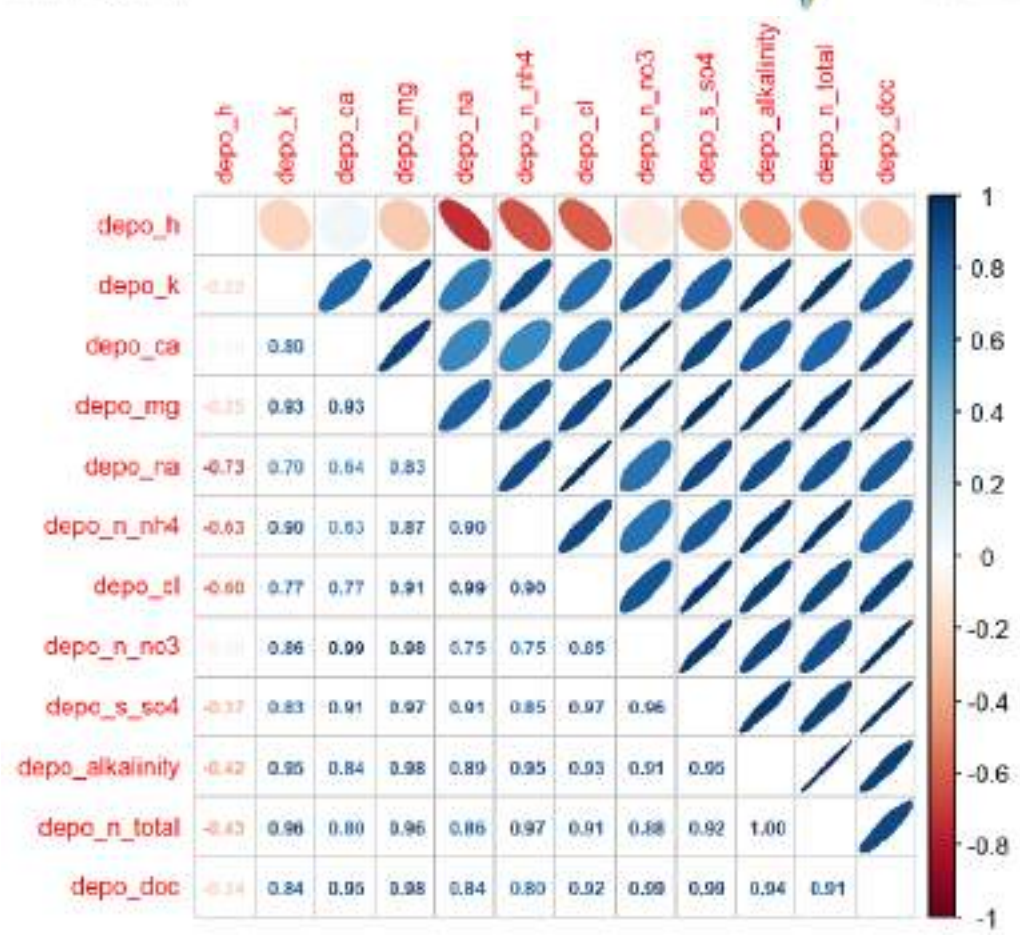

Figure 4.3.4. Pearson's correlation among Open field deposition variables at the forest site VEN1.

PCA on Throughfall and Open field data

Principal Component Analysis (PCA) results are consistent with the trends observed in Pearson's correlations (Figure 4.3.5). Depositions of nitrogen compounds group together, indicating a strong correlation, and are associated with positive PC1 values that correspond to the VEN1, VEN2, EMI1, and PIE1 forest sites, i.e. the sites affected by the highest nitrogen deposition. Negative PC1 values are associated with higher sulfur depositions and correspond to CAL1. *Open field* and *Throughfall* values are correlated each other, except for depo_DOC, being DOC higher in throughfall samples.

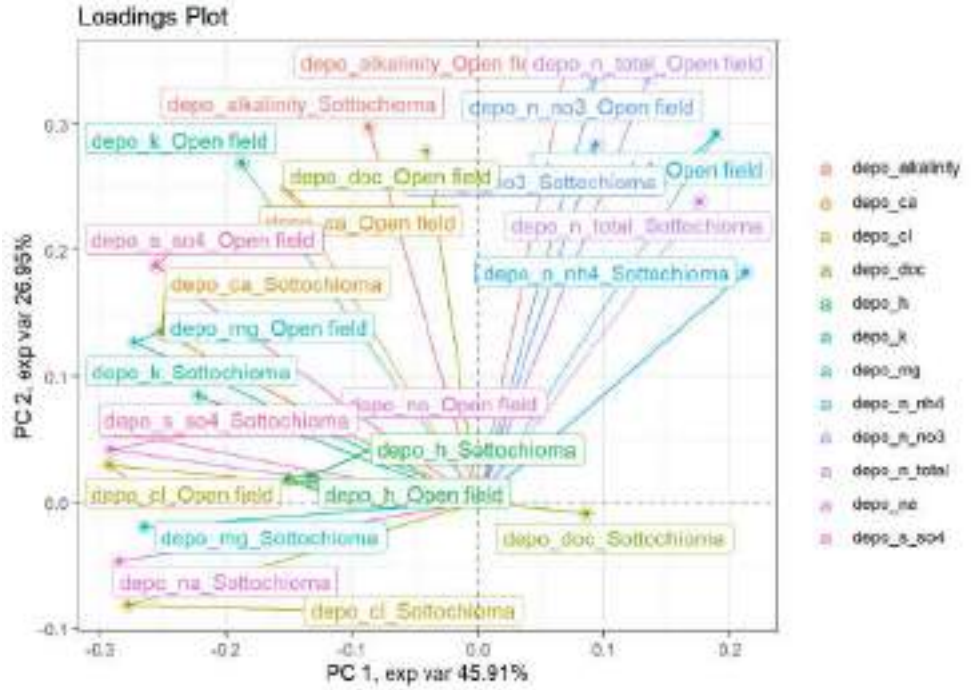

Figure 4.3.5. Results of the PCA on autoscaled data (→ continues).

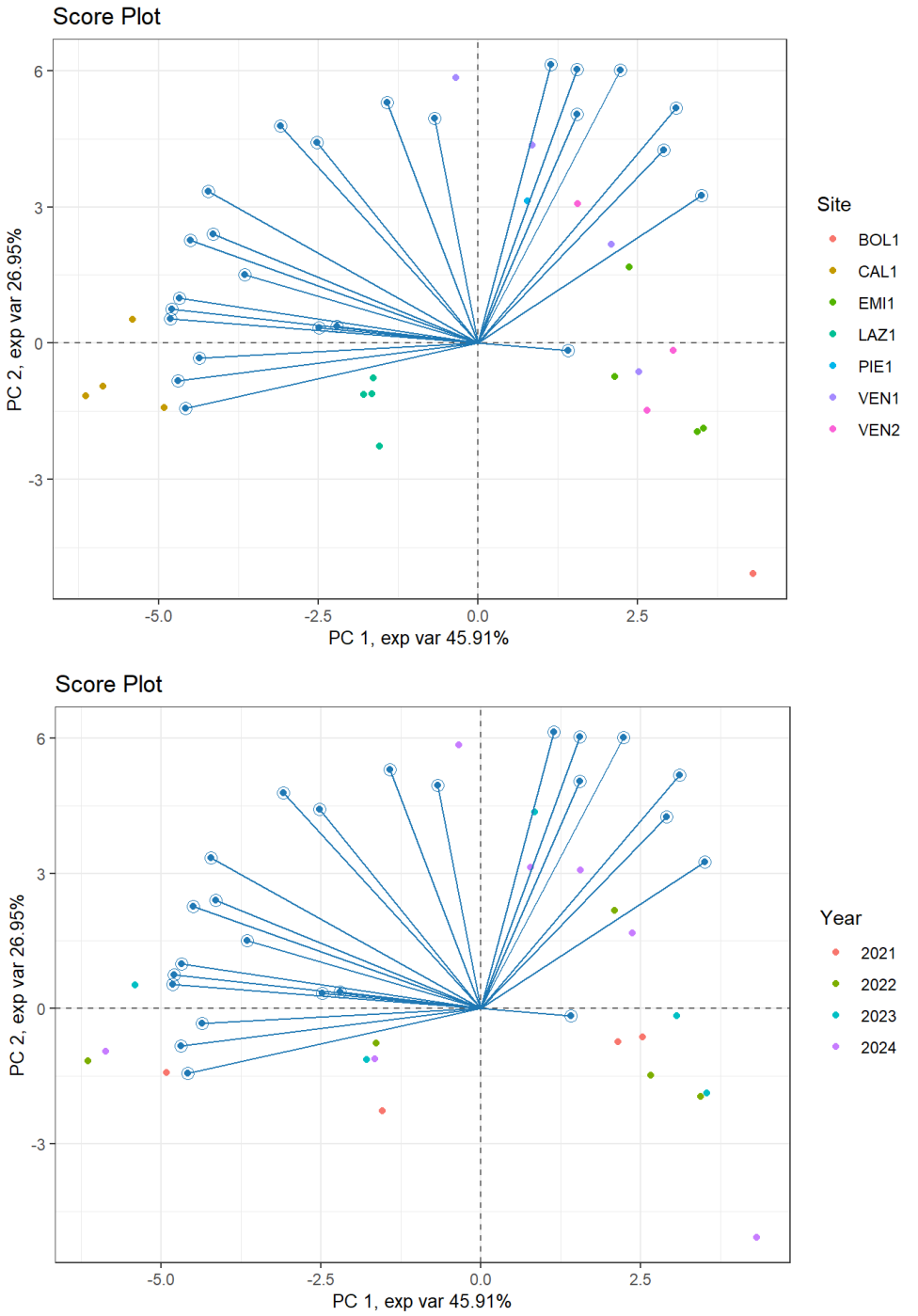

Figure 4.3.5. Results of the PCA on autoscaled data.

PCA on Throughfall data only

The PCA performed exclusively with *Throughfall data* shows results consistent with those obtained from both datasets, with nitrogen depositions separating from the other parameters, along PC1 (Figure 4.3.6). Positive values of PC2 are associated with the Mountain site BOL1 characterized by conifer forest, which show the lowest values of nitrogen and sulfur deposition.

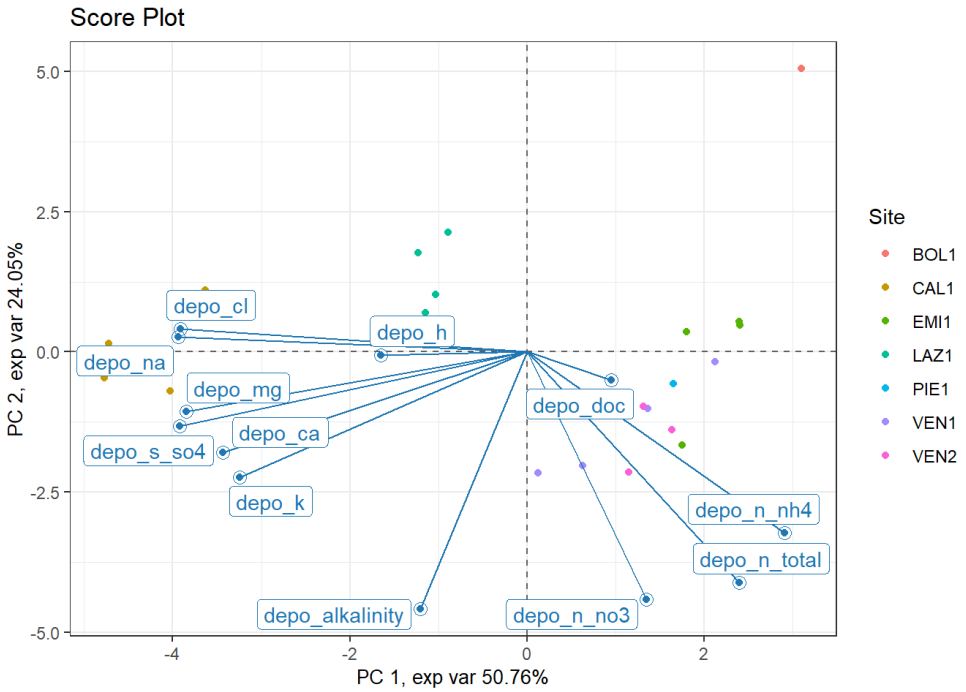

Figure 4.3.6. Results of the PCA on autoscaled data (Througfall data) (→ continues).

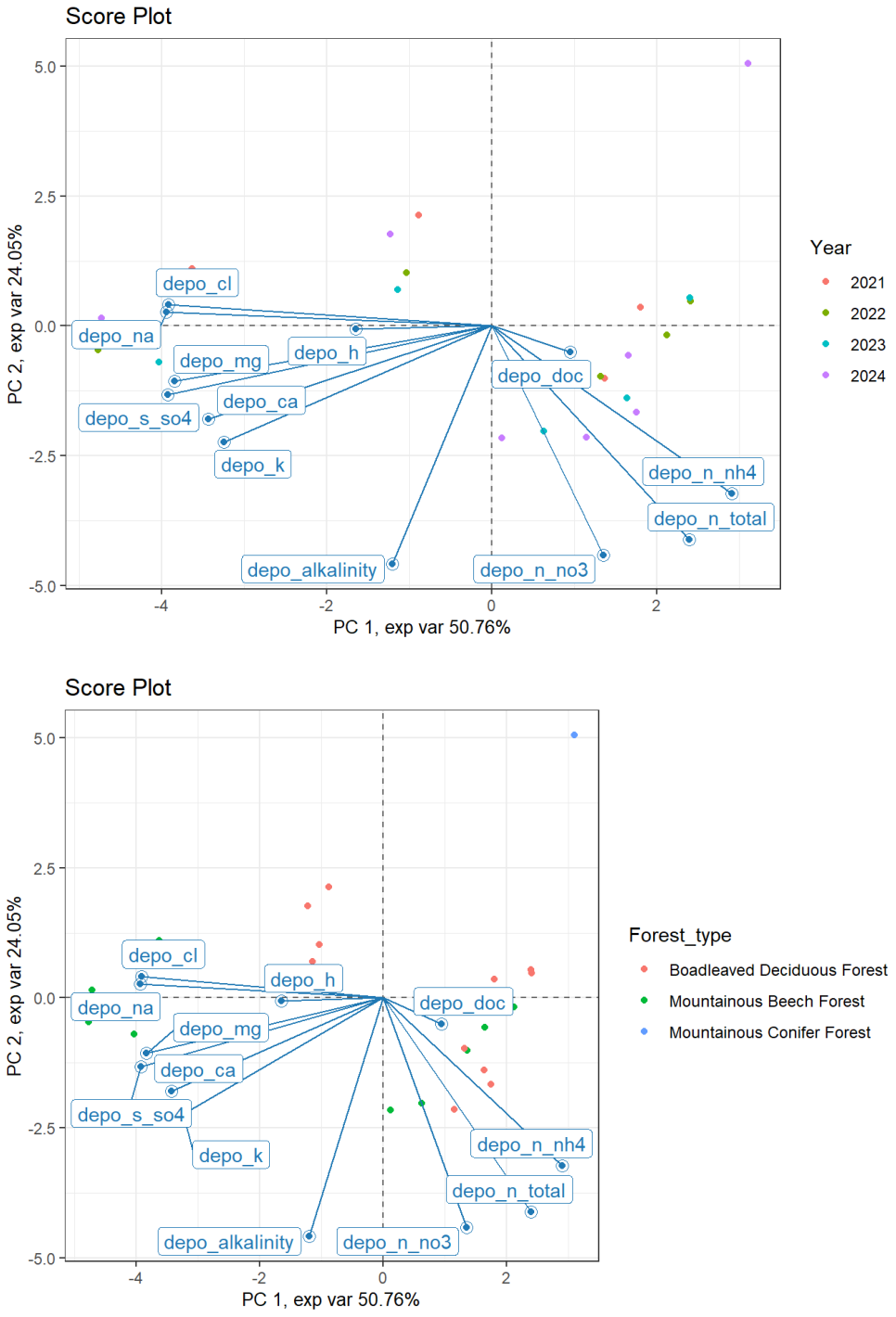

Figure 4.3.6. Results of the PCA on autoscaled data (Througfall data).

PCA on Open field data only

The PCA performed exclusively with *Open field data* shows results consistent with those obtained from both datasets, with nitrogen depositions separating from the other parameters, along PC2 (Figure 4.3.7). Negative values of PC1 are associated with an increasing gradient of sulfur deposition.

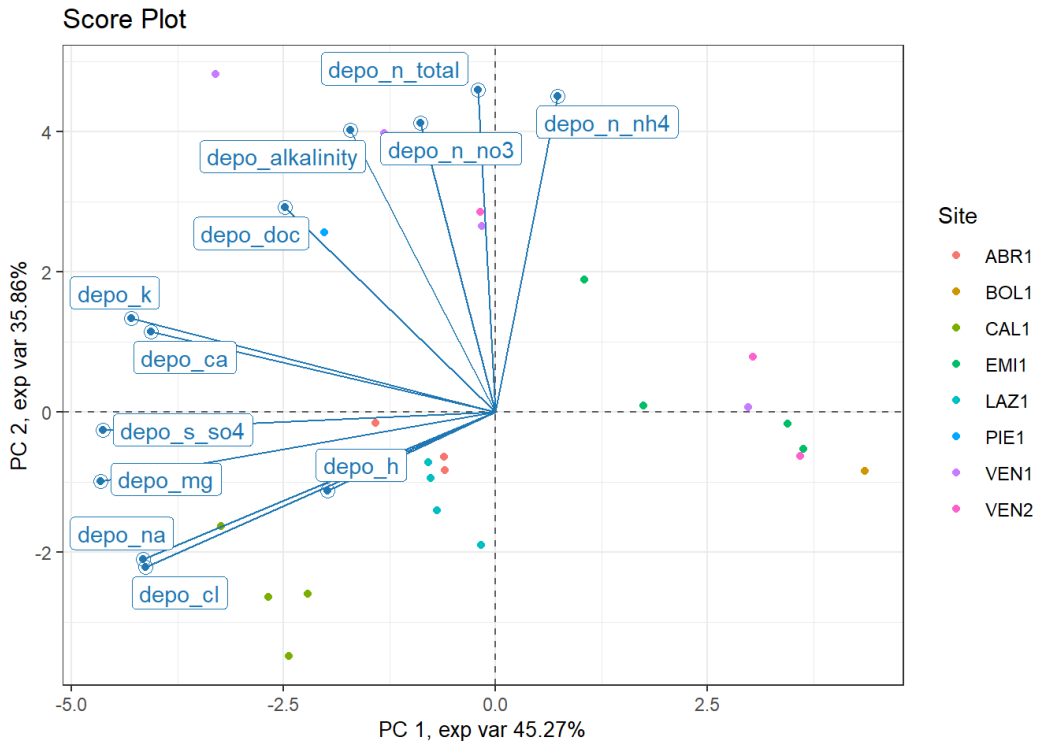

Figure 4.3.7. Results of the PCA on autoscaled data (Open field data) (→ continues).

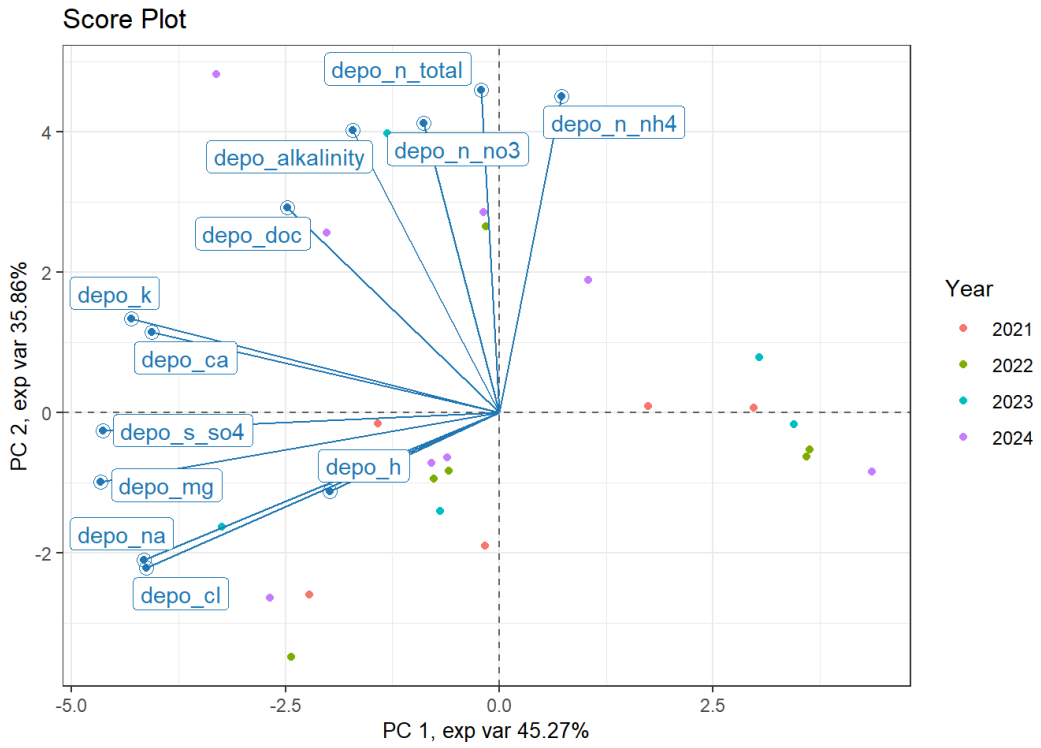

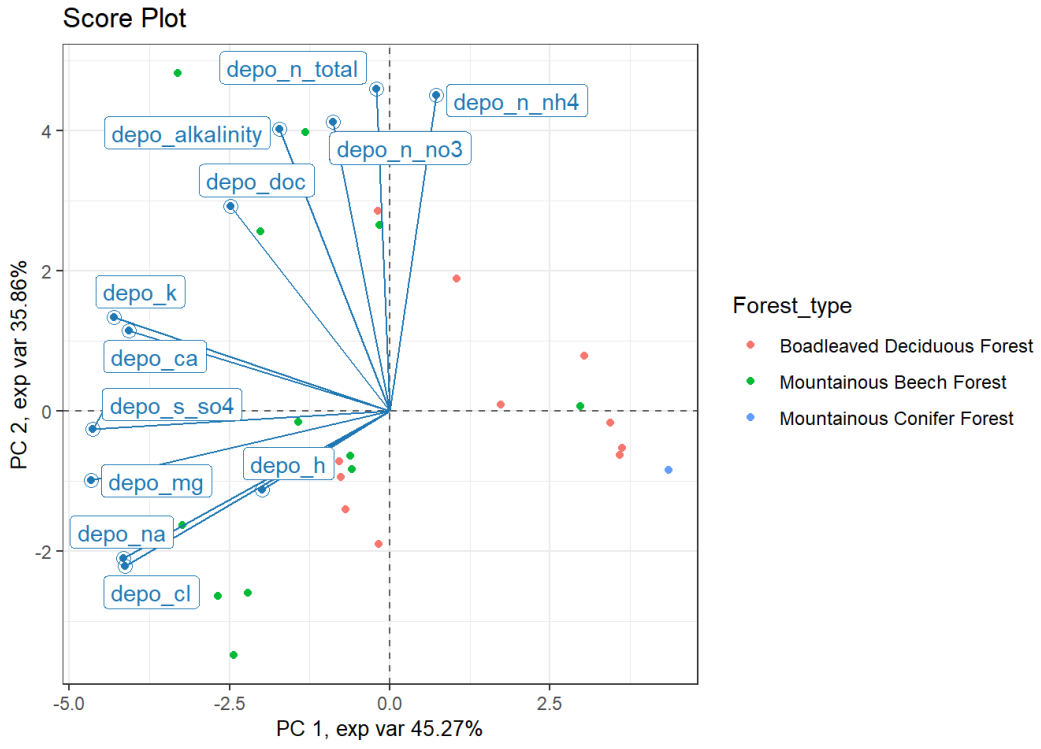

Figure 4.3.7. Results of the PCA on autoscaled data (Open field data).

4.4 Soil solution

4.4.1 Dataset

Table 4.4.1 provides an overview of the dataset. Soil solution data cover 25 years (1999-2023) in 8 forest sites of the project. Eleven key variables have been considered for this analysis.

Table 4.4.1 Overview of the available dataset.

Forest sites (8)	• ABR1 (Selva Piana) • BOL1 (Renon) • CAL1 (Piano Limina) • EMI1 (Carrega) • LAZ1 (Monte Rufeno) • PIE1 (Val Sessera) • VEN1 (Cansiglio) • VEN2 (Bosco Fontana)
Variables (11)	• pH • EC (dS) • K (mg l^{-1}) • Ca (mg l^{-1}) • Mg (mg l^{-1}) • N_NO3 (mg l^{-1}) • S_SO4 (mg l^{-1}) • Na (mg l^{-1}) • N_NH4 (mg l^{-1}) • Cl (mg l^{-1}) • total_N (mg l^{-1})
Years (25)	From 1999 to 2023

4.4.2 Results and discussion

4.4.2.1 Soil solution results

Figure 4.4.1 the distribution of the soil solution parameters in the two layers at the six forest types, whereas Figure 4.4.2 illustrates the trends of the variables over a 25-year period. The comparison between surface and deep data allows ready identification between the ions which essentially flow through the soil and those that undergo significant interactions. In the first case, concentration clearly increases with depth, as soil solution is concentrated by plant water uptake. In the second

case, ion concentration decreases markedly, indicating that the ion is being taken up by plants or microbiota, or is possibly chemically adsorbed by the mineral soil. Identification of ion release phenomena is more difficult, against the background of increasing concentration; however, checks made by comparing the depth trends with the depth trend for chloride suggest that release is very limited, possible exceptions being sulphate anion in EMI1.

Soil uptake and retention is especially heavy for K and nitrogen compounds, all major plant nutrients; further, K and ammonium are strongly adsorbed in soils with significant clay content (all but PIE1).

Retention, or not, of nitrogen compounds is of major interest, as their release in surface or subterranean water is a pollution phenomena of significant concern. Actual release has been observed in EMI1 and, on a lesser scale, in PIE1, VEN1 and CAL1; due to internal soil processes, such release invariably takes the form of nitrate, a most concerning pollutant.

The time trends in soil solution concentrations of the relevant analytes show a very large interannual variability, which is heavily influenced by the amount of rainfall, which controls the overall concentration of soil solutions. Specific statistical tests have failed to pinpoint significant changes, with a single exception which will be discussed further on.

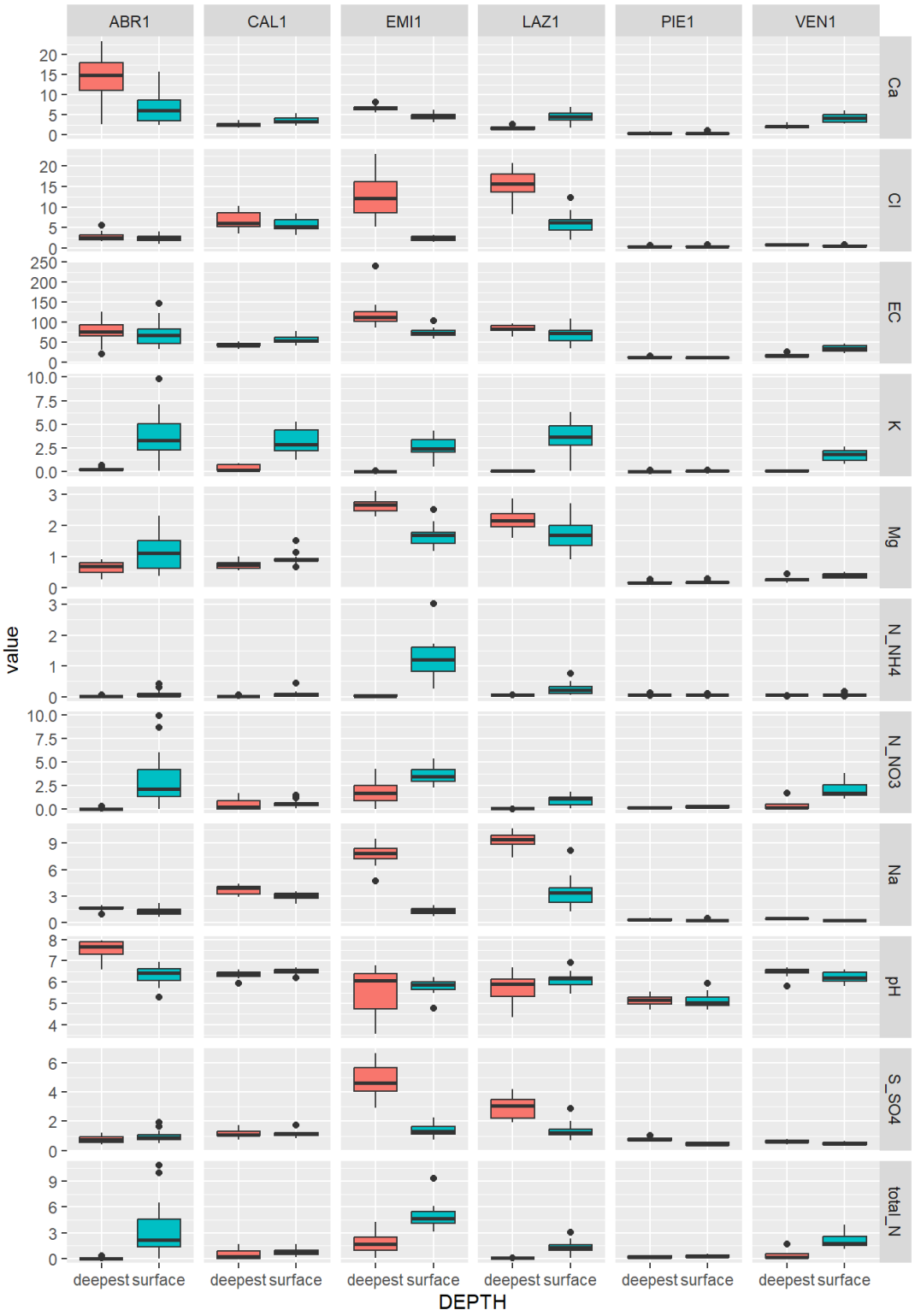

Figure 4.4.1. Boxplots showing the distribution of the soil solution parameters in the two layers at the six forest types.

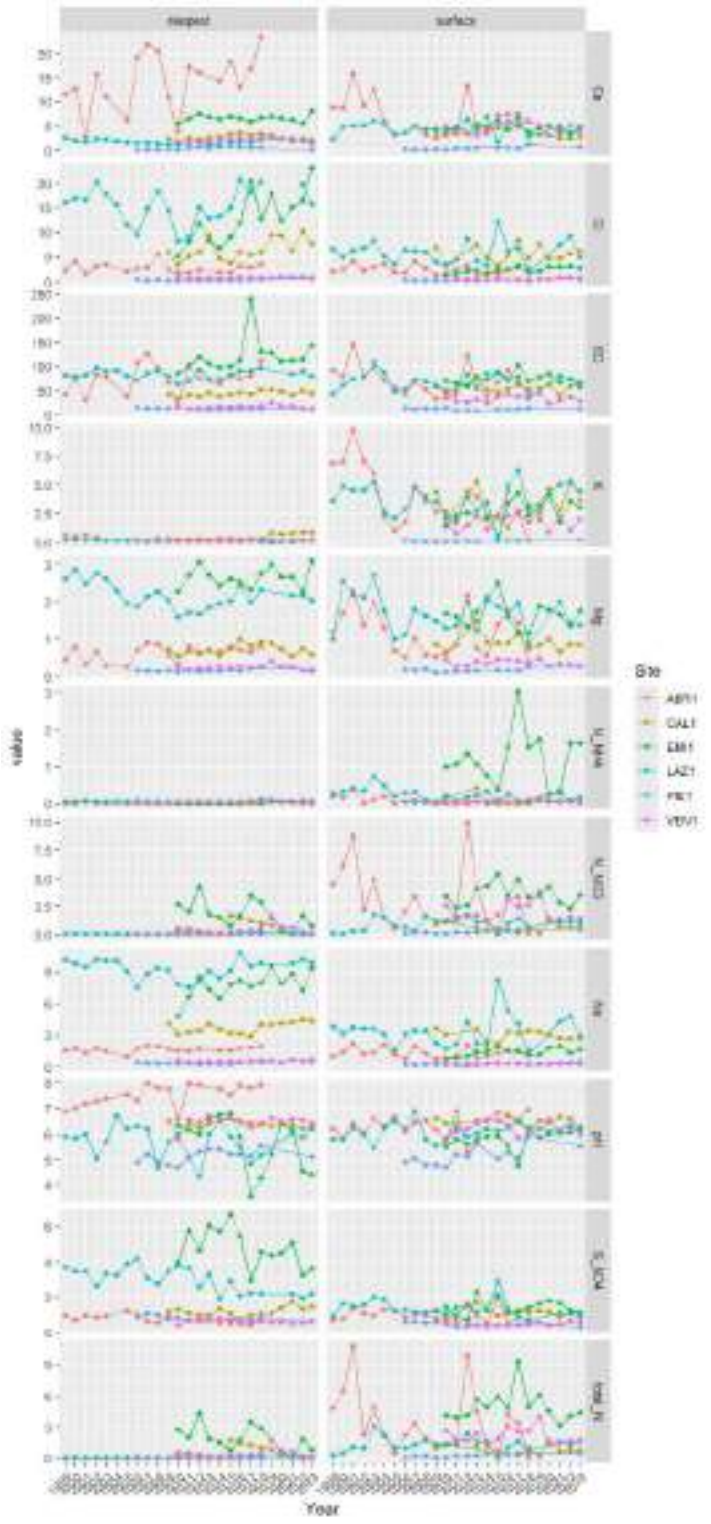

Figure 4.4.2. Trends of the 11 soil solution variables at the forest sites over a 25-year period.

The correlation among variables has been analyzed for each forest site over the years using Pearson's correlation method. As an example, we report here the results obtained for EMI1 (Figure 4.4.3), LAZ1 (Figure 4.4.4) and VEN1 (Figure 4.4.5).

Strong correlations are very frequent; this is, however, in a significant portion due to the large variations in overall concentration of the soil solution, which are primarily controlled by rainfall and secondarily by evapotranspiration.

It is indeed highly interesting to examine the cases for which poor or no correlations have been found. In this case, the most significant case is clearly the case of pH. This analysis clearly shows how soil solution pH is determined by very complex phenomena, involving plants, microbiota and the soil exchange complex. The influence of atmospheric deposition is then quite indirect, and has to be extracted through deeper analysis.

A most relevant case concerning pH is the case of the site EMI1, where the trend of decreasing pH in the deep samplers is rather striking, even if the high interannual variability restricts statistical significance. In this site, the variable most correlated with pH is soil solution electrical conductivity (EC), showing a negative correlation. Increasing EC is linked with high, and generally rising, levels of throughfall deposition, not including, however, the nitrogen compounds, and to a general trend of decreasing rainfall (see fig. 4.15). The result is represented by increasing concentrations of alkaline cations in the deep samplers; this condition prompts an increase in exchange phenomena; as the exchange complex of this soil contains a high amount of exchangeable hydrogen, such hydrogen is released in the soil solution, lowering pH. This interpretation is supported by the results obtained for site VEN1, where pH is also negatively correlated to the concentrations of Ca, Mg, and K, but positively with Na; in this case, the changes in exchange dynamics are seasonal or interannual, rather than being a long term trend, so showing up more clearly as correlation.

A positive feedback of this process is the penetration of ammonium to the deepest samplers, shifting nitrification downwards with further acidification effects.

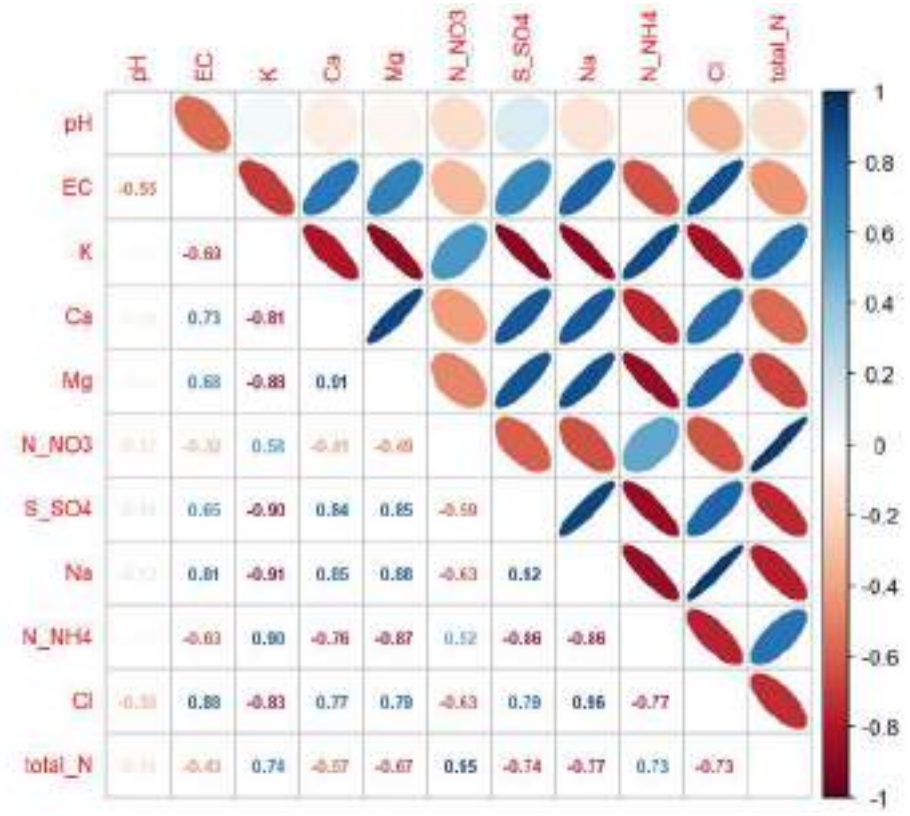

Figure 4.4.3. Pearson's correlation among soil solution variables at the forest site EMI1.

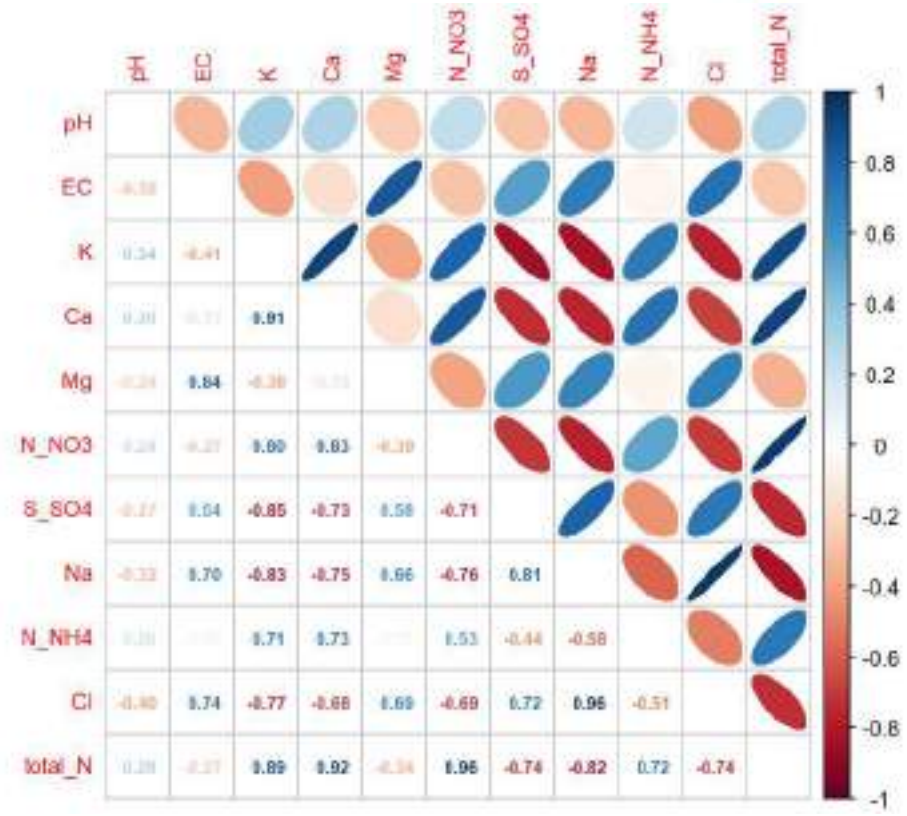

Figure 4.4.4. Pearson's correlation among soil solution variables at the forest site LAZ1.

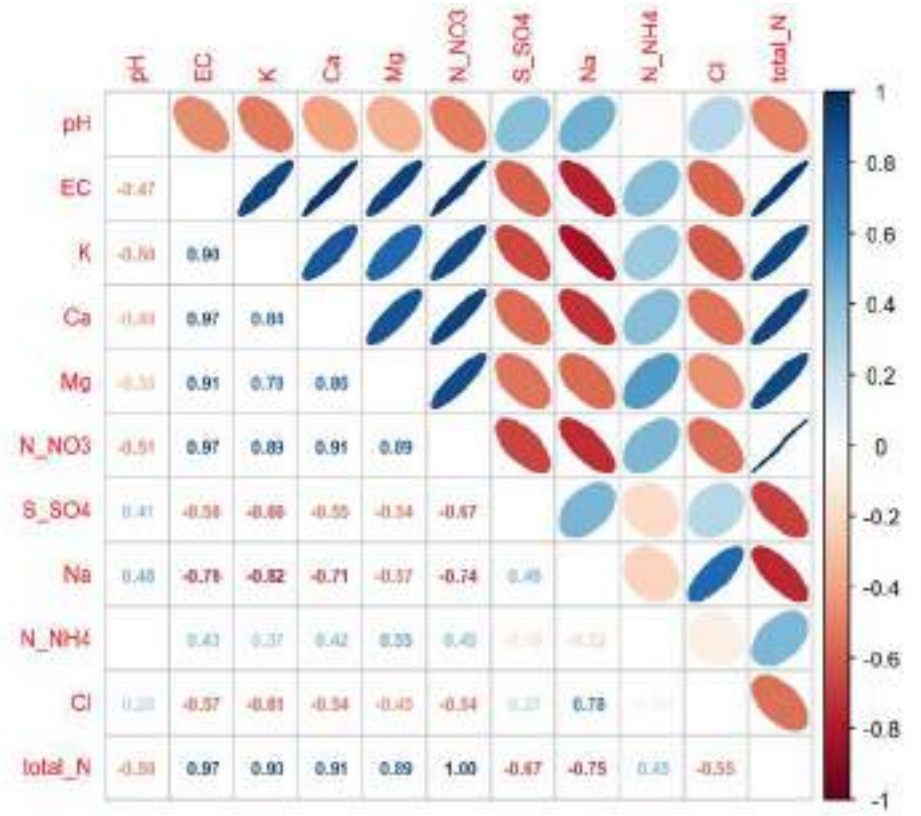

Figure 4.4.5. Pearson's correlation among soil solution variables at the forest site VEN1.

Principal Component Analysis (PCA) was performed on autoscaled data (Figure 4.4.6). Negative PC1 values indicate a rising gradient of all soil solution compounds, characterizing Broadleaved Deciduous Forests (BDF), while Mountainous Beech Forests (MBF) are distributed along the positive values of the axis.

Conductivity (EC) and Mg are the two parameters most strongly correlated with the negative values of the axis and are linked to the EMI1 site. Nitrogen compounds (N_NO3, N_NH4, and total_N), Ca and K show highest values in the quadrant with negative PC1 and positive PC2 values, corresponding to surface samples from EMI1, LAZ1, and ABR1. Deeper samples cluster at negative PC2 values. Within this group, samples from EMI1 and LAZ1 display elevated concentrations of S-SO4, Cl, and Na.

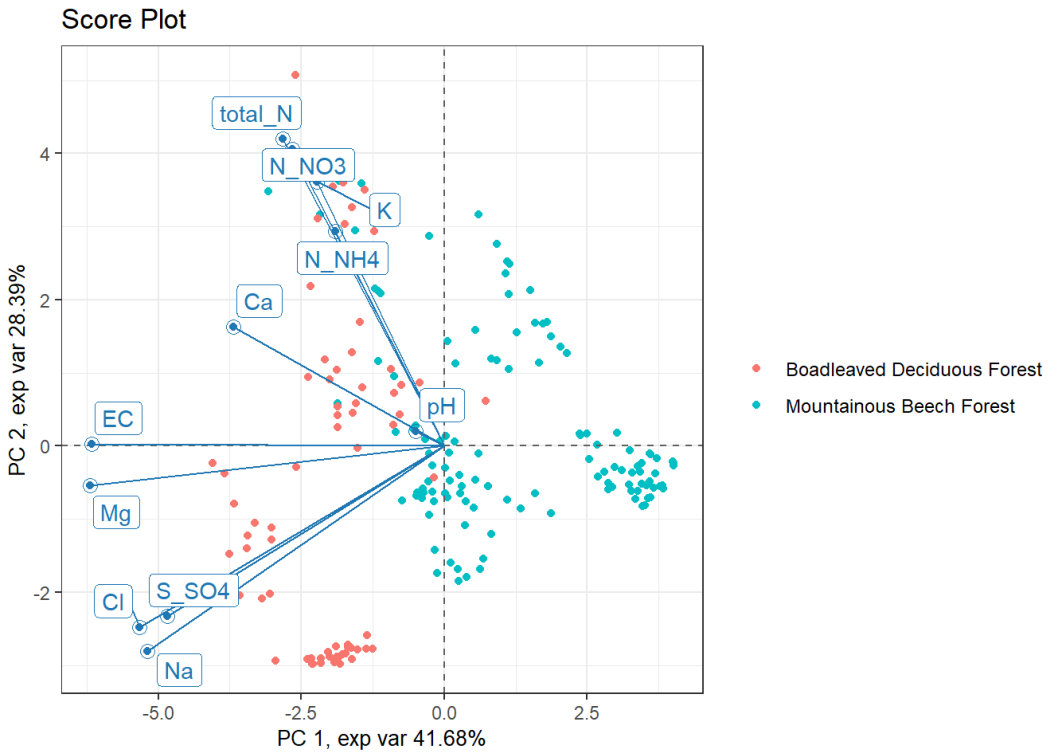

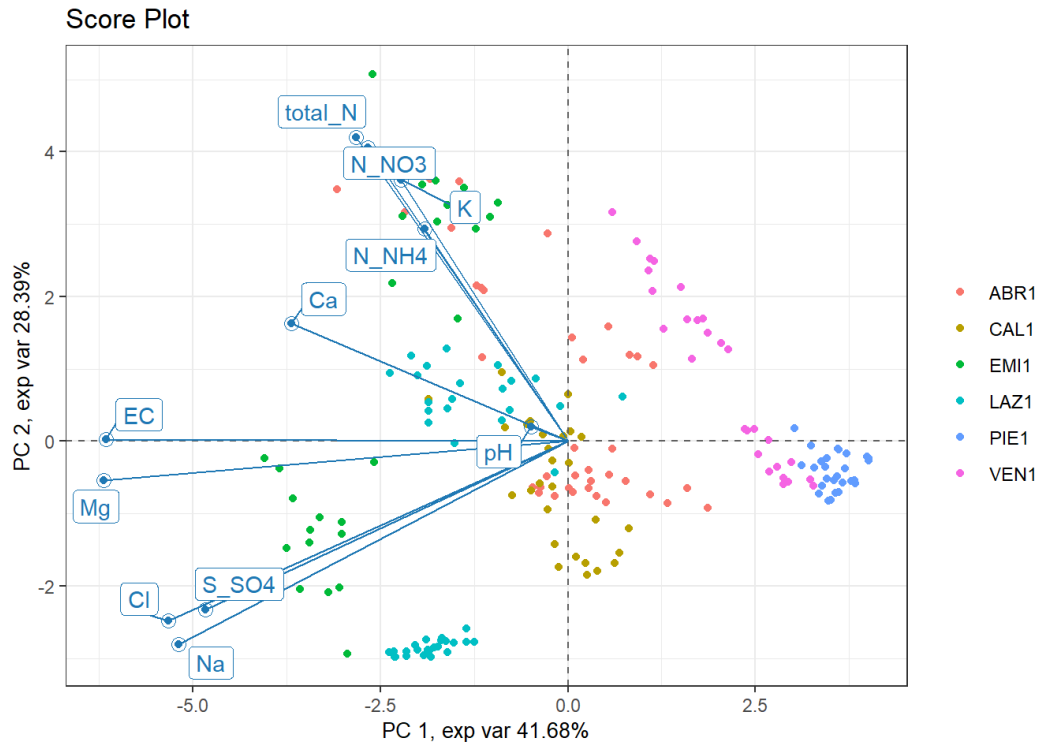

Figure 4.4.6. Results of the PCA on autoscaled data (→ continues).

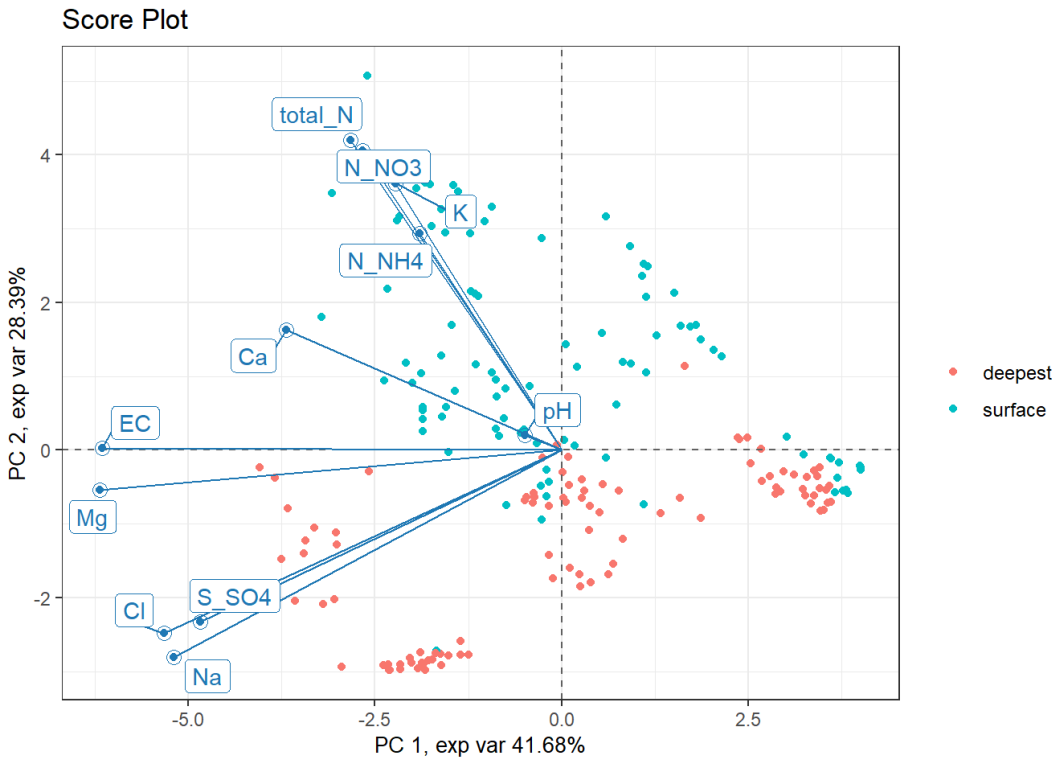

Figure 4.4.6. Results of the PCA on autoscaled data.

4.4.2.2 Testing the new indicator: estimated pollutant flows through the soil/forest system

Extended areas of Italian forests are subjected to some of the heaviest levels of atmospheric deposition of reactive forms of nitrogen, either oxidized (nitrate, NO_3^- anion) or reduced (ammonium cation, NH_4^+, Ferretti et al, 2014).

In addition to their complex effects on the forest and soil, reactive nitrogen forms are also of major concern as they can produce significant degradation of both surface and underground freshwater reservoirs, with risks for both aquatic ecosystems and sources of drinking water. As a consequence, it is important to assess whether atmospherically deposited reactive nitrogen is held within the forest ecosystems or it is released towards other environmental compartments.

Since the beginning of soil solution monitoring in high N-deposition areas, around 2010, it became evident that the risk of nitrogen, specifically nitrate, export, must be seriously considered. Evidence for this necessity is supplied by the regular detection of Nitrate-N, in significant concentrations, in the soil solutions sampled at depths of 60-70 cm. Such depths are considered, according to ICP-Forests (ICP-Forests, 2020) to represent the lower boundary of nitrogen biological uptake. Nitrate-

N detected at such depths is, then, likely to be actually moving out of the forest ecosystem towards either underground or surface waters.

A first attempt at estimating the actual amount of Nitrate-N flowing out of the soil was made by the use of the chloride tracer method introduced by Hruska et al (2012). This resulted in estimated positive flows for the sites EMI1, PIE1, VEN1 and CAL1 (Cecchini et al, 2021). The first three sites are located around the Po plain, and are interested by significant atmospheric depositions of reactive nitrogen. A large proportion of such deposition is actually made up of Ammonium-N, but analysis of soil solution trends revealed how ammonium is either retained or transformed into Nitrate-N, thus increasing the potential for Nitrate-N export. It was actually somewhat surprising to find out possible Nitrate-N export in CAL1 site, given that the site receives relatively small amounts of atmospheric deposition. This result was, then, explained by the very high precipitation volume of the site (>1000 $mm \cdot y^{-1}$), inducing quick flow through the soil and reducing the opportunities for nitrogen biological uptake.

It was however understood that the chloride tracer method relies on many assumptions, thus leaving uncertainties in the final results. In the context of the present LIFE project, it was then undertaken to test alternate methods, to obtain comparative estimates.

This initial testing phase concentrated on two sites, namely EMI1 and LAZ1. The selection is due to the fact that these two sites have quite similar forests and soils but are receiving quite different levels of N depositions. The fact that both stations lie essentially on flat terrain also reduces the complexity of fluxes' estimation.

SOIL-VEGETATION-ATMOSPHERE MODEL

The first and most logical possibility for flux estimates is the use of a soil-vegetation-atmosphere mathematical model (SVAT). A thorough literature and web search was then carried on to identify the most suitable model to be used, among the several existing ones.

The search resulted in the selection of the LWF-Brook90 model; this specific model was selected first because it was created and developed specifically for application to soil-forest ecosystems, within which all the validation tests have been carried out. The model has recently also been entirely re-engineered on the software side, making its use reasonably agile.

Actual running of the model revealed that it requires, as usual in such models, a large amount of input data, and that the results are heavily influenced by the quality of many such data.

A very high sensitivity was found with respect to meteorological data and to the data needed for estimating vegetation transpiration, especially data concerning the actual phenological state of the canopy, i.e. the times of leaf sprouting, senescence and fall.

Such sensitivities required an extended work of data search, checking and interpretation. Unfortunately, the data supplied by the meteorological sensors installed in the monitoring sites showed to be not the ideal source. This is primarily due to the relatively high frequency and extent of interruptions in data availability, extending as much as several years for EMI1 site. Also, there exist cases of strong disagreement between open field and 'in the plot' data, which are difficult to explain.

Search for meteorological data, then, turned to external sources. For EMI1 site, it was found that Emilia Romagna Region is running a highly developed system of meteorological data interpolation, supplying data for 500x500 m tiles and publicly accessible through the ERG5 portal (https://dati.arpae.it/dataset/erg5-interpolazione-su-griglia-di-dati-meteo). For plot LAZ1, a solution was found in the data provided by the Copernicus service: https://surfobs.climate.copernicus.eu; these offer a coarser resolution (0.1° to 0.25°) but are highly controlled and validated.

As a check for the significance of these data with respect to the monitoring sites, they were compared to the volumes recorded by deposition sampling. The results show how the ERG5 data are highly relevant for EMI1 site, while for LAZ1 site a limited overestimation in the Copernicus data is visible (Figure 4.4.7).

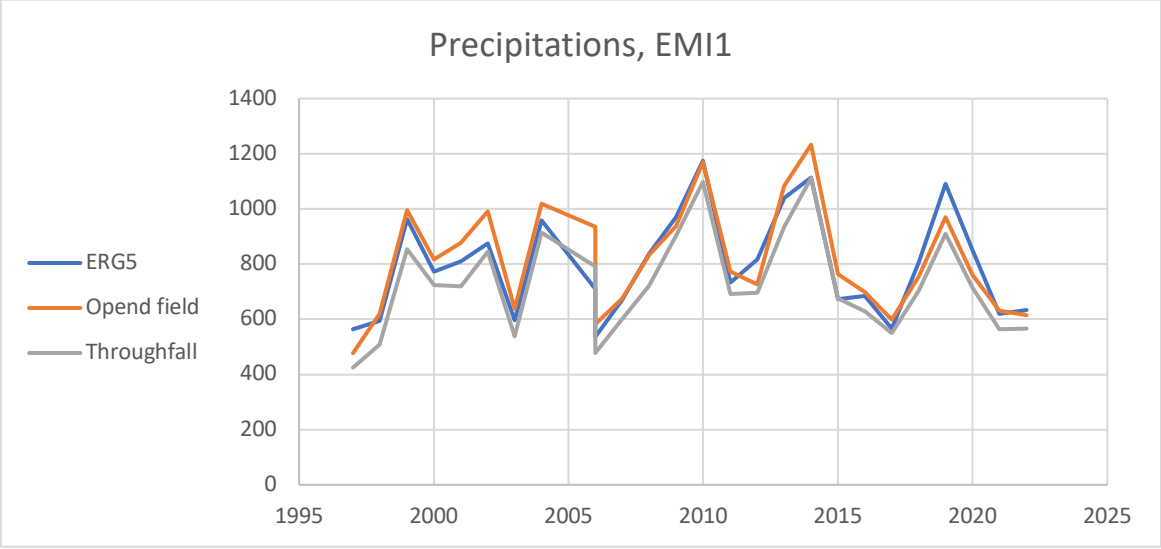

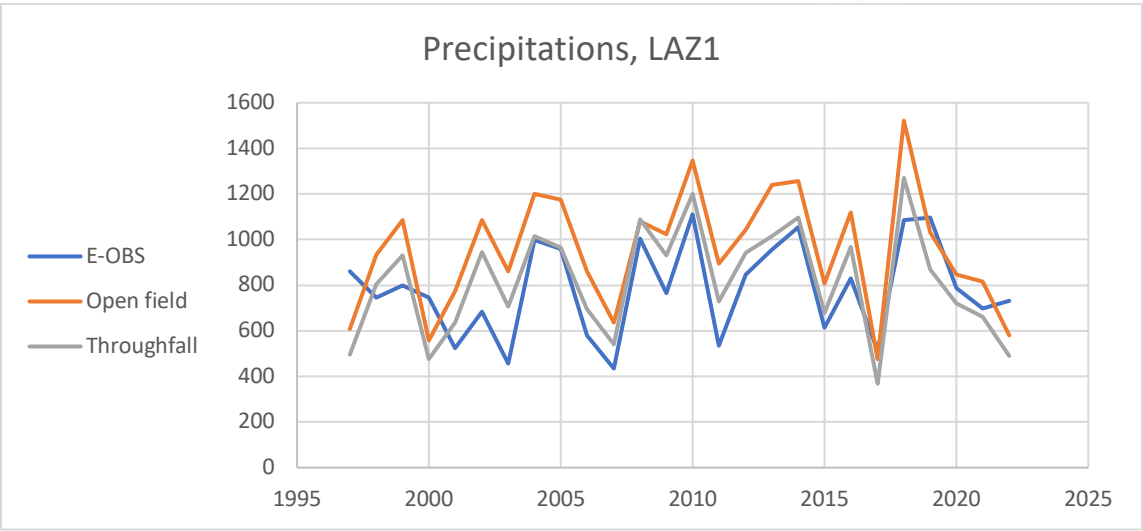

Figure 4.4.7. Yearly precipitation volumes for sites EMI1 (above) and LAZ1 (below.

In analyzing the figure, it has to be taken into account that:

- Deposition samplers are not built to prevent evaporation, while sampling and volume measurement are carried out weekly; it is then unavoidable for the recorded volume to be somewhat lower than the actual rainfall volume, as would be recorded by pluviometers.
- For the throughfall samplers, a further 'loss' of precipitation volume is represented by canopy interception.

Given these differences between measurement procedures, the agreement between volumes supplied by ERG5 and volumes recorded by deposition sampling must be considered especially good, while for the Copernicus data it still appears acceptable, given the serious difficulties encountered with all other possible sources.

For estimating the timings of the phenological phases of the canopy, missing direct observations, an original approach was adopted. This approach derives from internal analysis of ecosystem chemical data. Since the earliest attempts at estimating mass balances (Cecchini et al, 2019), it was observed how the concentrations of potassium (K) in throughfall samples follow a highly specific seasonal trend, which is completely independent of any trend of atmospheric deposition. This trend sees two strong maxima, in late spring and in early fall. These two maxima were then interpreted, also according to literature, as related to the evolution of the canopy. The first maximum is due to K release by young leaves, while the second one is due to release by senescent leaves. By finding out the dates of strong increases in K concentration or, better K/Na ratio, it then appeared possible to make an estimation of the dates of leaf sprouting and senescence.

The dates thus estimated agreed quite well with typical dates for the various oak species in central Italy, as known from experience. Especially, these approximations must be evaluated with respect to the default settings of LWF-Brook90, which were found to be removed by months from realistic actual dates for these Mediterranean sites.

Remote sensing data were used instead to estimate Leaf Area Index (LAI), a requested input parameter. A continuous estimate of LAI can be obtained from LANDSAT data, according to Orusa et al (2023).

PedoTransferFunctions

Concerning soil parameters, the basic soil data, i.e. soil texture, structure, bulk density and organic carbon content, were available from previous soil surveys undertaken in projects connected with the CONECOFOR network.

No direct soil hydrological measurements were, however, initially available. This is not an unusual condition in applied soil hydrological studies, the common solution being the use of the so-called PTF (PedoTransferFunctions). These are actually empirical, statistically obtained, relationships between important soil hydrological parameters and the kind of basic soil data listed above. As of today, all functions refer to the parameters used to reconstruct the soil water retention curve according to the van Genuchten equation (vGE) and the soil water conductivity curve according to the Mualem-van Genuchten equation.

The state of the art does offer a high variety of different PTFs; the LWF-Brook90 model allows either manual input of data, independently obtained, or internal calculation of parameters, with selection among three possible methods, namely the PTFs proposed by Puhlmann and von Wilpert (2011, hereafter 'Puhlmann') or Wessolek et al (2009, hereafter 'Wessolek') or otherwise the more complex approach of the Rosetta model (Zhang and Schaap, 2017).

Initial simulations using the three methods showed significantly different results. Search for the origin of such differences quickly revealed how the main divergences between the three PTFs lie in the estimates of soil saturated hydraulic conductivity (Ksat) and of the α parameter of van Genuchten equation. These are both critical parameters for water flux estimation, as the α parameter heavily influences the partition between gravitational, draining, water and retained water.

The values estimated by the various functions diverged for up to 2 orders of magnitude. The Puhlmann function produced the lowest Ksat values and the Wessolek function the highest (Tab.

4.4.2). Expert judgment suggested that the results from both Rosetta and Wessolek method were definitely too high with respect to the generally accepted values for the texture classes of the B horizons namely, silty clay loam for EMI1 and silty clay for LAZ1.

Table 4.4.2. Estimated and measured main soil hydraulic properties.

EMI1		Puhlmann estimates					
Horizon	**Low. Bound.**	***ths***	***thr***	***α***	***n***	***Ksat***	**Ksat meas.**
A	6	0.576	0.069	6.355	1.312	150.3	N/A*
E	38	0.506	0.069	3.975	1.233	37.3	1.79
Bt	57	0.473	0.069	8.700	1.174	10.3	0.17
Rosetta estimates							
A	6	0.551	0.097	0.273	1.559	66.7	N/A*
E	38	0.485	0.090	0.303	1.554	23.4	1.79
Bt	57	0.483	0.104	0.386	1.174	13.3	0.17
Wessolek estimates							
A	6	0.416	0.028	1.697	1.205	10.3	N/A*
E	38	0.416	0.028	1.697	1.205	10.3	1.79
Bt	57	0.428	0.053	4.321	1.165	34.4	0.17

LAZ1		Puhlmann estimates					
Horizon	**Low. Bound.**	**ths**	**thr**	**α**	**n**	**Ksat**	**Ksat meas.**
A	21	0.460	0.069	4.700	1.180	12.8	6.25
Bt	40	0.408	0.069	7.396	1.114	0.2	3.96
BC	63	0.348	0.069	5.731	1.114	0.1	2.29
Rosetta estimates							
A	21	0.442	0.090	0.504	1.458	11.9	6.25
Bt	40	0.455	0.125	0.637	1.322	3.3	3.96
BC	63	0.388	0.114	0.691	1.170	1.4	2.29
Wessolek estimates							
A	21	0.415	0.141	4.052	1.324	16.0	6.25
Bt	40	0.497	0.000	7.242	1.061	74.5	3.96
BC	63	0.453	0.163	4.947	1.170	18.4	2.29

α as 1/m; Ksat as $mm \cdot h^{-1}$

* too thin to measure

Given such significant differences, we decided to proceed to field measurement of Ksat. The measurements were carried on by using the constant-head hole permeameter commercially known as 'Amoozemeter' (Amoozegar and Warrick, 1986).

The results from the field measurements (Tab. 4.4.2) supported the hypothesis that the Puhlmann estimates were actually the better approximated. Actually, existing observations suggest that the differences between these estimates and the measured data are largely due to spatial variability in the thickness of the contrasting subsurface and deep soil horizons.

As a consequence of measurement results, new model simulations were carried on by setting Ksat at fixed at the measured values. The results of these simulations are showed in Figures 4.4.8 (results for EMI1) and 4.49 (results for LAZ1).

As can be gauged by the figure, the important difference remaining between the three PTFs lies in the partition between vertical, downwards, and lateral, downslope, flux, while total out-of-soil flux remains very similar. Summarizing, use of the Puhlmann function returns higher lateral fluxes than the other two functions. The actual reasons for such major difference are still the object of investigation. It has to be kept in mind that, at this stage, the only divergences allowed, between the three functions, are connected to the water retention curve. Examination of the van Genuchten parameters as estimated by the three functions showed a large, up to 2 orders of magnitude, difference in the parameter α; this parameter is strongly related to the air entry point, and then to the partition between free-draining and retained water. Actually, use of the Puhlmann and Wessolek functions results in substantially lower water contents at field capacity.

In terms of ecological significance, however, the differences should not be overstated. First, it has to be considered that LWF-Brook90 is, formally, a 1-D model; the 'lateral flux' estimation is obtained by a simplified subroutine whose actual purpose is to reduce errors in the estimate of downward flow. Furthermore, both lateral and downwards fluxes represent water that exits the soil to move to other components of the ecosystem. Clearly, the direct destination is somewhat different, being either surface or underground waters.

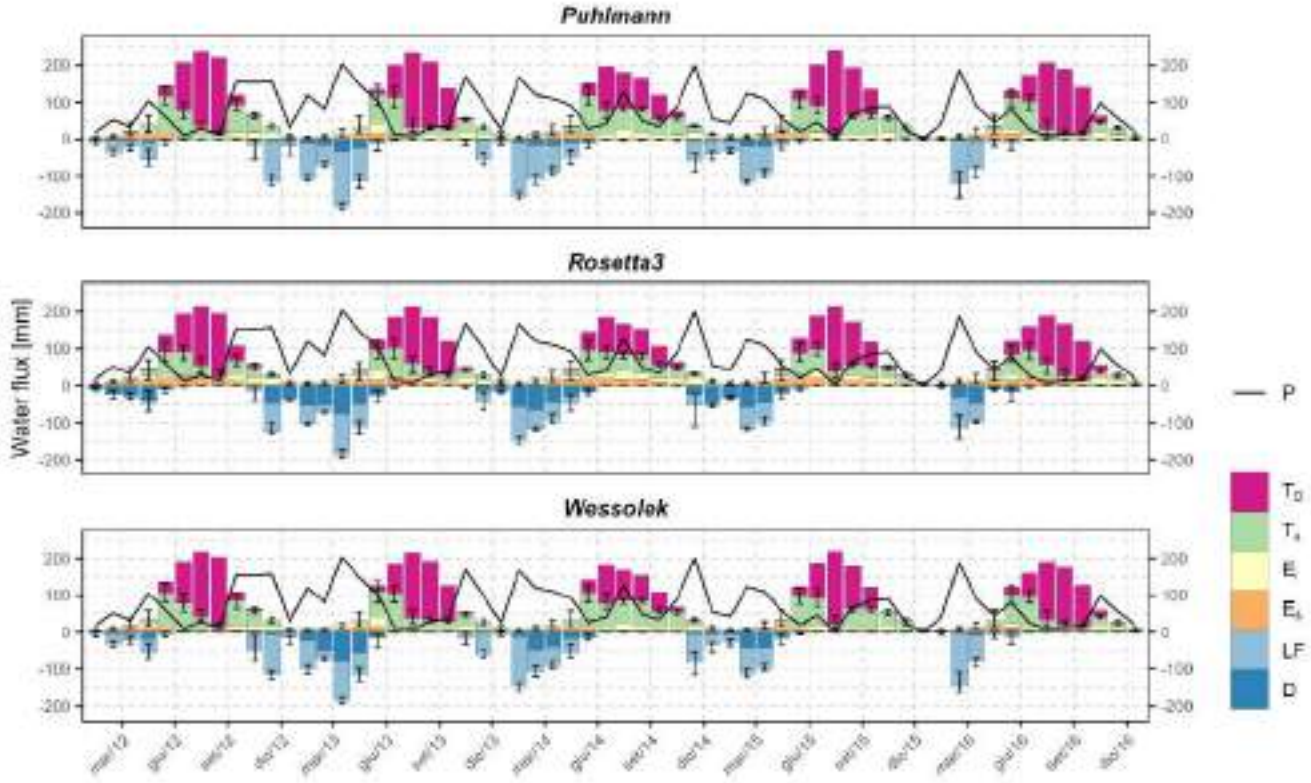

Figure 4.4.8. Water budget estimates for EMI1 site; water retention curves estimated through the listed PTFs, Ksat values as measured in the field. P = precipitation; T_D to E_s the various components of evapotranspiration; LF = lateral flow; D = drainage (downwards).

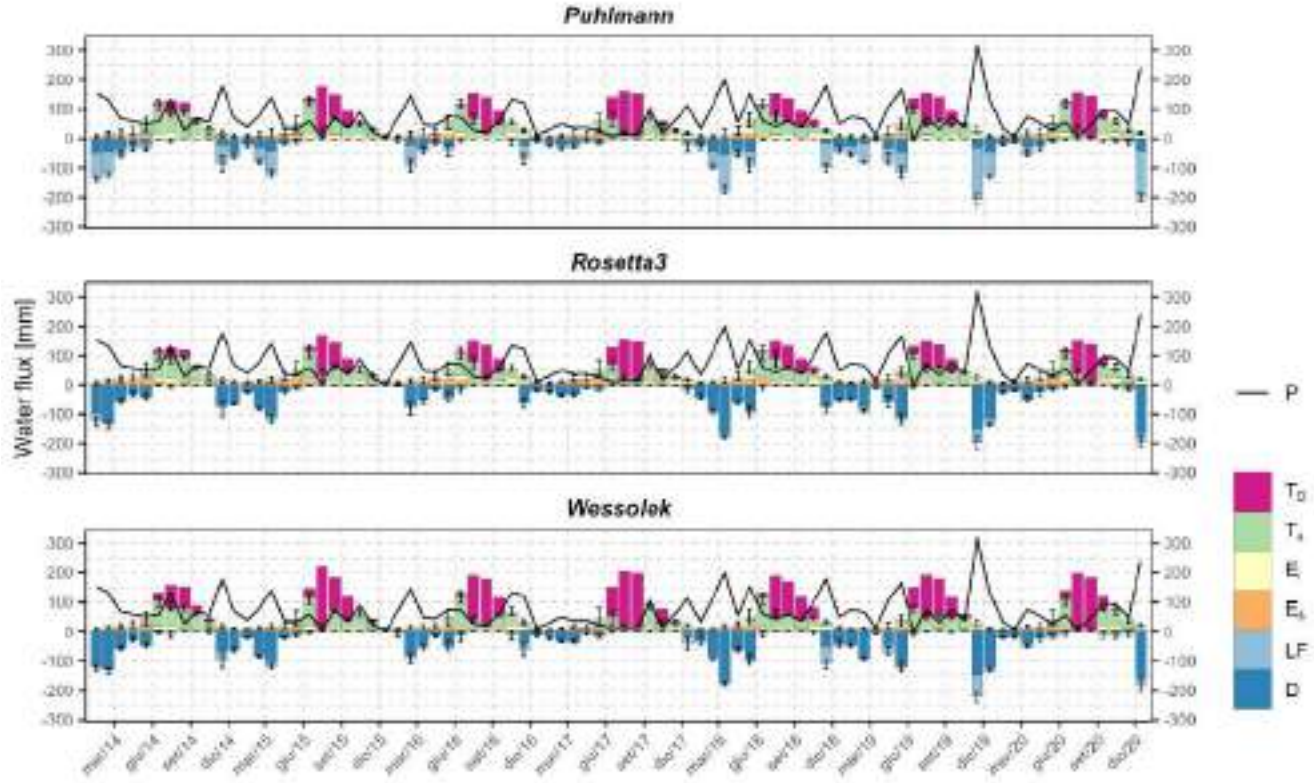

Figure 4.4.9. Water budget estimates for LAZ1 site; water retention curves estimated through the listed PTFs, Ksat values as measured in the field. P = precipitation; T_D to E_s the various components of evapotranspiration; LF = lateral flow; D = drainage (downwards).

The total outwards fluxes of water and nitrate, as estimated by LWF-Brook90, were finally compared with the estimates obtained by the chloride tracer method, see Tables 4.4.3 to 4.4.5. The comparison shows that the results from the chloride tracer method are reasonably comparable with the results from the SVAT model. Of course, the tracer method cannot estimate lateral flux, and this brings to a significantly lower estimate of total out-of-soil fluxes, but we maintain that it can supply a fully acceptable estimate of total out-of-soil pollutant flows in cases in which the conditions for applications of SVAT models are missing.

In parallel, we then led a full re-evaluation of the chloride tracer method itself; this was prompted by doubts about the nitrate fluxes found by Cecchini et al (2021) for site CAL1, turning up quite high with respect to the low deposition levels of the site. We speculated that, in certain site topographical settings, such as the shallow depression of CAL1 site, lateral fluxes could introduce a strong bias, due to shallow water being sampled in deep samplers. To obtain a summary evaluation, a multi-year integrated soil water flux index was calculated for all the sites for which an adequately large number of sampling years is available, see Table 4.4.6.

As can be seen, the index turns out quite different among the various sites; result can be summarized into three groups.

a) EMI1 and LAZ 1 show fairly small values, such as to consider the results quite realistic.
b) VEN1 site shows a significantly higher value. In this very gentle slope site, it is not possible to assess whether this value is physically realistic by simple comparison with the previous sites, due to the large difference of climate conditions. VEN1 is an alpine site, with much higher precipitation and much lower evapotranspiration, much precipitation being made up of snow, which is much more efficient in infiltrating and flowing through.
c) The values showed by all other sites are definitely unrealistic, being too high, suggesting that >80% rainwater flows out of the soil and then not allowing for adequate evapotranspiration. These sites are actually sited in depressions or on steep slopes. We must conclude that, at least in these sites, a more sophisticated approach, using some SVAT model working in 2-D or 3-D mode, would be necessary.

Table 4.4.3. Flux estimates according to the different methods used, EMI1 site.

		Puhlmann			Rosetta3			Wessolek		
	CI factor	Total	Lateral	Down	Total	Lateral	Down	Total	Lateral	down
2010	298	491	321	170	591	274	317	550	380	169
2011	140	210	144	67	236	80	157	238	134	104
2012	129	282	254	28	301	115	186	296	251	45
2013	247	553	457	95	562	269	293	573	353	220
2014	260	513	444	69	534	254	279	529	392	137
2015	177	262	204	57	274	112	162	260	155	104
2016	129	220	209	11	241	135	106	241	223	18
2017	86	45	40	4	36	1	35	78	72	6
2018	99	268	244	24	280	104	176	272	193	79
2019	110	430	398	32	446	243	204	440	384	56
2020	171	243	224	18	269	139	130	266	227	39
2021	112	196	175	21	208	81	127	207	169	38
2022	107	134	119	14	126	24	102	143	118	24
2023	68	220	198	22	230	80	150	233	192	41

Table 4.4.4. Flux estimates according to the different methods used, LAZ1 site.

		Puhlmann			Rosetta3			Wessolek		
	CI factor	Total	Lateral	Down	Total	Lateral	Down	Total	Lateral	down
2010	474	680	420	260	710	53	657	714	66	648
2011	359	200	78	122	208	9	199	214	9	204
2012	533	395	295	100	378	123	255	430	185	246
2013	335	503	242	261	506	9	497	530	52	478
2014	259	542	305	238	532	46	485	565	58	507
2015	188	253	137	117	258	23	235	264	24	240

		Puhlmann			Rosetta3			Wessolek		
	Cl factor	Total	Lateral	Down	Total	Lateral	Down	Total	Lateral	down
2016	293	282	140	142	284	13	271	313	55	258
2017	190	143	58	85	122	1	121	157	44	113
2018	115	594	348	246	597	33	565	627	94	533
2019	N/A	672	452	220	661	96	565	700	116	584
2020	N/A	354	216	138	343	32	311	354	71	283
2021	309	392	217	175	386	30	356	417	58	359
2022	295	310	166	143	309	12	297	330	86	244
2023	283	331	158	174	332	20	312	357	60	296

2019-2020 no soil solution sampling

Table 4.4.5. N_NO_3 outflows from the soil, ($kg \cdot ha^{-1}$), site EMI1, according to the different approaches (note: there is no outflow of N_NO_3 from LAZ1 site).

Year	Cl fac.	Puhlmann		Rosetta3		Wessolek	
		Lateral	Down	Lateral	Down	Lateral	Down
2010	8.00	8.60	4.56	7.34	8.50	10.19	4.53
2011	2.90	2.99	1.39	1.66	3.26	2.78	2.16
2012	5.55	10.92	1.20	4.94	7.99	10.79	1.93
2013	4.50	8.32	1.73	4.90	5.33	6.42	4.00
2014	3.89	6.65	1.03	3.80	4.18	5.87	2.05
2015	1.32	1.52	0.43	0.84	1.21	1.16	0.78
2016	2.19	3.54	0.19	2.29	1.79	3.78	0.30
2017	2.96	1.37	0.14	0.03	1.20	2.47	0.21
2018	2.82	6.95	0.68	2.96	5.01	5.50	2.25
2019	1.58	5.73	0.46	3.50	2.94	5.53	0.81
2020	1.04	1.37	0.11	0.85	0.79	1.38	0.24
2021*	ns	ns	ns	ns	ns	ns	ns
2022	1.81	2.01	0.24	0.41	1.72	1.99	0.41
2023	0.51	1.48	0.16	0.60	1.12	1.43	0.31

** In 2021, median concentration of N_NO_3 in the deepest samplers was below limit of quantification*

Table 4.4.6. Indexes of water flux within the soil, as obtained by the chloride tracer method, for project sites.

Site	ABR1	BOL1	CAL1	EMI1	LAZ1	PIE1	SAR1	TOS2	VEN1	VEN2
W. retention index	0.936	0.670	0.861	0.244	0.324	0.921	N/A	N/A	0.634	Water table

Conclusions

The experimental work carried on within the LIFE20 GIE/IT/000091 - LIFE MODERn (NEC) project has demonstrated that actual quantitative estimates of pollutant fluxes through the soil are presently possible in certain conditions, namely in sites with flat or very gentle topography.

Use of basic, 1-D, SVAT models, when supported by adequate data, supplies more accurate estimates of the partition between lateral and downwards flux in water that leaves the soil. On the other hand, use of the chloride tracer method, which requires many less data and is completely feasible with data existing within the ICP-Forests surveys, supplies results which are not significantly less valid.

Both methods appear to be restricted to use in sites with simple topography; more sophisticated approaches should be set up for the other sites.

4.5 Faunal diversity

4.5.1 Dataset

Table 4.5.1 provides an overview of the dataset. Data on faunal diversity represent a new indicator data cover the 10 forest sites of the LIFE project in the two central years (2023 and 2024). Variables on species richness and evennes and diversity indices have been considered for this analysis.

Table 4.5.1. Overview of the available dataset.

Forest sites (10)		• ABR1 (Selva Piana) • BOL1 (Renon) • CAL1 (Piano Limina) • EMI1 (Carrega) • LAZ1 (Monte Rufeno) • PIE1 (Val Sessera) • SAR1 (Marganai) • TOS2 (Cala Violina) • VEN1 (Cansiglio) • VEN2 (Bosco Fontana)
Variables (11)	Acoustic Indices	• ADI: Acoustic Diversity Index • AEI: Acoustic Evenness Index
	Diversity of bats	• Species richness • Species evenness
	Diversity of birds	• Species richness • Species evenness

	Diversity of soil microarthropods (QBS)	• QBS-ar • n°euedaphic • n°hemiedaphic • n°epidaphic
	e-DNA	• Species richness
Years (2)		2023 and 2024

4.5.2 Results and discussion

Acoustic indices

Figure 4.5.1 presents the distribution of the Acoustic Diversity Index (ADI) and the Acoustic Evenness Index (AEI). The highest ADI values, which correspond to the lowest AEI values, were observed at the SAR1 site, in contrast to the VEN2 site.

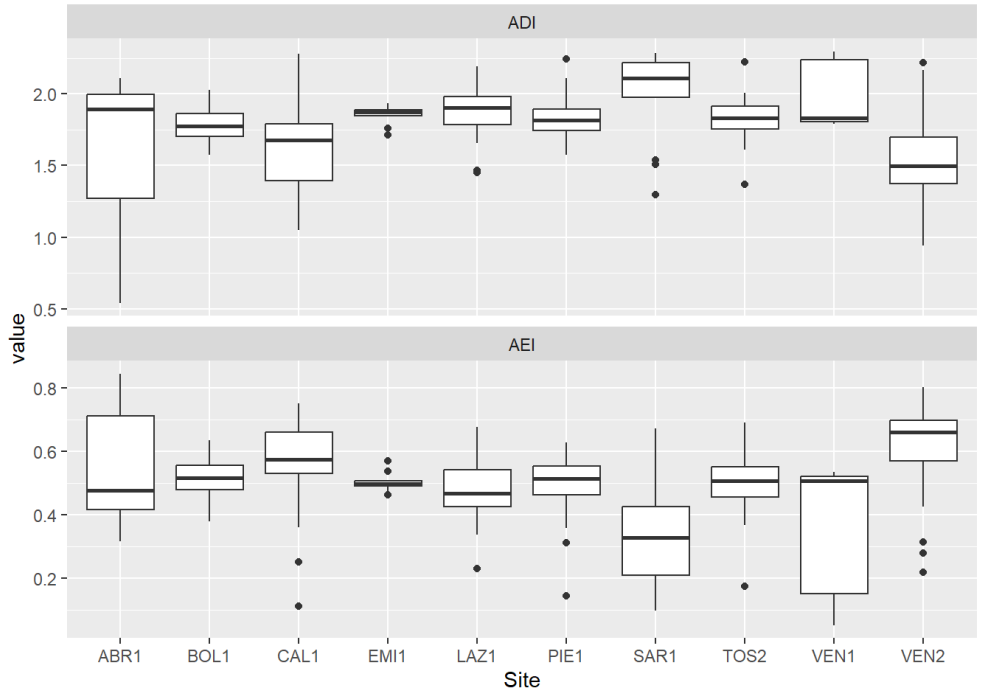

Figure 4.5.1. Distribution of ADI and AEI values among the 10 forest sites.

Comparing the ADI and AEI values between 2023 and 2024, LAZ1 and VEN2 show the highest ADI and the lowest AEI in 2024 (Figure 4.5.2; $p<0.05$).

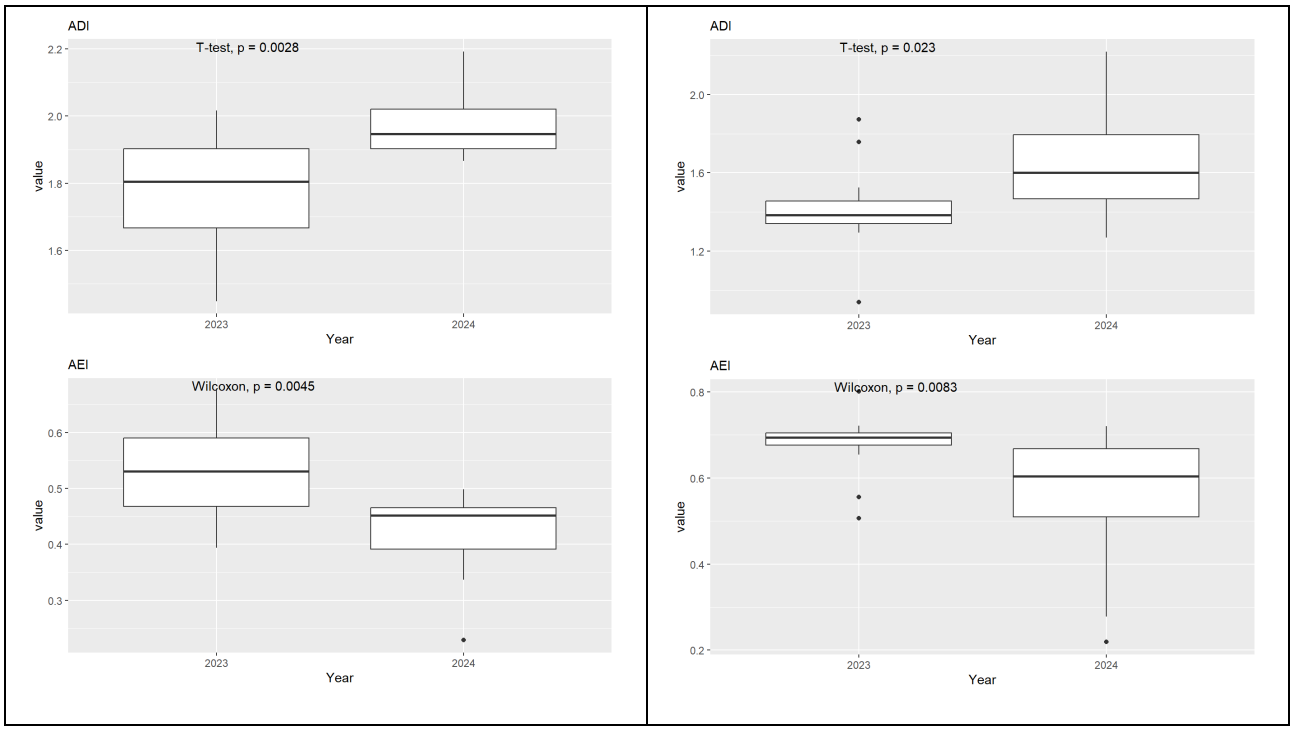

Figure 4.5.2. Comparison between years of the values of ADI and AEI at LAZ1 (left) and VEN2 (right) forest sites.

Diversity of bats

Figure 4.5.3 shows the distribution of bat evenness and diversity across the ten forest sites. The highest values of evenness have been found in CAL1 and LAZ1, while CAL1 and SAR1 show the highest species richness.

Figure 4.5.4 reports the total number of detections of each bat species in each year by forest site, useful to understand the permanence of each species in the site.

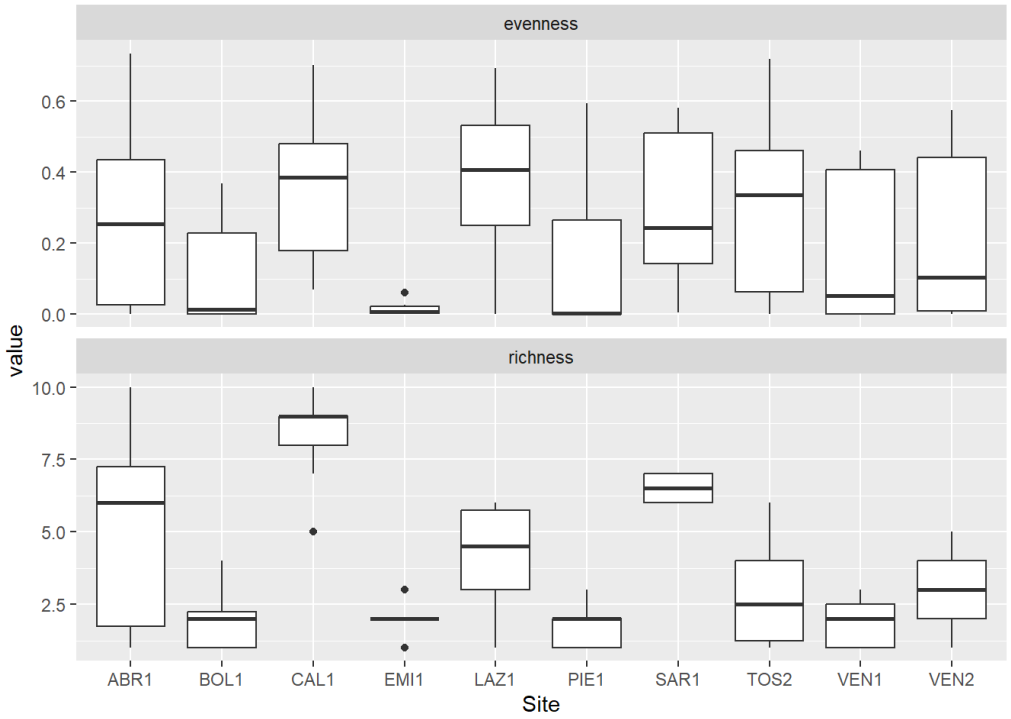

Figure 4.5.3. Distribution of bat evenness and diversity across the ten forest sites.

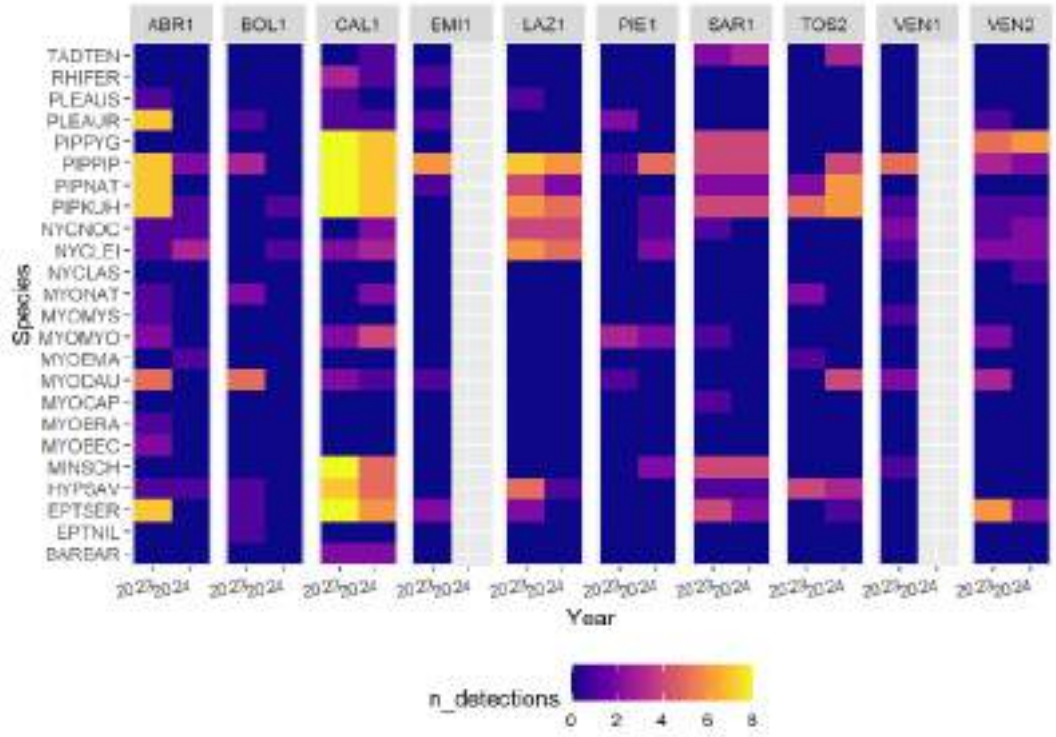

Figure 4.5.4. Distribution of the total number of detections of each bat species in each year by forest site.

The values recorded in each site for richness and evenness are compared between the two years of the project. The normality assumptions withing groups is checked using the Shapiro test: if values in both Year follow the normal distribution the T-test was used, otherwise the Wilcoxon Rank Sum Test was adopted. CAL1 and LAZ1 show lower values of evenness in 2024 compared to 2023 (Wilcoxon test; $p<0.05$) with a low species richness in 2024 in LAZ1 (Figure 4.5.5).

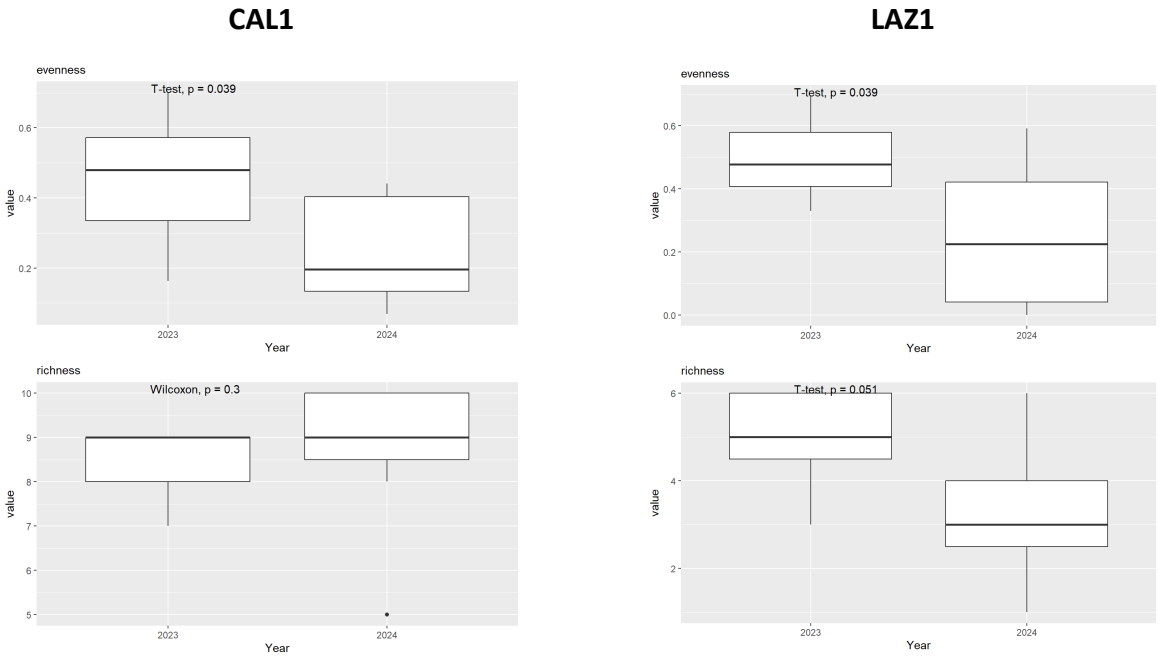

Figure 4.5.5. Distribution of bat evenness and diversity in the two years for CAL1 and LAZ1 forest sites.Results of the Wilcoxon test.

Table 4.5.2 reports the list of species detected over the two years. The total number of species detected over the two-year period at each site ranges from 6-7 for EMI1 and VEN1 to 16-17 for ABR1 and CAL1 (see Fig. 4.5.6 above). A comparison of bat species richness between the two years at each site (see Fig. 4.5.6 below) reveals that some sites, such as CAL1, PIE1 and TOS2, experienced an increase in the number of species, whereas the other sites exhibited a decline in the number of records.

Table 4.5.2. List of bat species detected in the two years for each of the ten forest sites.

Site	Year	Species
ABR1	2023	EPTSER, HYPSAV, MYOBEC, MYOBRA, MYODAU, MYOMYO, MYOMYS, MYONAT, NYCLEI, NYCNOC, PIPKUH, PIPNAT, PIPPIP, PLEAUR, PLEAUS
	2024	HYPSAV, MYOEMA, NYCLEI, NYCNOC, PIPKUH, PIPPIP
BOL1	2023	EPTNIL, EPTSER, HYPSAV, MYODAU, MYONAT, PIPPIP, PLEAUR
	2024	NYCLEI, PIPKUH
CAL1	2023	BARBAR, EPTSER, HYPSAV, MINSCH, MYODAU, MYOMYO, NYCLEI, PIPKUH, PIPNAT, PIPPIP, PIPPYG, PLEAUR, PLEAUS, RHIFER
	2024	BARBAR, EPTSER, HYPSAV, MINSCH, MYODAU, MYOMYO, MYONAT, NYCLEI, NYCNOC, PIPKUH, PIPNAT, PIPPIP, PIPPYG, PLEAUR, RHIFER, TADTEN
EMI1	2023	EPTSER, MYODAU, PIPNAT, PIPPIP, PLEAUR, RHIFER
LAZ1	2023	EPTSER, HYPSAV, NYCLEI, NYCNOC, PIPKUH, PIPNAT, PIPPIP, PLEAUS
	2024	HYPSAV, NYCLEI, NYCNOC, PIPKUH, PIPNAT, PIPPIP
PIE1	2023	MYODAU, MYOMYO, PIPPIP, PLEAUR
	2024	MINSCH, MYOMYO, NYCLEI, NYCNOC, PIPKUH, PIPPIP
SAR1	2023	EPTSER, HYPSAV, MINSCH, MYOCAP, MYOMYO, NYCNOC, PIPKUH, PIPNAT, PIPPIP, PIPPYG, TADTEN
	2024	EPTSER, HYPSAV, MINSCH, PIPKUH, PIPNAT, PIPPIP, PIPPYG, TADTEN
TOS2	2023	HYPSAV, MYOEMA, MYONAT, PIPKUH, PIPNAT
	2024	EPTSER, HYPSAV, MYODAU, PIPKUH, PIPNAT, PIPPIP, TADTEN
VEN1	2023	MINSCH, MYODAU, MYOMYS, NYCLEI, NYCNOC, PIPKUH, PIPPIP
VEN2	2023	EPTSER, MYODAU, MYOMYO, NYCLEI, NYCNOC, PIPKUH, PIPPIP, PIPPYG, PLEAUR
	2024	EPTSER, NYCLAS, NYCLEI, NYCNOC, PIPKUH, PIPPIP, PIPPYG

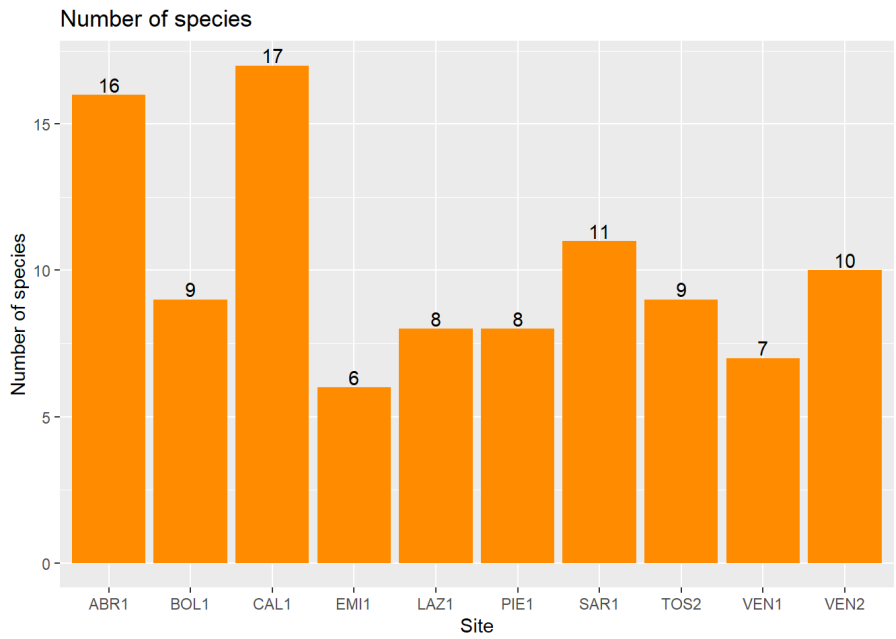

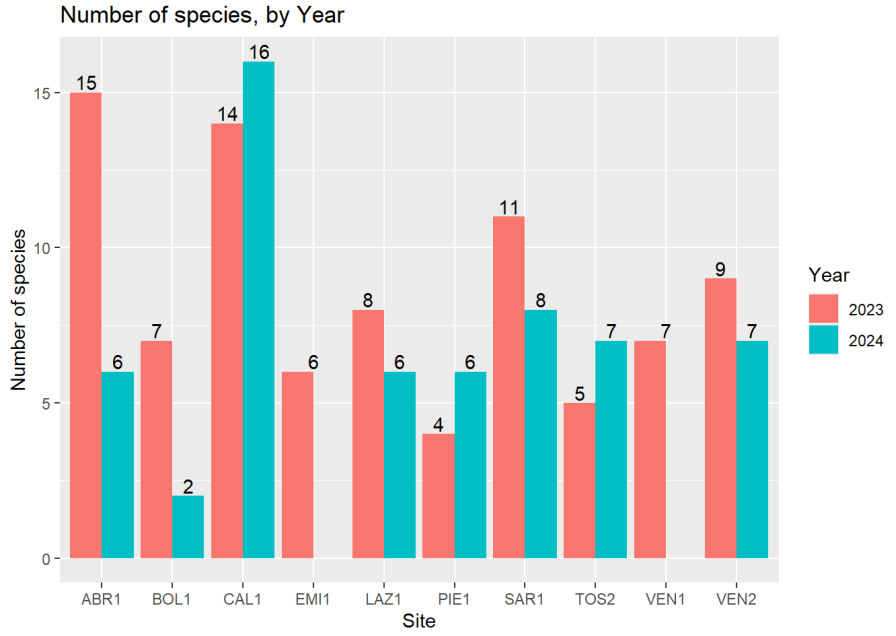

Figure 4.5.6. Number of bat species detected at each of the 10 forest sites (above) and for each year (below).

Diversity of birds

Figure 4.5.7 presents the number of bird species detected at each site and for each year, respectively. The sites with the highest diversity are BOL1 (35 species) and CAL1 (30 species).

Conversely, PIE1 (13 species) and VEN1 (11 species) had the lowest diversity among the forest sites. Over the two sampling years (2023 and 2024), an increase in biodiversity was observed at BOL1 (22 vs 27 species), CAL1 (21 vs 25 species), PIE1 (9 vs 10), and VEN2 (18 vs 19 species).

Figure 4.5.8 lists the bird species with their detection values recorded during the morning hours (4 to 8 a.m.), indicating that the majority of recordings occur between 4 and 5 a.m.

Figure 4.5.9 provides the list of bird species with their detection values at each forest site.

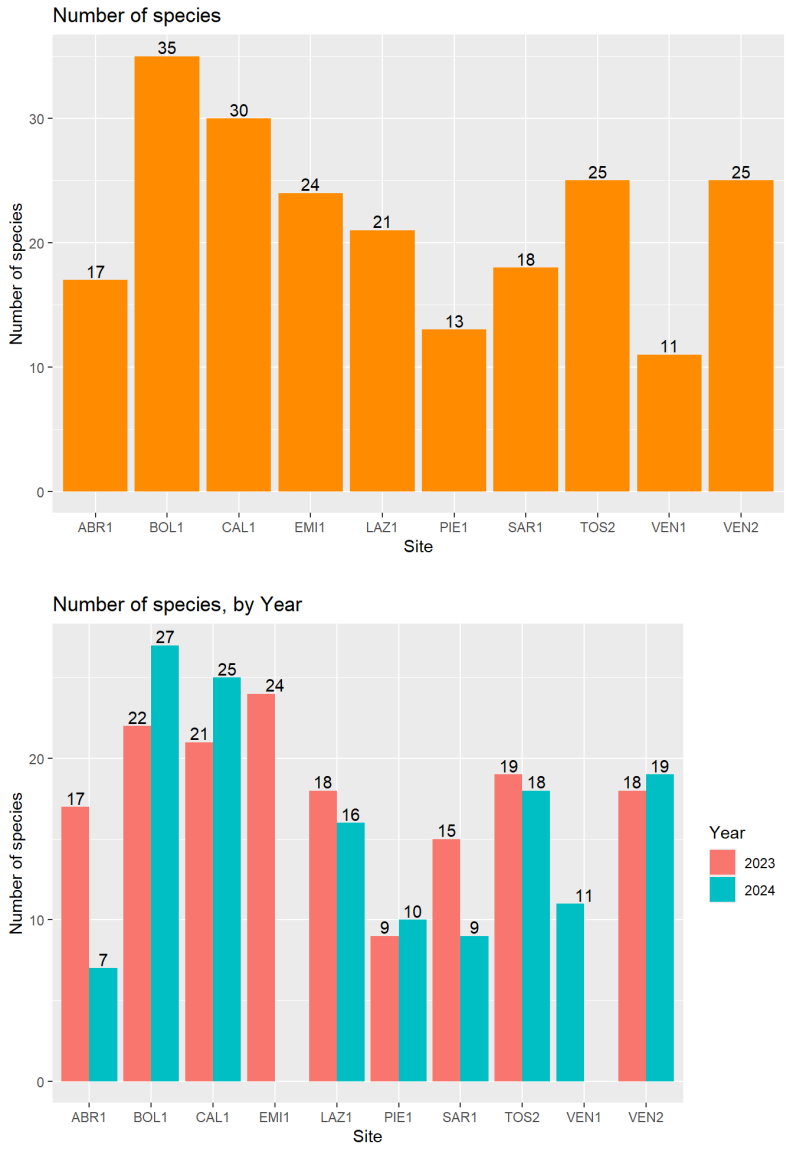

Figure 4.5.7. Number of bird species detected at each of the 10 forest sites (above) and for each year (below).

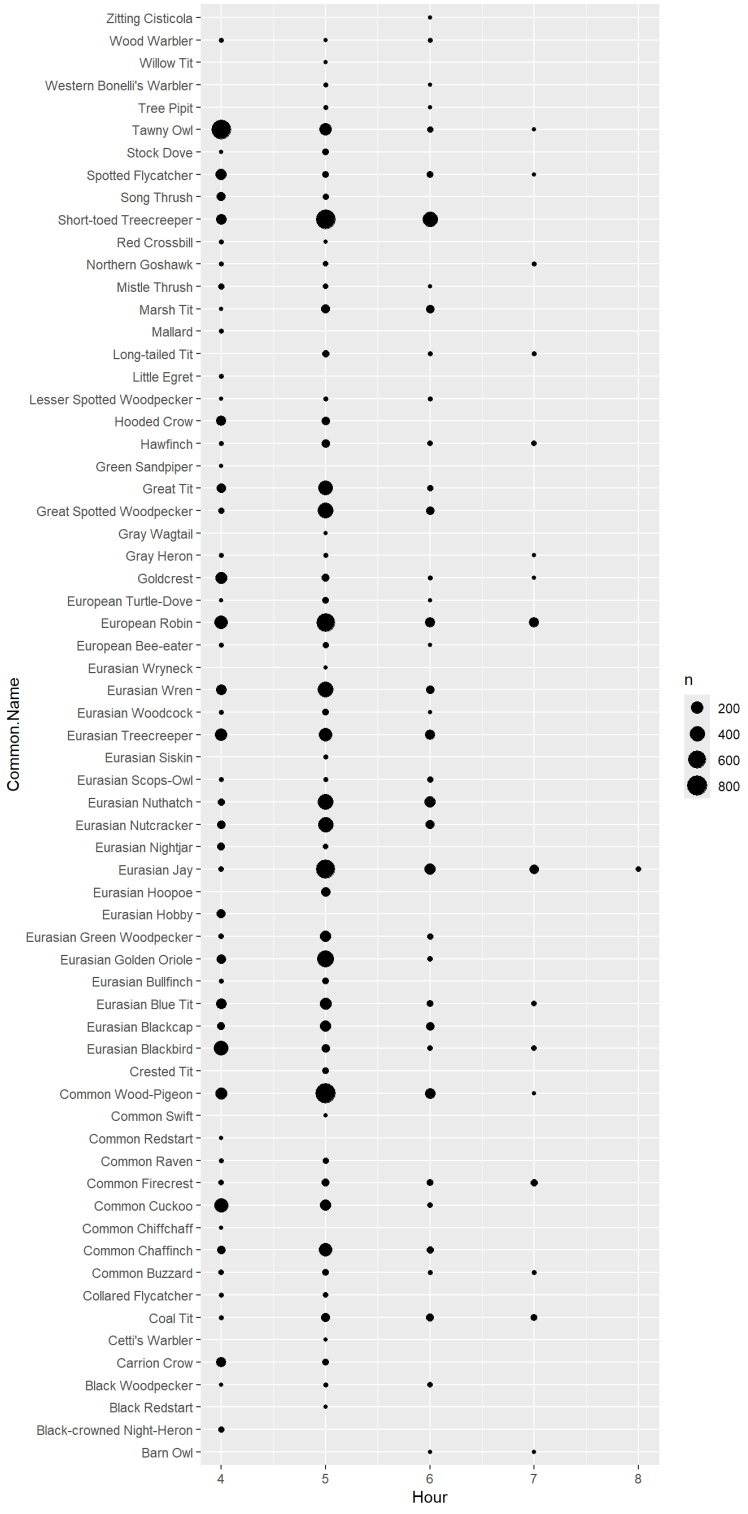

Figure 4.5.8. List of bird species with their detection values in the hours of the morning.

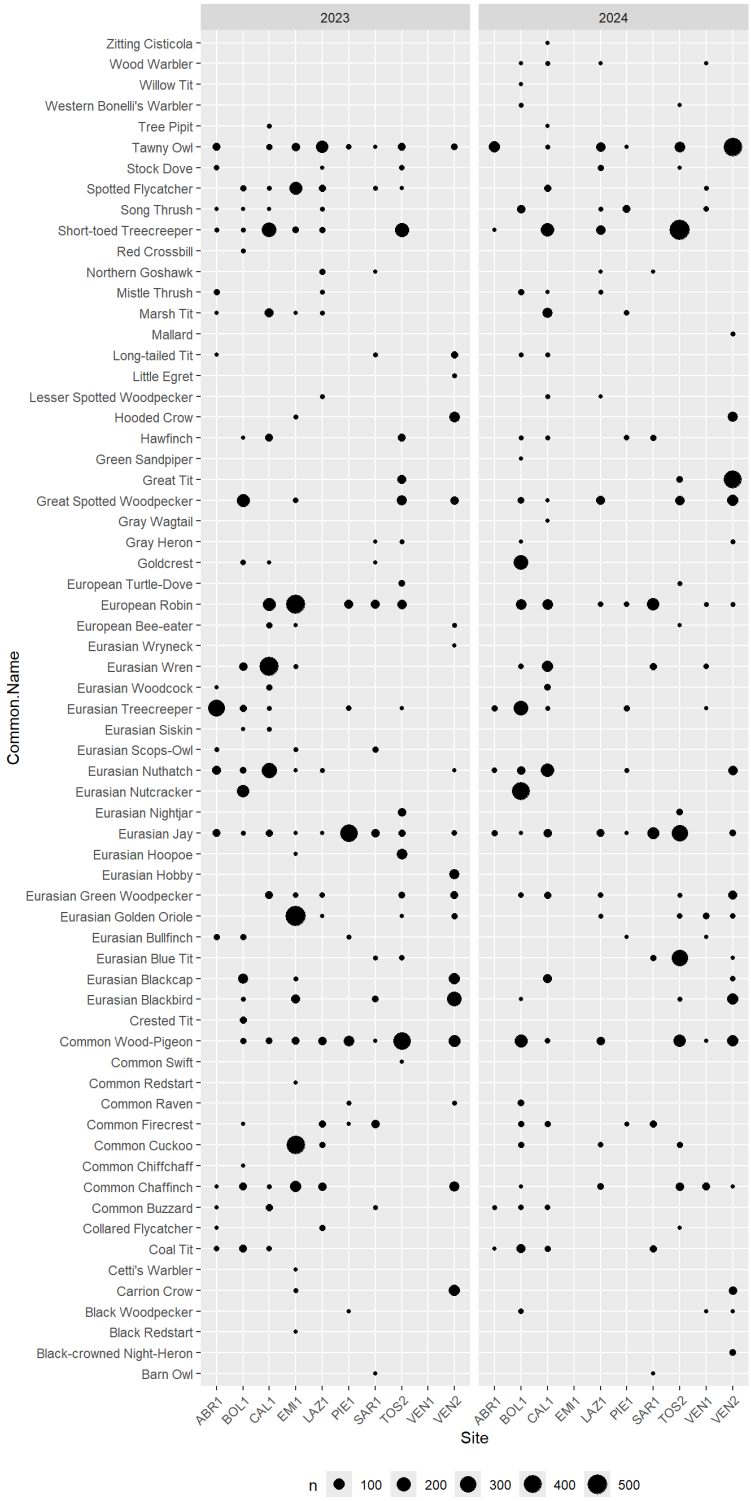

Figure 4.5.9. List of bird species with their detection values at each forest site.

Diversity of soil microarthropods (QBS)

Figure 4.5.10. reports the values of the QBS-ar at the 10 forest sites in the two years of the project (2023 and 2024).

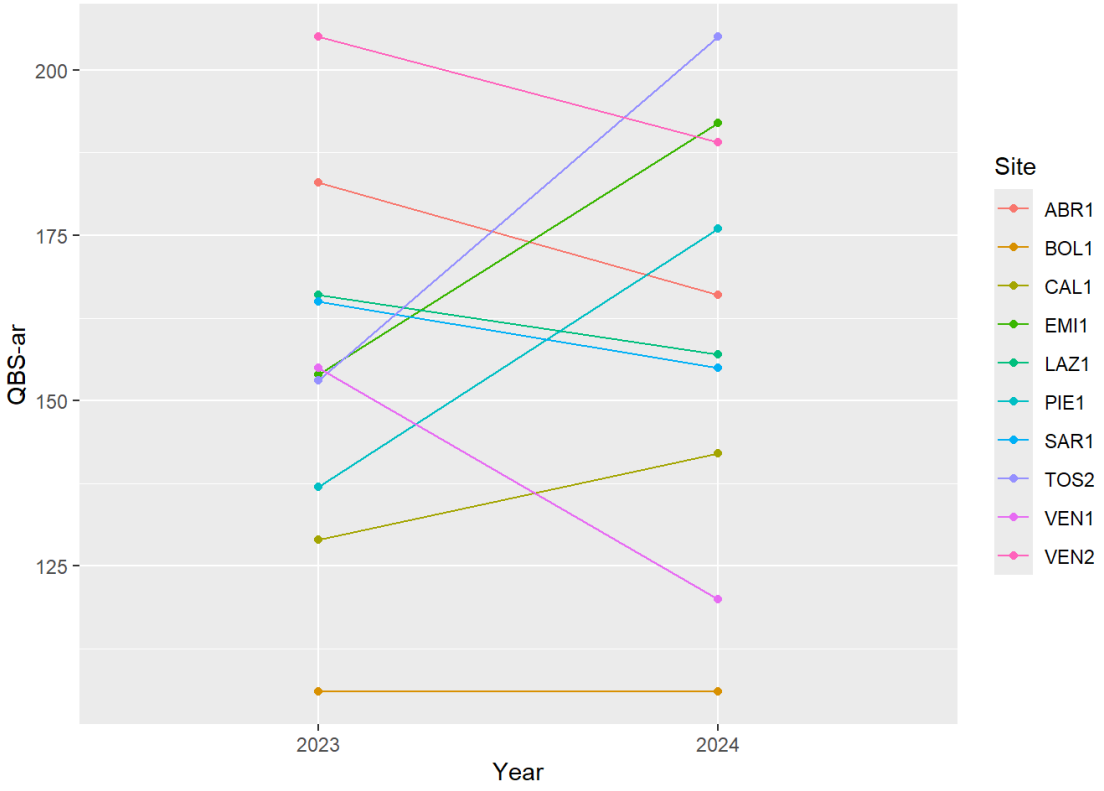

Figure 4.5.10. Trends of the QBS-ar at the 10 forest sites in the two years of the project.

Figure 4.5.11 shows the distribution of the species of the three groups of macroartropods (epidaphic, hemiedaphic, euedaphic) in the four forest types.

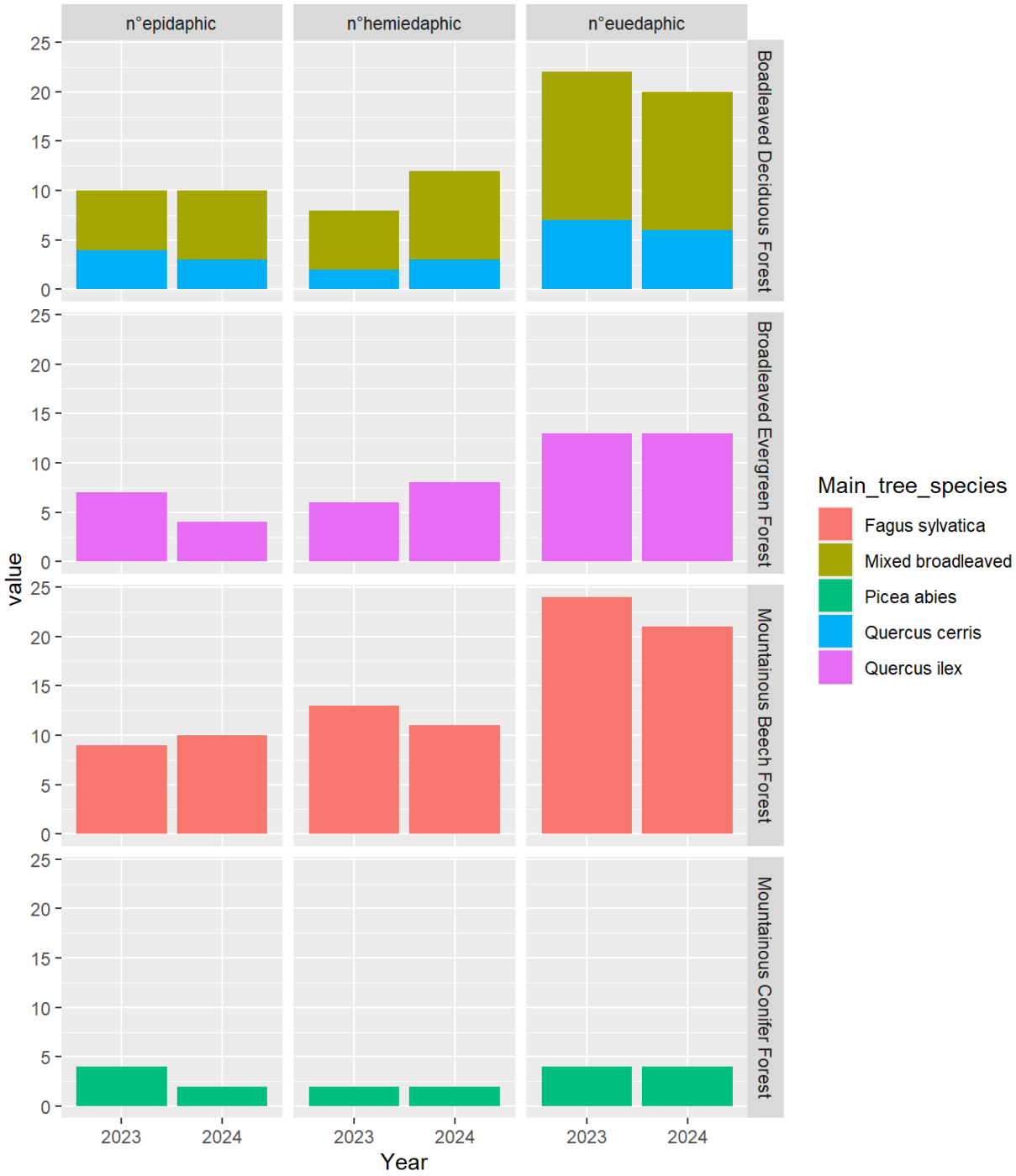

Figure 4.5.11. Distribution of the species of the three groups of macroartropods (epidaphic, euedaphic, hemiedafic) in the four forest types.

Environmental DNA (e-DNA)

Figure 4.5.12 reports the distribution of the relative frequencies of the genera of vertebrates found on the e-DNA in the samples of soils collected in the ten forest sites, with the indications of the forest type and the tree species.

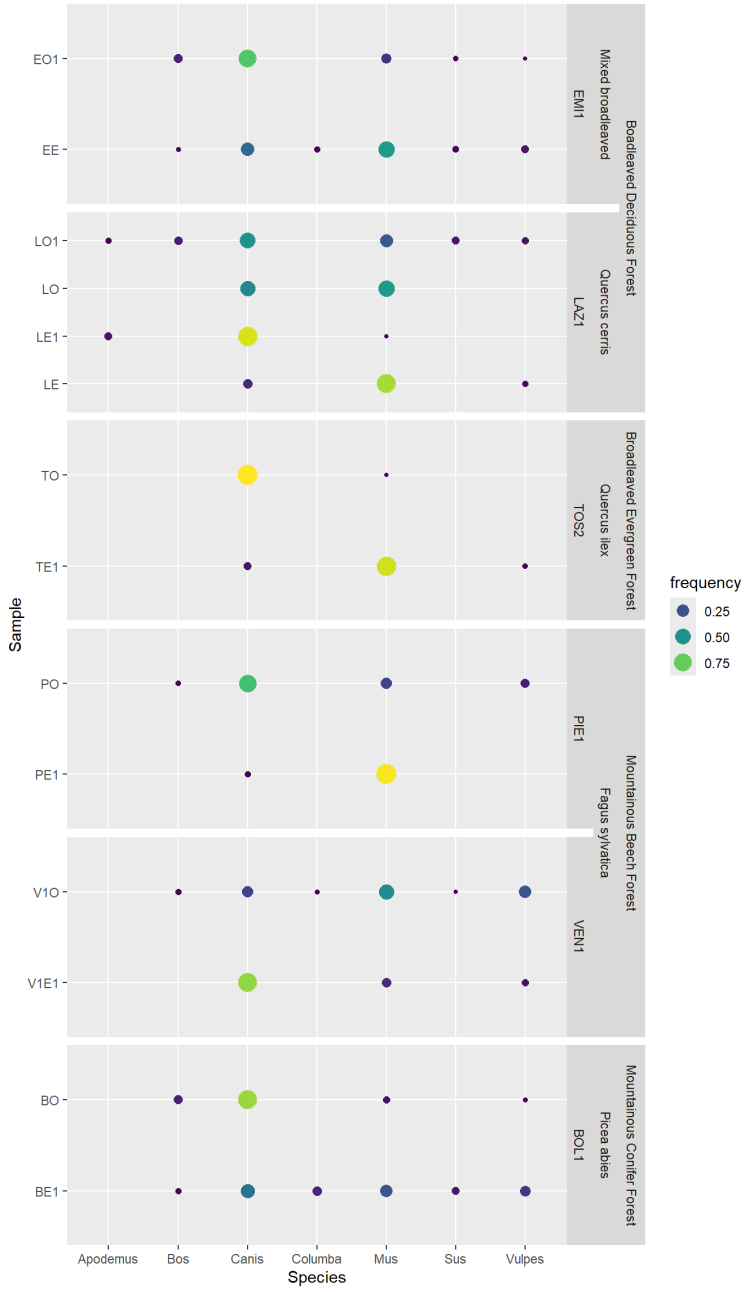

Figure 4.5.12. Distribution of the relative frequencies of the genera of vertebrates found on the e-DNA in the samples of soils collected in the ten forest sites, with the indications of the forest type and the tree species.

4.6 Epiphytic lichens

4.6.1 Dataset

Table 4.6.1 provides an overview of the dataset. The data on lichen diversity were collected during 3 surveys (2019, 2020, and 2023-2024) in the 10 forest sites of the project. Ten key variables have been considered for this analysis.

Table 4.6.1. Overview of the available dataset.

Forest sites (10)	• ABR1 (Selva Piana) • BOL1 (Renon) • CAL1 (Piano Limina) • EMI1 (Carrega) • LAZ1 (Monte Rufeno) • PIE1 (Val Sessera) • SAR1 (Marganai) • TOS2 (Cala Violina) • VEN1 (Cansiglio) • VEN2 (Bosco Fontana)
Variables (10)	• LDV_TREE: Lichen Diversity Value at the tree level • %LDV_MACRO: % LDV of macrolichens (foliose and fruticose species) • %LDV_NITRO: % LDV of nitophytic species • %LDV_OLIGO: % LDV of oligotrophic species • NSP_TREE: Number of species at the tree level • %SP_MACRO: % of species of macrolichens • %SP_NITRO: % of species of nitophytic lichens • %SP_OLIGO: % of species of oligotrophic lichens • FRUT_BIOMASS: biomass of fruticose lichens • FRUT_NSP: Number of species of fruticose lichens
Years (4)	2019, 2020, 2023-2024

4.6.2 Results and discussion

Lichen Diversity Values (LDV)

A total of 120 lichens has been sampled over the years (Tab. 4.6.2): 76 crustose (63%), 33 foliose (28%), 11 fruticose species (9%). The list includes 7 nitrophytic species (i.e., lichens occurring in situations from rather to highly eutrophicated) and 58 oligotrophic species (i.e., lichens not resistant to eutrophication or that are resistant to a very weak eutrophication). Further, 39 lichens of the list

are species which exclusively occur on old trees in ancient, undisturbed forests or in semi-natural habitats.

*Table 4.6.2. List of lichen species found during the survey on Lichen Diversity Value (LDV). Growth form (Gf): C= crustose lichen; F= foliose; FR= fruticose. Eutrophication (Eut): O= oligotrophyc species; N= nitrophytic species. * species which exclusively occur on old trees in ancient, undisturbed forests or in semi-natural habitats.*

Lichen species	
** Acrocordia cavata (Ach.) R.C. Harris*	Gf: C; Eut: O
Alyxoria varia (Pers.) Ertz & Tehler	Gf: C; Eut: O
Amandinea punctata (Hoffm.) Coppins & Scheid.	Gf: C
Anaptychia ciliaris (L.) A. Massal.	Gf: FR
Arthonia atra (Pers.) A. Schneid.	Gf: C; Eut: O
** Arthonia didyma Körb.*	Gf: C
Arthonia punctiformis Ach.	Gf: C; Eut: O
Arthonia radiata (Pers.) Ach.	Gf: C
Arthonia sp.	Gf: C
** Arthonia stellaris Kremp.*	Gf: C; Eut: O
Arthopyrenia sp.	Gf: C
Athallia cerinella (Nyl.) Arup, Frödén & Søchting	Gf: C
Athallia cerinelloides (Erichsen) Arup, Frödén & Søchting	Gf: C; Eut: N
** Bacidia rosella (Pers.) De Not.*	Gf: C
Bacidia rubella (Hoffm.) A. Massal.	Gf: C
Bactrospora patellarioides (Nyl.) Almq. var. patellarioides	Gf: C; Eut: O
Blastenia herbidella (Hue) Servit	Gf: C
** Buellia disciformis (Fr.) Mudd*	Gf: C; Eut: O
Buellia griseovirens (Sm.) Almb.	Gf: C; Eut: O
Buellia s.l.	Gf: C
Caloplaca sp.	Gf: C
Candelaria concolor (Dicks.) Stein	Gf: F; Eut: N
Candelariella reflexa (Nyl.) Lettau	Gf: C; Eut: N
Candelariella xanthostigma (Ach.) Lettau	Gf: C
** Cetrelia olivetorum (Nyl.) W.L. Culb. & C.F. Culb.*	Gf: F; Eut: O
** Chaenotheca chrysocephala (Ach.) Th. Fr.*	Gf: C; Eut: O
** Cladonia caespiticia (Pers.) Flörke*	Gf: FR; Eut: O
Cladonia coniocraea (Flörke) Spreng.	Gf: FR
** Cladonia parasitica (Hoffm.) Hoffm.*	Gf: FR; Eut: O
Cladonia sp.1	Gf: FR
Cladonia sp.2	Gf: FR
Coenogonium pineti (Ach.) Lücking & Lumbsch	Gf: C; Eut: O
Dendrographa decolorans (Sm.) Ertz & Tehler	Gf: C
Evernia prunastri (L.) Ach.	Gf: FR
Flavoparmelia caperata (L.) Hale	Gf: F
Flavoparmelia soredians	Gf: F
** Fuscidea stiriaca (A. Massal.) Hafellner*	Gf: C; Eut: O
Graphis pulverulenta (Pers.) Ach.	Gf: C; Eut: O
Graphis scripta (L.) Ach.	Gf: C; Eut: O
** Gyalecta carneola (Ach.) Hellb.*	Gf: C; Eut: O
Gyalecta sp.	Gf: C
** Gyalecta truncigena (Ach.) Hepp*	Gf: C; Eut: O
Gyalolechia flavorubescens (Huds.) Søchting, Frödén & Arup var. flavorubescens	Gf: C
Hyperphyscia adglutinata (Flörke) H. Mayrhofer & Poelt	Gf: F; Eut: N
Hypogymnia physodes (L.) Nyl.	Gf: F; Eut: O

Lichen species	
* *Imshaugia aleurites (Ach.) S.L.F. Mey.*	Gf: F; Eut: O
Lecanora argentata s.l.	Gf: C; Eut: O
Lecanora carpinea (L.) Vain.	Gf: C
Lecanora chlarotera Nyl. subsp. Chlarotera	Gf: C
Lecanora expallens Ach.	Gf: C; Eut: O
* *Lecanora intumescens (Rebent.) Rabenh.*	Gf: C
* *Lecanora strobilina (Spreng.) Kieff.*	Gf: C; Eut: O
Lecanora symmicta (Ach.) Ach.	Gf: C; Eut: O
Lecidella elaeochroma (Ach.) M. Choisy var. elaeochroma f. elaeochroma	Gf: C
Lepra albescens (Huds.) Hafellner	Gf: C
Lepra amara (Ach.) Hafellner	Gf: C
* *Lepra slesvicensis (Erichsen) Hafellner*	Gf: C; Eut: O
Lepraria sp. 1	Gf: C
Lepraria sp. 2	Gf: C
* *Lobaria pulmonaria (L.) Hoffm.*	Gf: F; Eut: O
Melanelixia fuliginosa (Duby) O. Blanco, A. Crespo, Divakar, Essl., D. Hawksw. & Lumbsch	Gf: F
Melanelixia glabratula (Lamy) Sandler & Arup	Gf: F
Melanelixia subaurifera (Nyl.) O. Blanco, A. Crespo, Divakar, Essl., D. Hawksw. & Lumbsch	Gf: F
* *Melanohalea elegantula (Zahlbr.) O. Blanco, A. Crespo, Divakar, Essl., D. Hawksw. & Lumbsch*	Gf: F
* *Micarea prasina Fr.*	Gf: C; Eut: O
* *Mycoporum antecellens (Nyl.) R.C. Harris*	Gf: C; Eut: O
Naetrocymbe punctiformis (Pers.) R.C. Harris	Gf: C; Eut: O
* *Nephroma parile (Ach.) Ach.*	Gf: F; Eut: O
Normandina pulchella (Borrer) Nyl.	Gf: C
Opegrapha sp.	Gf: C
* *Opegrapha vermicellifera (Kunze) J.R. Laundon*	Gf: C; Eut: O
Parmelia saxatilis (L.) Ach.	Gf: F
Parmelia sulcata Taylor	Gf: F
* *Parmeliella testacea P.M. Jørg.*	Gf: C; Eut: O
* *Parmeliella triptophylla (Ach.) Müll. Arg.*	Gf: C; Eut: O
Parmelina pastillifera (Harm.) Hale	Gf: F
Parmelina tiliacea (Hoffm.) Hale	Gf: F
Parmeliopsis ambigua (Hoffm.) Nyl.	Gf: F; Eut: O
Parmotrema perlatum (Huds.) M. Choisy	Gf: F; Eut: O
Peltigera praetextata (Sommerf.) Zopf	Gf: F; Eut: O
* *Pertusaria coccodes (Ach.) Nyl.*	Gf: C
Pertusaria coronata (Ach.) Th. Fr.	Gf: C; Eut: O
* *Pertusaria flavida (DC.) J.R. Laundon*	Gf: C; Eut: O
Pertusaria hymenea (Ach.) Schaer.	Gf: C; Eut: O
* *Pertusaria leioplaca (Ach.) DC.*	Gf: C; Eut: O
Pertusaria pertusa (L.) Tuck. var. pertusa	Gf: C; Eut: O
* *Pertusaria pustulata (Ach.) Duby*	Gf: C; Eut: O
Pertusaria sp.	Gf: C
Phaeophyscia orbicularis (Neck.) Moberg	Gf: F; Eut: N
Phlyctis agelaea (Ach.) Flot.	Gf: C; Eut: O
Phlyctis argena (Spreng.) Flot.	Gf: C; Eut: O
Physcia adscendens H. Olivier	Gf: F; Eut: N
Physcia sp.	Gf: F
Physcia stellaris (L.) Nyl.	Gf: F
Physcia tenella (Scop.) DC.	Gf: F
Physconia sp.	Gf: F
Physconia venusta (Ach.) Poelt	Gf: F; Eut: O
Platismatia glauca (L.) W.L. Culb. & C.F. Culb.	Gf: F; Eut: O

Lichen species	
Pleurosticta acetabulum (Neck.) Elix & Lumbsch	Gf: F
** Porina aenea (Wallr.) Zahlbr*	Gf: C; Eut: O
** Porina borreri (Trevis.) D. Hawksw. & P. James*	Gf: C; Eut: O
** Porina coralloidea P. James*	Gf: C; Eut: O
Pseudevernia furfuracea (L.) Zopf var. furfuracea	Gf: F; Eut: O
** Pseudoschismatomma rufescens (Pers.) Ertz & Tehler*	Gf: C; Eut: O
Punctelia subrudecta (Nyl.) Krog	Gf: F
** Pyrenula macrospora (Degel.) Coppins & P. James*	Gf: C; Eut: O
** Pyrenula nitida (Weigel) Ach.*	Gf: C; Eut: O
Ramalina farinacea (L.) Ach.	Gf: FR
** Ramalina fraxinea (L.) Ach.*	Gf: FR
Ramalina sp.	Gf: FR
** Ricasolia virens (With.) H.H. Blom. & Tønsberg*	Gf: F; Eut: O
Scoliciosporum umbrinum (Ach.) Arnold	Gf: C
Scytinium lichenoides (L.) Otálora, P.M. Jørg. & Wedin	Gf: C
Scytinium teretiusculum (Wallr.) Otálora, P.M. Jørg. & Wedin	Gf: C
Tephromela atra (Huds.) Hafellner var. atra	Gf: C; Eut: O
** Usnea hirta (L.) F.H. Wigg.*	Gf: FR; Eut: O
** Varicellaria hemisphaerica (Flörke) I. Schmitt & Lumbsch*	Gf: C; Eut: O
** Waynea stoechadiana (Abbassi Maaf & Cl. Roux) Cl. Roux & P. Clerc*	Gf: C
Xanthoria parietina (L.) Th. Fr.	Gf: F; Eut: N
Zwackhia viridis (Ach.) Poetsch & Schied.	Gf: C; Eut: O

At the plot level, the total number of species ranges from 11 (PIE1) to 38 (CAL1) in 2019, from 14 (PIE1) to 38 (LAZ1) in 2020, and from 10 (SAR1 and VEN2) to 42 (LAZ1) in 2023/24 (Table 4.6.3). At the tree level, the mean number of species ranges 3-16 in 2019, 4-17 in 2020 and 3-18 in 2023/24. Lichen Diversity Values (LDV) are between 36.2 (PIE1) and 107 (LAZ1) in 2019, between 40.7 (PIE1) and 106.4 (LAZ1) in 2020, and between 11.8 (SAR1) and 101.9 (LAZ1) in 2023/24.

Of the six sites surveyed in 2019, 2020, and 2023/24, most showed little change in LDVs, except EMI1 and VEN1, which increased from 39.3 to 63.1 and 59.3 to 72, respectively.

Table 4.6.3. Plot and tree level descriptive statistics of lichen diversity at the 10 forest sites.

Site Code	Total number of species (plot level)			Mean number of species (tree level)			Mean LDV (tree level)		
	2019	2020	2023-24	2019	2020	2023-24	2019	2020	2023-24
ABR1	27	31	36	14	14	16	83.4	82.8	82.8
CAL1	38	41	36	12	13	13	50.2	53.4	52.7
EMI1	16	15	20	6	5	5	39.3	40.9	63.1
LAZ1	34	38	42	16	17	18	107	106.4	101.9
PIE1	11	14	13	3	4	4	36.2	40.7	36.3
VEN1	25	24	25	9	9	10	59.3	65.3	72

BOL1	17	7	52.5
SAR1	10	3	11.8
TOS2	15	7	61.9
VEN2	10	5	35.8

The total number of species detected over the years at each site ranges from 10 for SAR1 and VEN2 to 42 and 46 for CAL1 and LAZ1 respectively (see Fig. 4.6.1 above). A comparison of lichen species richness between the years at each site (see Fig. 4.6.1 below) reveals that some sites, such as ABR1 and LAZ1, experienced an increase in the number of species, whereas the other sites exhibited a fluctuating trend between years.

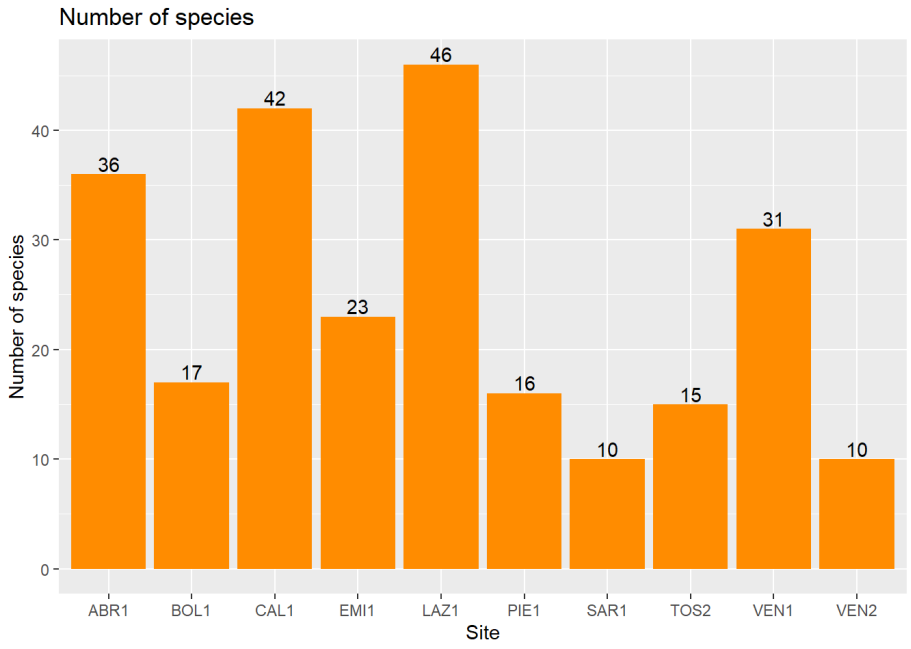

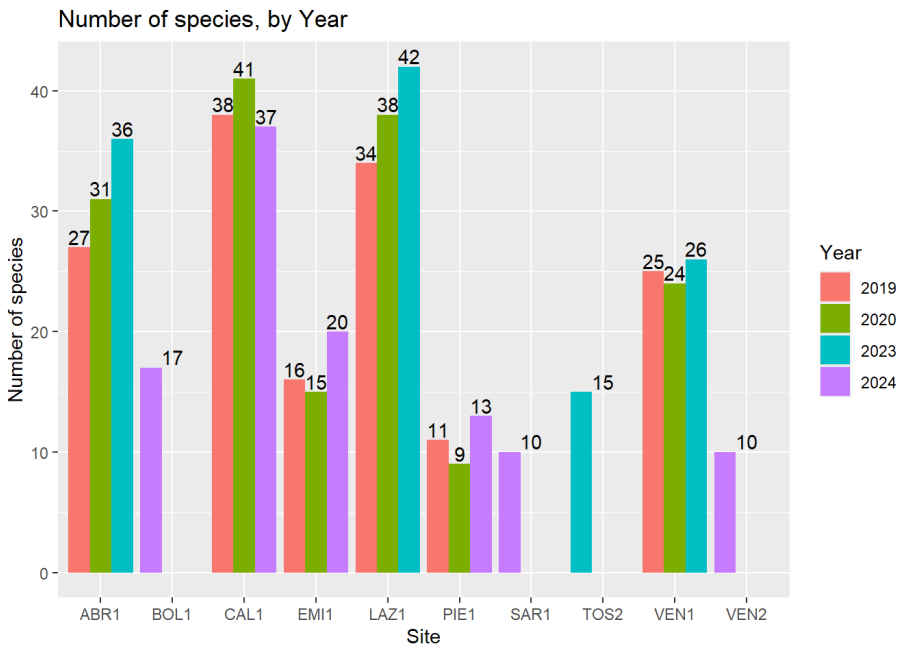

Figure 4.6.1. Number of lichen species detected at each of the 10 forest sites (above) and for each year (below).

Lichen functional diversity

Starting from the lichen diversity assessment (LDV, species richness, abundance and composition), the lichen functional groups has been considered to obtain additional information based on lichen responses to air pollution and climate change, allowing for early warning responses to forest environmental changes. In particular, the following parameters were taken into account:

- %LDV_MACRO: % LDV of macrolichens (foliose and fruticose species)
- %LDV_NITRO: % LDV of nitophytic species
- %LDV_OLIGO: % LDV of oligotrophic species

Figure 4.6.2 illustrates the trend of the functional groups in the four years, by forest type (above) and site (below).

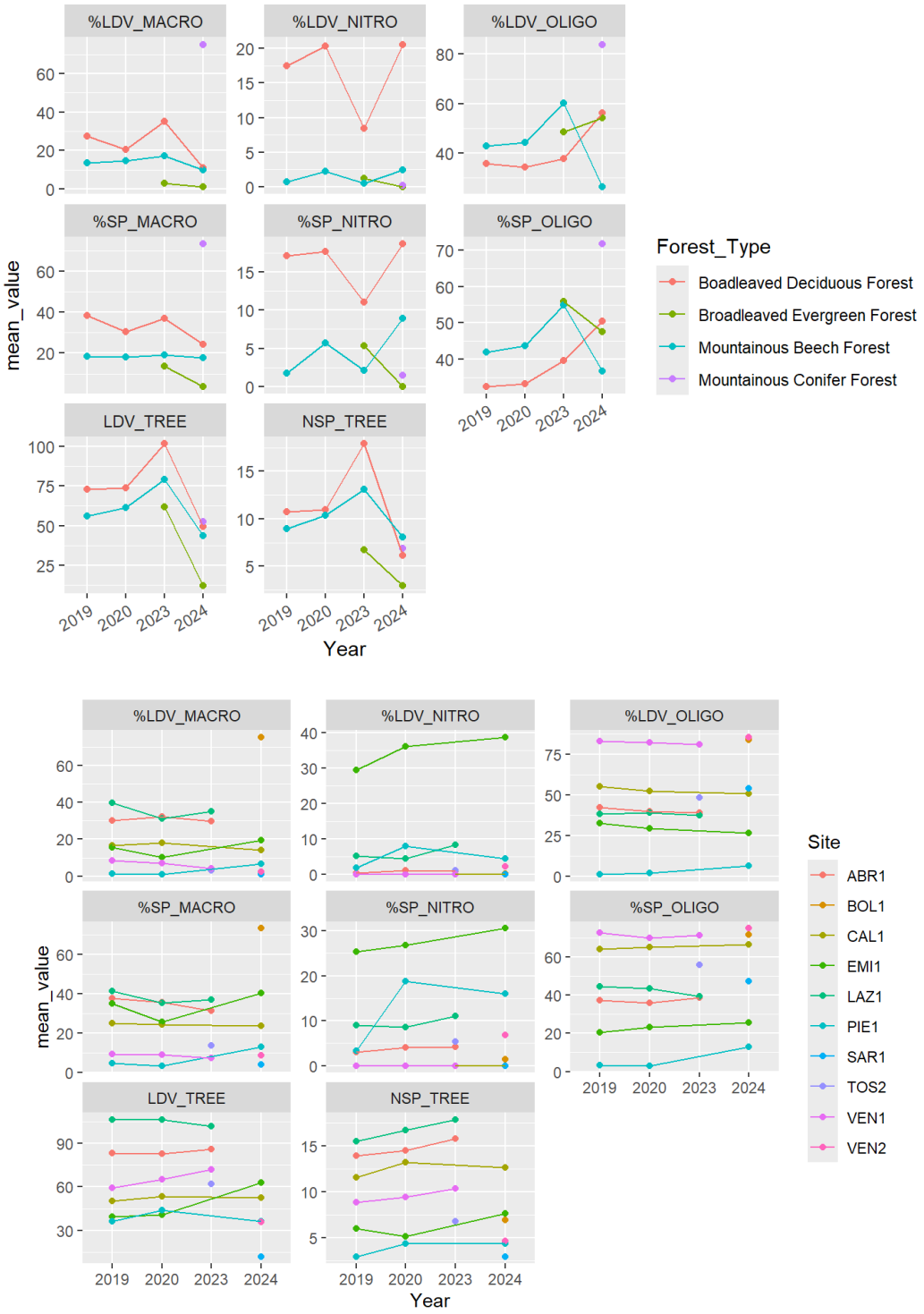

Figure 4.6.2. Trends of the lichen functional diversity at the 10 forest sites in the four years of survey, by forest type (above) and forest site (below).

Fruticose lichens

Fruticose lichens, and especially hair lichens, are particularly sensitive to pollution and climate change, as their large surface area to mass ratios filters moisture and elements from the air, and they have strongly declined in areas with atmospheric pollution and intensive forestry. This makes this functional group a useful indicator of air pollution and climate change in forest ecosystems.

Overall, 23 species of fruticose lichens were recorded in 5 out of 10 forest sites (Figure 4.6.3). The plots host between 3 (LAZ1, ABR1) and 16 taxa (BOL1). The Renon spruce forest (BOL1), in addition to being the site with the highest species richness (16 taxa), also exhibited the highest values of biomass of epiphytic fruticose lichens fallen to the ground, with a clear dominance of *P. furfuracea* (Table 4.6.4).

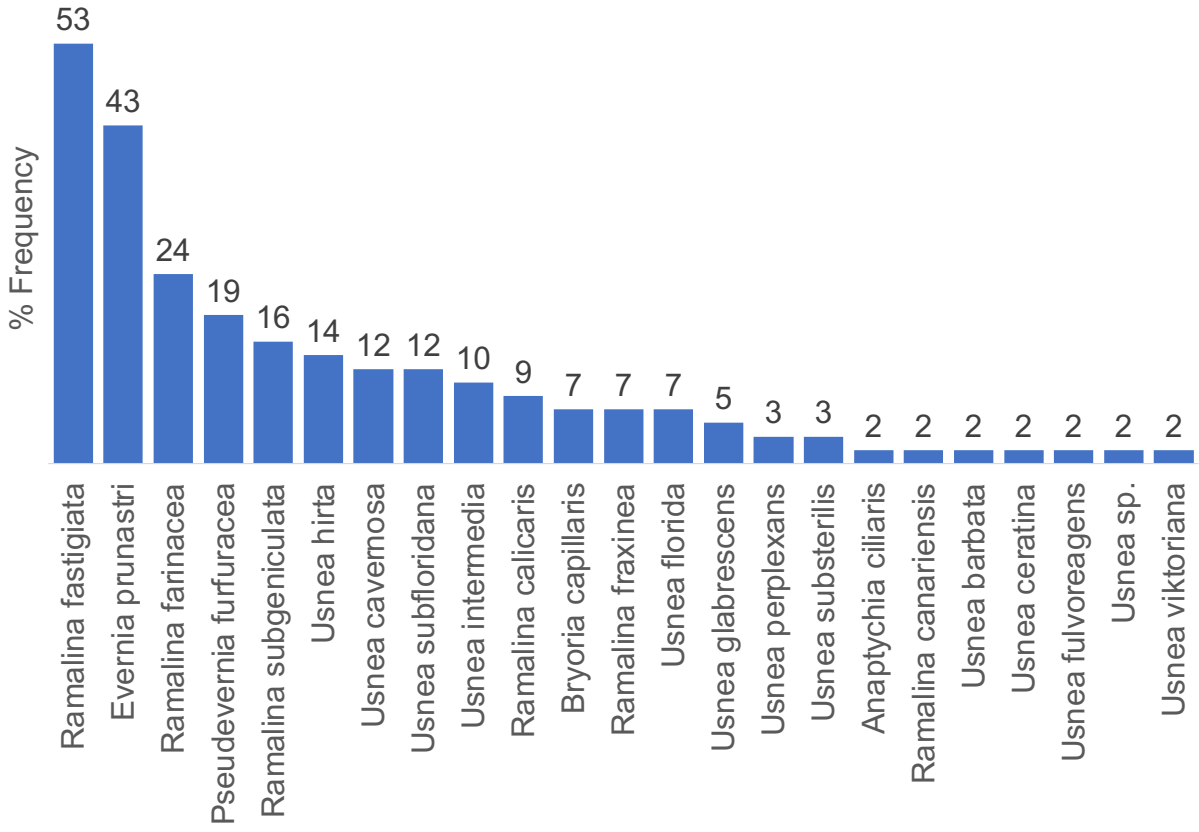

Figure 4.6.3. List of epiphytic fruticose lichens fallen to the ground species detected at 5 out of the 10 forest sites of the project.

Table 4.6.4. Species richness and biomass of fruticose lichens. Forest type: MBF: Mountainous Beech Forest, MCF: Mountainous Conifer Forest, BDF: Boadleaved Deciduous Forest, BEF: Broadleaved Evergreen Forest.

Forest type	Site	N species	Weight (g)	
			Mean ± SD	Cumulative total
MBF	**ABR1**	3	0.138 ± 0.194	1.65
	VEN1	6	0.457 ± 0.585	5.48
BDF	**LAZ1**	3	0.087 ± 0.083	1.045
BEF	**SAR1**	6	1.061 ± 1.041	12.728
MCF	**BOL1**	16	30.180 ± 18.309	301.804

Lobaria pulmonaria

The large foliose species *Lobaria pulmonaria* (L.) Hoffm. is very sensitive to air pollution and in large decline throughout Europe. Several studies demonstrated its suitability both as a flagship and as an umbrella species for nature conservation, since it is easy to identify, and it is associated with many other rare or endangered forest dwelling organisms.

The foliose lichen *Lobaria pulmonaria* was detected in two out of the 10 plots: VEN 1 Pian di Cansiglio, rare (1 tree), and CAL1 Piano Limina, abundant (19 trees; 37%). In sites SAR1 and ABR1 it is present only outside the plot. In the two plots where it is present, *Lobaria pulmonaria* shows a good state of conservation and vitality (Figure 4.6.4). This indicator species is predominantly abundant at the tree level (45% of trees with > 10 thalli). Most trees contain thalli with meristematic ascending lobes (60%). Young thalli are sporadic (40%) to absent (35%). Vegetative propagules (soredia and isidia) are always present, although mostly sporadic. Fruit bodies are present in only 10% of the trees detected.

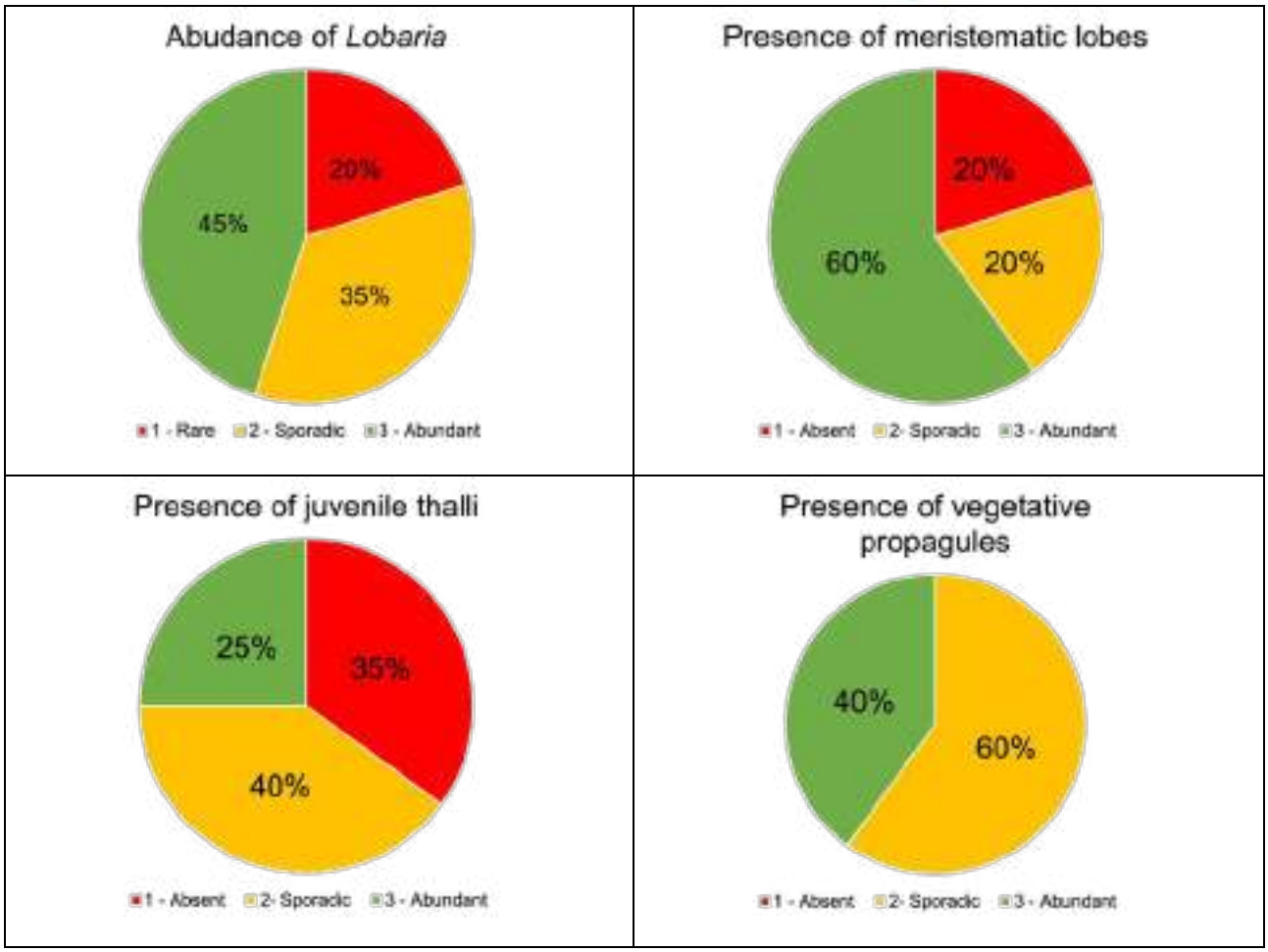

Figure 4.6.4. Descriptive statistics on the presence and vitality of Lobaria pulmonaria *detected at the forest sites of VEN1 and CAL1.*

4.7 Ground vegetation

4.7.1 Dataset

Table 4.7.1 provides an overview of the dataset. Ground vegetation data cover 21 years (1999-2024) in the 10 forest sites of the project. Seven key variables have been considered for this analysis.

Table 4.7.1. Overview of the available dataset.

Forest sites (10)	• ABR1 (Selva Piana) • BOL1 (Renon) • CAL1 (Piano Limina) • EMI1 (Carrega) • LAZ1 (Monte Rufeno) • PIE1 (Val Sessera) • SAR1 (Marganai) • TOS2 (Cala Violina) • VEN1 (Cansiglio) • VEN2 (Bosco Fontana)
Variables (7)	Species composition • Species Richness • Species Density Compositional Diversity • MAX CD Specific Leaf Area • Leaf area (mm^2) • Dry mass (mg) • SAL (Specific Leaf Area, $mm^2\ mg^{-1}$) • Species ecology (Ellenberg indices)
Years (21)	From 1999 to 2024

4.7.2 Results and discussion

Ground vegetation layers

Figure 4.7.1 illustrates the distribution of percentage cover of each layer in the 10 forest types over the two years of the project. Figure 4.7.2 shows the distribution of the height of arboreal and shrubby layers in the 10 forest types over the two years of the project.

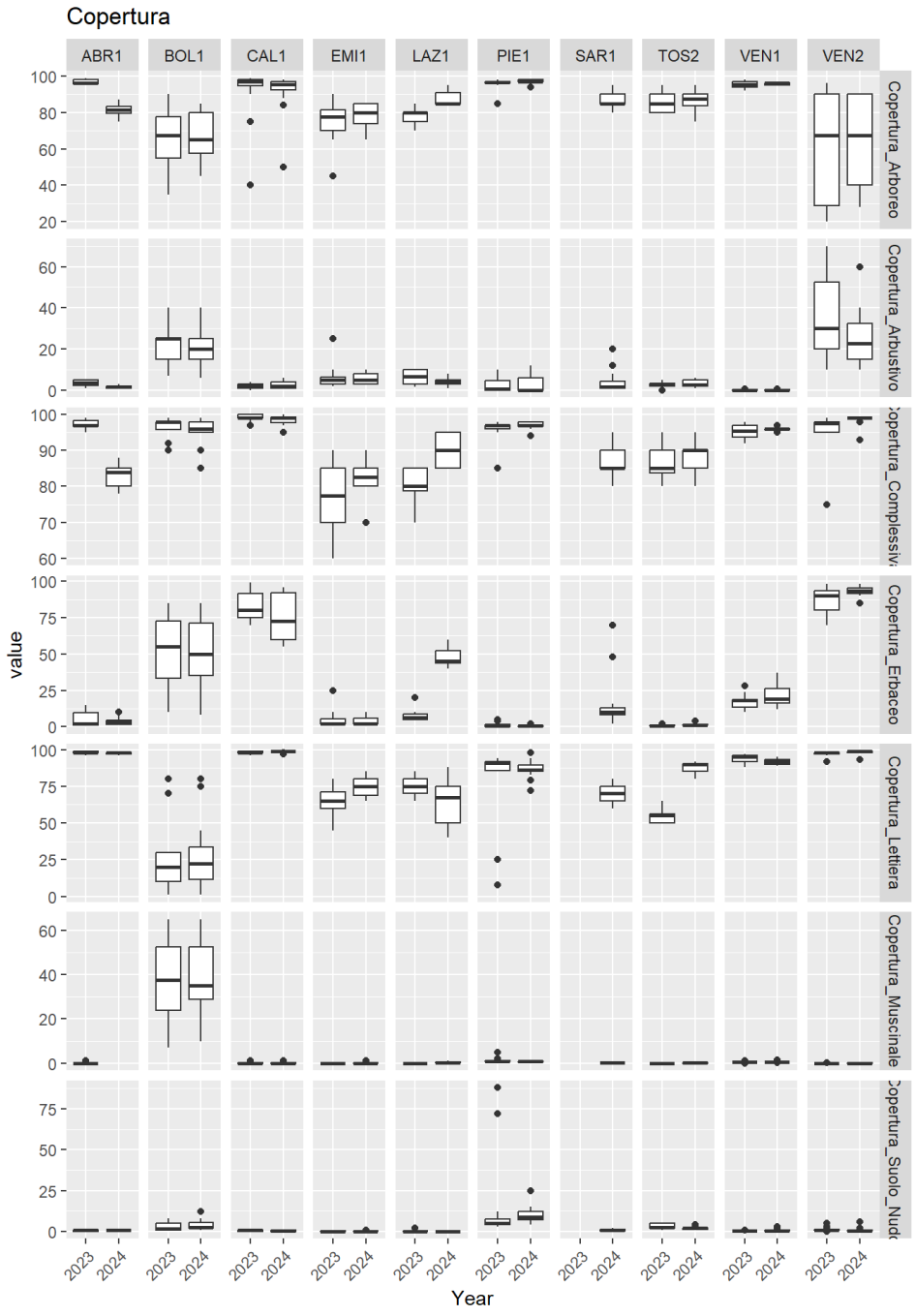

Figure 4.7.1. Boxplots showing the distribution of percentage cover of each layer in the 10 forest types over the two years of the project.

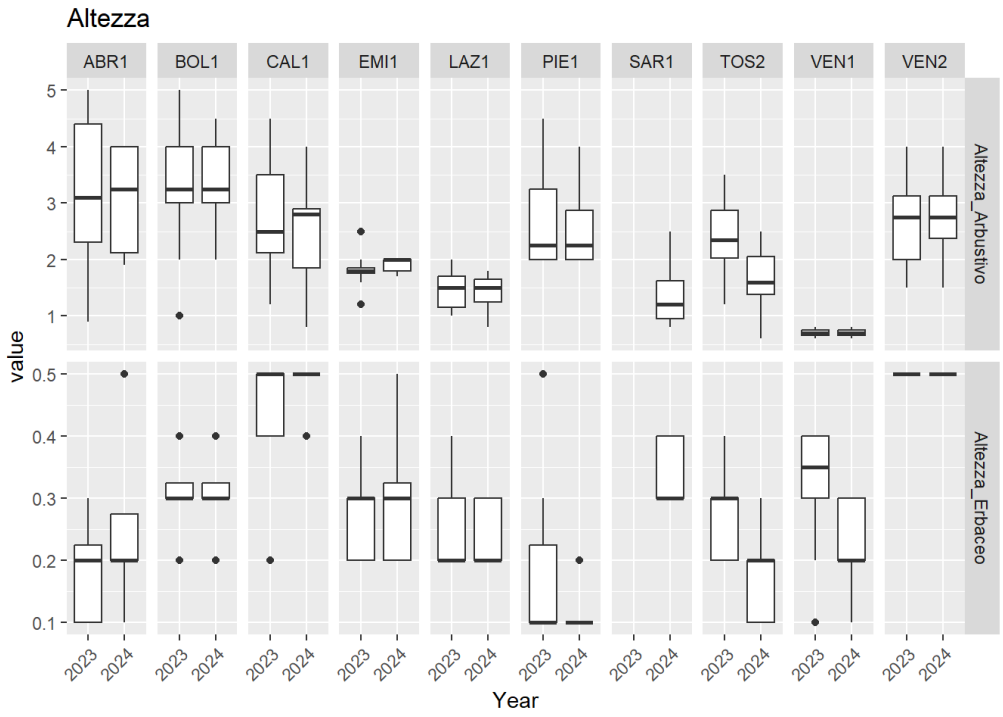

Figure 4.7.2. Boxplots showing the distribution of the height of arboreal and shrubby layers in the 10 forest types over the two years of the project.

Species composition

Plant species were listed in the four layers (1: arboreal layer; 2: shrubby layer; 3: herbaceous layer; 4: mossy layer) both by forest site and by forest type. As an example, Figure 4.7.3 shows mean species coverage and its changes at the BOL1 site across the two project years. Figure 4.7.4 displays the list obtained for Broadleaved Evergreen Forest (BEF).

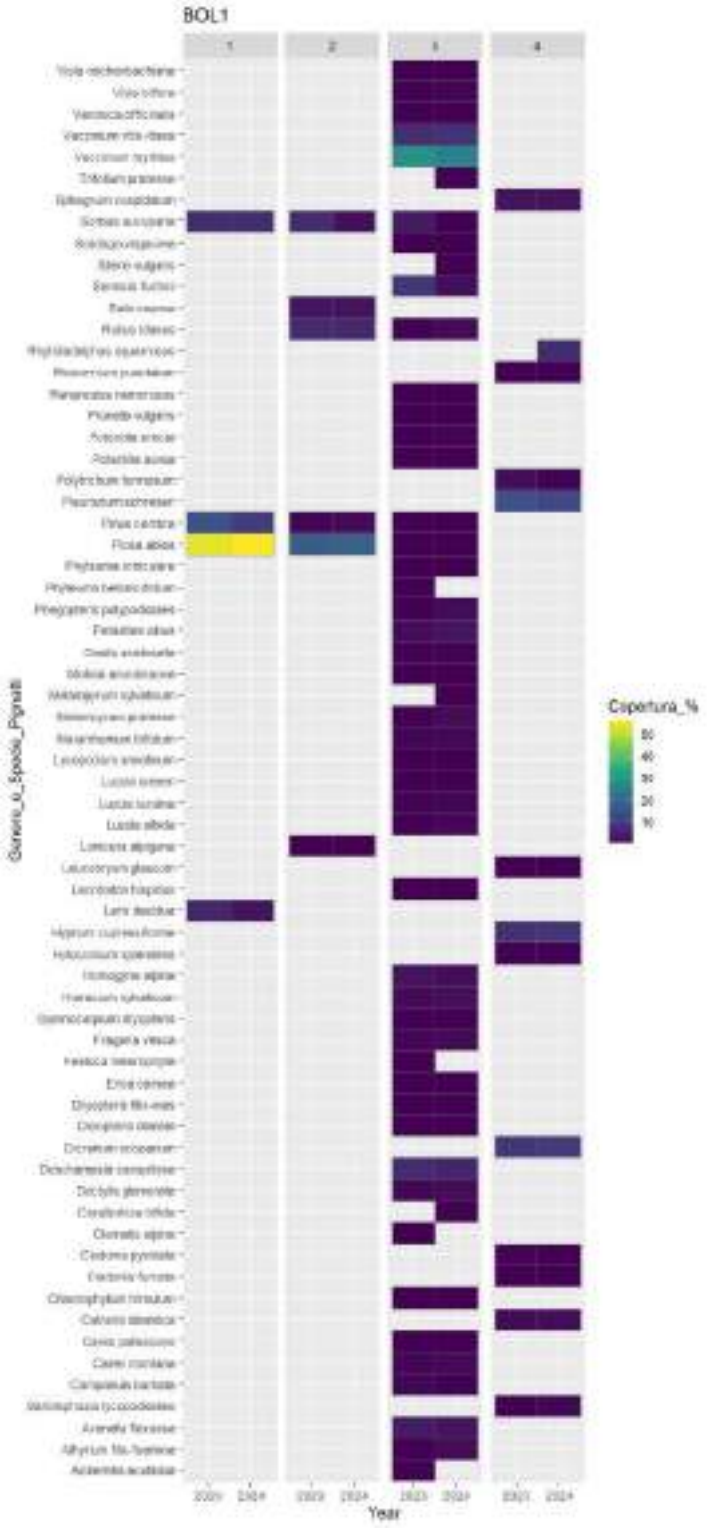

Figure 4.7.3. List of species, detected at BOL1 over the two of the project. For each species the mean cover (%) in the four layers is reported.

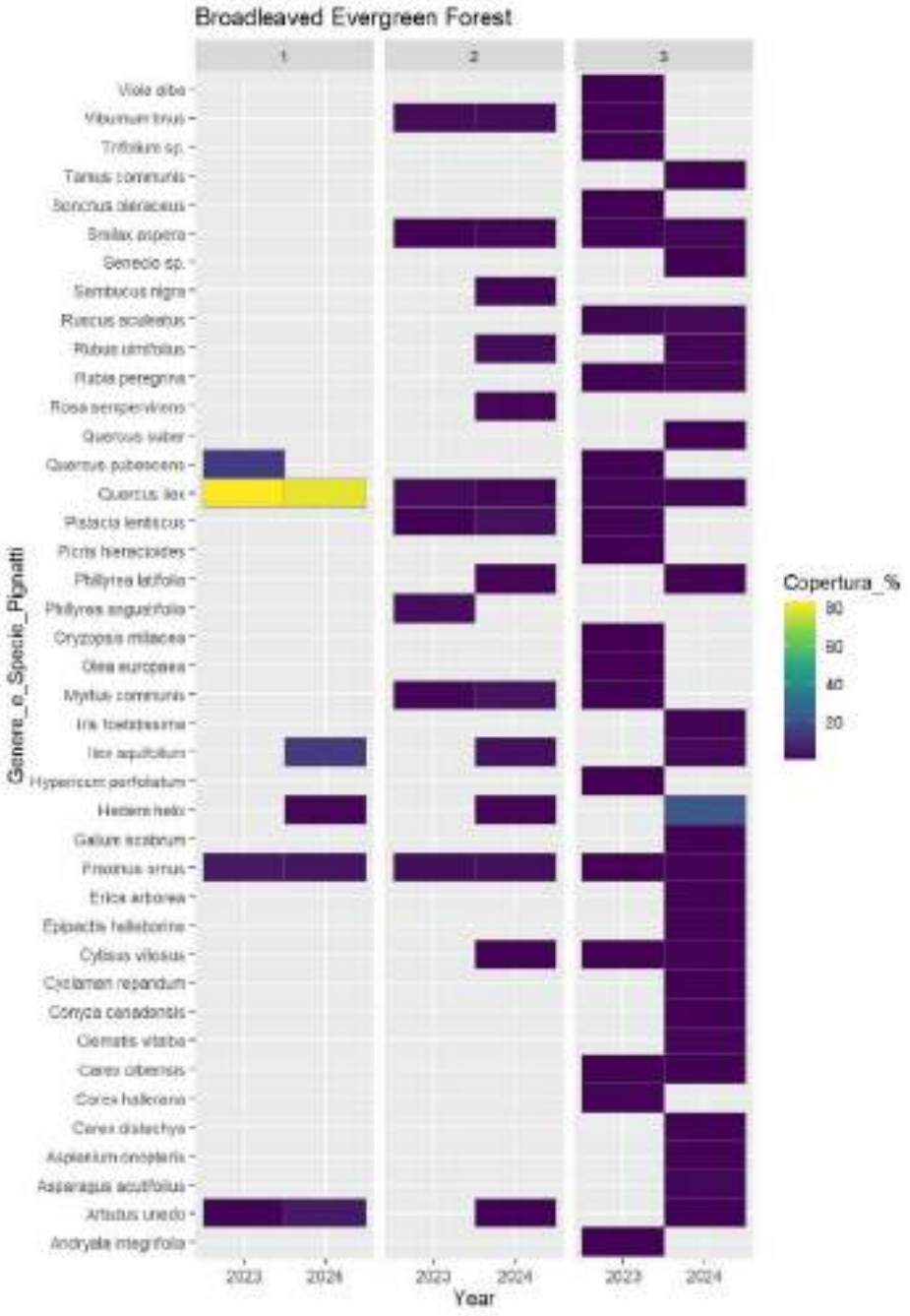

Figure 4.7.4. List of species, detected at BEF over the two of the project. For each species the mean cover (%) in the four layers is reported.

Figure 4.7.5 shows the trends of species richness at the 10 forest sites from 1999 to 2024.

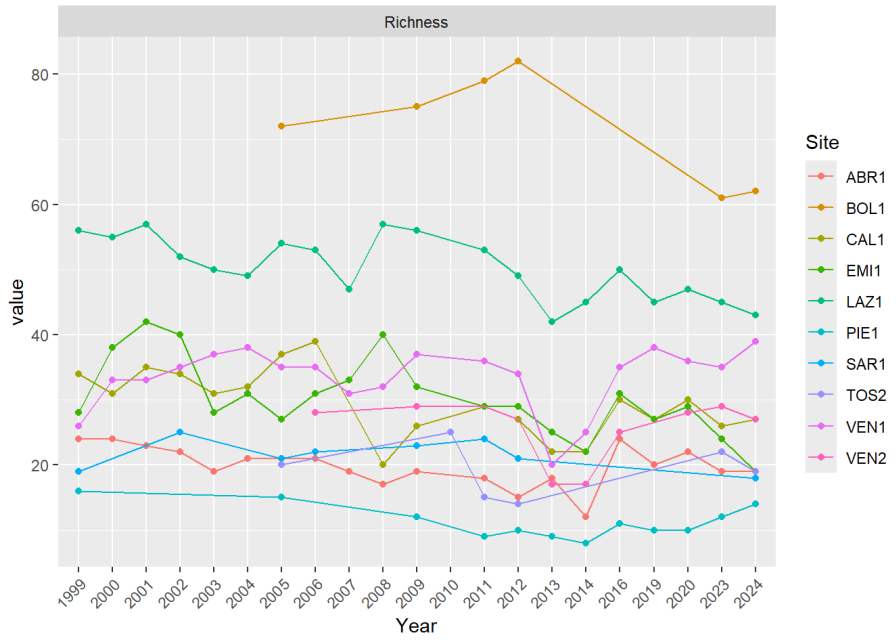

Figure 4.7.5. Trends of species richness at the 10 forest sites from 1999 to 2024.

Compositional Diversity

Figure 4.7.6 illustrates the distribution of the new indicator compositional diversity (MAX CD) at the 10 forest sites of the project, whereas Figure 4.7.7 shows its trend over the years.

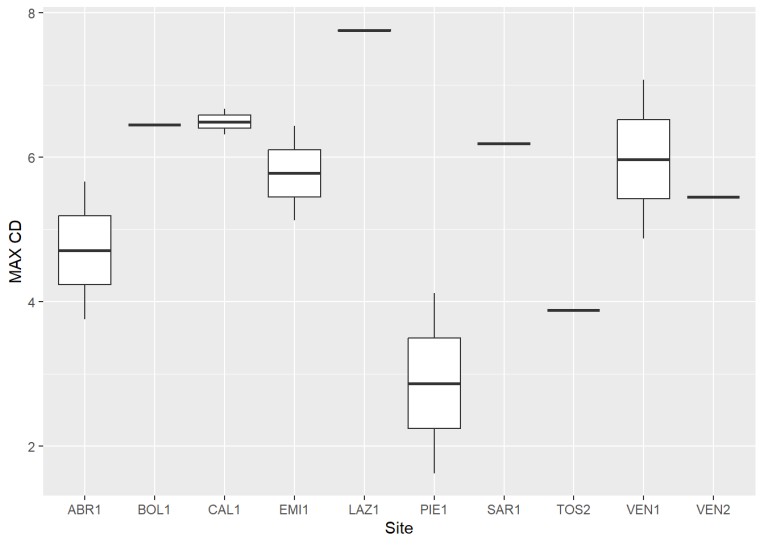

Figure 4.7.6. Boxplots showing the distribution of the variable Max CD in the 10 forest types of the project.

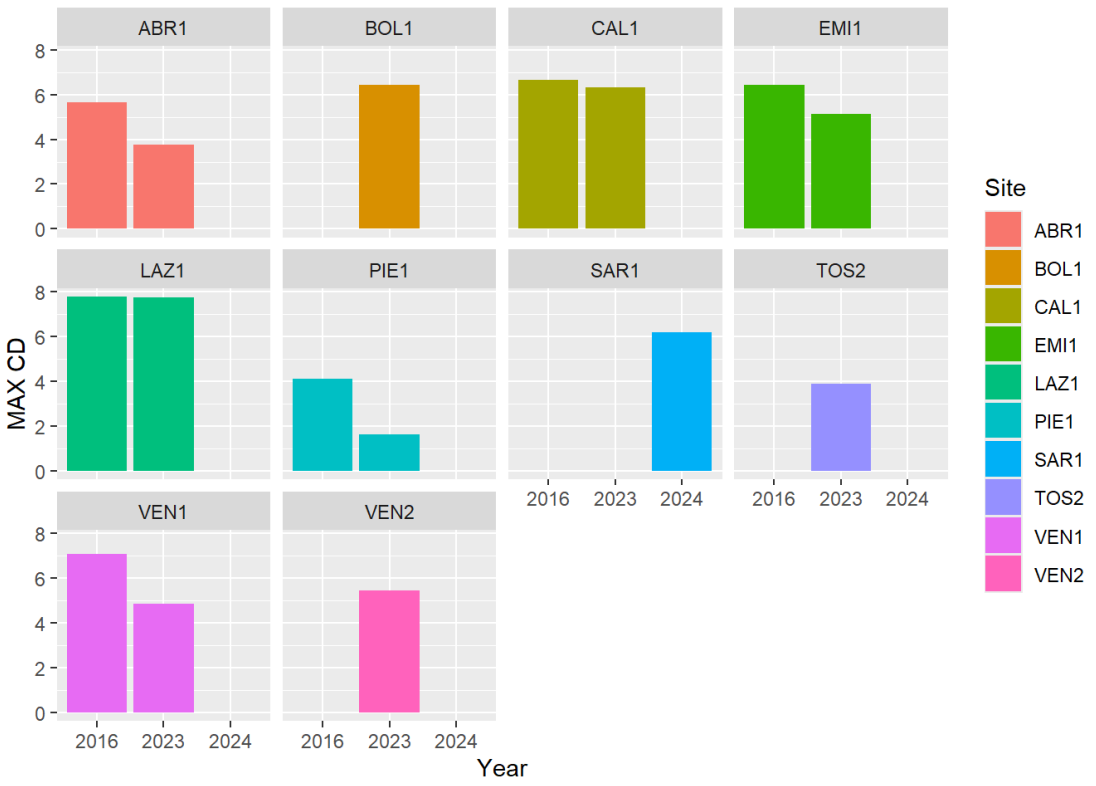

Figure 4.7.7. Trends of Max CD detected at the 10 forest sites of the project in the years 2016, 2023 and 2024.

Specific Leaf Area

Dry mass, leaf area, and Specific Leaf Area (SLA) were measured at the 10 forest sites of the project during 2023–2024 and analysed by forest type. Results for Broadleaved Deciduous Forests (BDF) and Broadleaved Evergreen Forests (BEF) are shown in Figures 4.7.8 and 4.7.9; Mountainous Beech Forests (MBF) and Mountainous Conifer Forests (MCF) are shown in Figure 4.7.10 and 4.7.11.

Broadleaved Deciduous Forests (BDF)

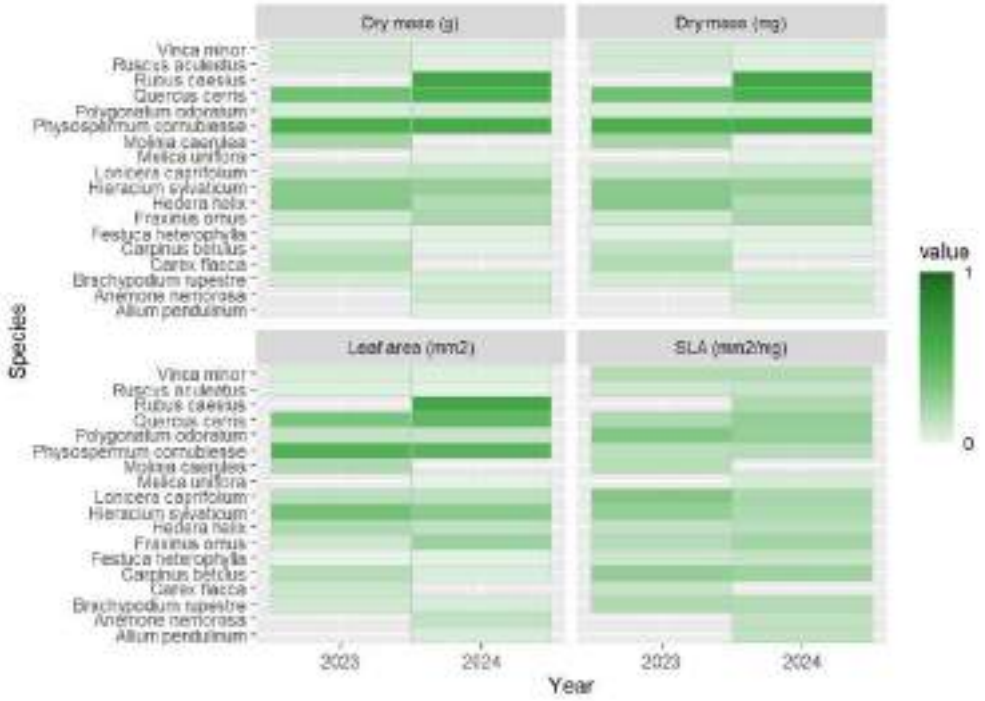

Figure 4.7.8. List of species with their dry mass, leaf area, and SLA obtained for Broadleaved Deciduous Forests (BDF).

Broadleaved Evergreen Forests (BEF)

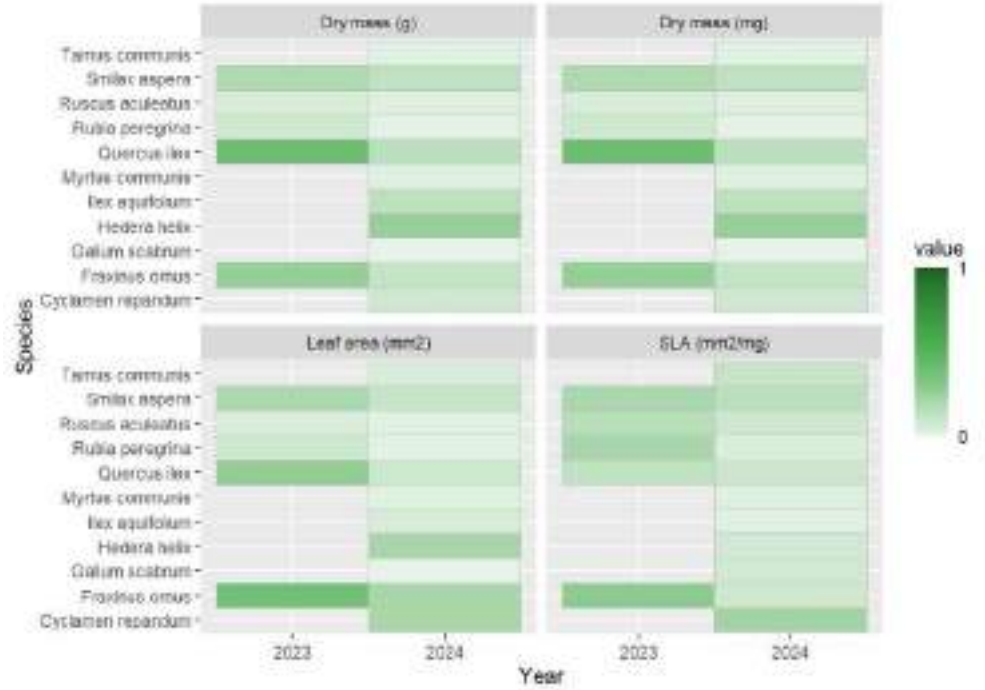

Figure 4.7.9. List of species with their dry mass, leaf area, and SLA obtained for Broadleaved Evergreen Forests (BEF).

Mountainous Beech Forests (MBF)

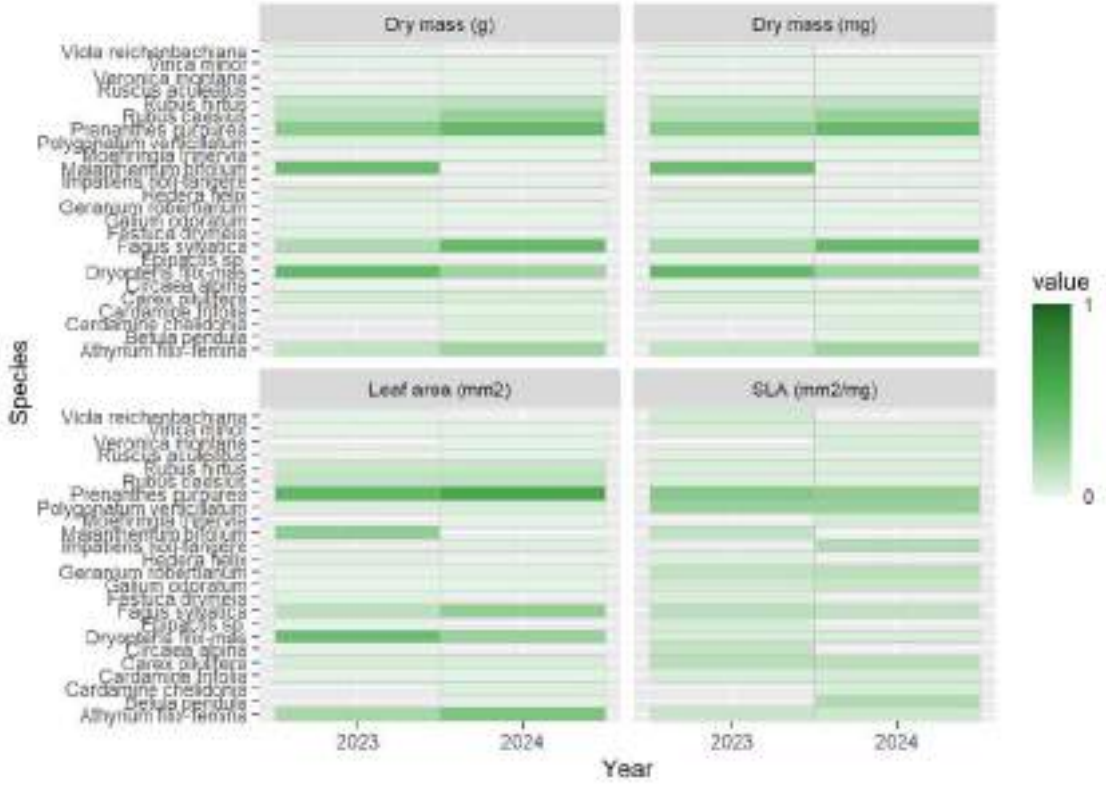

Figure 4.7.10. List of species with their dry mass, leaf area, and SLA obtained for Mountainous Beech Forests (MBF).

Mountainous Conifer Forests (MCF)

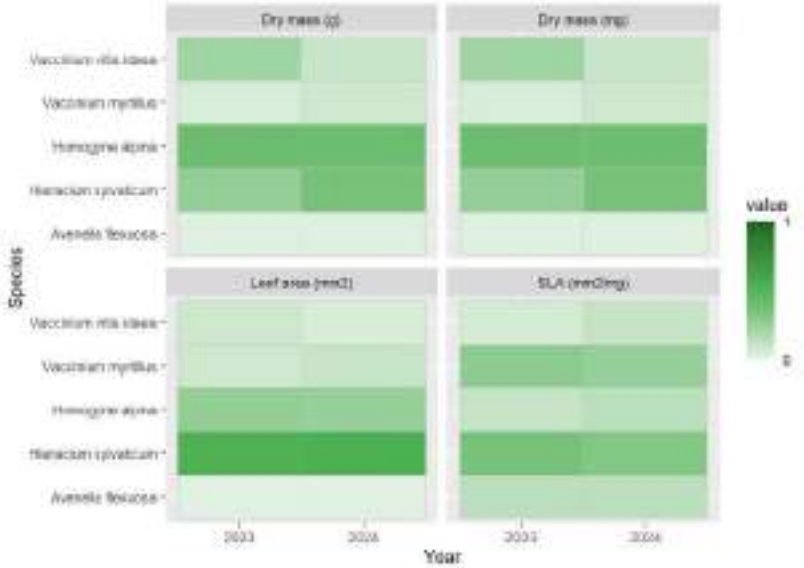

Figure 4.7.11. List of species with their dry mass, leaf area, and SLA obtained for Mountainous Conifer Forests (MBF).

Species ecology

Ellenberg's ecological indices, which describe the ecological requirements of each species for light availability (Ell-Light), humidity (Ell_moisture), temperature (Ell_Temp), nutrients (Ell_Nutrients), and soil acidity (Ell_Reaction), were used to identify potential trends in the time series.

For each ecological aspects, the nine index classes were grouped into three tertiles (see Campetella et al. 2005 modified). For instance, for light levels, the first tertile (classes 1, 2, 3) includes species that grow in low-light enviroments, the second tertile (classes 4, 5, 6) features generalist species, and the third tertile (classes 7, 8, 9) includes those in very bright environments. This applies similarly to other ecological factors as well.

Graphs depicting the trends over the years of the species grouped in the first and third tertiles (number of species and frequency) were obtained for each forest site (Figure 4.7.12) and for forest types (Figure 4.7.13). Figure 4.7.12 presents an illustrative example for ABR1, whereas Figure 4.7.13 shows the results for Mountainous Beech Forests.

Figure 4.7.12. Ellenberg's ecological indices: trends of the species (number and relative frequency) belonging to the first and the third tertile from 1999 to 2024 at the forest site ABR1.

Figure 4.7.12. Ellenberg's ecological indices: trends of the species (number and relative frequency) belonging to the first and the third tertile from 1999 to 2024. Results are categorized for Mountainous Beech Forests.

4.8 Crown condition

4.8.1 Dataset

In this report the results of crown condition assessment on the 10 forest "core" plots belonging to NEC network are shown. In addition, the assessment was carried out on the whole of the 31 ICP Forests Level II plots (CON.ECO.FOR.) and on the 261 ICP Forests Level I plots. The entire dataset ranges for a timespan from 1996 to 2024, allowing to individuate species-specific and site-specific

trends. General trends at national level are highlighted by the Level I survey. The results indicate a general increase of defoliation and mortality with a linear significant trend from 2010, in relation to extreme drought and heat waves, windstorms and pest attacks. Results concerning the extensive Level I survey were published by Bussotti et al. (2024).

Table 4.8.1 provides an overview of the dataset. Crown condition data cover 29 years (1996-2024) in the 10 forest sites of the project. Eight key variables have been considered for this analysis.

Table 4.8.1. Overview of the available dataset.

Forest sites (10)	• ABR1 (Selva Piana) • BOL1 (Renon) • CAL1 (Piano Limina) • EMI1 (Carrega) • LAZ1 (Monte Rufeno) • PIE1 (Val Sessera) • SAR1 (Marganai) • TOS2 (Cala Violina) • VEN1 (Cansiglio) • VEN2 (Bosco Fontana)
Variables (8)	Defoliation • Def M (average defoliation per area, %) • Def >25 (defoliation greater than 25%) • Def >60 (defoliation greater than 60%) • Def >85 (defoliation greater than 85%) • Def =100 (defoliation of 100%) Symptoms • LEAV (spread of symptoms on leaves) • BRAN (spread of symptoms on branches) • TR (spread of symptoms on the stem)
Years (29)	From 1996 to 2024

4.8.2 Results and discussion

Figure 4.8.1 shows the trends of the variables in the surveys (time span 1996-2024).

Figure 4.8.1. Trends of the variables related to crown condition at the 10 forest sites in the period 1996-2024.

The correlation among variables has been studied for each forest site over the years (Pearson's correlation). Figure 4.55 provides an example of the results obtained for ABR1 (Figure 4.8.2, above) and CAL1 (Figure 4.8.2, below).

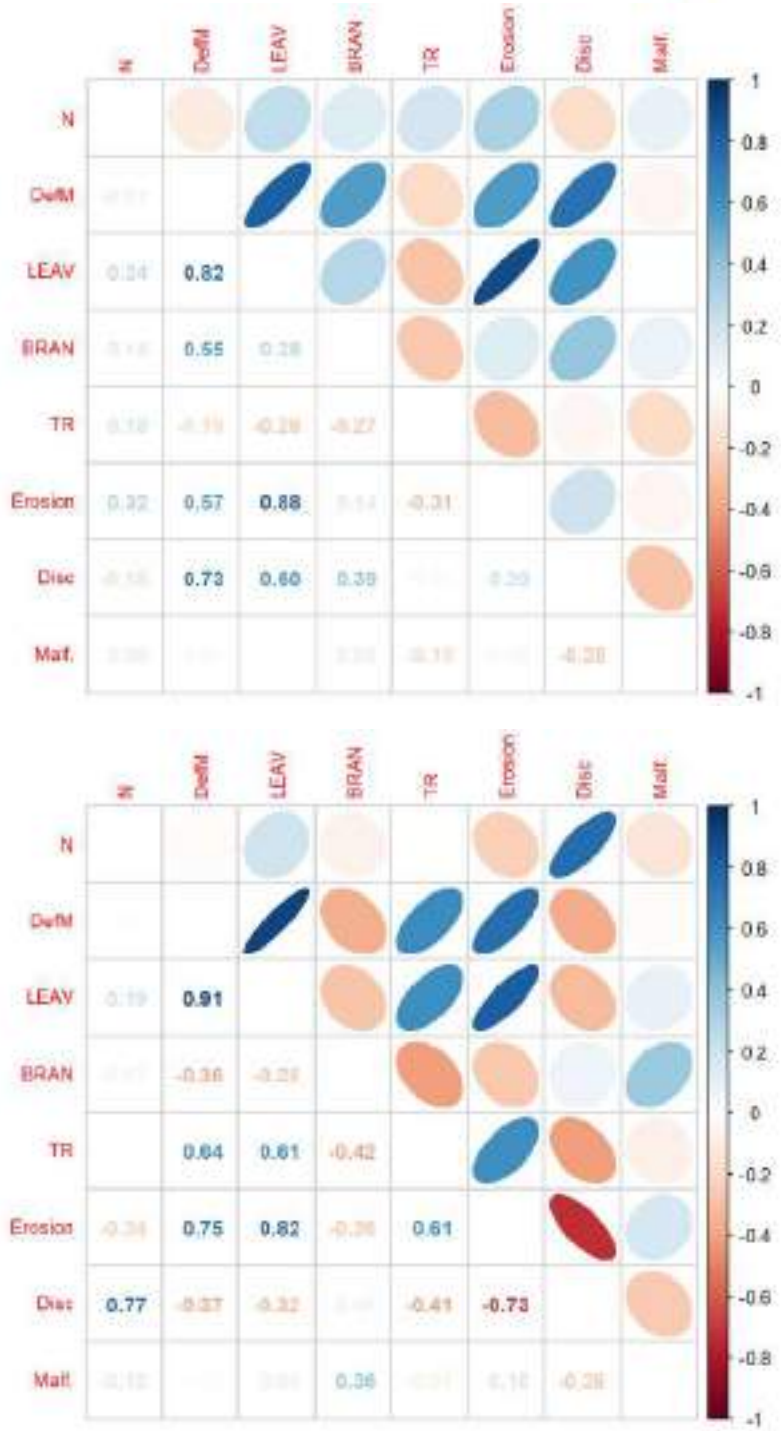

Figure 4.8.2. Pearson's correlation among variables over the years for ABR1 (above) and CAL1 (below).

Analysis of forest sites reveals varying defoliation patterns over time. Figure 4.8.3 compares the responses of *Fagus sylvatica* stand of the siteABR1 and *Quercus ilex* stand of TOS2 plots. ABR1 shows

a sudden and strong increase of the number of defoliated trees between 2016 and 2018, as consequence of the late frost that affected the beechwoods in Central and Southern Apennines in 2016, and the next extreme drought and heat wave occurred in 2017. The high rates of defoliated trees in recent years are to be connected to the increasing conditions of drought and higher summer temperatures. TOS2 shows high rates of defoliated trees, that is to be expected in Mediterranean conditions. However, also for this species defoliation is increasing in recent years because of harshening climatic conditions and pest attacks.

Other relevant findings concern EMI1 (*Quercus petraea* and *Quercus cerris*) plot, with high mortality of *Q. petraea* trees subsequent dry years, and the alpine coniferous forests (not in the core NEC network) FRI1 and TRE1, withPicea abies, destroyed respectively by Ips typographus attacks and Vaia windstorm.

Symptoms were analyzed from a timespan from 2005 to 2019, when comparable methods were applied. Symptoms on leaves (erosions, discolorations, malformations) were prevalent with respect to symptoms on branches and stem. The diffusion of symptoms is correlated to defoliation; thus it evidences the impact of disturbances on tree crown integrity.

ABR1	

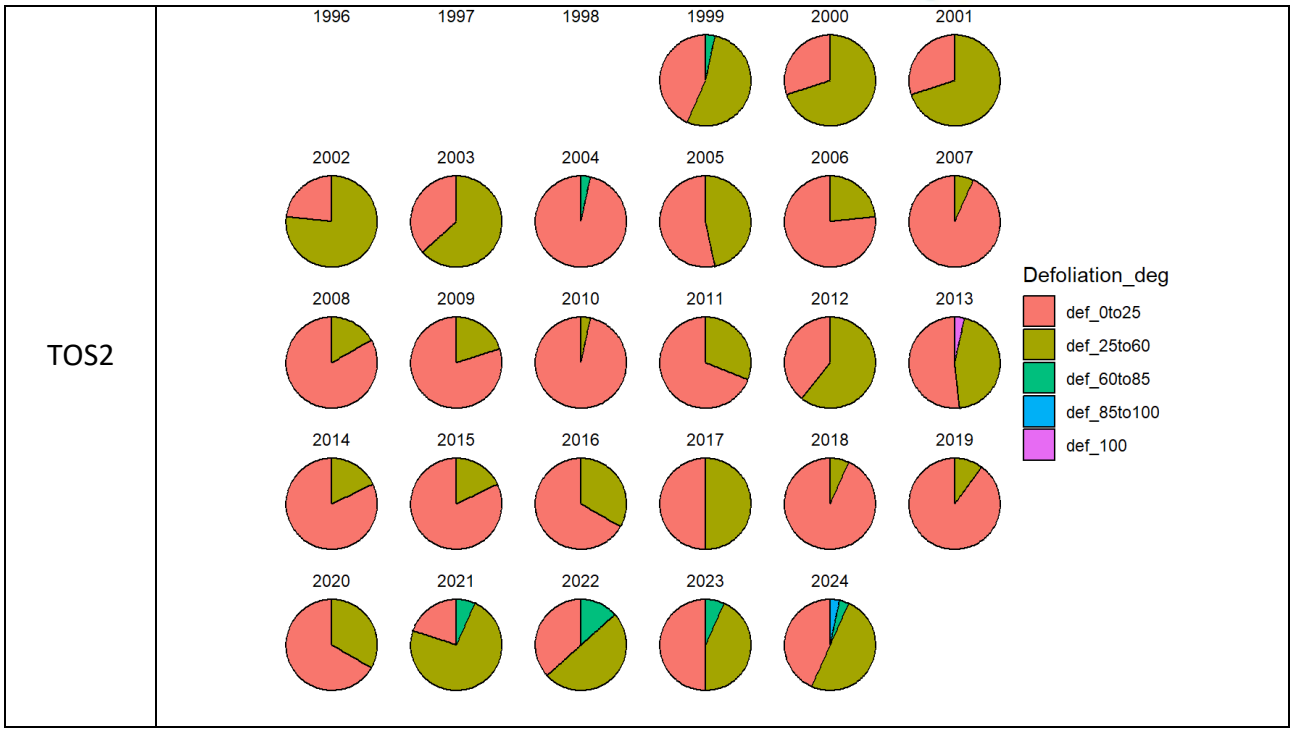

Figure 4.8.3. Pie-charts showing the distribution of the percentage of classes of defoliation in the considered period.

Principal Component Analysis (PCA) on autoscaled data (Figure 4.8.4) shows that sites with symptoms and defoliation – mainly Broadleaved Deciduous Forests (e.g., VEN2, EMI1), and Broadleaved Evergreen Forests (SAR1, TOS2) are associated to positive PC1 values. In contrast, negative PC1 values correspond to MBF (ABR1, VEN1, CAL1) and MCF (BOL1), which have low symptoms and defoliation.

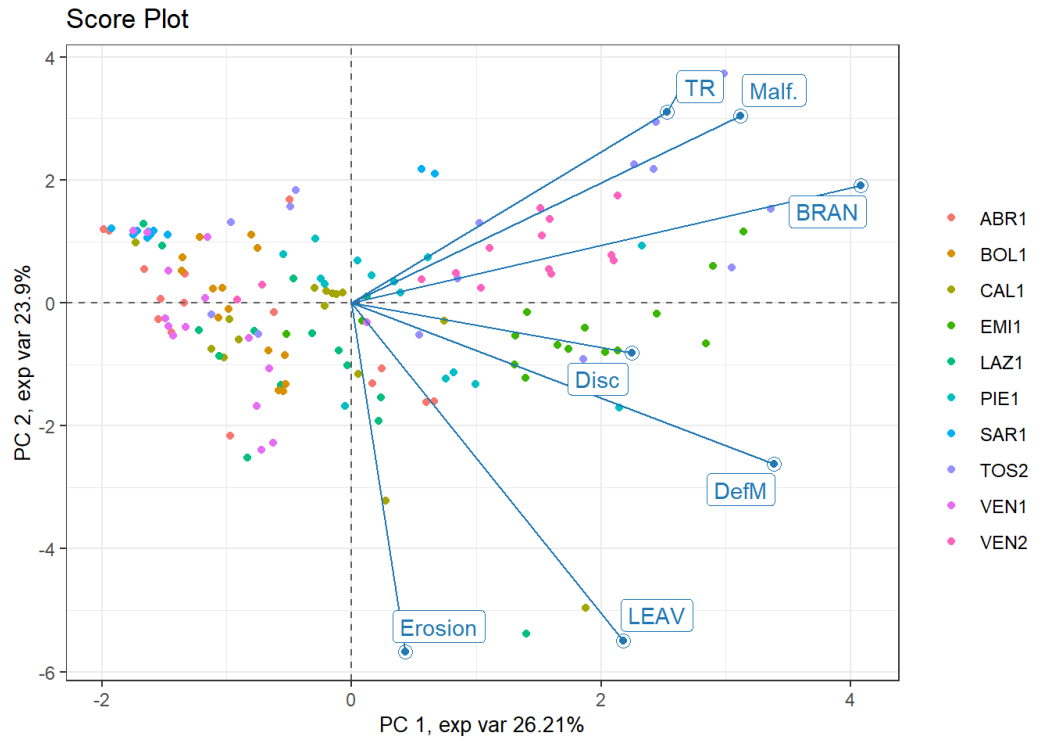

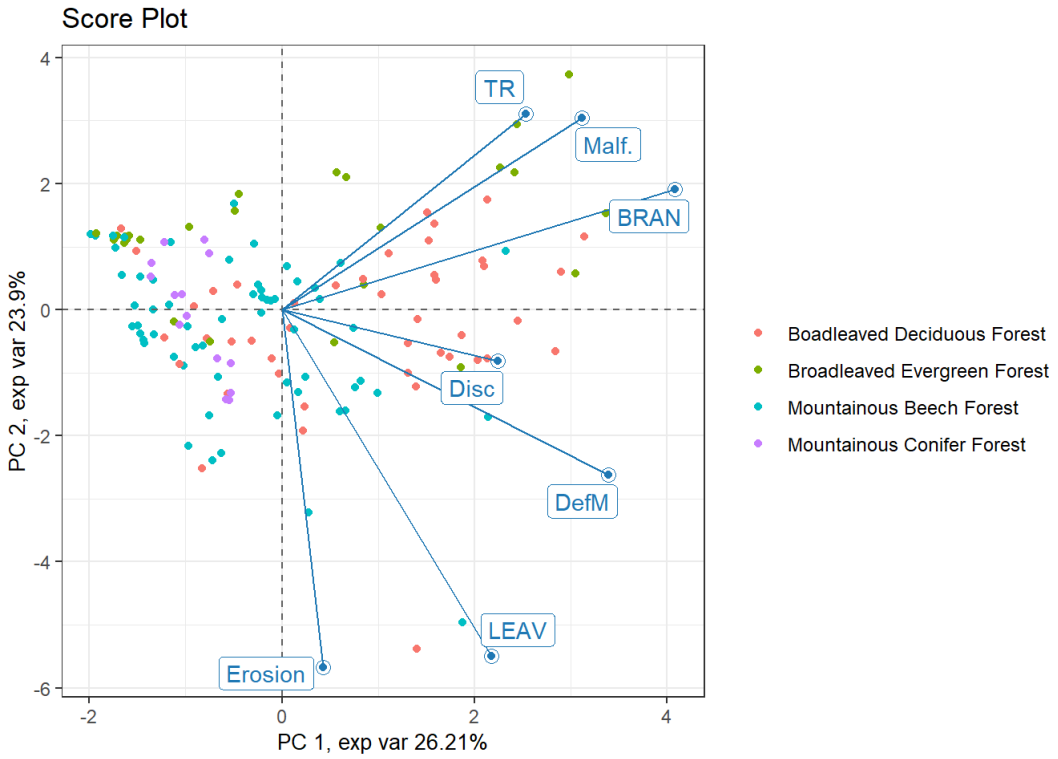

Figure 4.8.4. Results of the PCA on autoscaled data.

4.9 Chlorophyll fluorescence and content

4.9.1 Dataset

Table 4.9.1 provides an overview of the dataset. Chlorophyll data cover 9 forest sites in the 2 central years of the project (2023 and 2024). Ten key variables have been considered for this analysis.

Table 4.9.1. Overview of the available dataset.

Forest sites (9)	• ABR1 (Selva Piana) • CAL1 (Piano Limina) • EMI1 (Carrega) • LAZ1 (Monte Rufeno) • PIE1 (Val Sessera) • SAR1 (Marganai) • TOS2 (Cala Violina) • VEN1 (Cansiglio) • VEN2 (Bosco Fontana)
Variables (10)	Chlorophyll fluorescence parameters • Fv/Fm • PSIo • Sm • PI(abs) • IP-phase • Pitot • Chl Leaf morphology parameters • LA (Leaf Area, 15 leaves, cm^2) • DW (Dry Weight, 15 leaves, g) • SLA (Specific Leaf Area, $cm^2\ g^{-1}$)
Years (2)	2023 and 2024

4.9.2 Results and discussion

The analysis of Chlorophyll a Fluorescence (ChlaF), with the Prompt Fluorescence (PF) technique, is a simple and quick non-destructive method that gives information on the state and functionality of photosystems. JIP-test parameters are considered as a proxy for photosynthetic efficiency. The application of this technique on tall trees in forests was tested in previous European projects.

Within LIFE Modern(NEC) the photosynthetic properties of leaves were assessed jointly with the sampling for foliar chemistry during the years 2023-2024. The parameters measured were: FV/FM (maximum quantum yield of photons in dark adapted leaves); PSI_0 (capacity to move a trapped electron into the ETC – Electron Transport Chain – at the PSII side); Sm (pool of the electron carriers); IP-phase (measure of the efficiency of the electron flux through PSI to reduce the final acceptors of the electron transport chain); Performance Indices: PIabs - Performance Index (potential) for energy conservation from photons absorbed by PSII to the reduction of intersystem electron acceptors; PItot: Performance index (potential) for energy conservation from photons absorbed by PSII to the reduction of PSI end acceptors. In addition, leaf morphological parameters such as dry weight (DW), leaf area (LA) and specific leaf area (SLA = LA/DW) were assessed. Chlorophyll content was assessed by a chlorophyll-meter (optical device for non-destructive measurement of the pigment content) and expressed in arbitrary units.

Figure 4.9.1 shows the trends of the variables in the two years of the project (2023 and 2024).

Figures 4.9.2 provides a comparison of the distribution of the variables in the two years, while in Figure 4.9.3 the plots are categorized by forest types.

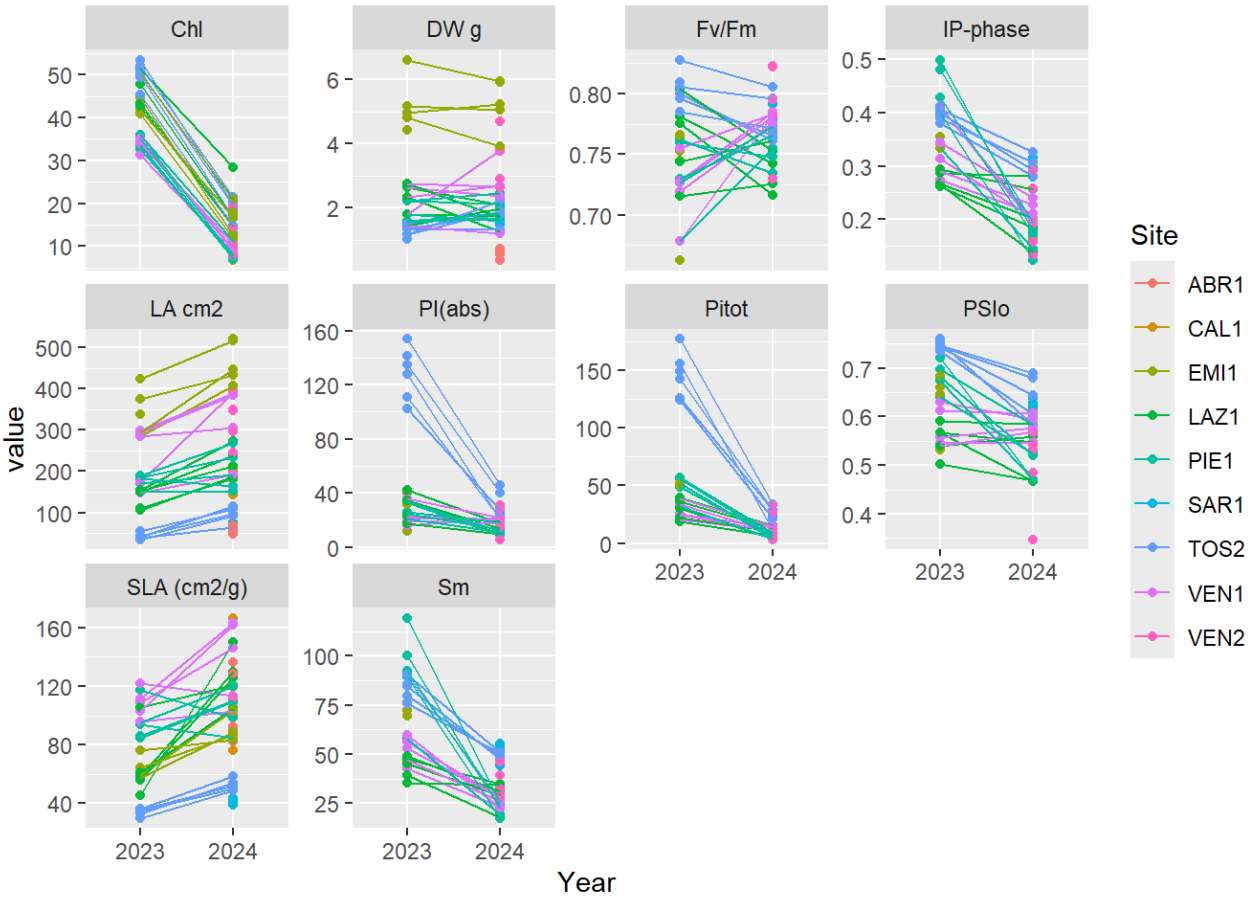

Figure 4.9.1. Trends of the 10 variables related to chlorophyll fluorescence at 9 forest sites in 2023 and 2024.

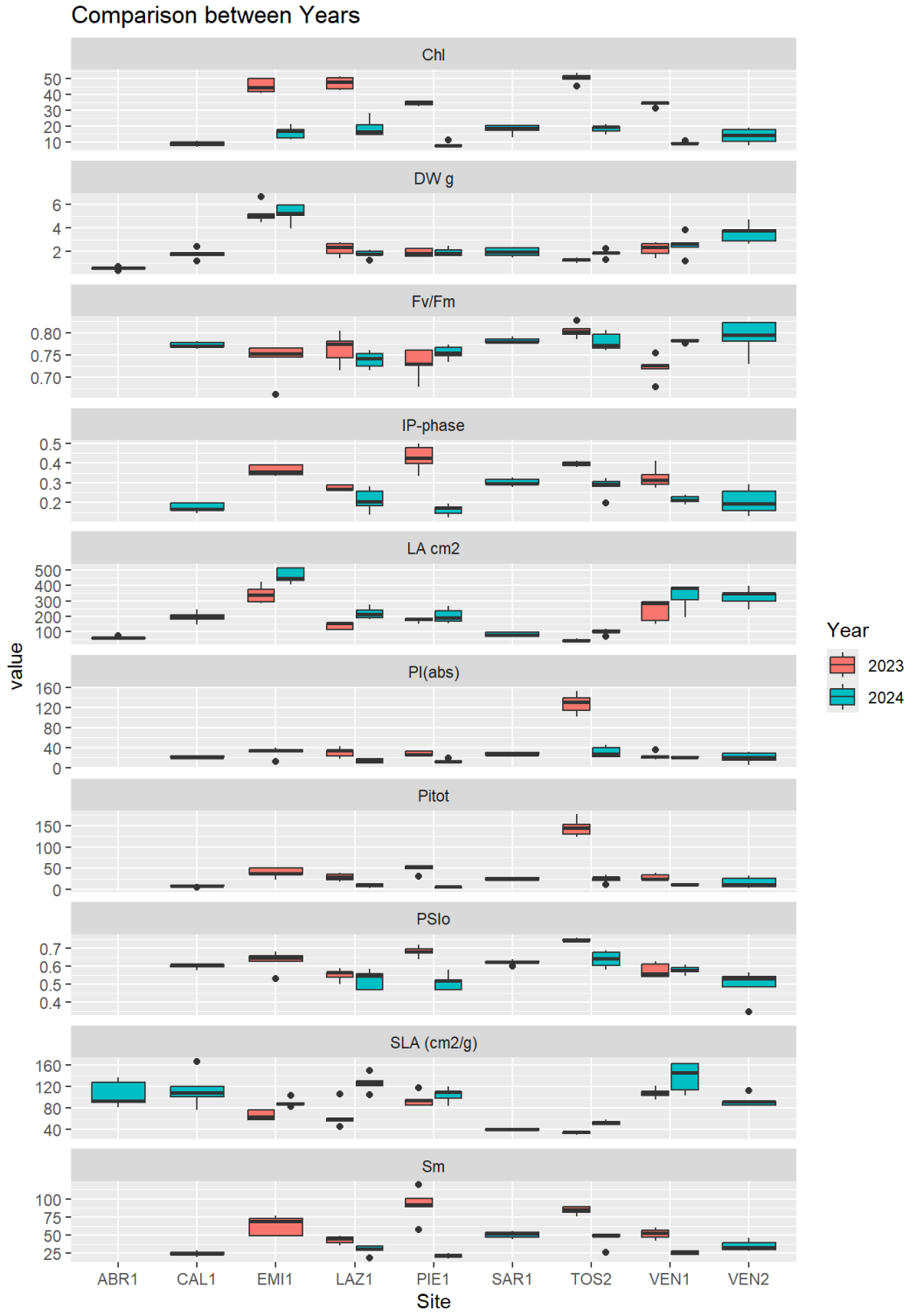

Figure 4.9.2. Boxplots with the distribution of the variables in the two years.

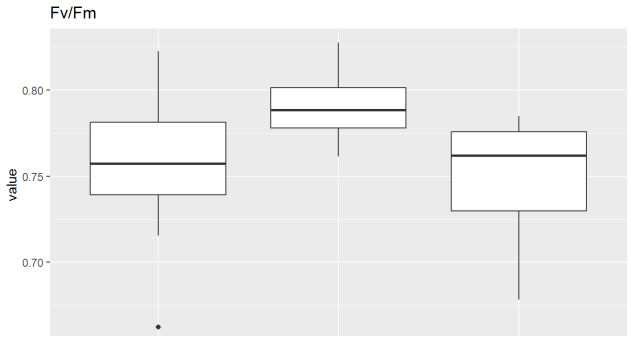
Fv/Fm
value
0.80
0.75
0.70

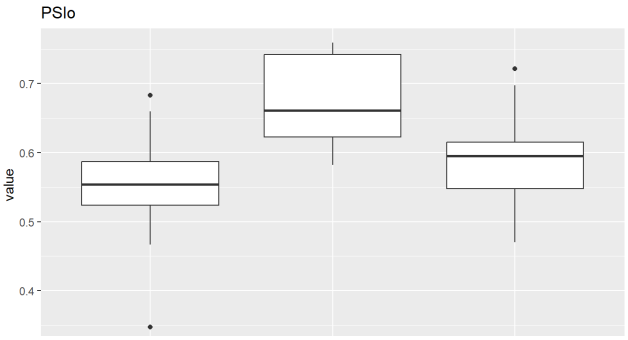
PSIo
value
0.7
0.6
0.5
0.4

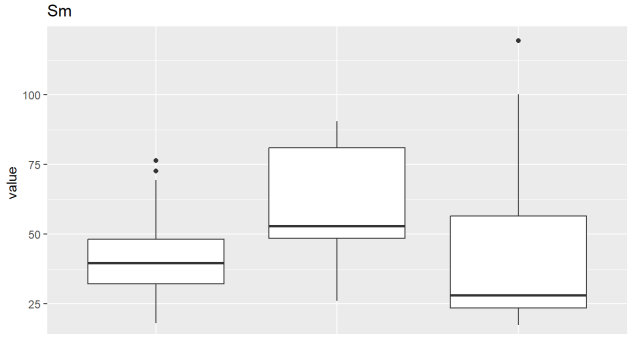
Sm
value
100
75
50
25

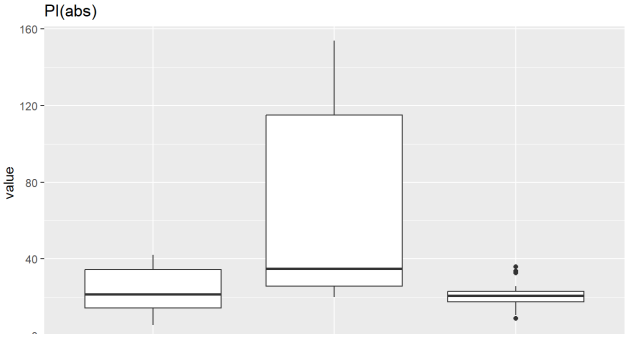
PI(abs)
value
160
120
80
40

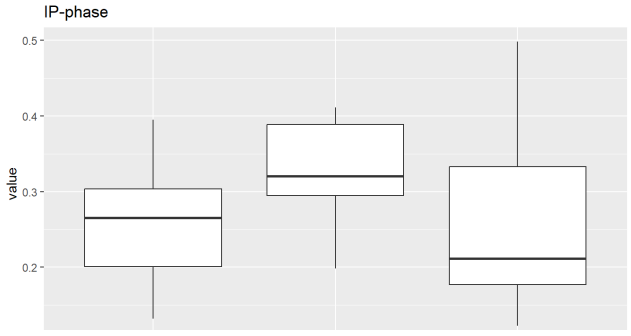
IP-phase
value
0.5
0.4
0.3
0.2

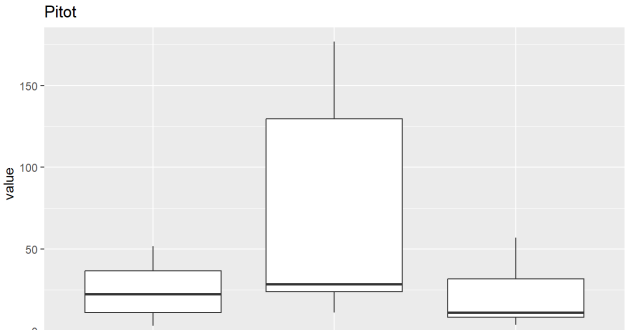
Pitot
value
150
100
50

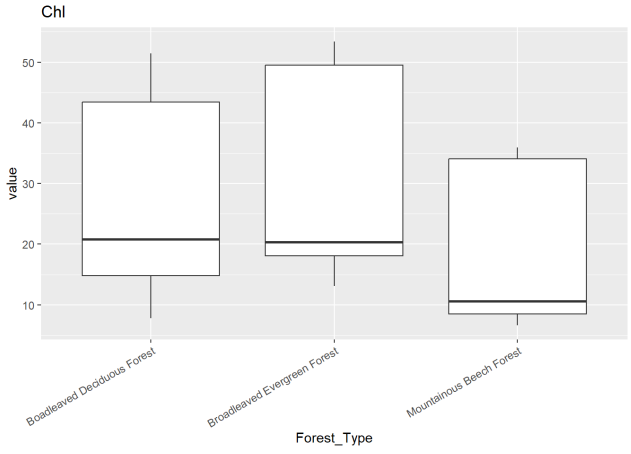
Chl
value
50
40
30
20
10
Boadleaved Deciduous Forest
Broadleaved Evergreen Forest
Mountainous Beech Forest
Forest_Type

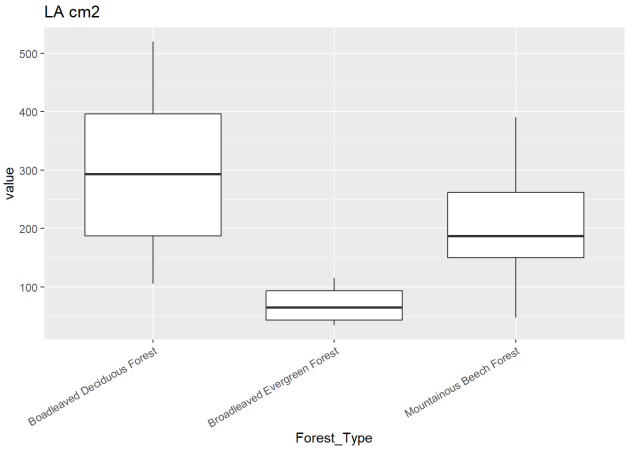
LA cm2
value
500
400
300
200
100
Boadleaved Deciduous Forest
Broadleaved Evergreen Forest
Mountainous Beech Forest
Forest_Type

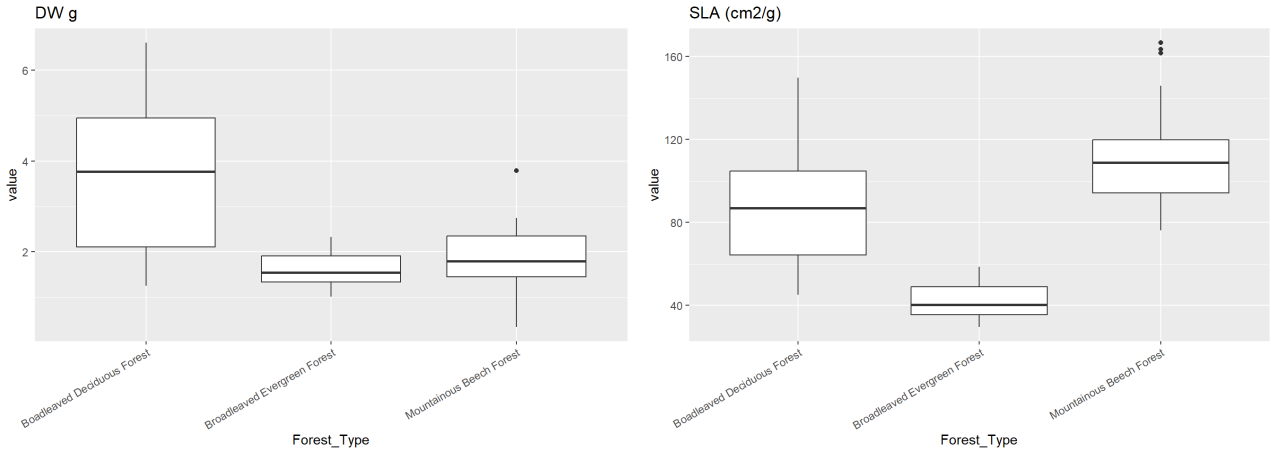

Figure 4.9.3. Boxplots with the distribution of the variables by forest types.

Principal Component Analysis (PCA) was performed on autoscaled data (Figure 4.9.4). Positive PC1 values indicated higher fluorescence parameters (e.g. PSIo, Pitot, PI(abs), IP-phase, Chl, Sm), which characterize the results from PIE1 and TOS2 during the 2023 survey. Negative PC1 values correspond to greater SLA measured during the 2024 survey at VEN1 and VEN2 sites.

The 2023 and 2024 surveys are distinguished along PC2, with 2024 observations showing higher Fv/Fm (TOS2) and lower measurements of IP-phase, Chl, Sm. The site EMI1 is characterized by high values of dry weight (DW).

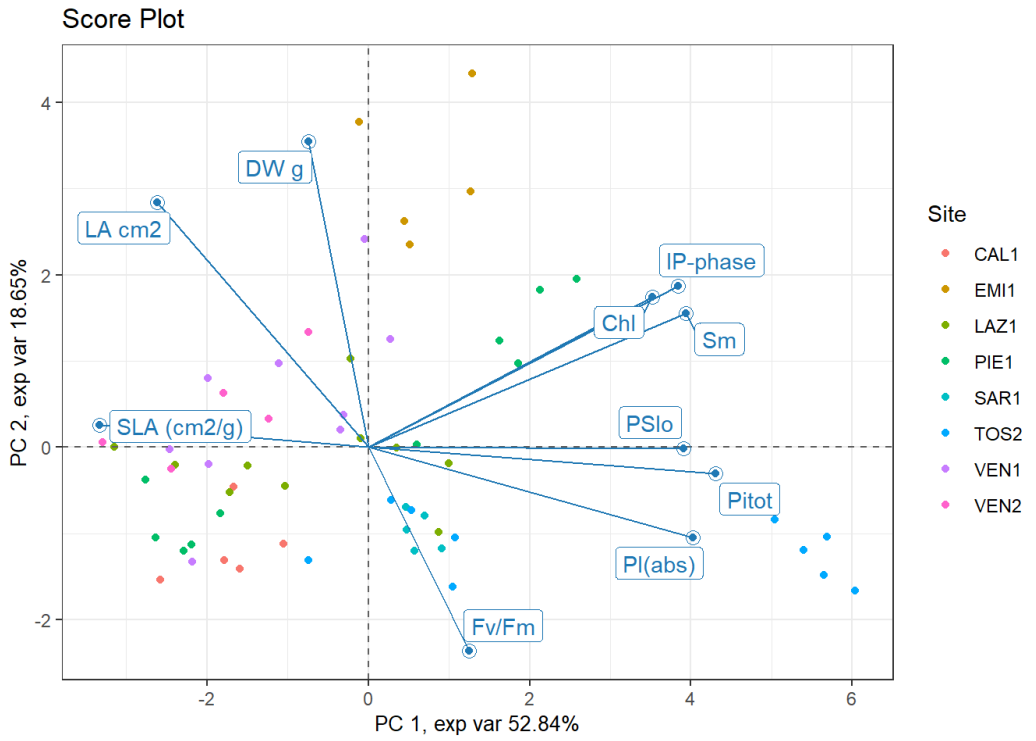

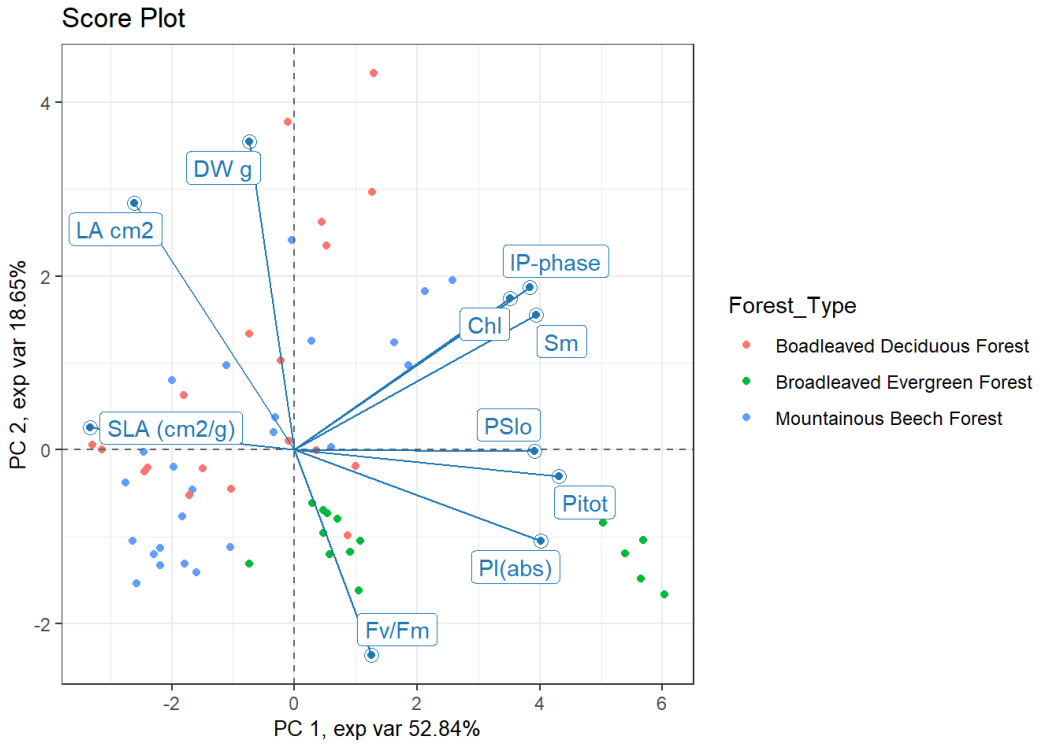

Figure 4.9.4. Results of the PCA on autoscaled data (→ continues).

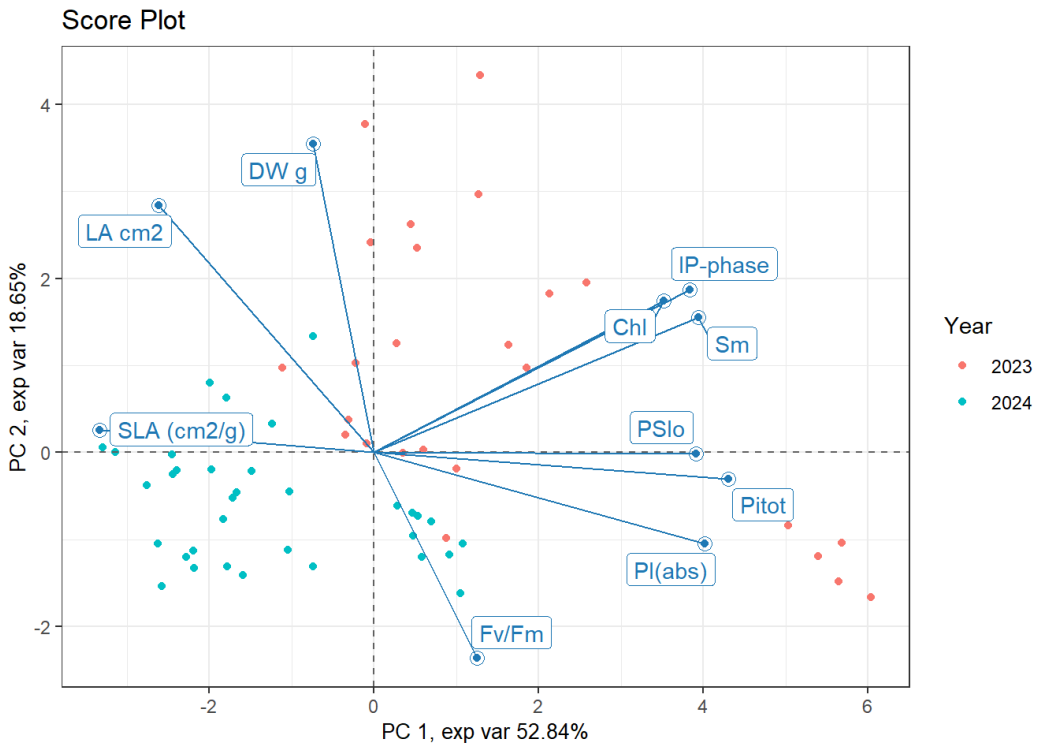

Figure 4.9.4. Results of the PCA on autoscaled data.

The results are preliminary and further data analysis are needed to define baseline values and evaluate oscillations for the construction of long-term trends. Possible factors for trend and year-to-year oscillation include: (i) N fertilization and worsening of the tree nutritional status that affect the construction of the photosynthetic apparatus; (ii) leaf photobleaching due to high temperature and solar irradiation; (iii) pest attacks.

4.10 Foliar chemistry

4.10.1 Dataset

Table 4.10.1 presents an overview of the dataset. The data on foliar chemistry cover the two central years of the project (2023 and 2024) across 10 forest sites. The analysis includes 9 variables.

Table 4.10.1. Overview of the available dataset.

Forest sites (10)	• ABR1 (Selva Piana) • BOL1 (Renon) • CAL1 (Piano Limina) • EMI1 (Carrega) • LAZ1 (Monte Rufeno) • PIE1 (Val Sessera) • SAR1 (Marganai) • TOS2 (Cala Violina) • VEN1 (Cansiglio) • VEN2 (Bosco Fontana)
Variables (12)	• C (g kg^{-1}) • N (g kg^{-1}) • S (g kg^{-1}) • P (g kg^{-1}) • K (g kg^{-1}) • Ca (g kg^{-1}) • Mg (g kg^{-1}) • Ca/Mg • N/P
Years (2)	2023 and 2024

4.10.2 Results and discussion

Figure 4.10.1 compares the distribution of the variables across the two years of the project, grouping the 10 sites by forest type. All parameters show low variability between the two surveys.

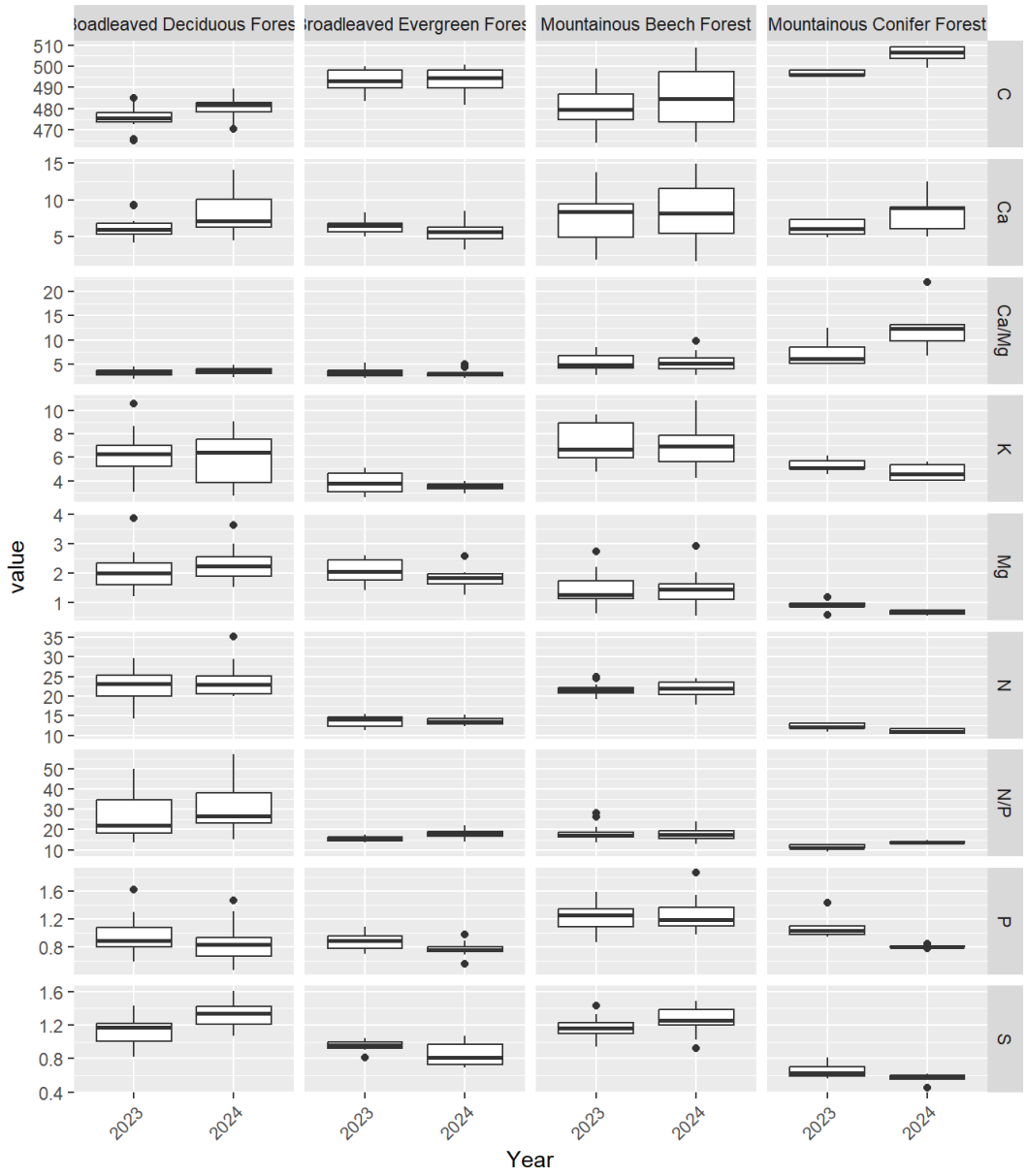

Figure 4.10.1. Boxplots with the distribution of the variables in the two years.

The correlation among variables has been studied for each forest type over the years (Pearson's correlation). Figure 4.10.2 provides an example of the results obtained for Boadleaved Deciduous Forests (BDF, Figure 4.10.2, above) and Broadleaved Evergreen Forests (BEF Figure 4.10.2, below).

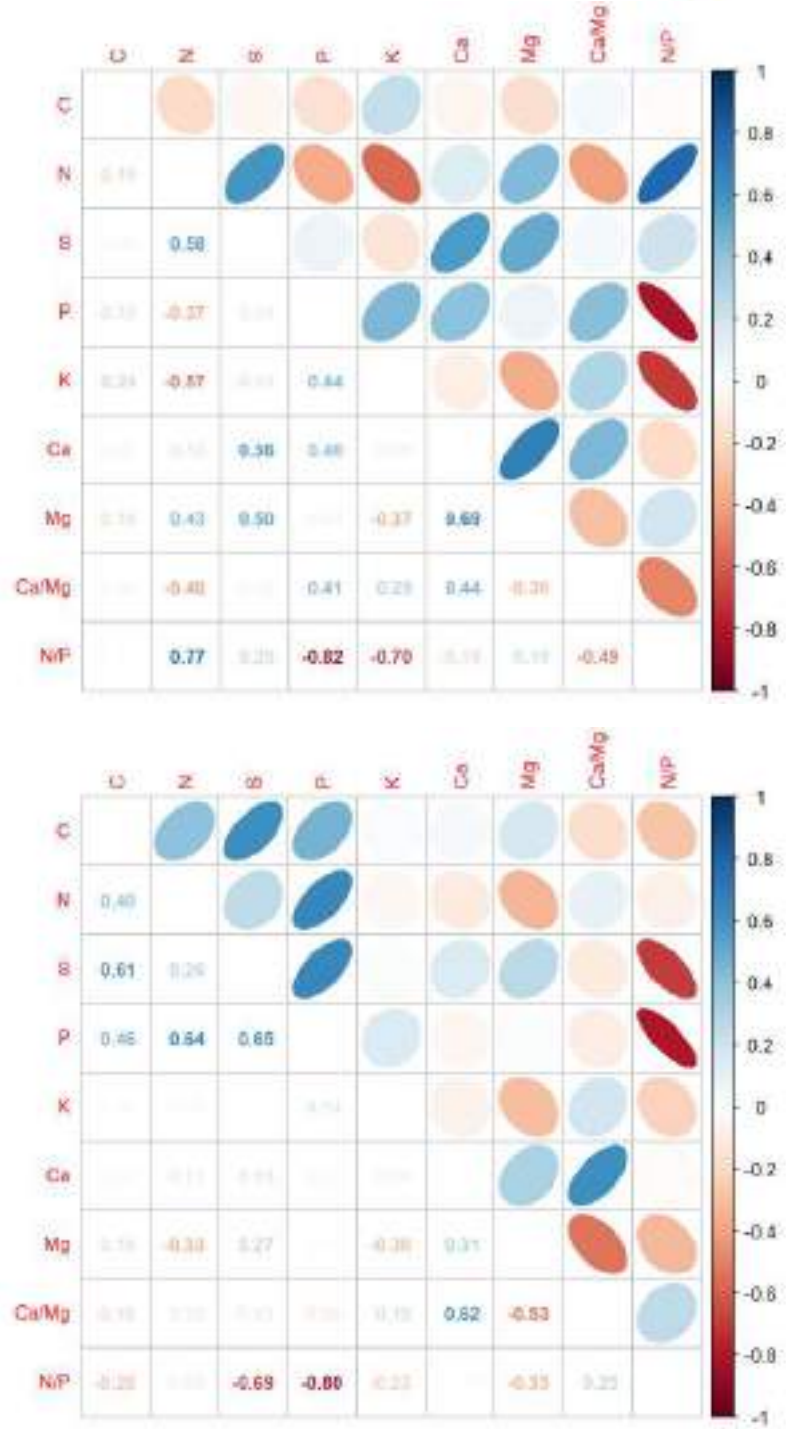

Figure 4.10.2. Pearson's correlation among variables over the years for Boadleaved Deciduous Forests (BDF, above) and Broadleaved Evergreen Forests (BEF, below).

Principal Component Analysis (PCA) was performed on autoscaled data (Figure 4.10.3). Positive values of PC1 reflect an increasing gradient of foliar Carbon content (C), whereas negative value of the axis are associated with increased Sulfur (S) and Nitrogen (N) levels. The BOL1, SAR1 and TOS2 sites show high values of C. The EMI1 Site shows higher concentrations of Mg and increased N:P ratio. The ABR1, CAL1 and VEN1 sites shows high value of Ca, K and P.

Observations belonging to the same forest type groups together:

- Broadleaved Evergreen Forests (SAR1, TOS2) and Mountainous Conifer Forests (BOL1) are characterized by high values of C.
- Boadleaved Deciduous Forests (EMI1) are characterized by high values of S, N, Mg and N/P.
- Mountainous Beech Forests (ABR1, CAL1 and VEN1) are characterized by high values of Ca, K, P.

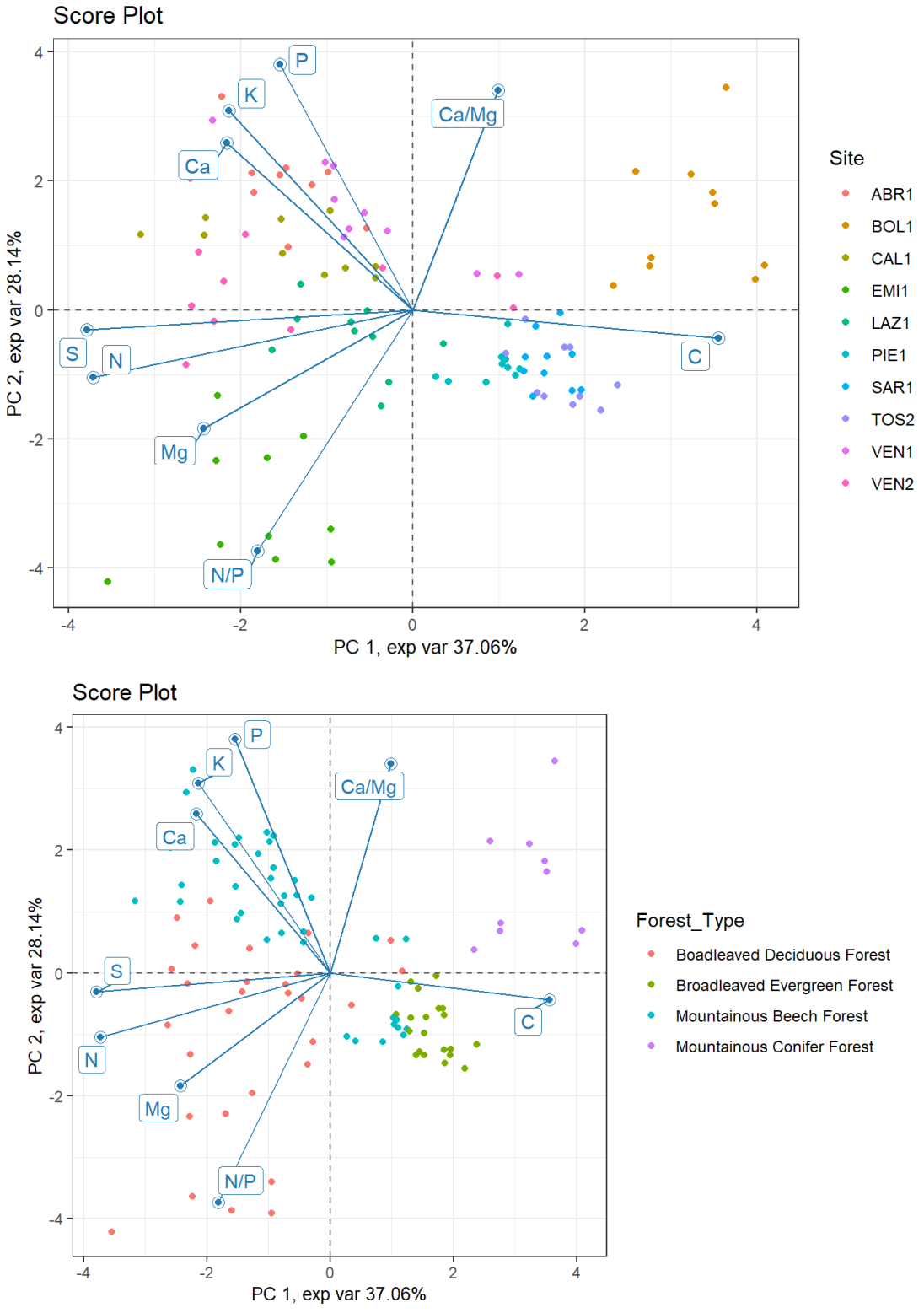

Figure 4.10.3. Results of the PCA on autoscaled data.

4.11 Forest growth

4.11.1 Dataset

Table 4.11.1 presents an overview of the dataset. The data on forest growth spans 1997 to 2020 across 10 forest sites. The analysis includes 12 variables. The surveys are 6 and are the base to provide variables dynamics and trends. Tree biomass (Volume) in relation with forest age, stand current growth capacity (IcV) and its current growth phase (ImV), together, are the main variables able to represent forests' overall biological state and can be considered as the main explanatory and responsive variables (Dobbertin 2005) providing a sensitive response to impacts. Indeed a healthy and vital forest grows according to a consolidated pattern that may highlight any disturbances influencing the forest's growth environment, atmosphere, and soil.

Table 4.11.1. Overview of the available dataset.

Forest sites (10)	• ABR1 (Selva Piana) • BOL1 (Renon) • CAL1 (Piano Limina) • EMI1 (Carrega) • LAZ1 (Monte Rufeno) • PIE1 (Val Sessera) • SAR1 (Marganai) • TOS2 (Cala Violina) • VEN1 (Cansiglio) • VEN2 (Bosco Fontana)
Variables (12)	• Tree density (n ha-¹) • Mortality (n ha-¹) • Ingrowth (n ha-¹) • Basal area (total) (m^2 ha-¹) • Mean dbh (cm) • Mean height (m) • Dom dbh (cm) • Top height (m) • Volume (m^3 ha-¹) • Age (years) • ImV (Volume Increment, mean, m^3 ha-¹) • IcV annuo (Yearly Volume Increment, m^3 ha-¹)
Years (7)	1997, 2000, 2005, 2010, 2015, 2020

4.11.2 Results and discussion

Figure 4.11.1 shows the trends of the variables in the six surveys (time span 1997-2020). Plot ages at the last survey vary from the minimum of 65 to the maximum of 200 years. All structural variables analyzed are consistent with forest ages and main tree species ecology.

Figure 4.11.2 provides the distribution of the variables by categorizing the plots in four forest types: Broadleaved deciduous forest (3 plots); Broadleaved evergreen forest (2 plots); Mountainous beech forest (4 plots); Mountainous conifer forest (1 plot).

Values and trends are shaped by forest age and trees species auto-ecology in the frame of changing climate conditions. Volume, as we can see, has a positive trend for all forest types meaning that those forests are still growing at the ages considered and also suggesting their good “health and vitality” conditions.

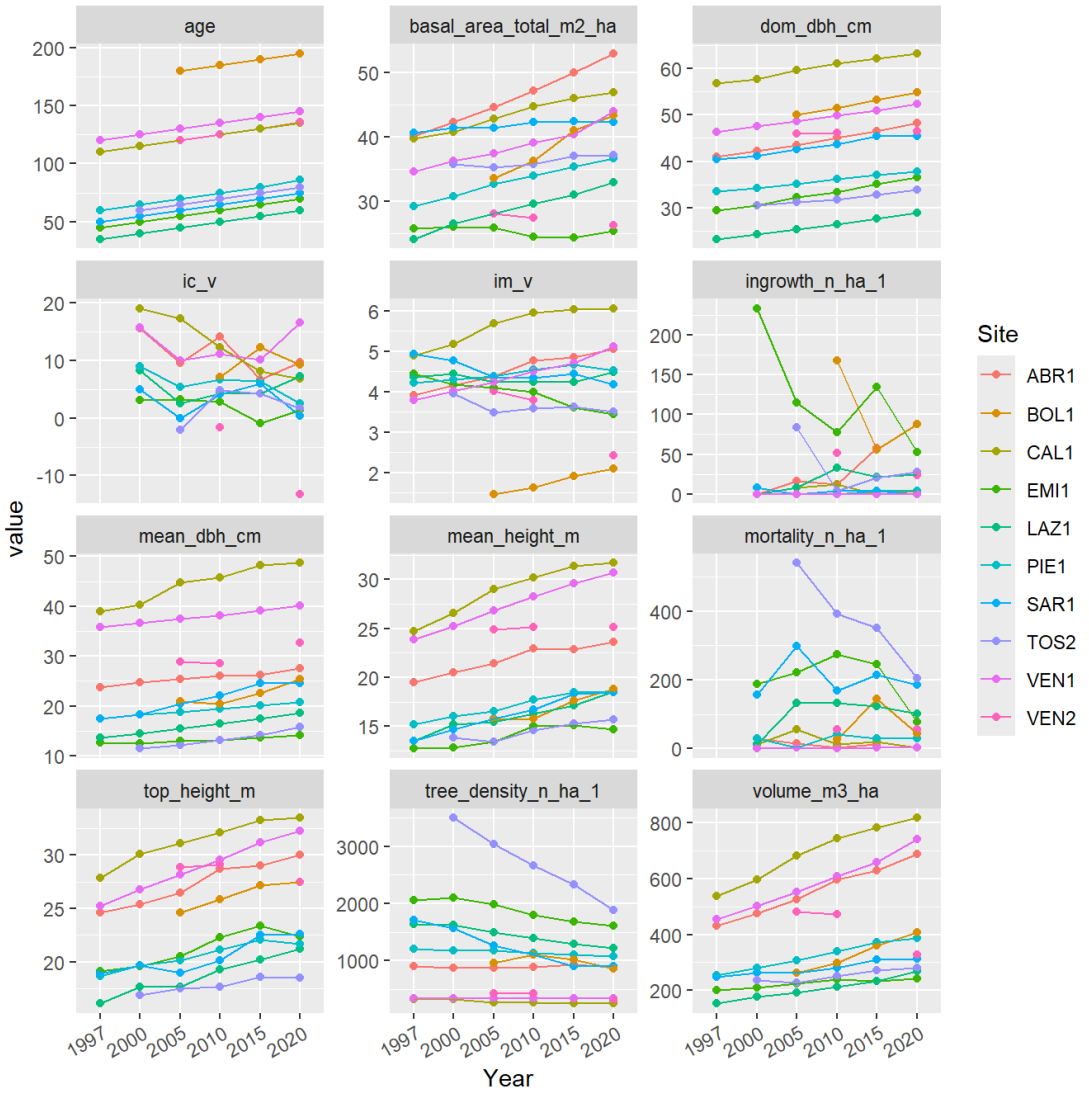

Figure 4.11.1. Trends of the 12 variables related to forest growth assessment at the 10 forest sites in the period 1997-2020.

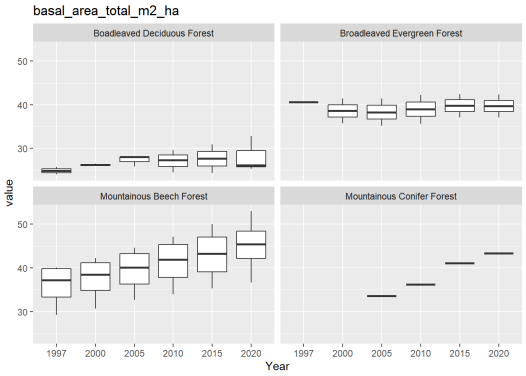
basal_area_total_m2_ha
Boadleaved Deciduous Forest
Broadleaved Evergreen Forest
Mountainous Beech Forest
Mountainous Conifer Forest
value
Year

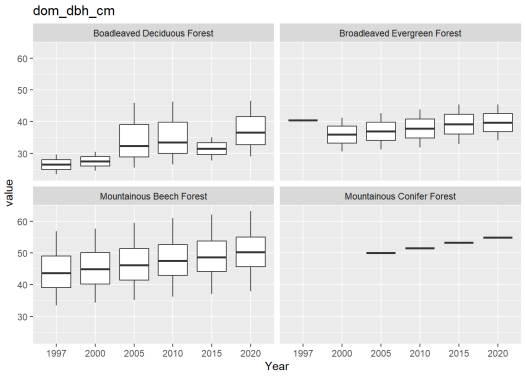
dom_dbh_cm
Boadleaved Deciduous Forest
Broadleaved Evergreen Forest
Mountainous Beech Forest
Mountainous Conifer Forest
value
Year

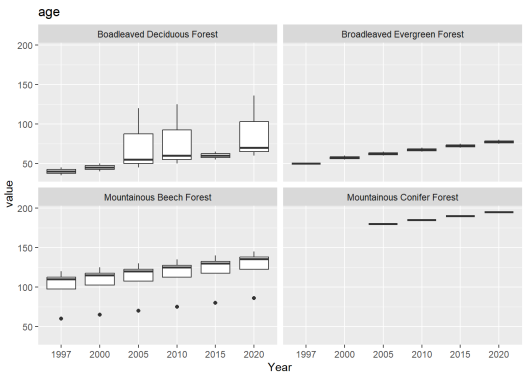
age
Boadleaved Deciduous Forest
Broadleaved Evergreen Forest
Mountainous Beech Forest
Mountainous Conifer Forest
value
Year

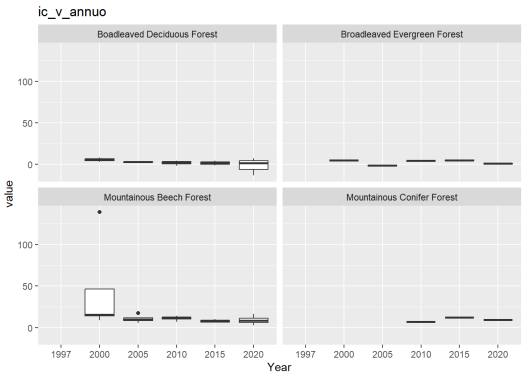
ic_v_annuo
Boadleaved Deciduous Forest
Broadleaved Evergreen Forest
Mountainous Beech Forest
Mountainous Conifer Forest
value
Year

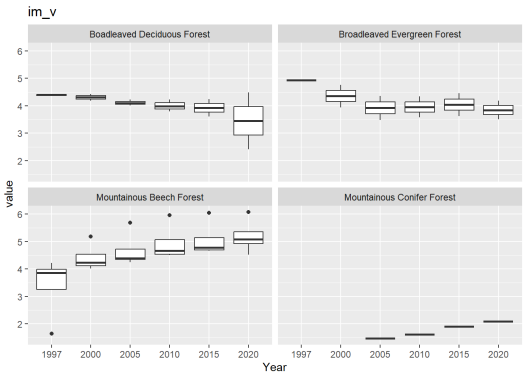
im_v
Boadleaved Deciduous Forest
Broadleaved Evergreen Forest
Mountainous Beech Forest
Mountainous Conifer Forest
value
Year


ingrowth_n_ha_1
Boadleaved Deciduous Forest
Broadleaved Evergreen Forest
Mountainous Beech Forest
Mountainous Conifer Forest
value
Year

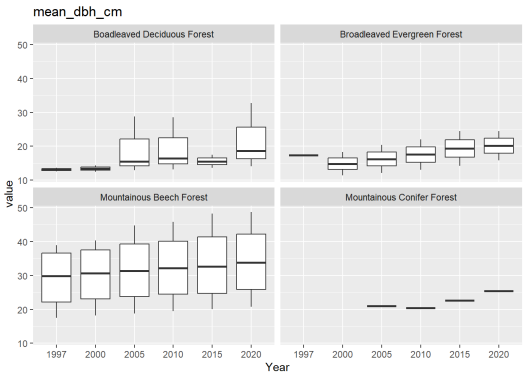
mean_dbh_cm
Boadleaved Deciduous Forest
Broadleaved Evergreen Forest
Mountainous Beech Forest
Mountainous Conifer Forest
value
Year

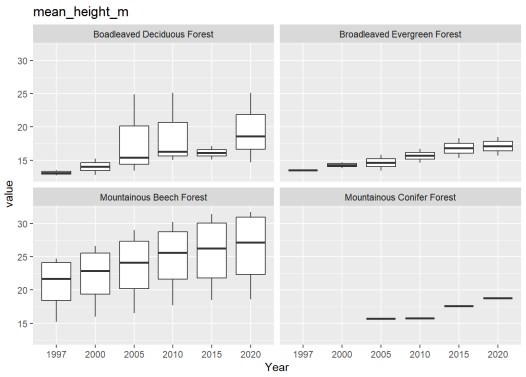
mean_height_m
Boadleaved Deciduous Forest
Broadleaved Evergreen Forest
Mountainous Beech Forest
Mountainous Conifer Forest
value
Year

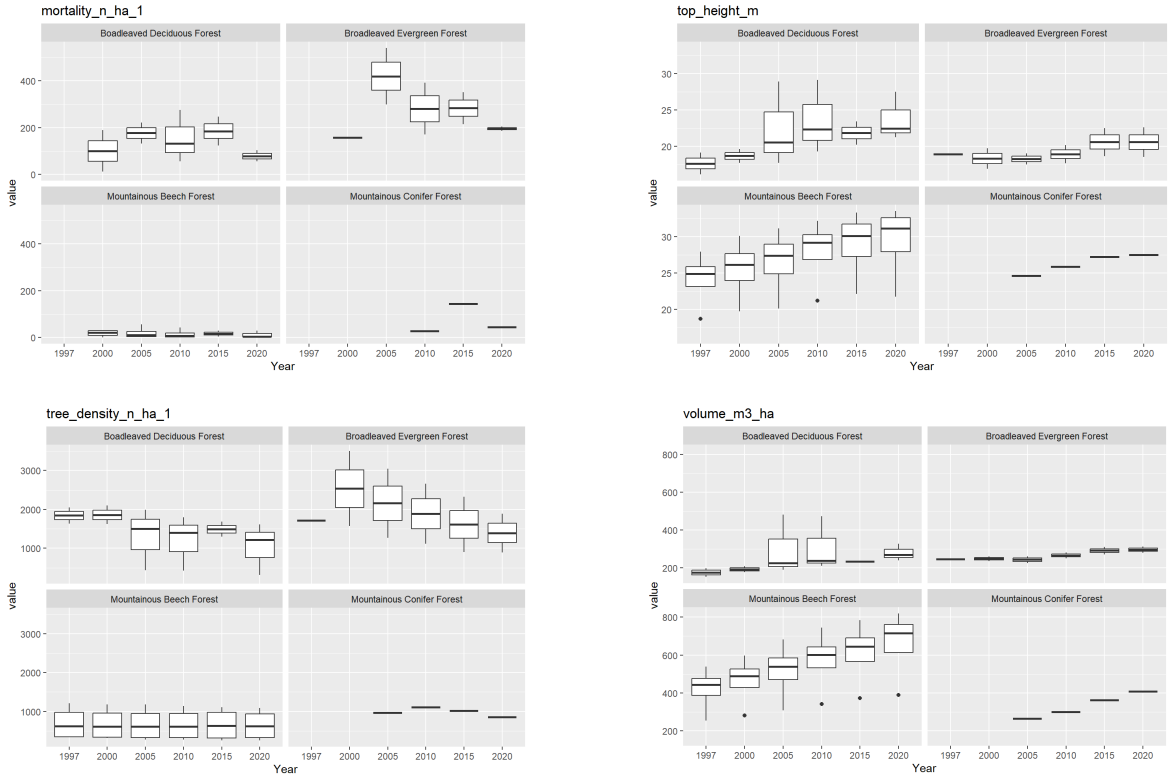

Figure 4.11.2. Boxplots showing the distribution of the variables over the measuring period at the four forest types.

The correlation among variables has been studied for each forest type over the years (Pearson's correlation). Figure 4.11.3 provides an example of the results obtained for Mountainous Beech Forests (MBF).

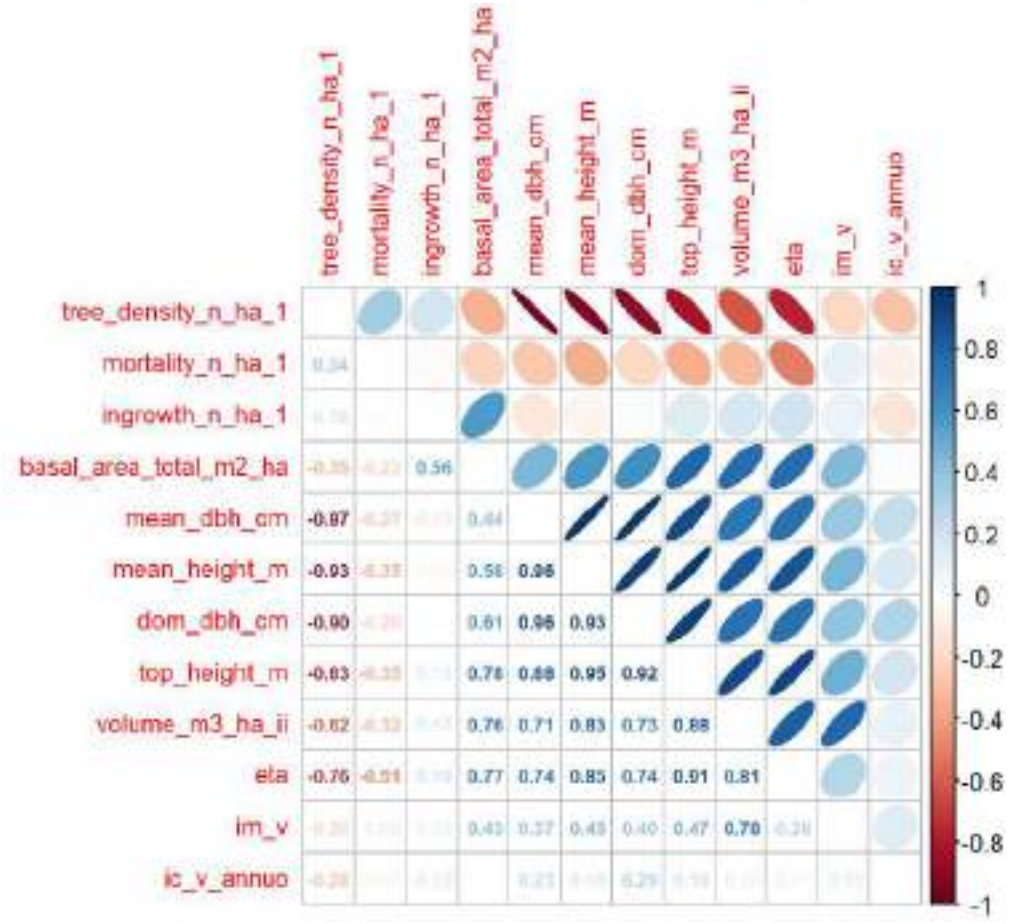

Figure 4.11.3. Pearson's correlation among variables over the years for Mountainous Beech Forests (MBF).

4.12 Ozone injury

4.12.1 Dataset

Table 4.12.1 presents an overview of the dataset. The data on ozone injuries to plants spans 2018 to 2024 across 5 forest sites. The analysis includes the percentage of symptomatic species in the LESS (%) and the percentage of symptomatic leaves per branch (scores 0-3).

Table 4.12.1. Overview of the available dataset.

Forest sites (5)	• ABR1 (Selva Piana) • EMI1 (Carrega) • LAZ1 (Monte Rufeno) • PIE1 (Val Sessera) • VEN1 (Cansiglio)
Variables (2)	Symptoms of ozone injuries on plants: • % of symptomatic species • % of symptomatic leaves (scores from 0 to 3)
Years (7)	From 2018 to 2024

4.12.2 Results and discussion

Figure 4.12.1 shows the trends of the % of symptomatic species in the LESS at the five forest sites form 2018 to 2024. An overall increasing trend of symptomatic species is observed for beech forest sites in 2023 and 2024 (see also Figure 4.12.2).

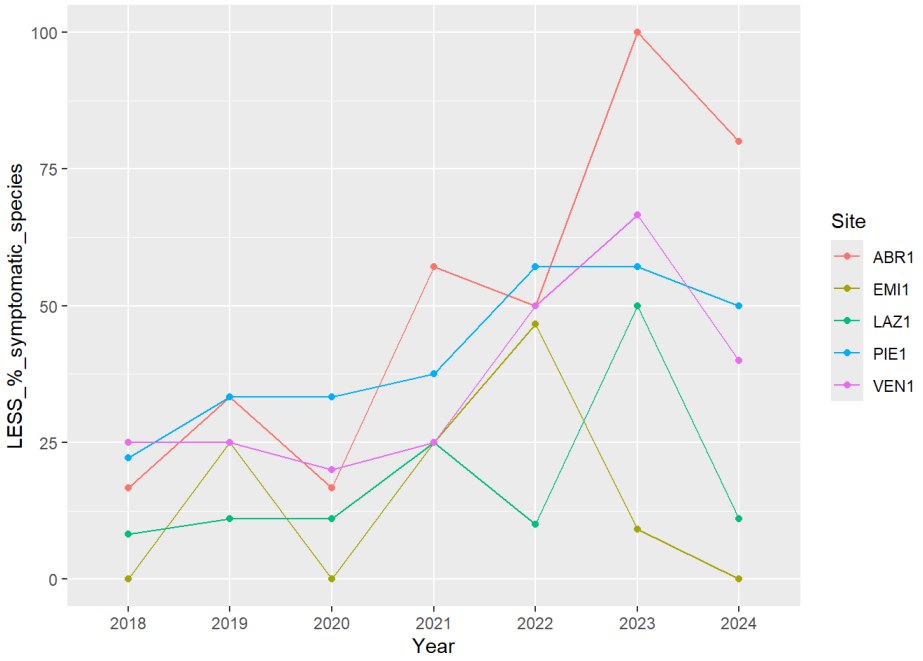

Figure 4.12.1. Trends of the % of symptomatic species in the LESS at the five forest sites in the period 2018-2024.

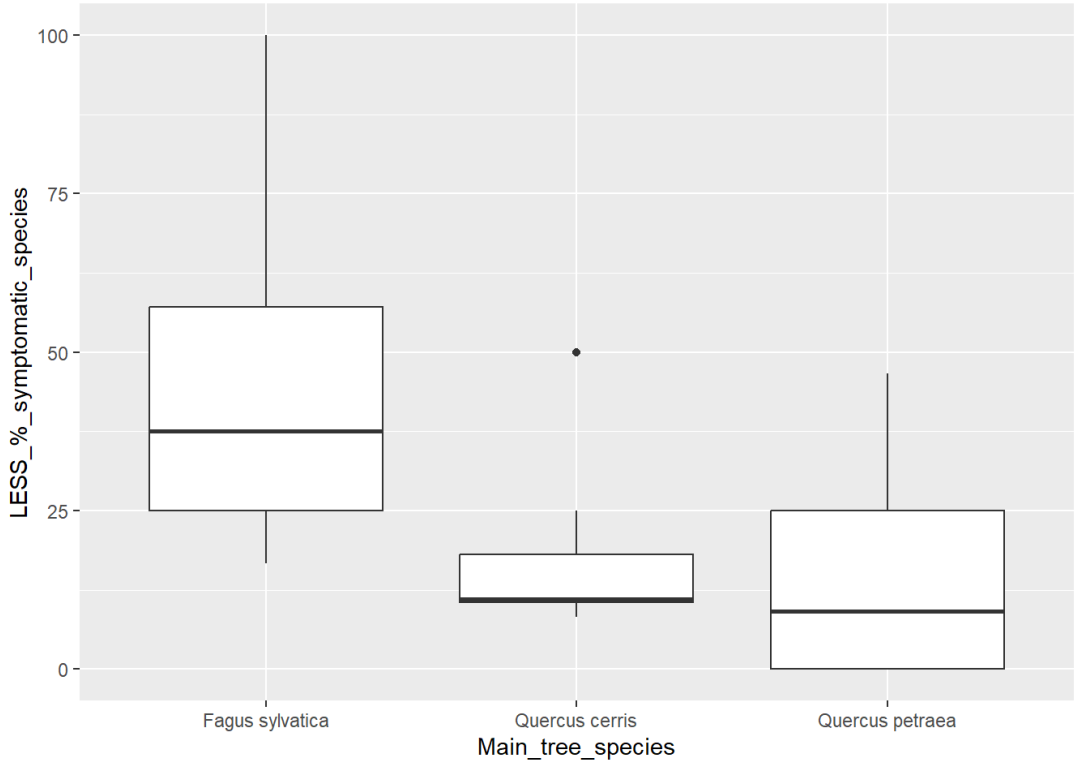

Figure 4.12.2. Boxplot with the distribution of the % of symptomatic species in the LESS among the different main tree species.

By analyzing individual forest sites, we can observe differences in the proportion of the score classes of symptomatic leaves over the time span considered. Figure 4.12.3 provides examples of two sites with contrasting trends: in the EMI1 plot, no symptomatic leaves have been observed over the years (score 0); whereas the VEN1 site shows a high incidence of symptomatic leaves per branch (score classes 2 and 3).

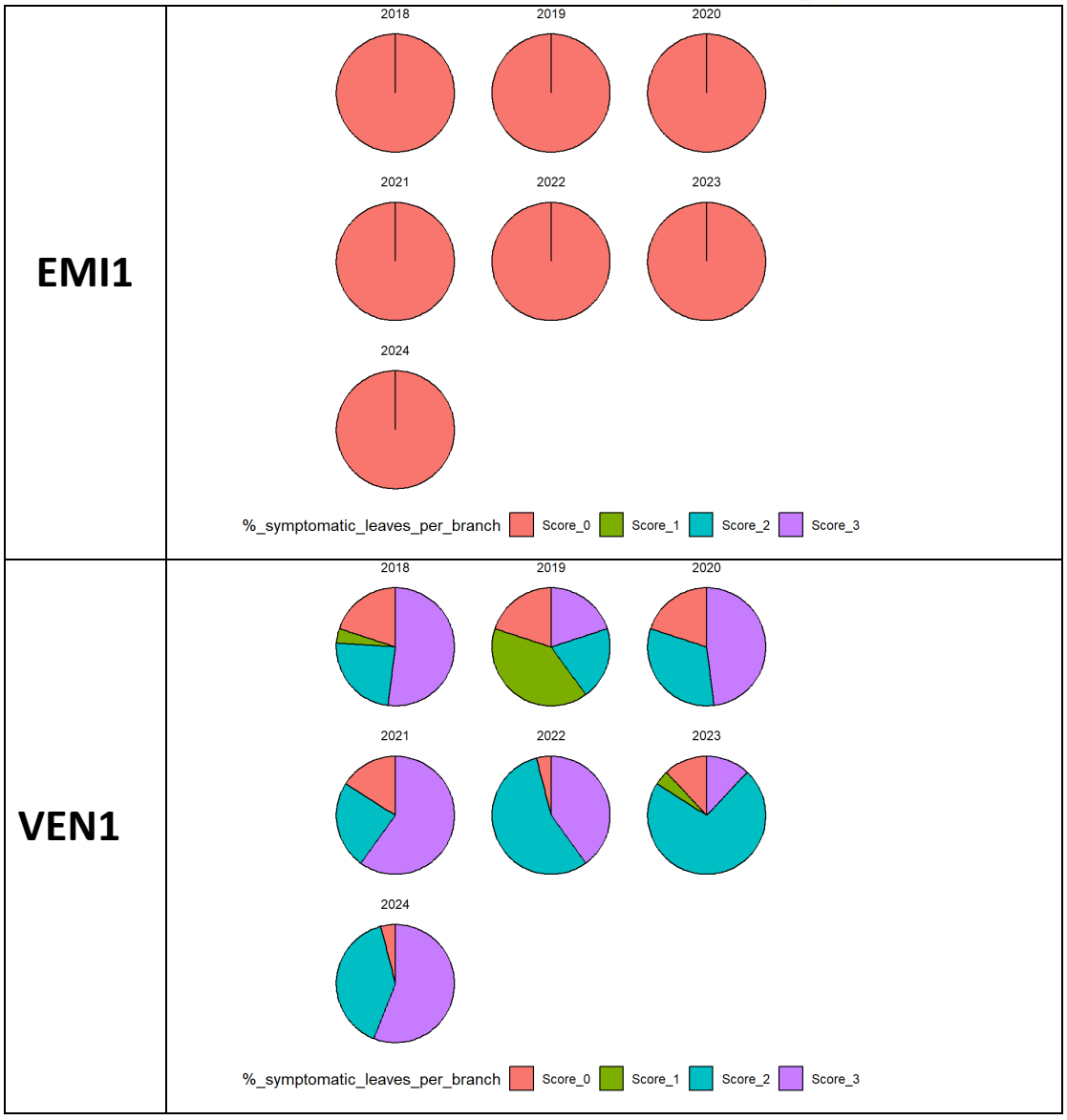

Figure 4.12.3. Pie-charts showing the distribution of the percentage of classes of symptomatic leaves per branch in the considered period.

4.13 Plant phenology

4.13.1 Dataset

Table 4.13.1 shows the sites and the metrics extracted from the analysis of the Copernicus Sentinel-2 Normalized Difference Vegetation Index (S2 NDVI) time series carried out with the R package "Sen2Rts". The R package has been developed specifically for processing S2 time series and for

extracting seasonal phenological key parameters (Ranghetti, 2021). We processed S2 NDVI time series for a total of seven forest sites discarding project's sites BOL1 (Renon), SAR1 (Marganai) and TOS2 (Cala Violina) covered by evergreen species. Processing covered the period 2018 to 2024 to estimate, for each site and year, dates for the start and end of season; phenological metrics for 2024 and for sites ABR1, EMI1, LAZ1, TOS2, VEN1, VEN2 were used for validation though comparison with available field observations.

Table 4.13.1. Overview of the forest sites, metrics and years for the Remote Sensing processing.

Forest sites (7)	• ABR1 (Selva Piana) • CAL1 (Piano Limina) • EMI1 (Carrega) • LAZ1 (Monte Rufeno) • PIE1 (Val Sessera) • VEN1 (Cansiglio) • VEN2 (Bosco Fontana)
Variables (2)	• SOS: Start of Season • EOS: End of Season
Years (7)	2018, 2019, 2020, 2021, 2022, 2023, 2024

4.13.2 Results and discussion

4.13.2.1 Remote sensing phenological metrics

For each project's site, we extracted time series of NDVI from multi-spectral NIR (near infrared) and red S2 reflectance bands (S2 B8 and B4, respectively). NDVI is a proxy of the greenness and it is an indicator of the vegetative cycle of plants: phenology can be estimated from the NDVI curve (Figures 4.13.1 and 4.13.2). Satellite measurements are influenced by surface and atmospheric conditions at the site on each acquisition date, NDVI values can be affected by noise and/or data gaps that are corrected during data processing (e.g., smoothing, gap filling, function fitting) before implementing the algorithm for the identification of phenological metrics.

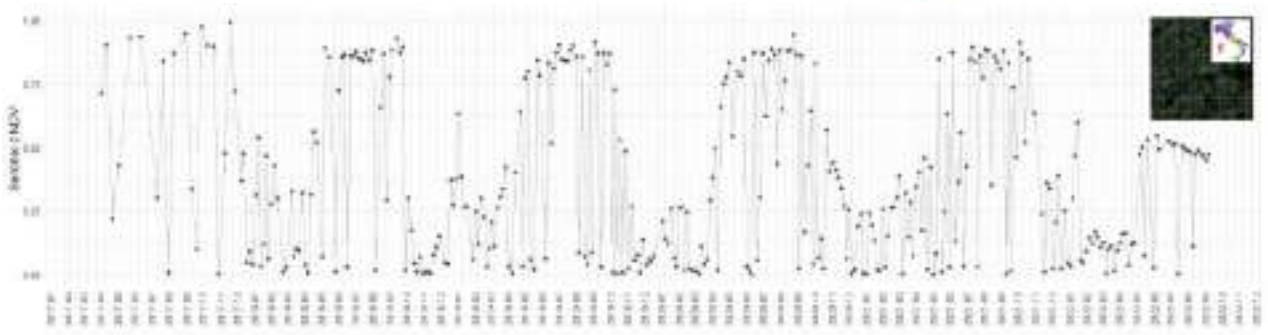

Figure 4.13.1. Example of the raw NDVI time series from S2 acquisition dates for the EMI1 SITE (top box where the site location is overlaid on the S2 pixel grid 10 m x 10 m, white grid lines).

Figure 4.13.2 illustrates the output of NDVI time series after processing and the estimated phenological metrics start and end of the season (SOS and EOS) for each year (vertical dashed line) and for site LAZ1.

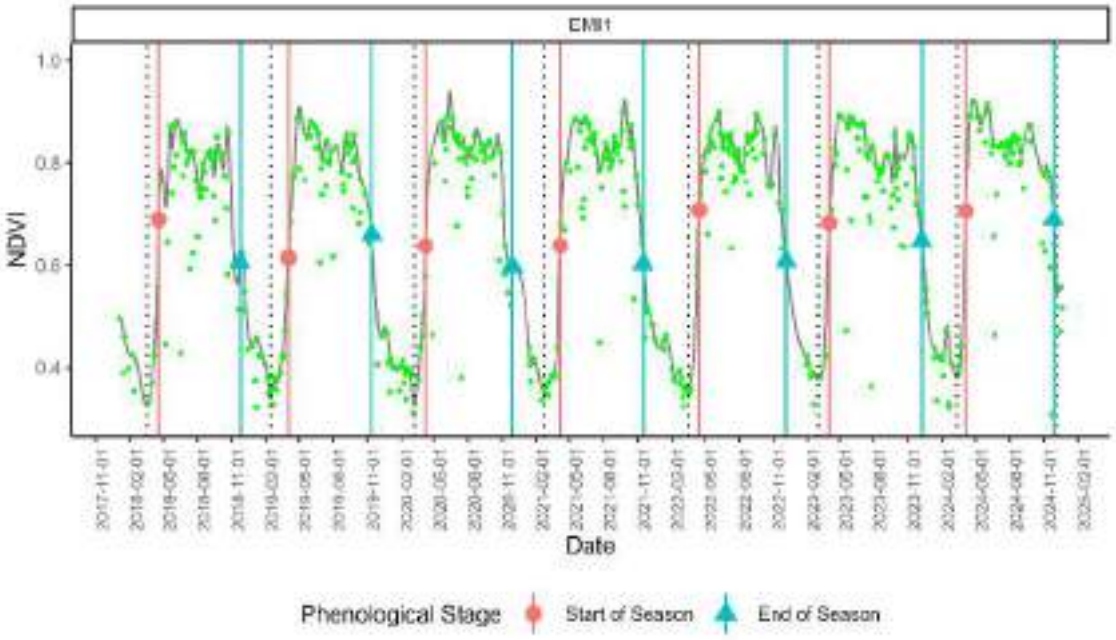

Figure 4.13.2. Example of the S2 NDVI raw data (green dots) and cleaned NDVI time series (continuous line) and phenological metrics derived with the "Sen2Rts" algorithm; start of season (SOS) and end of season (EOS) for the LAZ1 site. Vertical lines show the vegetative cycles identify by the algorithm.

Depending on the site and the year, noise and/or signal disturbance in the times series could not be fully removed thus preventing the estimation of the metrics: Table 4.13.2 summarizes sites and years for which the start and end of season dates were estimated and are part of the project's deliverable.

Table 4.13.2. Sites and years processed to the final start and end of season metrics after cleaning of the NDVI times series.

Site	2018	2019	2020	2021	2022	2023	2024
ABR1	x	x	x	x	x	x	x
CAL1		x	x	x	x	x	x
EMI1	x	x	x	x	x	x	x
LAZ1	x	x	x	x	x	x	x
PIE1		x	x		x	x	
VEN1		x	x		x	x	x
VEN2	x	x	x	x	x	x	x

Table 4.13.3 shows the RS estimated metrics for the multi-annual dataset; start of season shows more consistent results across the year (lowest date variability from year to year). Indeed, SOS dates vary across years from a minimum of 14 days (CAL1) to a maximum of 43 days (PIE1); while EOS from a minimum of 23 days (EMI1) to a maximum of 54 days (VEN1).

Table 4.13.3. Sites and years processed to the final start and end of season metrics after cleaning of the NDVI times series.

Site	2018		2019		2020		2021		2022		2023		2024	
	SOS	EOS	SOS	EOS	SOS	EOS	SOS	EOS	SOS	EOS	SOS	EOS	SOS	EOS
ABR1	07/05	29/10	24/05	24/10	19/04	27/11	01/05	05/12	01/05	20/10	31/05	05/11	24/04	21/10
CAL1	-	-	27/04	11/11	20/04	25/10	20/04	04/10	25/04	03/11	13/04	18/11	14/04	12/11
EMI1	18/04	24/11	04/04	14/11	07/04	27/11	06/04	16/11	16/04	07/12	02/04	07/12	05/04	28/11
LAZ1	26/04	16/11	04/05	16/11	23/04	10/11	26/04	11/11	28/04	06/12	29/04	02/12	09/04	26/11
PIE1	-	-	06/06	10/10	24/04	29/10	-	-	16/05	16/10	09/05	07/11	-	-
VEN1	-	-	19/04	05/12	13/04	14/11	-	-	28/04	26/01	18/04	04/12	16/04	06/10-
VEN2	17/04	26/10	13/04	16/11	02/04	21/10	31/03	10/12	05/04	11/11	24/03	25/11	25/03	23/11

Remote sensing SOS and EOS metrics for project sites ABR1, EMI1, LAZ1, VEN1, VEN2 and the year 2024 were compared to field observations for validation purposes (Table 4.13.4). Agreement between field observations and remote sensing estimates is also illustrated in Figure 4.13.3 through scatter plots.

Table 4.13.4. Start of Season (RS SOS) and End Of Season (EOS) phenological metrics derived from remote sensing (RS) for the validation field sites in 2024.

Site	RS SOS	RS EOS
ABR1	24/04/2024	21/10/2024
EMI1	05/04/2024	28/11/2024
LAZ1	09/04/2024	26/11/2024
VEN1	16/04/2024	06/10/2024
VEN2	25/03/2024	23/11/2024

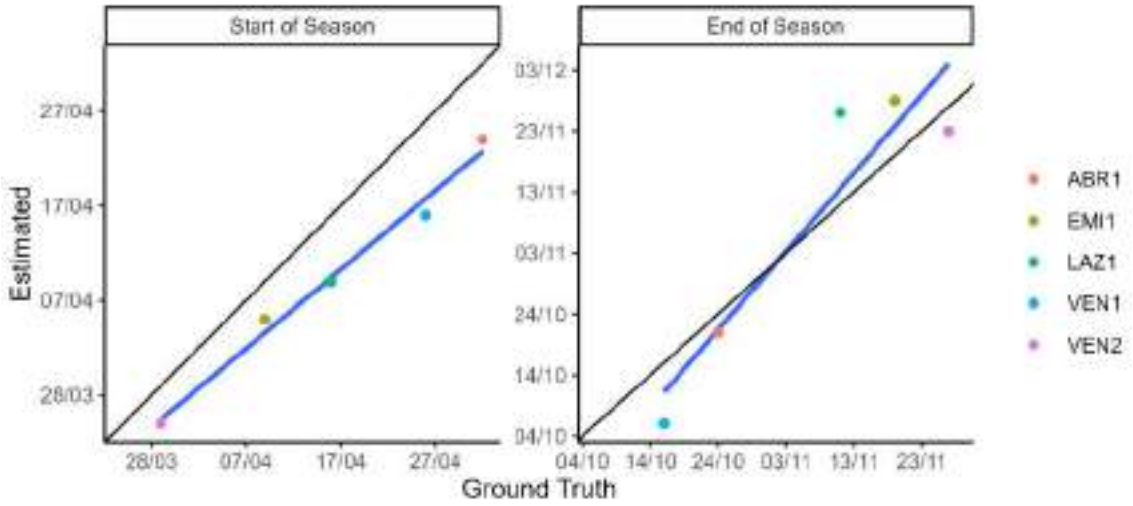

Figure 4.13.3. For the start and end of season phenological metrics: comparison between field observations/measurements (x-axis) and RS estimations (y-axis) for the year 2024 when field observations were available for validation.

The RS-derived estimates agreed with field observations with R^2=0.98 (RMSE=7.0) and R^2=0.86 (RMSE=9.3) for the start and end of season, respectively. The results confirm that the end of season/senescence phenological stage is more difficult to estimate compared to the start of season/green up (Ling et al., 2022) although these accuracy metrics reveal a more than satisfactory agreement with field observations. The lowest accuracy achieved in the estimation of the EOS metric could also explain the largest multi-annual variability observed for this parameter from remote sensing estimations.

Extensive validation should be carried out to further confirm these results and to this aim collecting field observations is necessary over large areas and multiple years to calibrate and validate remote sensing techniques.

4.13.2.2 Ground-base phenological assessment

Phenological observations from the ground were carried out in selected plots. The results are reported in terms of flushing (bud sprouting in spring months) and foliar senescence (color turning) in autumn. The results of the 2024 assessment were compared with the phenological variables in the same plots assessed during the period 2004-2006 (Figure 4.13.4).

The budburst time does not change substantially between 2024 and the 2004-2006 years; however, it seems that the whole flushing period, from budburst to complete leaf distension, appears shorter in the last year.

The period of leaf senescence in deciduous trees, from the onset of leaf yellowing to complete desiccation of the leaves on the crown, is more variable between sites, species and years. The onset of yellowing may be anticipated in summer months and depends on the stress factors encountered during the summer.

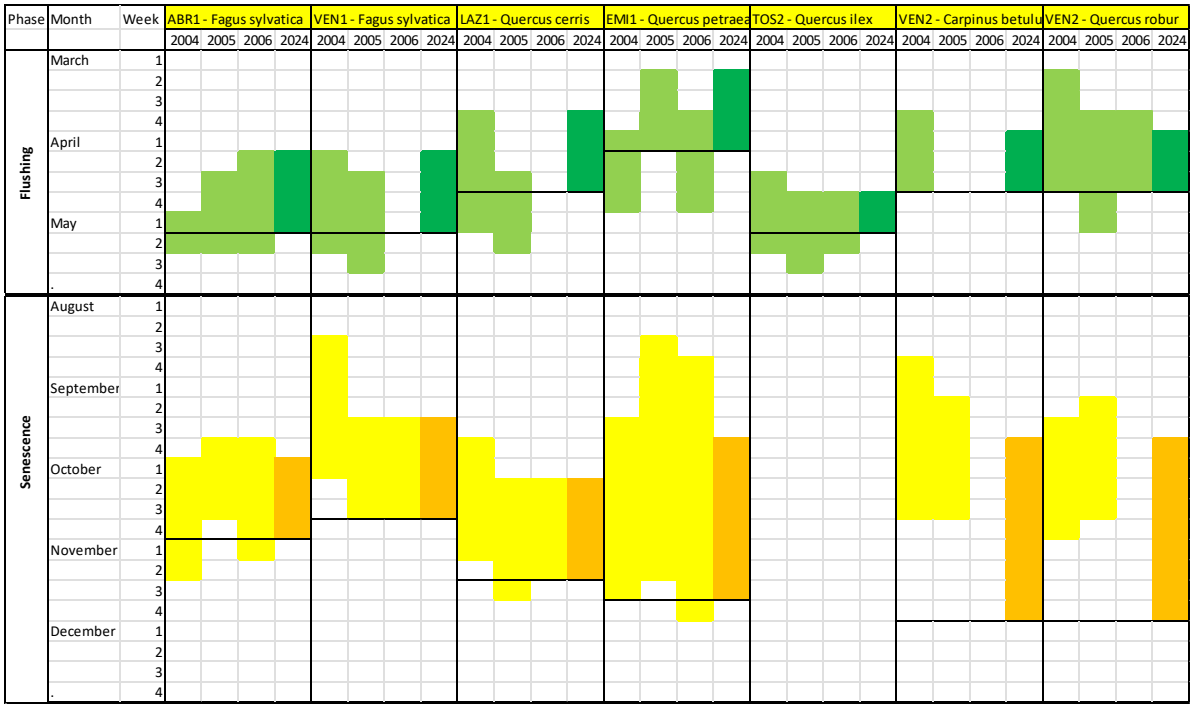

Figure 4.13.4. Ground-based phenological assessment.

5. Freshwater ecosystems: results

This chapter summarizes the results from the freshwater sites, with each paragraph detailing the descriptive statistics for each indicator.

5.1 Chemical indicators

5.1.1. Present status in relation to acidification, eutrophication and nitrogen enrichment

The ionic composition of the study lakes and streams is shown in Figure 5.1.1, based on the water chemistry data of 2023-2024, while a comparison of the freshwater sites focusing on indicators of acidification and trophic status is presented in Figure 5.1.2.

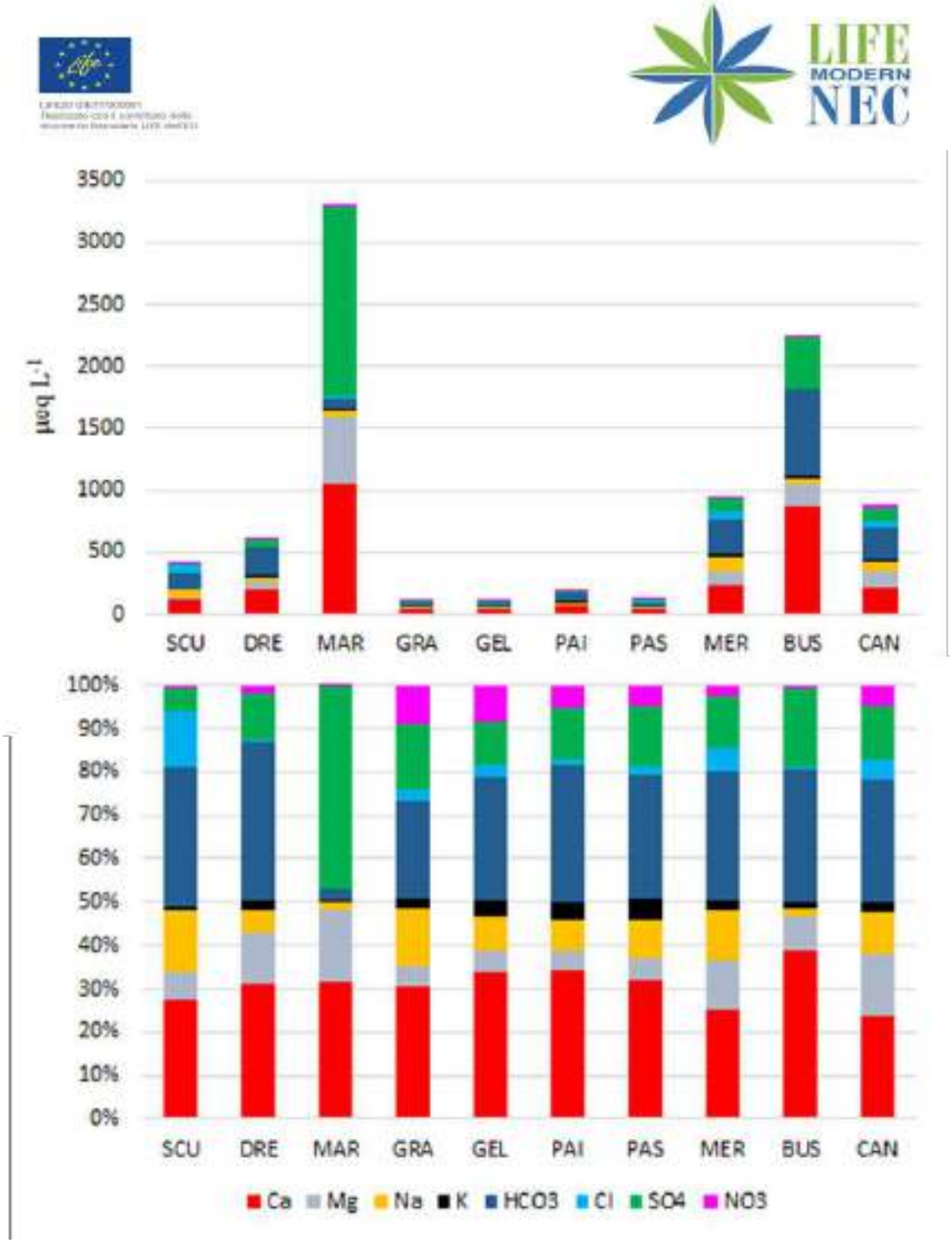

Figure 5.1.1. Ionic composition (absolute concentrations and relative construction to the total ionic content) of the study sites based on chemical analysis of samples collected in 2023-2024.

The study sites are mainly characterised by dilute waters, with low conductivity (5-50 µS cm^{-1} at 20 °C) and low ionic concentrations (sum of all ions: < 1000 µeq L^{-1}). Exceptions are stream BUS (107µS cm^{-1} and 2250 µeq L^{-1}) and lake MAR, characterised by moderately mineralised waters (170 µS cm-1 and 3300 µeq L-1). Calcium and bicarbonate are the dominant cation and anion, respectively, in

all sites (both contributing 25-40% to the total sum of ions) except MAR where SO4 is much more important than at the other sites (contributing almost 50% of the total ionic content). The presence of minerals containing CaSO4 and MgSO4 in the lake bedrock may explain the different ionic composition at this site. Mg and Na concentrations and contributions are rather variable (between 4 and 17% and between 2 and 14%, respectively), while K and Cl are mainly present in low amounts. Slightly higher concentrations of the salts Na and Cl were detected at lakes MER and SCU (Fig. 5.1).
The selected sites are representative of a wide range of pH and ANC (Acid Neutralizing Capacity), two of the key indicators in the NEC Directive monitoring scheme. More generally, pH and ANC are widely used indicators in the evaluation of freshwater sensitivity to acidification. In Europe, the value of 20 µeq L^{-1} has been identified as the minimum level required for ecosystem protection under UNECE protocols, even if critical limits may vary depending on the target group of organisms. In the high Alps, an ANC limit of 30 µeq L^{-1} has been suggested (Raddum and Skjelkvåle 2001).
The two rivers and Lake MER are characterised by a good buffer capacity, with high ANC (above 200 µeq L^{-1}) and pH close or above 7.5. However, especially in the case of CAN, acidic episodes with sudden and sharp decrease of ANC may occur, for instance in consequence of heavy rainfalls (Rogora et al., 2012). The mountain lakes are slightly (SCU, DRE, MAR) or highly sensitive (GRA, GEL, PAS) to acidification, with pH varying between 6.2 (GRA) to values close to or above 7.0 (Fig. 5.2a). It should be highlighted that high altitude lakes are still exposed to potential acidification episodes at snowmelt (early summer), when alkalinity and pH may drop due to the flushing of water delivering acidifying compounds to the lake in a short time. Recently, it has also been shown that during this critical period the relative contribution of nitrate (NO_3) to lake acidity has increased compared to that of sulfate (SO_4) (Rogora et al., 2013).
Phosphorus concentrations indicate oligotrophic or ultraoligotrophic conditions in all sites (P-PO_4 < 4 µg L^{-1}; total P between 2 and 8 µg L^{-1}), which are also confirmed by the low Chl-a values in lakes (mainly below 5 µg L^{-1}). However, on some occasions, a few lakes showed higher Chl concentrations than expected (e.g. 10 µg L^{-1} in PAS in September 2023, > 20 µg L^{-1} in PAI in September 2024) (Fig. 5.2b). A tendency towards more eutrophic conditions in relation to N deposition or climate change has been reported for some mountain lakes (e.g. Burpee et al., 2022; Oleksy et al., 2020) and the effect of N as a eutrophying agent has been evaluated by working groups within the ICP WATERS (Thrane et al., 2021). This aspect is also presently under investigation in lakes PAI and PAS, using time series dating back to the 1980s. However, in these lakes, other factors, such as fish stocking, may also contribute to a eutrophying effect by altering the lake trophic food web (Cammarano and Manca, 1997).

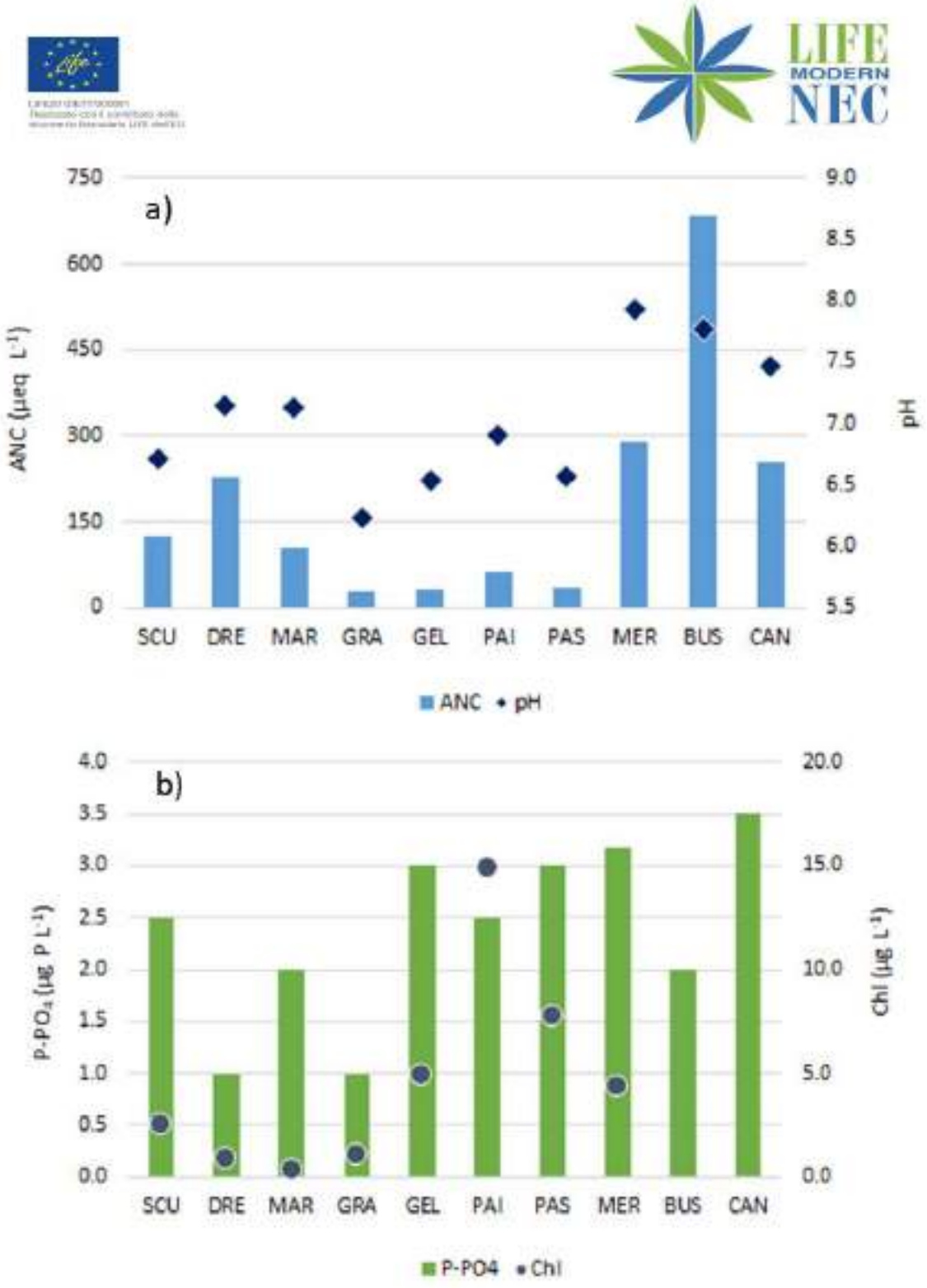

Figure 5.1.2. Average values (2023-2024) of pH and Acid Neutralising Capacity (ANC) (a) and orthophosphate (P-PO4) and chlorophyll a (b) in the 10 freshwater sites.

A focus on nitrogen compounds concentrations is shown in Fig. 5.1.3, where the freshwater sites are compared considering both the absolute concentrations of inorganic ($N\text{-}NO_3$ and $N\text{-}NH_4$) and organic nitrogen and their relative contribution to total N.

Figure 5.1.3. Concentrations of nitrate, ammonium and organic N (above) and their relative contribution to total N in the freshwater sites (average data 2023-2024).

The highest NO_3 concentrations are found in the lowland subalpine sites (MER and CAN, about 300 and 600 µg L^{-1}); rather high values also characterise the Alpine sites (80-220 g L^{-1}) while lower concentrations were found in the Apennine site SCU. Ammonium is present in low amounts, mainly below 10 µg L^{-1} (20-25 µg L^{-1} in lakes MER and SCU). The latter sites also show the highest concentrations of organic N (210-240 µg L-1 with respect to 75-100 µg L^{-1} in the other sites) and in lake SCU organic N is by far the dominant form (76%). On the other hand, organic N is almost negligible in lake MAR (6 µg L^{-1}), contributing to less than 3% of total N. NO_3 is also dominant in the other alpine lakes (60-70% of total N), except PAS where inorganic and organic N are equally important. NO_3 is the dominant form of N in the stream sites too (68-85%) (Fig. 5.1.3).

Total organic carbon (TOC) varies from extremely low values (0.15 mg L^{-1} in MAR) to above 2.0 mg L^{-1} in SCU, reflecting the organic matter content. The lowest concentrations are found in the high-altitude sites, while higher values characterised the water of lowland rivers and lakes; however, TOC may vary significantly in different periods of the year in relation e.g. to heavy rainfall, as occurred in lake SCU in 2024. As expected, TOC correlated with ON, with the highest concentration of both variables in lakes SCU and MER.

The absolute concentrations and the relative importance of inorganic versus organic N may reflect different levels of N atmospheric loads; however, catchment characteristics, particularly vegetation cover, play an important role in regulating the effective N inputs to freshwater (Marchetto et al. 1994; Kopacek et al. 2005). Recently, Kopacek et al. (2024) put in evidence how the concentrations of organic N in mountain lakes in the Tatras are increasing, due to a combined effect of reduced acid deposition and climate change (more heavy rainfall events). This hypothesis warrants to be investigated in Alpine lakes too, where time series allow an evaluation of the changing contribution of the different forms of N.

5.2 Biological indicators

5.2.1 Epilithic diatoms

Diatom assemblages were collected simultaneously in lakes and rivers to support ecosystem assessment and comparisons. A total of 195 *taxa* were identified to the highest taxonomic level possible, mainly at species and sub-species. Forty-eight taxa were present with abundances higher than 3%. Specifically, in lakes a total of 164 taxa, belonging to 41 genera, and in rivers a total of 66 taxa, belonging to 22 genera have been detected. For the complete list of species and codes see Annex B3.2.

Across the lakes, the most species-rich groups were achnanthoid taxa (15), *Nitzschia* (14 each), *Eunotia* (13) and fragilarioid taxa (13), while all other genera were represented by less than ten taxa. The most common and abundant species were *Achnanthidium minutissimum*, *Achnanthidium lineare*, *Denticula tenuis*, *Navicula notha*, *Psammothidium scoticum* (Fig. 5.2.1A).

In rivers, the most species-rich groups were *Gomphonema* (13), achnanthoid taxa (12), and fragilarioid taxa (7), while all other genera were represented by less than five taxa. The most common and abundant species were *Achnanthidium microcephalum*, *Achnanthidium sublineare*, *Fragilaria perminuta* (Fig. 5.2.1B).

Diatom assemblages were characterized using common diversity metrics for both ecosystems: total abundance, taxa richness, Shannon–Wiener diversity, and Pielou's evenness (Magurran, 2004).

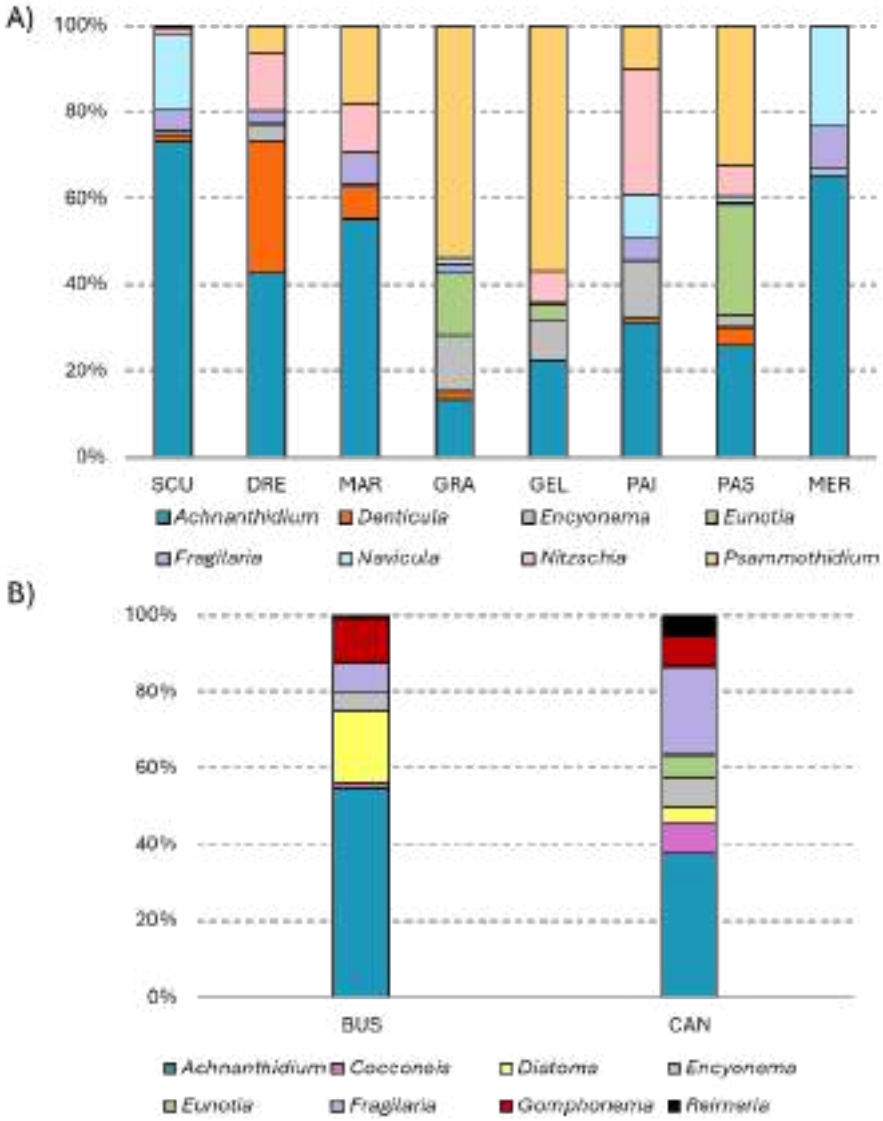

Figure 5.2.1. Percent occurrence of the main genera of diatoms in terms of abundance found in the studied lakes (A) and rivers (B).

The diversity indices presented in Table 5.2.1 provides a comparative assessment of diatom community structure in lakes (blue) and rivers (green). In lakes, species richness and Shannon diversity showed wide variation, with richness ranging from 28 to 59 taxa and diversity from 2.08 to 5.04. Evenness values were also variable ranging from 0.43 to 0.86), indicating that some lakes hosted uneven communities dominated by a few taxa (e.g., MAR), whereas others displayed highly balanced assemblages (e.g., PAS and PAI).

In rivers, by contrast, richness and diversity values fell within a narrower range (34–44 taxa; 4.26–4.67), and Evenness was consistently high (>0.80). While this might indicate more balanced

community structures, the lower variability observed is also likely influenced by the smaller number of river sites (n = 2) compared to lakes (n = 8). Overall, diatom assemblages in lakes appear to display greater variability in community structure, reflecting the broader environmental heterogeneity of lacustrine habitats, whereas river sites, based on the limited dataset available, showed comparatively uniform patterns.

Table 5.2.1. Diversity indices of diatom communities in various lakes (in blue) and rivers (in green). Reported metrics include the total number of individuals counted (Ntot), number of genera, species richness, Shannon diversity index (H), and evenness.

Sites	No. tot	No. genera	No. species	Shannon index	Evenness
SCU	420	15	32	3.49	0.7
DRE	435	21	39	4.16	0.79
MAR	426	14	28	2.08	0.43
GRA	413	21	46	4.07	0.74
GEL	419	20	45	4.53	0.83
PAI	415	18	36	4.43	0.86
PAS	359	28	59	5.04	0.86
MER	423	15	29	3.11	0.64
BUS	452	16	34	4.26	0.84
CAN	407	17	44	4.67	0.86

5.2.2 Macroinvertebrates

Macroinvertebrate assemblages were surveyed in parallel in both lakes and rivers to enable cross-system comparisons. A total of 1355 individuals were captured both in lakes and rivers (910 in lakes and 445 in rivers). Percent occurrences of the main taxonomic groups are shown in Figure 5.2.2. The complete list of macroinvertebrates taxa and codes is provided in Annex B3.2.

Across the lakes (Fig. 5.2.2A), Chironomidae and Oligochaeta dominate the assemblages (with relative abundance in the range of 2-97% and 1-66% respectively). MER and SCU sites stand out for a richer and more varied lake community. In addition to Oligochaeta (Naididae and Lumbriculidae) and Chironomidae (Chironomini, Orthocladiinae, Diamesinae, Tanypodinae), a notable presence of

Bivalvia (26%), Ephemeroptera (18%), and Trichoptera (11%) and Hirudinea (2%) in SCU, and of Bivalvia (8% including also invasive species such as *Corbicula fluminea*), Diptera Ceratopogonidae (8%), Hirudinea (2%), Crustacea Isopoda (2%) were observed. This pattern suggests that the lower-altitude sites provide environmental conditions (e.g., warmer temperatures, longer growing seasons, higher primary production) that foster greater biodiversity and more complex food webs.

In lotic waters with high dissolved oxygen and relatively swift currents (Fig. 5.2.2B), except Chironomidae always occurring with relatively high abundances (5-83%), EPT taxa typically increase in importance (Ephemeroptera: 4-40%, Plecoptera: 4-28%, Trichoptera: 5-22%), reflecting their ecological affinity for oxygen-rich, fast-flowing environments. Oligochaeta lack in GRAo, DREi, and PAIi, corresponding to low organic-matter availability, whereas they are markedly abundant in PAIo (67%) and MERo (95%), where the occurrence of aquatic plants and organic-matter is higher. Among watercourses, the larger ones (BUS and CAN) show a more diverse and widespread fauna across major taxonomic groups (Oligochaeta, Hirudinea, Ephemeroptera, Plecoptera, Trichoptera, Diptera, Chironomidae), indicative of their true riverine character and of the larger catchment contributing to their diversification. MERo stands out the other river types showing a very simple assemblage structure that includes only Oligochaeta (Naididae) and Chironomidae (Tanypodinae).

To describe macroinvertebrate assemblages, the most commonly applied diversity indices (Magurran 2004) total abundance, taxa richness, and diversity indices (Shannon–Wiener and Pielou) were quantified for the two ecosystem types enabling comparative analyses of structure and diversity (Tab. 5.2.2). The Shannon-Wiener index was chosen as it summarizes species diversity by accounting for both richness and relative abundance, and Pielou's evenness as it standardizes the diversity by the maximum possible diversity given the observed number of taxa, yielding a value between 0 and 1 where 1 indicates complete evenness. The results indicate a strong correlation among No. tot, No. taxa, and Shannon-Wiener diversity, and a negative one between No. taxa and Pielou evenness, likely reflecting multicollinearity among these metrics rather than independent ecological signals.

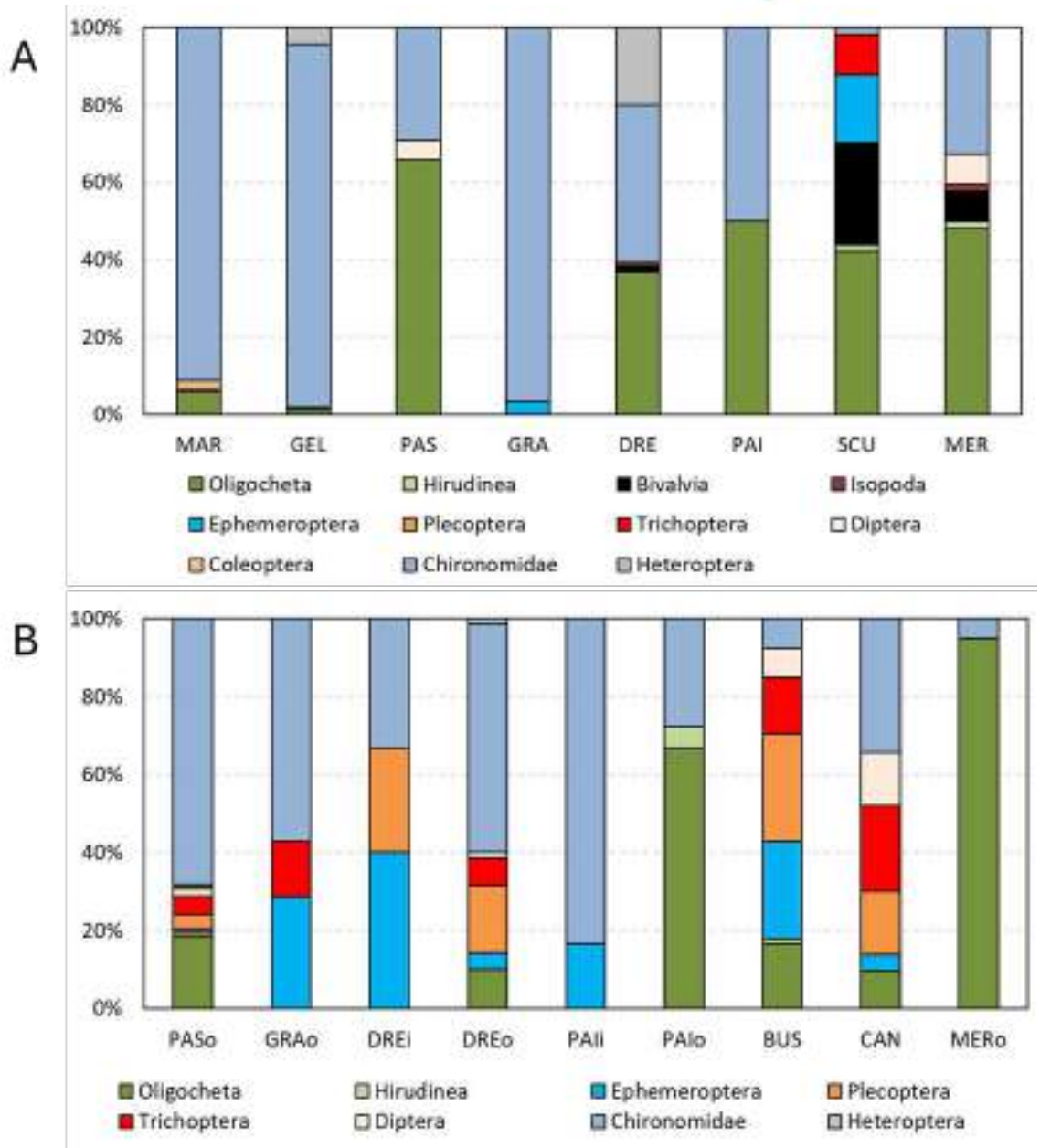

Figure 5.2.2. Percent occurrence of the main taxonomic groups in the studied lakes (A) and rivers (B). i: inlet, o=oulet. Lake/River distribution follows a high to low altitude gradient.

Tab 5.2.2. Diversity indices for macroinvertebrates assessed across lakes (in blue), rivers, and inlets and outlets of lakes (in green). Reported metrics include total abundance (No. tot), taxa richness (No. taxa), Shannon-Wiener diversity index, and Pielou evenness. i: inlet, o=oulet. Lake/River distribution follows a high to low altitude gradient.

Sites	No. tot	No. Taxa	Shannon	Evenness
MAR	137	10	1.3	0.4
GEL	326	10	1.7	0.5
PAS	41	6	1.2	0.6
GRA	31	5	1.3	0.7
DRE	264	11	1.8	0.5
PAI	2	2	0.7	1.0
SOJ	58	10	1.9	0.7
MER	52	13	2.1	0.6
GRAo	7	5	1.6	0.9
PASo	206	21	2.2	0.4
DRESi	45	15	2.5	0.8
DRESo	70	19	2.5	0.7
PAIi	6	4	1.2	0.9
PAIo	18	7	1.5	0.6
BUS	145	26	2.7	0.6
CAN	73	31	3.1	0.7
MERo	20	4	1.0	0.7

6. Studying relationships among indicators and stressors

This chapter presents the findings of the analyses conducted to examine the relationships between indicators and stressors in both forest and freshwater ecosystems.

6.1 Forest ecosystems: an integrated analysis

According to the conceptual scheme in Figure 3.1.1 (§ 3.1), integrated analyses were performed to investigate the relationships among groups of environmental variables (drivers) that may influence ecosystem responses (ecological indicators) relevant to the project. The following paragraphs illustrate the key findings for forest ecosystems:

- Relationship between lichens and atmospheric depositions
- Relationship between ozone concentrations and ozone symptoms
- Relationship between foliar analysis, deposition and defoliation
- Relationship between bird and bat diversity
- Relationship between different biodiversity groups.

6.1.1 Relationship between lichens and atmospheric depositions

To test the responses of lichen communities (species composition) and functional diversity in relation to atmospheric pollution and climatic variables, we considered the values of atmospheric deposition 1 year and 2 years before lichen sampling, and we performed a multivariate analysis.

Pearson's correlation was used to analyse variable relationships at each forest site. Figure 6.1.1 presents the results obtained for LAZ1. All nitrogen deposition variables are strongly linked and inversely related to sulfur deposition. The proportion of nitrophytic species (%LDV_NITRO) is positively related to nitrogen depositions, while oligotrophic species (%LDV_OLIGO) decrease, indicating effective indicator response.

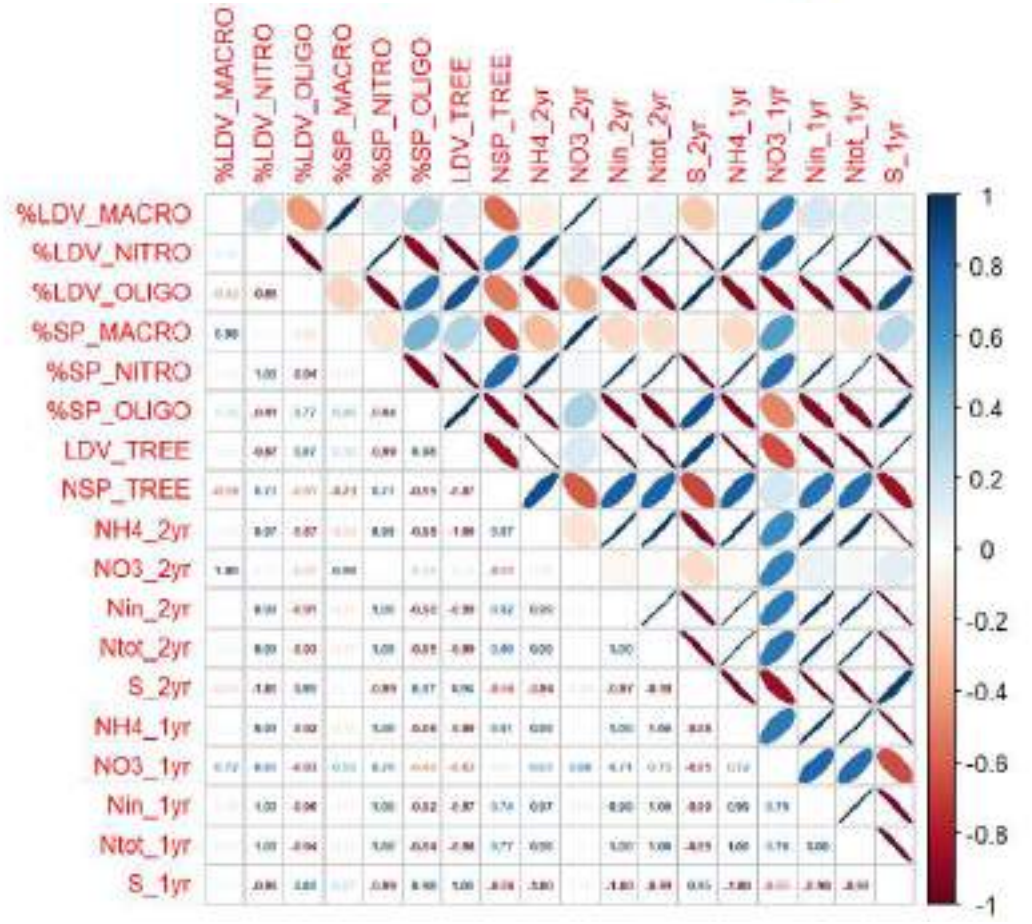

Figure 6.1.1. Pearson's correlation among variables over the years at the forest site LAZ1.

Forest sites were grouped into two groups (high and low nitrogen deposition) based on the median value of total nitrogen deposition (Ntot_1yr), and the responses of lichen functional diversity was tested (Kruskal Wallis test; Figure 6.1.2). Sites with lower nitrogen deposition show significantly higher LDV values (LDV_TREE; $p<0.05$) and macrolichens (%LDV_MACRO; $p<0.01$) than sites with higher nitrogen deposition. The response of nitrophytic (%LDV_NITRO) and oligotrophic species (%LDV_OLIGO) is not significant ($p>0.05$).

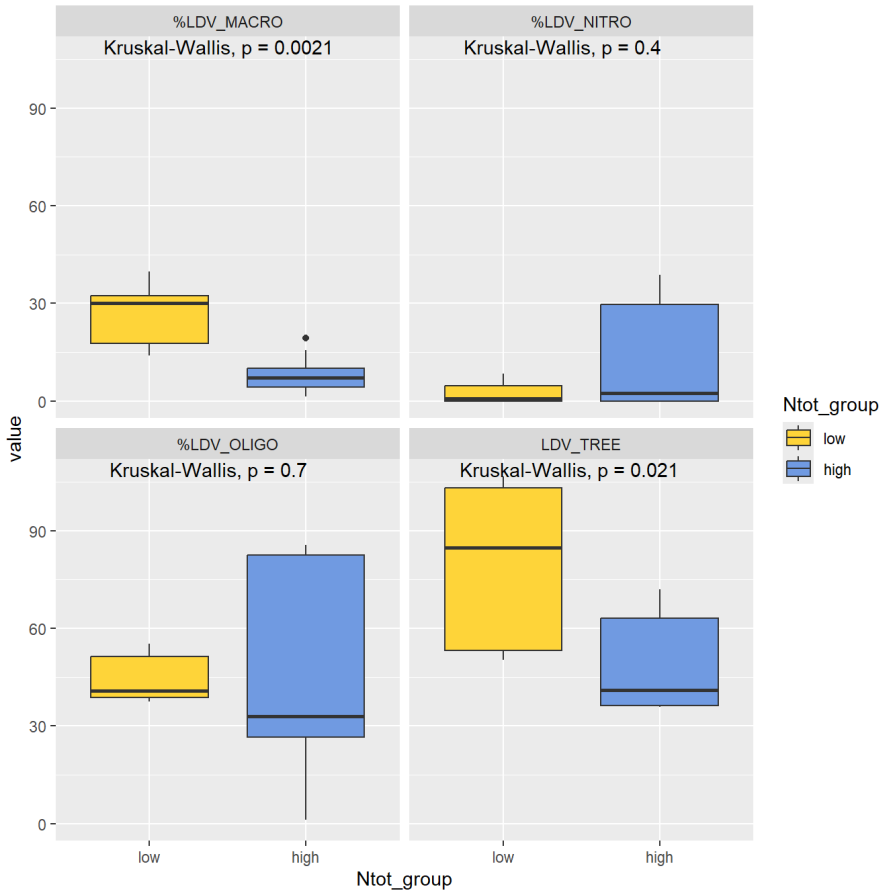

Figure 6.1.2. Boxplots with the distribution of functional diversity in the two groups of sites (low and high total nitrogen). Results of the non-parametric Kruskal Wallis test are also reported.

To study the response of species composition to nitrogen depositions and climatic variables a Non-Metric MultiDimensional Scaling (NMDS) was performed with the results of the surveys carried out during the project (2023 and 2024). For each site, the % of occurrence of each species out of the total number of occurrences at the site was calculated. To reduce the influence of the most frequent species, data were transformed by mean of the square root of the percentages. Environmental variables: i) average temperature for the period 1981-2010 (data source: https://www.reterurale.it/agroclima, owned by the Ministry of Agricultural, Food, Forestry and Tourism Policies (Mipaaft) and the Council for Agricultural Research and Analysis of Agricultural Economics - Agriculture and Environment Research Center,CREA-AA); ii) coordinates, precipitation and canopy deposition data for 2011 (the last FutMon year); iii) binary variable: C (conifer yes/no) and D (deciduous yes/no). Environmental variables were log transformed.

Figure 6.1.3 presents the results of the NMDS. NMDS1 identifies an altitudinal gradient, with holm oak forests and low-altitude mixed forests (TOS2, VEN2, and SAR1) distributed along the positive values of the axis, which correspond to greater air temperature. Sites with the highest nitrogen deposition and the lowest lichen richness (PIE1 and EMI1) are found along negative values of NMDS2, while sites with the highest species composition (ABR1, LAZ1, and VEN1) are associated to the positive values of the axis.

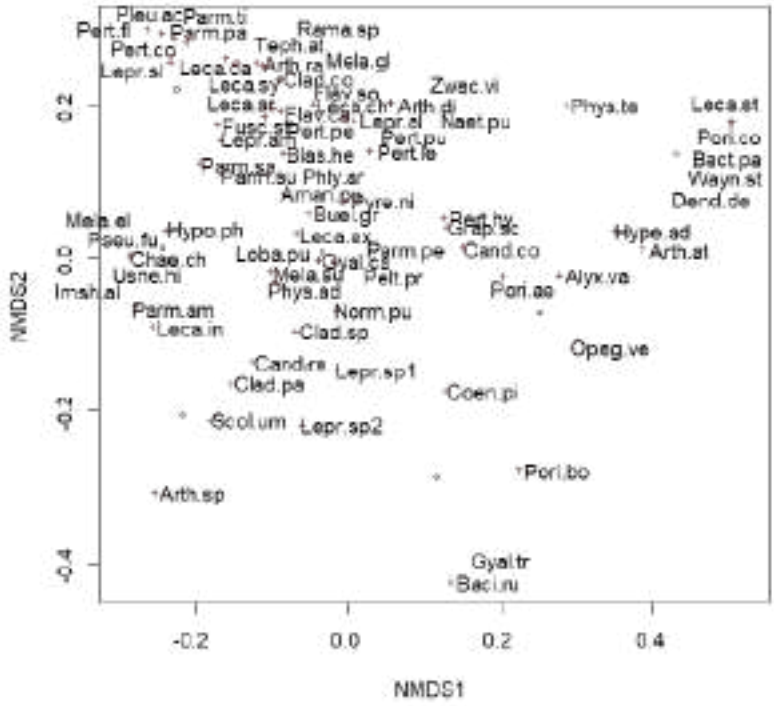

Figure 6.1.3. Results of the NMDS (→ continues).

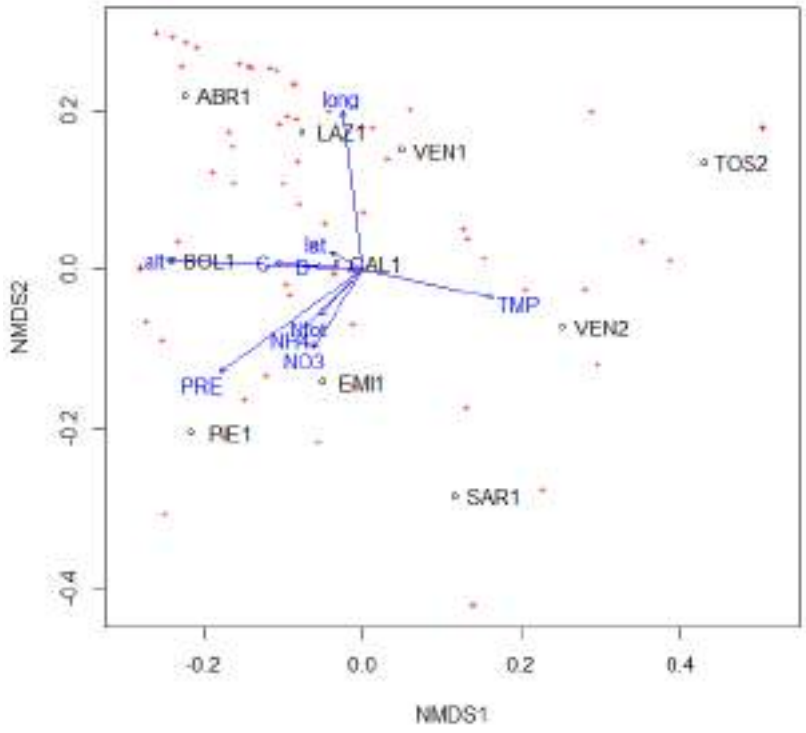

Figure 6.1.3. Results of the NMDS.

To study the response of lichen functional diversity to the levels of nitrogen and sulfur deposition recorded respectively one year and two years before the lichen surveys, a PCA was used as explorative unsupervised multivariate analysis (Figure 6.1.4).

PC1 reflects a gradient of nitrogen deposition, characterizing the PIE1 and EMI1 sites, which exhibit the highest values of nitrophytic species (%LDV_NITRO, %SP_NITRO). Negative PC1 and positive PC2 values relate to ABR1 and LAZ1, which have the greatest lichen species richness in terms of macrolichens (%LDV_MACRO), LDV (LDV_TREE), and number of species (NSP_TREE). The negative values of PC2 correspond to a sulfur deposition gradient primarily linked to CAL1, reflecting a prevalence of oligotrophic species (%SP_OLIGO, %LDV_OLIGO).

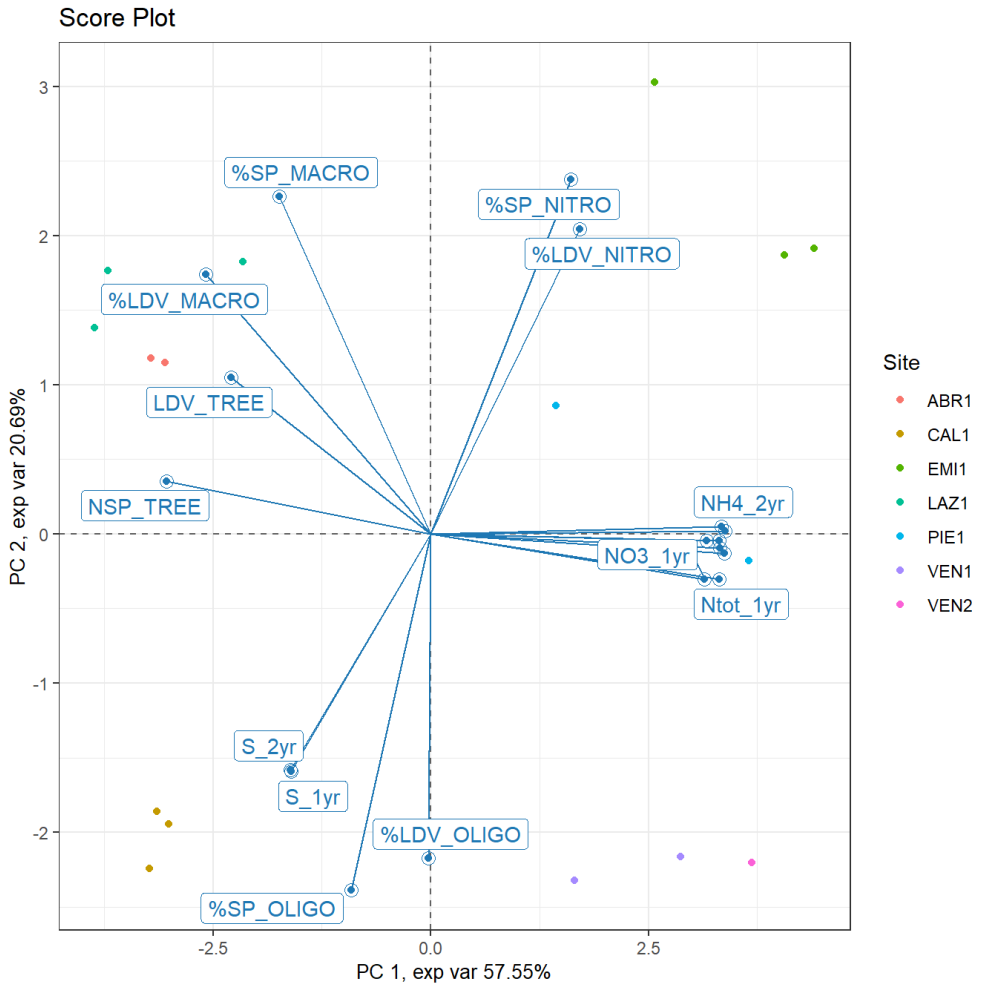

Figure 6.1.4. Results of the PCA on autoscaled data.

6.1.2 Relationship between ozone concentrations and ozone symptoms

In this section the relationship between ozone concentrations and leaf injuries (expressed as percentages) is explored using beta regression models.

The coefficient estimates β_i can be interpreted in terms of odds ratio:

$$OR := \frac{\frac{\mu_B}{1-\mu_B}}{\frac{\mu_A}{1-\mu_A}} = e^{c\beta_i}$$

where μ is the modelled mean of the distribution, $c>0$ is the i-th covariate increment, $\mathbf{x\_A}=[x_1,\ldots,x_i,\ldots,x_n]$, $\mathbf{x\_B}=[x_1,\ldots,x_i+c,\ldots,x_n]$

Thus

- if $OR>1$ there is a positive effect of x_i on μ
- if $OR<1$ there is a negative effect of x_i on μ
- if $OR=1$ there is no effect of x_i on μ.

Before model fitting, the percentages of response variables are converted such that they range in the [0, 1] interval. Models are fitted separately for each Main tree species: *Quercus petraea* and *Fagus sylvatica*.

The model fitted for *Quercus petraea* shows that the levels of ozone (annual mean) have a statistically significant effect on the percentage of symptomatic species (Table 6.1.1; $p<0.05$), whereas any significant relationship is found for *Fagus sylvatica* (Table 6.1.2; $p>0.05$). These findings may be due to the limited dataset available.

Table 6.1.1. Results of the beta regression model fitted for Quercus petraea*.*

```
## **Quercus petraea**
## [1] "n_obs: 6"
## [1] "perc_symptomatic_species ~ O3_Annual_mean + O3_Growing_season_mean + AOT40 + POD0 + POD1"
##
## Call:
## betareg::betareg(formula = as.formula(f), data = gr)
##
## Randomized quantile residuals:
##     Min      1Q  Median      3Q     Max
## -0.0106  0.0019  0.0156  0.0277  0.0660
##
## Coefficients (mu model with logit link):
##                         Estimate Std. Error z value Pr(>|z|)
## (Intercept)             -882.52        NaN     NaN      NaN
## O3_Annual_mean           -64.53      26.79  -2.409    0.016 *
## O3_Growing_season_mean   290.06        NaN     NaN      NaN
## AOT40                    -84.76        NaN     NaN      NaN
## POD0                     624.40        NaN     NaN      NaN
## POD1                    -405.27        NaN     NaN      NaN
##
## Phi coefficients (phi model with identity link):
##       Estimate Std. Error z value Pr(>|z|)
## (phi)    749.2      510.4   1.468    0.142
##
## Exceedence parameter (extended-support xbetax model):
##         Estimate Std. Error z value Pr(>|z|)
## Log(nu)   -4.939        NaN     NaN      NaN
## ---
## Signif. codes:  0 '***' 0.001 '**' 0.01 '*' 0.05 '.' 0.1 ' ' 1
##
## Exceedence parameter nu: 0.0072
## Type of estimator: ML (maximum likelihood)
## Log-likelihood: 12.64 on 8 Df
## Number of iterations in BFGS optimization: 468
```

Table 6.1.2. Results of the beta regression model fitted for Fagus sylvatica*.*

```
## **Fagus sylvatica**
## [1] "n_obs: 18"
## [1] "perc_symptomatic_species ~ O3_Annual_mean + O3_Growing_season_mean + AOT40 + POD0 + POD1"
##
## Call:
## betareg::betareg(formula = as.formula(f), data = gr)
##
## Randomized quantile residuals:
##     Min      1Q  Median      3Q     Max
## -1.6852 -0.4900 -0.1618  0.6776  3.1209
##
## Coefficients (mu model with logit link):
##                       Estimate Std. Error z value Pr(>|z|)
## (Intercept)            14.2702     7.5212   1.897   0.0578 .
## O3_Annual_mean          5.8500     4.2752   1.368   0.1712
## O3_Growing_season_mean -5.1462     4.8336  -1.065   0.2870
## AOT40                  -1.0331     0.8662  -1.193   0.2330
## POD0                   -4.9376     6.3707  -0.775   0.4383
## POD1                    3.3698     4.5076   0.748   0.4547
##
## Phi coefficients (phi model with identity link):
##       Estimate Std. Error z value Pr(>|z|)
## (phi)    19.65      12.81   1.534    0.125
##
## Exceedence parameter (extended-support xbetax model):
##         Estimate Std. Error z value Pr(>|z|)
## Log(nu)  -1.4413     0.8771  -1.643      0.1
## ---
## Signif. codes:  0 '***' 0.001 '**' 0.01 '*' 0.05 '.' 0.1 ' ' 1
##
## Exceedence parameter nu: 0.2366
## Type of estimator: ML (maximum likelihood)
## Log-likelihood: 5.228 on 8 Df
## Number of iterations in BFGS optimization: 60
```

6.1.3 Relationship between foliar analysis, deposition and defoliation

In this section the relationship between foliar analysis, depositions and defoliation values is investigated. Tree-level foliar analysis data have been aggregated to obtain the mean values for each site and year. For deposition data, only throughfall deposition was considered. For crown condition, only mean defoliation (DefM) was used.

Principal Component Analysis (PCA) was performed on autoscaled data (Figure 6.1.5). The first principal component (PC1) reveals a gradient of increasing nitrogen deposition, which aligns with high values of nitrogen and N:P ratios detected in foliar samples. This gradient characterizes the EMI1, VEN2, and PIE1 sites. The CAL1, LAZ1, and VEN1 sites are distributed along negative PC1 values and are linked to sulfur depositions and the deposition of other elements (Ca, Na, Mg, Cl, K), which correspond to the elevated foliar Ca, K, P and Ca:Mg ratios. Defoliation shows only a weak correlation with negative PC1 and PC2 values.

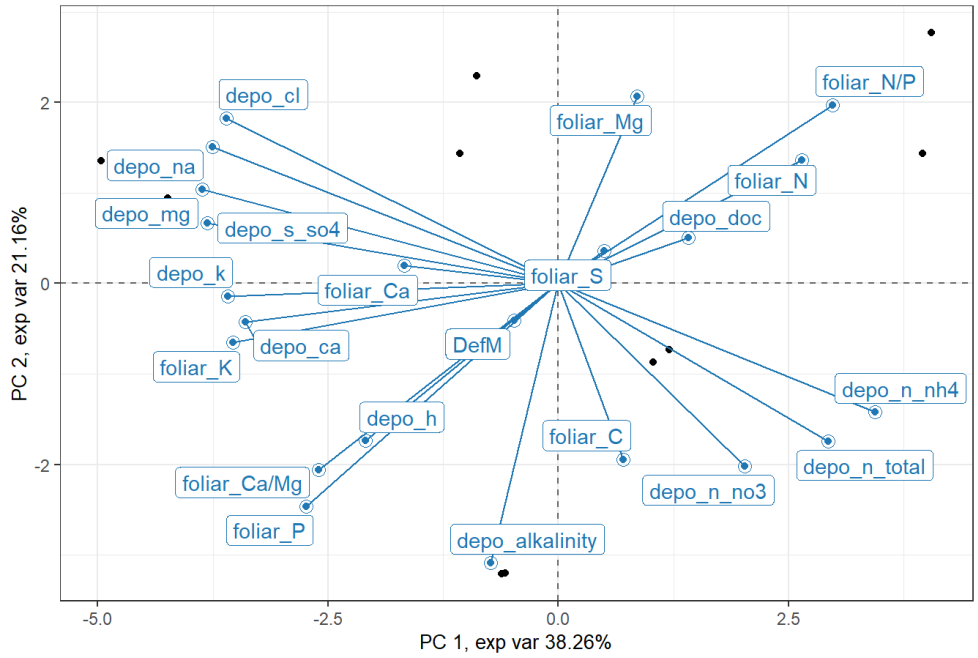

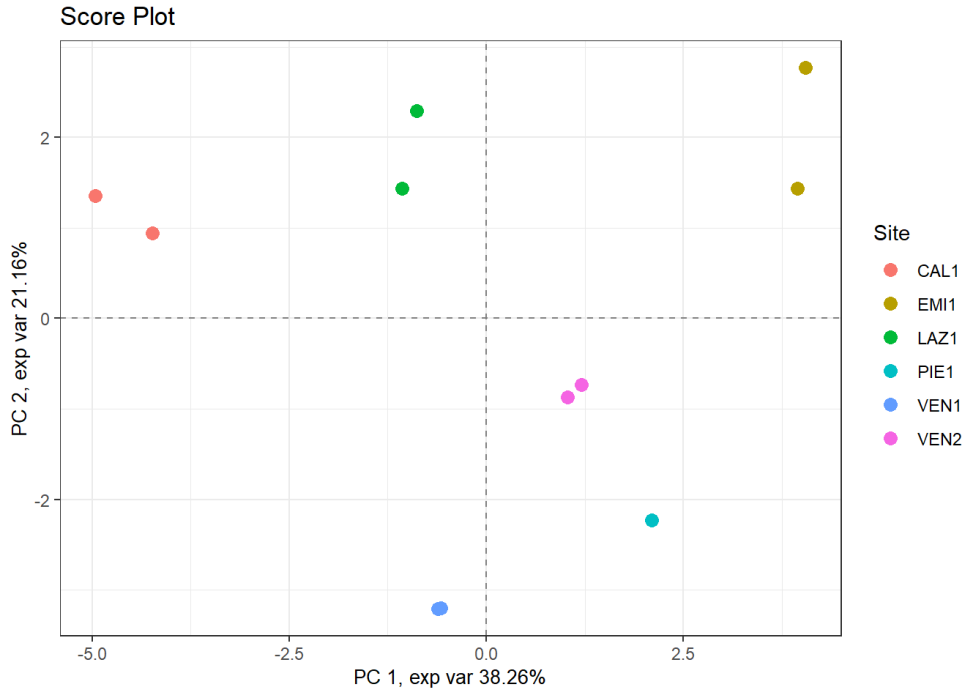

Figure 6.1.5. Results of the PCA on autoscaled data.

6.1.4 Relationship between bird and bat diversity

A dataset was created to analyze the relationship between bats and birds, which records the number of bird species detected in a single day at each site. This metric serves as a measure of bird richness, similar to bat richness. PCA was performed on autoscaled data of bird and bat indices (Figure 6.1.6). Bird species richness and bat richness and evenness are distinctly separated along PC2, showing opposite patterns. CAL1, VEN2, and TOS2 have higher bird richness values, while bat diversity is higher at ABR1, CAL1, SAR1 and LAZ1. In contrast, EMI1, TOS2, VEN2 and BOL1 have the lowest levels of bat richness, and ABR1 and PIE1 show the lowest bird richness.

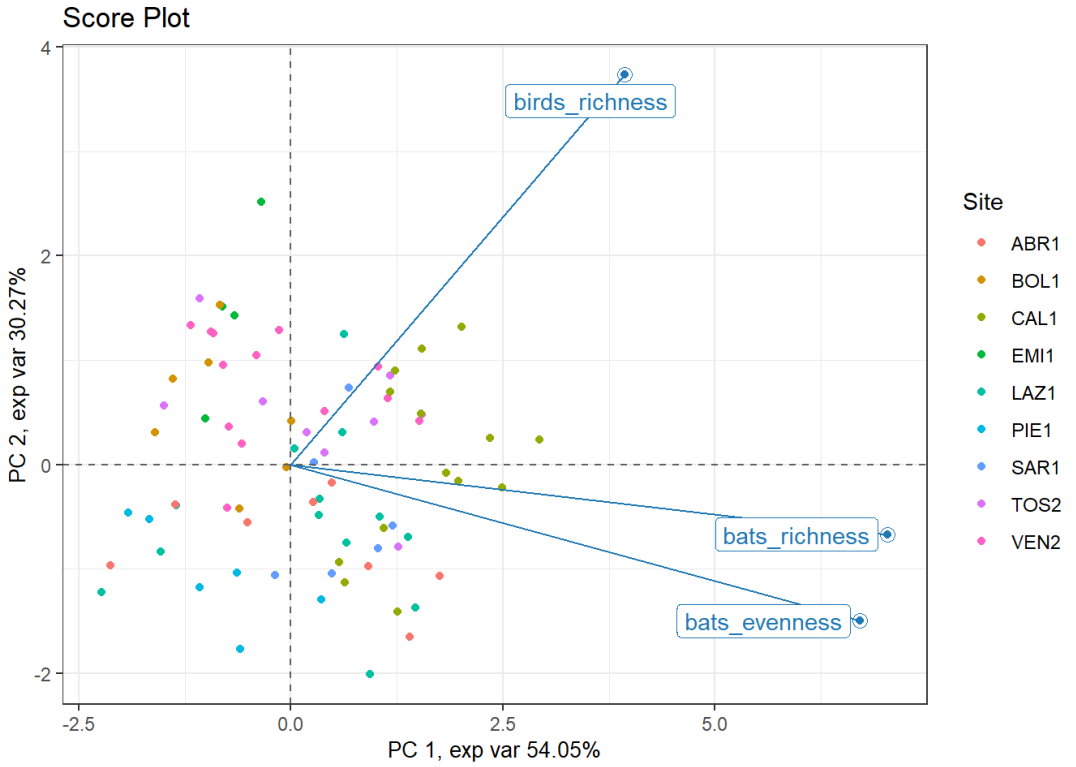

Figure 6.1.6. Results of the PCA on autoscaled data.

6.1.5 Relationship between different biodiversity groups

The congruence among the four taxonomic groups (lichens, herbaceous plants, bats and birds) was analyzed based on their species richness detected during the survey 2023 (Table 6.1.3) across the forest sites with shared datasets (8 out of the 10 forest sites; as lichen diversity data were collected at different sites over 2023 and 2024, the dataset was treated as a single survey and attributed to 2023). Regression analysis (Pearson r) shows a positive correlation between lichen and bat diversity (r=0.66) and between birds and herbaceous plants (r=0.53).

Table 6.1.3. Species richness of the four groups of taxa recorded in the sites of the project in the year 2023.

Site	Lichens	Bats	Birds	Ground Vegetation *
ABR1	36	15	17	17
BOL1	17	7	22	46
CAL1	37	14	21	24
EMI1	20	6	24	22
LAZ1	42	8	18	42
PIE1	13	4	9	9
TOS2	15	5	19	20
VEN2	10	9	18	22

** Herbaceous species.*

Figure 6.1.7. Pearson's correlation among groups of taxa in the 9 forest sites in 2023.

The PCA confirms Pearson's correlations (Figure 6.1.8): lichen and bat diversity correlate with each other and with positive PC2 values, associated with the Mountainous Beech Forests of ABR1 and CAL1. Ground vegetation and bird diversity correlate with each other and align with negative PC2 values in relation to the Broadleaved Deciduous Forest of LAZ1 and the Mountainous Conifer Forest (BOL1). Positive values of PC1 identify the sites with the lowest values of biodiversity (TOS2, PIE1, EMI1 and VEN2).

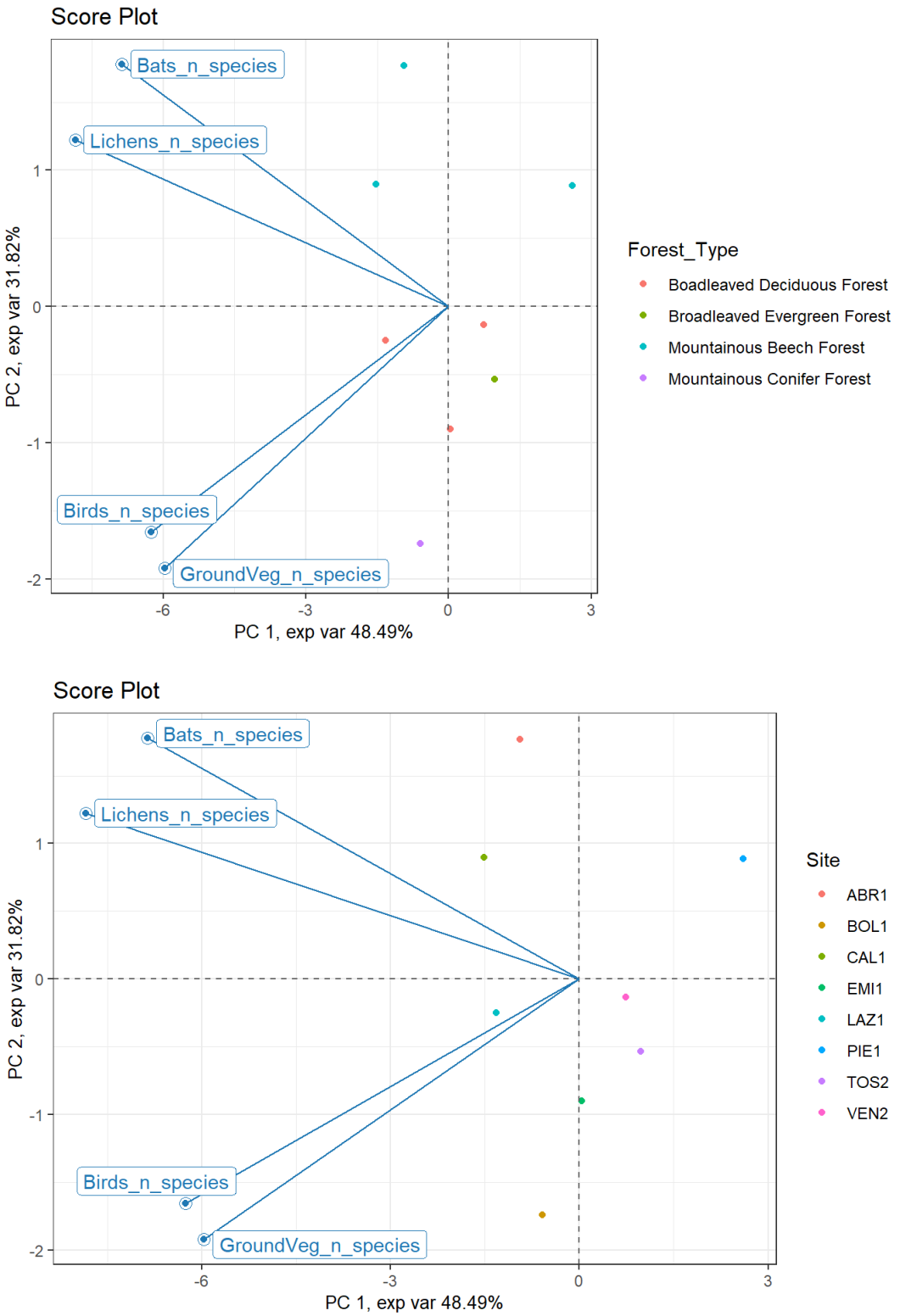

Figure 6.1.8. Results of the PCA on autoscaled data.

Multiple Factor Analysis (MFA)

To examine the relationships among the four taxonomic groups in terms of species composition rather than of species richness, we analyzed their presence/absence matrix using a Multiple Factor Analysis (MFA). This multivariate method is designed to analyze datasets in which variables are arranged in distinct groups, and it facilitates the organization and visualization of complex data tables. The MFA performs individual PCAs and integrated their results within a multidimensional space. In our case, the four taxonomic groups contain many separate variables represented by the presence/absence values of each species (Figure 6.1.9).

Tables 6.1.4 to 6.1.6 and Figures 6.1.9 to 6.1.12 present the results of the MFA. The first three dimensions of the MFA account for over the 50% of variance (Table 6.1.4).

Table 6.1.4. Results of the MFA: variance, % of variance and cumulative % of variance.

	Dim.1	Dim.2	Dim.3	Dim.4	Dim.5	Dim.6	Dim.7
Variance	3.283	2.641	2.566	2.356	2.012	1.694	1.549
% of var.	20.39	16.41	15.94	14.63	12.49	10.52	9.62
Cumulative % of var.	20.39	36.79	52.73	67.36	79.86	90.38	100.00

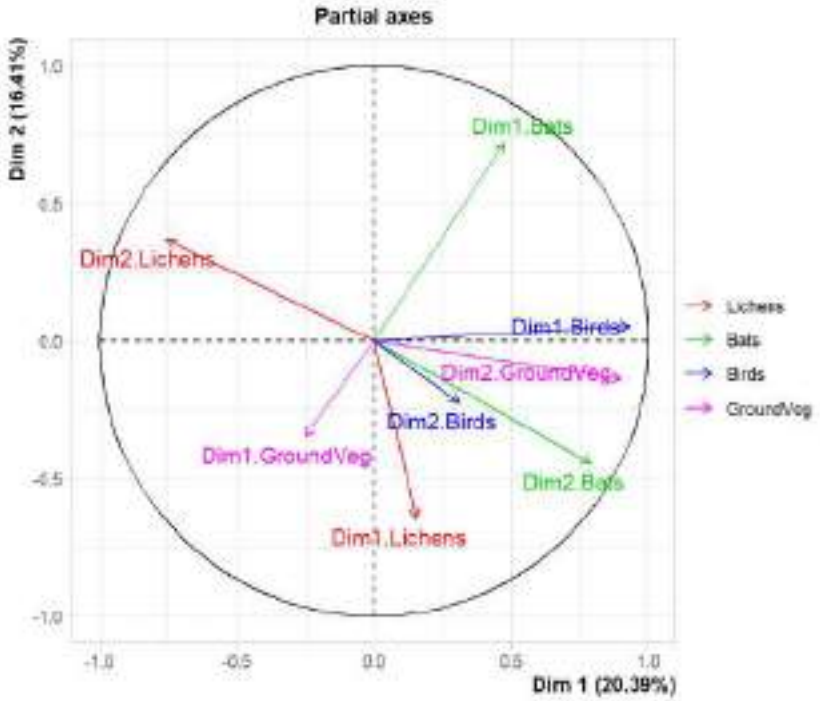

Figure 6.1.9. Results of the MFA: partial axes.

The site TOS2 accounts for most of the variance in the first dimension (87.8%) and separates from the other sites for its diverse species composition (Fig. 6.1.10 and Table 6.1.5). Positive values of Dim.2 are primarily associated with the site ABR1 (62.3%), whereas most other sites are distributed along negative values of this axis. The Mountainous Conifer Forest of BOL1 contributes the most to the variability of the Dim.3 (55.4%), along with VEN2 (21.4%).

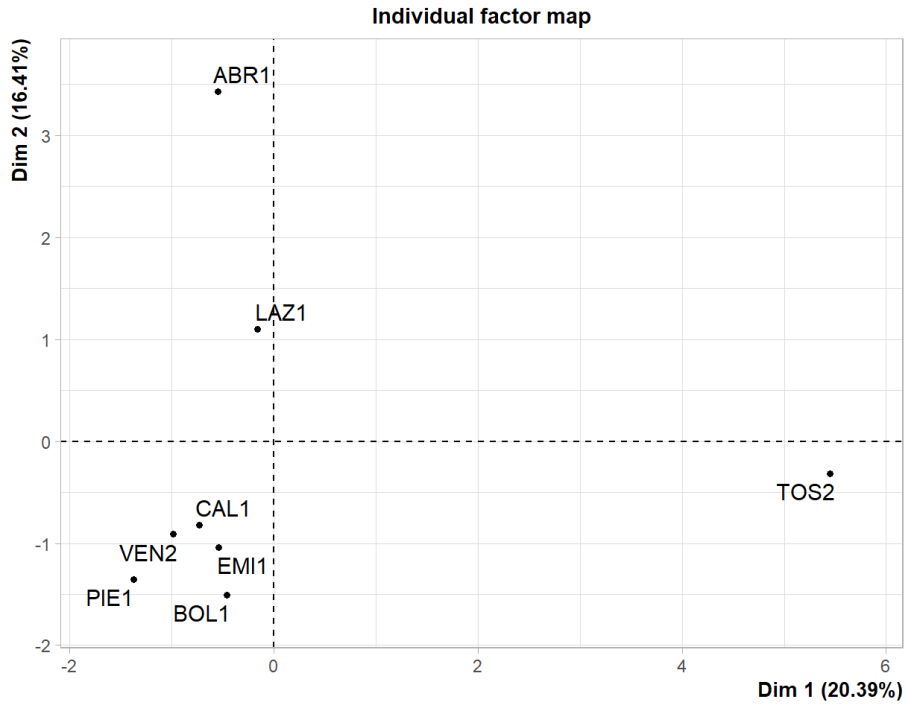

Figure 6.1.10. Results of the MFA: individual factor map.

Table 6.1.5. Results of the MFA: values of coordinates, contribute and sqaure cosine for the 8 forest sites.

Site	Dim.1			Dim.2			Dim.3		
	Coord	Contr	COS2	Coord	Contr	COS2	Coord	Contr	COS2
ABR1	-0.545	1.265	0.020	3.432	**62.350**	0.787	0.873	4.154	0.051
BOL1	-0.462	0.985	0.015	-1.510	13.067	0.165	3.066	**55.418**	0.679
CAL1	-0.731	2.572	0.042	-0.822	4.037	0.053	-0.824	4.178	0.053
EMI1	-0.539	1.047	0.021	-1.039	4.838	0.077	-1.409	9.164	0.142
LAZ1	-0.159	0.140	0.003	1.099	8.274	0.149	-0.623	2.735	0.048
PIE1	-1.372	3.302	0.055	-1.356	4.008	0.053	1.138	2.904	0.038
TOS2	5.451	**87.816**	0.982	-0.318	0.370	0.003	-0.113	0.048	0.000
VEN2	-0.986	2.872	0.050	-0.912	3.055	0.043	-2.379	21.400	0.294

With respect to the cross congruence between the four taxon groups, the MFA supports the PCA findings, showing correlations between lichen and bat communities, as well as between birds and herbaceous plants (Figure 6.1.11; Table 6.1.6). Species compositions across all four groups correlate similarly with Dim.1 (values from 21.8% to 29.4%). Birds exhibit the strongest association with Dim.1 (29.4%), lichen communities characterize the Dim.2 (32.7%), and herbaceous species align with the Dim.3 of the MFA (34.2%).

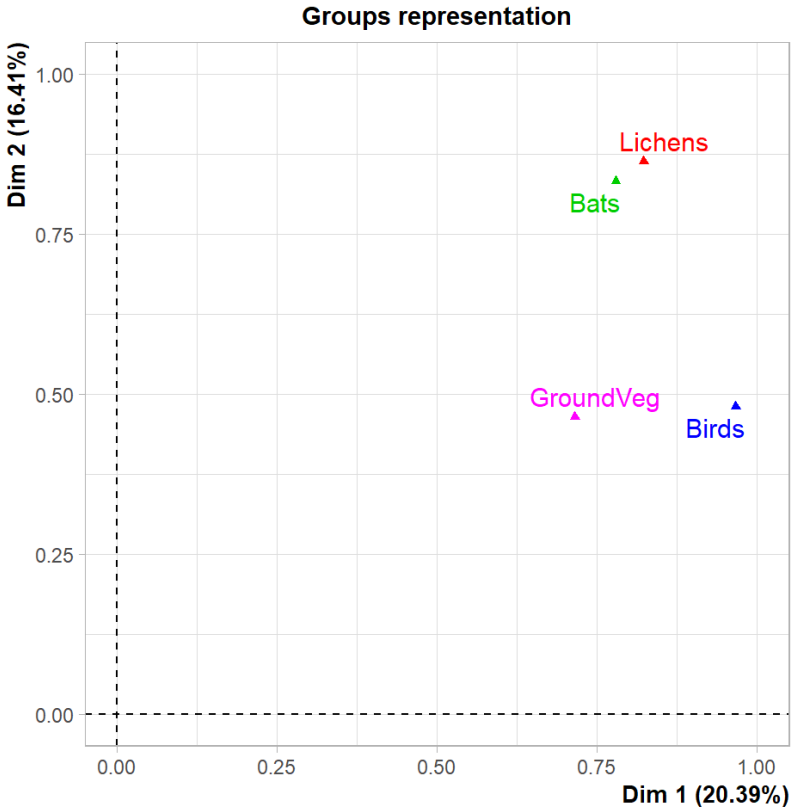

Figure 6.1.11. Results of the MFA: groups representation.

Table 6.1.6. Results of the MFA: values of coordinates, contribute and sqaure cosine for the four biodiversity groups.

Group	Dim.1			Dim.2			Dim.3		
	Coord	Contr	COS2	Coord	Contr	COS2	Coord	Contr	COS2
Lichens	0.822	25.052	0.201	0.864	**32.695**	0.221	0.519	20.218	0.080
Bats	0.779	23.730	0.257	0.833	31.535	0.294	0.517	20.143	0.113
Birds	0.966	**29.440**	0.332	0.481	18.193	0.082	0.653	25.452	0.151
Herbaceous plants	0.715	21.777	0.200	0.464	17.577	0.084	0.877	**34.187**	0.300

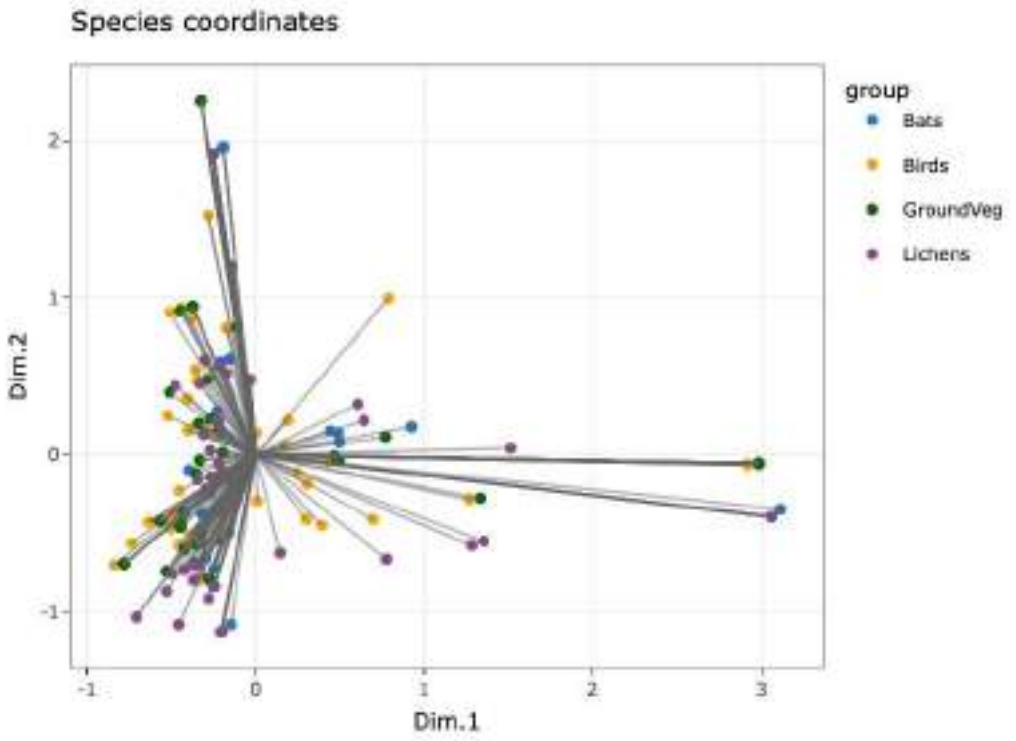

Figure 6.1.12. Results of the MFA: species coordinates.

6.2 Freshwater ecosystems: an integrated analysis

6.2.1. Relationships among chemical and environmental variables and sites

The relationships among chemical and selected environmental variables were assessed by regression analysis (Pearson r) based on the average data (log-transformed) of 2023-24 (Fig. 6.2.1). A cluster analysis (Ward's method, Euclidean distance) was applied to identify the main site subgroups according to chemical parameters (Fig. 6.2.2).

Significant correlations were found between conductivity on one side and major solute (Ca, Mg, SO_4). Alkalinity also correlated, even if not significantly, with pH and base cations. No correlations emerged among nutrients (P, N, Si) and TOC, apart from the correlation between TOC and organic N. Among the environmental variables, altitude and catchment area were negatively and positively related, respectively, to most of the chemical variables, as an effect of the higher concentrations of both ions and solutes in the lowland, wide-catchments sites. Nitrogen deposition was not correlated to NO_3 water content, indicating that NO_3 is regulated by several factors besides

atmospheric inputs, such as soil and vegetation cover in the catchments or in-lake and in-stream processes (Burpee et al., 2022).

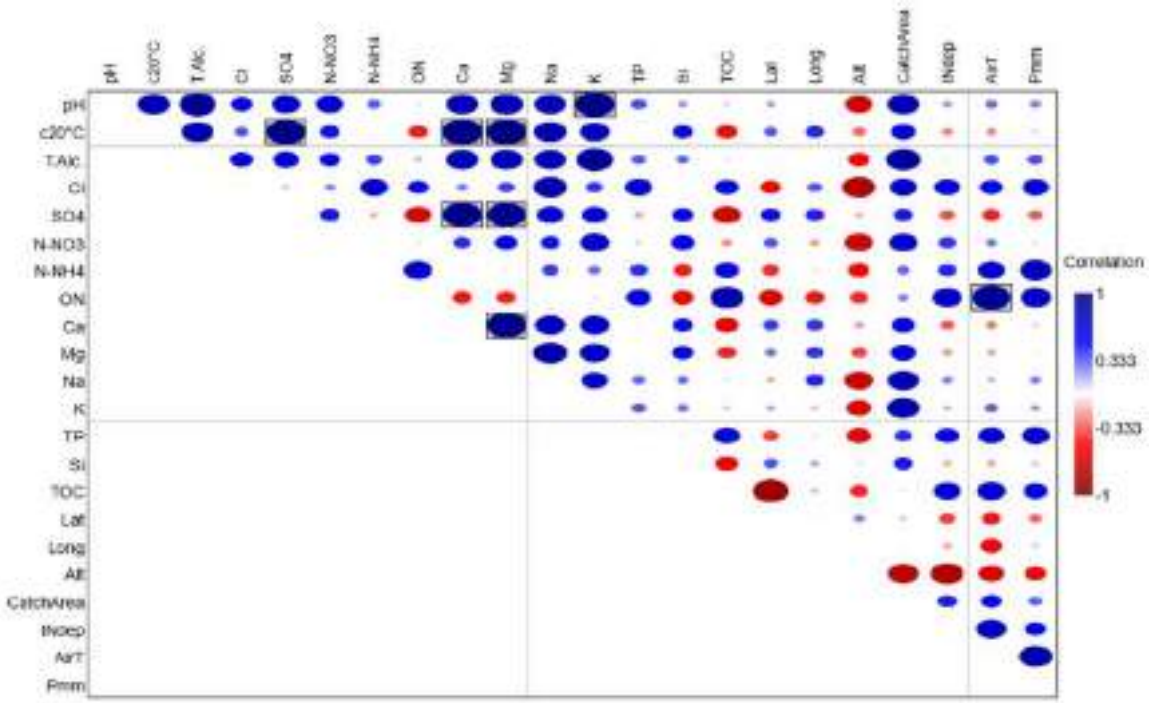

Figure 6.2.1. Regression analysis (Pearson's correlation, Bonferroni correction) based on chemical data of 2023-24. Squares indicate significant correlations (p<0.05)

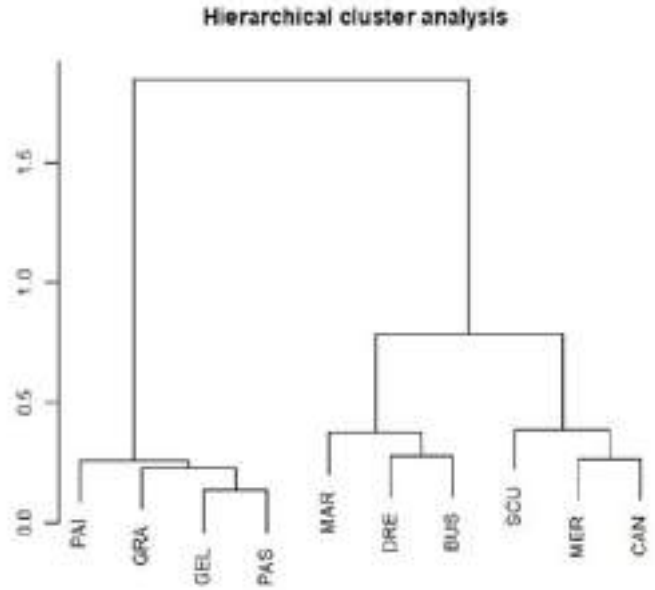

Figure 6.2.2. Cluster analysis applied to the chemical data (14 variables) collected on the study sites in 2023-24.

Three main subgroups were identified by cluster analysis: a first group including the high altitude lakes in the Western Alps PAI, PAS, GRA and GEL, which are characterised by the lowest pH and ANC (6.5 and 20-50 µeq L^{-1} as average values) (i.e. highest sensitivity to acidification) and the lowest concentrations of the major ions (conductivity < 10 µS cm^{-1} at 20 °C); a second group including both river and lake mountain sites (MAR, DRE and BUS), with well-buffered waters (ANC > 300 µeq L^{-1}) and a moderate to high solute content (cond. approx. 100 µS cm^{-1}); a third group, including the medium-low altitude sites (SCU, MER, CAN), characterised by intermediate ANC values (around 200 µeq L^{-1}) and the highest concentrations of NO_3, nutrients and TOC (NO_3 > 300 µg L^{-1} with respect to 120-200 µg L^{-1} of the other groups; TOC 1.6 mg L^{-1} with respect to 0.7-0.3 mg L^{-1}). In summary, the analysis confirmed a separation of sites based on geographical features, mainly altitude, and catchment characteristics (area and land cover).

It can be concluded that the selected sites are representative of a wide range of sensitivity to atmospheric pollution, namely to acidification and N enrichment. Despite being all oligotrophic, the sites also cover a range of nutrient and TOC concentrations, being suitable to assess the eventual eutrophying effects of N deposition. Long-term chemical data collected at these sites on a regular basis may provide useful information on NEC indicators and their change in time in response to changing deposition and other drivers; they can also be used in conjunction with biological indicators (see next paragraph) to assess the overall status of sensitive freshwater ecosystems.

6.2.2. Temporal trends in response to deposition and climate change

Time series of chemical data exist for some of the sites belonging to the ICP WATERS and LTER network: the high-altitude lakes PAS, PAI, GEL and GRA, the alpine stream BUS and the subalpine sites MER and CAN. To assess the long-term trends in acid sensitive high-altitude lakes in response to changing deposition, the newly collected data (2023-24) were used to update the time series and trend significance and slope of selected chemical variables analysed with the Mann-Kendall Test (MKT; Hirsch and Slack 1984) and Sen's slope estimator (Sen, 1968). Other ICP WATERS sites located in the Western Alps, not included in the MODERn NEC project, and covering a range of acidification sensitivity, were considered in the analysis (8 lakes in total; Table 6.2.1; Fig. 6.2.3), to get a more representative evaluation of lake chemical evolution (for details on these sites, see Rogora et al., 2022). Data from the samplings performed in the late-autumn period were used, being representative of a more stable condition of lake chemistry with respect to the snowmelt period (Rogora et al., 2013). PAS and PAI were monitored regularly, while irregular surveys were conducted

on the other lakes. Consequently, the number of samplings over the period 1984-2024 varied from one site to the other, from a minimum of 18 to 41.

*Table 6.2.1. Results of trend analysis on the time series data of 7 high altitude lakes covering the period 1984-2024 (lake MUI not included in the trend analysis). Trend significance according to the Mann Kendall Test: * p <0.05; ** p<0.01; *** p<0.001; n.s. not significant Sen's slope; units: pH unit y^{-1}; SO, NO_3, BC, ANC µeq L^{-1} y^{-1}. Significant positive and negative trends are shown in red and blue, respectively.*

Time series	n	p	Sen's slope
pH GEL	18	**	0.026
SO_4 GEL	19	***	-0.648
NO_3 GEL	19	***	-0.422
BC GEL	19		-0.028
ANC GEL	19	***	0.997
pH GRA	20	**	0.019
SO_4 GRA	20	***	-0.694
NO_3 GRA	20	***	-0.557
BC GRA	20	*	-0.904
ANC GRA	20	**	0.829
pH VAS	23	**	0.012
SO_4 VAS	23	***	-1.070
NO_3 VAS	21	***	-0.531
BC VAS	23		0.092
ANC VAS	22	***	1.794
pH VAI	20		0.007
SO_4 VAI	20	***	-1.145
NO_3 VAI	18	***	-0.417
BC VAI	20		-0.193
ANC VAI	19	**	1.727
pH SFO	18	***	0.023
SO_4 SFO	18		-0.324
NO_3 SFO	18	**	-0.492
BC SFO	18		-0.233
ANC SFO	18	***	0.874
pH LPI	41	***	0.009
SO_4 LPI	41	***	-0.960
NO_3 LPI	41	***	-0.276

Time series	n	p	Sen's slope
BC LPI	41		-0.113
ANC LPI	41	***	1.141
pH LPS	41	***	0.030
SO_4 LPS	41	***	-0.866
NO_3 LPS	41	***	-0.396
BC LPS	41	**	-0.327
ANC LPS	41	***	0.947

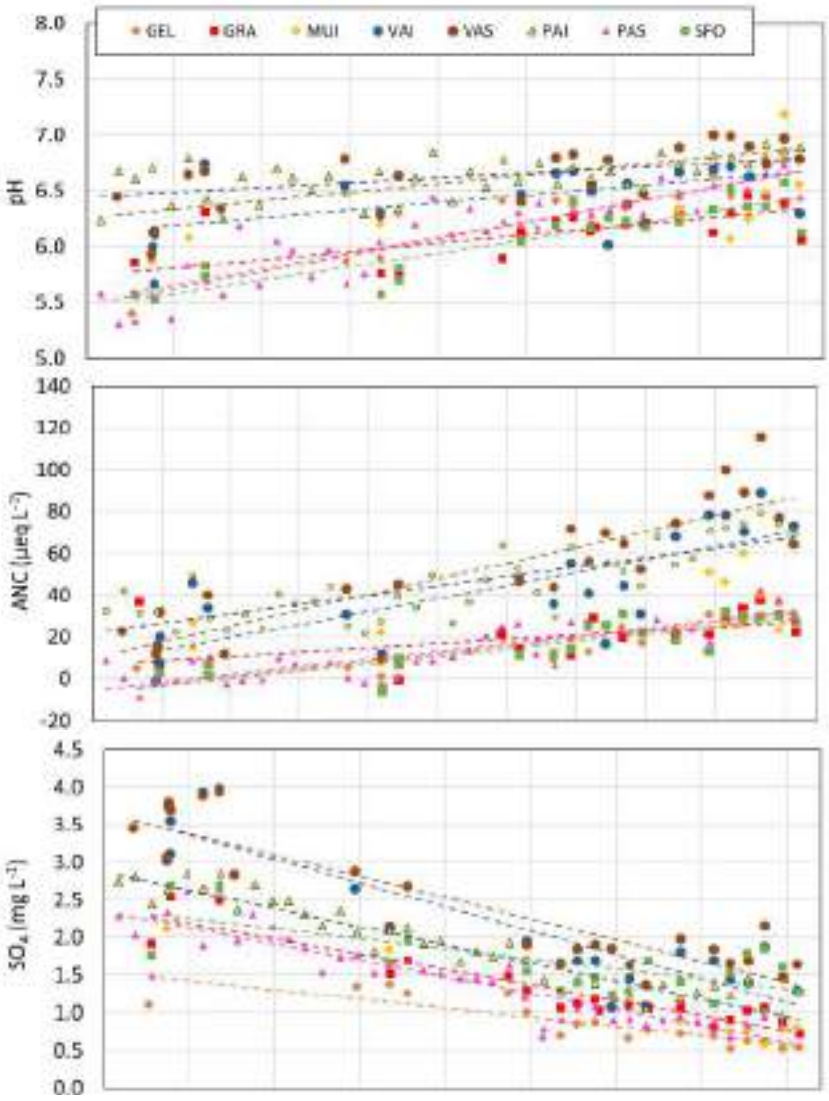

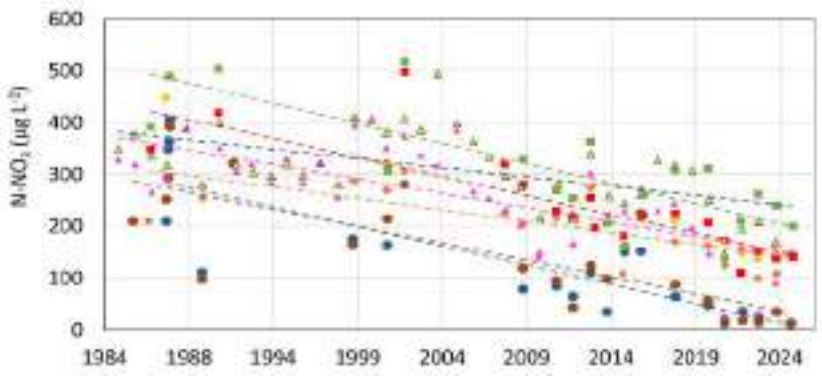

Figure 6.2.3. Trends of pH, ANC, SO_4 and NO_3 in 8 high altitude lakes based on annual data collected in late summer-early autumn. Regression lines indicate significant trends (p<0.01) according to the Mann-Kendall Test.

Significant negative trends of SO_4 (p<0.001 according to MKT) were found in all the lakes except SFO, with slope between -0.7 and -1.1 µeq L^{-1} y^{-1}. Nitrate also decreased significantly in all lakes (slope between -0.3 and -0.5 µeq L^{-1} y^{-1}), while pH and ANC increased (slope 0.01-0.02 pH unit y^{-1}; 0.8-1.1 µeq L^{-1} y^{-1} or even higher in VAI and VAS). Base cations decreased but not significantly (Tab. 6.3). Time series plots showed that SO_4 concentrations almost halved in the lakes; the steepest decline occurred until around 2010, then concentrations stabilised in all the lakes. These trends are a direct consequence of the decreasing SO_4 deposition occurring in the study area since the 1980s (Rogora et al., 2016). On the other hand, nitrogen deposition decreased later and to a lesser extent, causing a delayed response of NO_3 in surface water: indeed, a shift towards lower NO_3 concentrations in the study lakes can be seen only since 2008 (Figure 6.2.4). All lakes, particularly PAS, PAI, VAS and VAI, had very low concentrations of NO_3 in 2020: this has been related to the temporary decrease of N deposition in 2020 as an effect of the decreased NO_x emission during the pandemic period (Rogora et al., 2022). The trends overall confirm a chemical recovery from acidification. However, the most sensitive lakes (GEL, GRA, PAS) are still characterised by rather low pH (below or close to 6.5) and ANC (< 30 µeq L^{-1}). Furthermore, despite the temporary minimum in 2020, average NO_3 levels in the most impacted lakes (GEL, GRA, PAI, PAS) are still around 200 µg L^{-1} and seem to have stabilised in the very recent years. N deposition in the lake area is still high compared to critical loads, especially for sensitive ecosystems such as oligotrophic lakes where atmospheric inputs represent the main nitrogen source (Rogora et al., 2016).

Time series of weekly and monthly data are available for the two stream sites, BUS and CAN, since the 1980s and since 2002, respectively. Indeed, a monthly or even higher frequency has been recommended for stream site monitoring, considering the higher variability of chemical indicators in relation to hydrology (ICP WATERS 2025). These data allow an evaluation of the long-term but also seasonal change of acid-sensitivity and N saturation indicators. Trends of ANC and NO_3 in CAN

are shown in figure 5.7: both variables show a rather high variability, with values ranging mostly between 100 and 350 µeq L^{-1} and 400-1000 µg L^{-1}, respectively. The site can be considered not particularly sensitive towards acidification and ANC showed a positive trend, from about 200 µeq L^{-1} in the early 1980s to 250 µeq L^{-1} as average annual values; however, acidic episodes may occur in correspondence with heavy rainfalls, with ANC dropping below 100 µeq L^{-1} (e.g. 79 µeq L^{-1} in October 2014; 72 µeq L^{-1} in October 2021). NO_3 showed an increasing tendency until 2004-2005, then decreased in the period 2006-2020, with sharp oscillation in the last few years. Long-term change in NO_3 concentration at this site has been related to the pattern of N deposition in the area, but climate drivers have proved to contribute to the short-term variability (Rogora et al., 2012). To assess the present N saturation condition of this river catchment, Stoddard's approach (Stoddard, 1994) was applied to monthly NO_3 data of recently collected data (2022-2024; Figure 6.2.5). Stoddard (1994) defined four progressive stages of N saturation in forested catchments based on changes in seasonality and levels of nitrate leaching in streams. Based on these criteria, CAN can be classified for stage 2 of N saturation (no month with NO_3 <= 3 µeq L^{-1} and >= 3 months in the growing season with NO_3 < 50 µeq L^{-1}), where the nitrogen cycle is dominated by nitrate leaching.

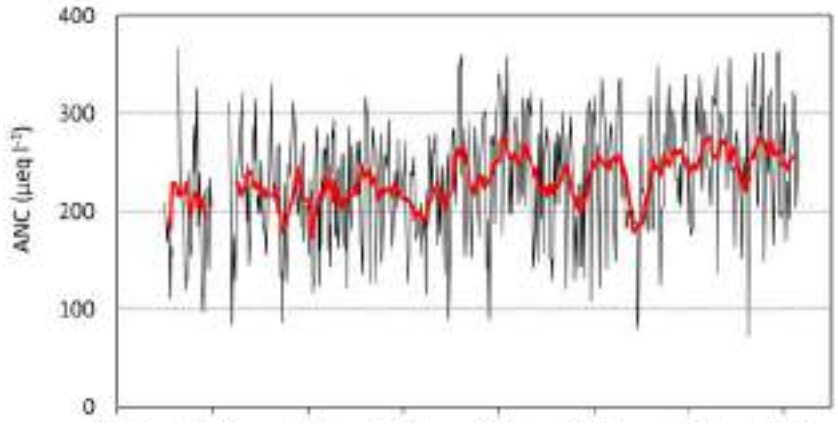

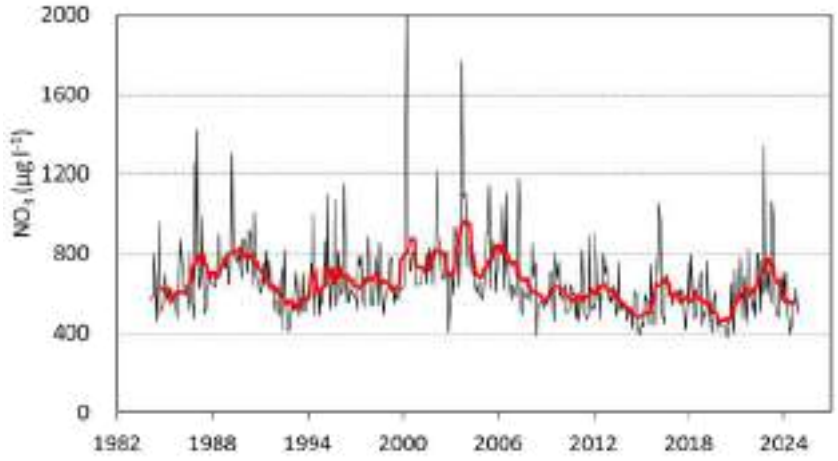

Figure 6.2.4. Trends of ANC and NO_3 concentration in CAN in the period 1984-2024 based on monthly data. Red line: 12-point running average.

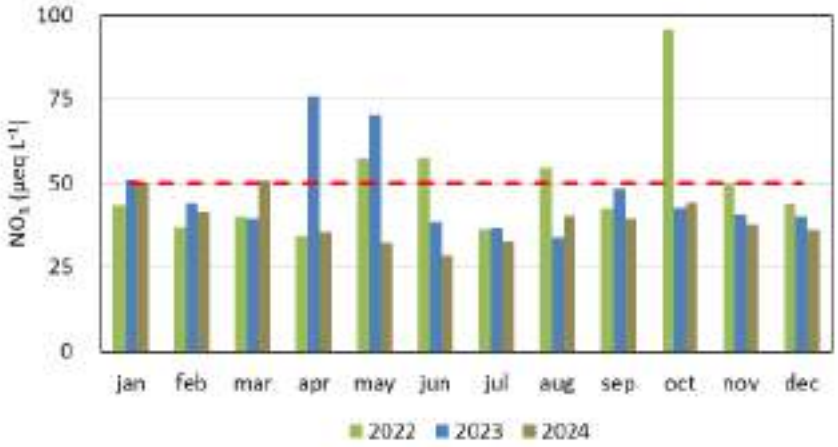

Figure 6.2.5. Monthly concentrations of NO_3 in river CAN in 2022, 2023 and 2024 compared with the critical limit of 50 µeq L^{-1}.

In summary, the main chemical indicators indicate a limited sensitivity of the selected sites to acidification, also in consideration of the evident chemical recovery that occurred in the most sensitive sites in the last two decades. Present level of ANC are mainly above the critical limits normally assumed for freshwater (e.g. 50 µeq L^{-1}); however, acidic episodes may still occur in particular conditions such as snowmelt and may be fostered by specific meteo-hydrological conditions (e.g. heavy rainfalls). Despite recent decline in NO_3 concentrations, the selected sites can be considered sensitive to N deposition and its effects, also in terms of nutrient enrichment. The eutrophying effect of P and N deposition should be considered, possibly in combination with climate-related drivers, by using simple and reliable proxies of lake productivity. With the

decreasing impact of acidifying compounds, other air pollutants may become more important, requiring specific monitoring and targeted indicators.

6.2.3 Relationships among diatoms and macroinvertebrates and environmental variables

For both diatoms and macroinvertebrates, mean temperature (Tmean) and precipitation (PCNP) data from June to August 2023 were included in the analyses (correlation tests and Canonical Correspondence Analysis). In examining the relationships between diatom assemblages and environmental variables (altitude, Tmean, and PCNP), no significant correlations were detected, suggesting that diatom distribution is more strongly influenced by water chemistry. In line with this, a significant negative correlation was found between species richness and pH (Spearman's r = –0.67, p = 0.039) (Fig. 6.2.6).

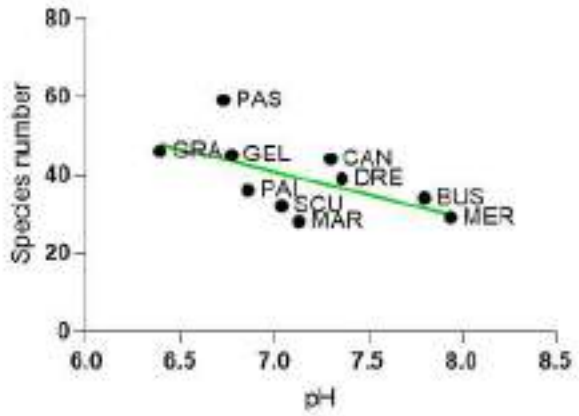

Figure 6.2.6. Correlation between pH and diatom species richness in lakes and rivers.

This pattern indicates that lower pH conditions tend to favor higher diatom richness, while more alkaline environments support fewer species. Such a relationship suggests that acid-tolerant taxa may increase in number under more acidic conditions, broadening overall richness, whereas in alkaline systems, community composition becomes more restricted. This highlights the sensitivity of diatom assemblages to pH as a key factor structuring biodiversity in both lakes and rivers (Cesarini et al., 2025).

To investigate acidification, diatoms were classified according to their pH requirements following van Dam et al. (1994) (Fig. 6.2.7). This system, which categorizes diatom species based on seven ecological factors, has been widely applied for deriving indicator values in surface water monitoring

and quality assessment. According to their pH range, diatoms are assigned to six occurrence groups, allowing lake communities to be described in terms of the relative abundance (%) of each group (ICP Waters, 2010).

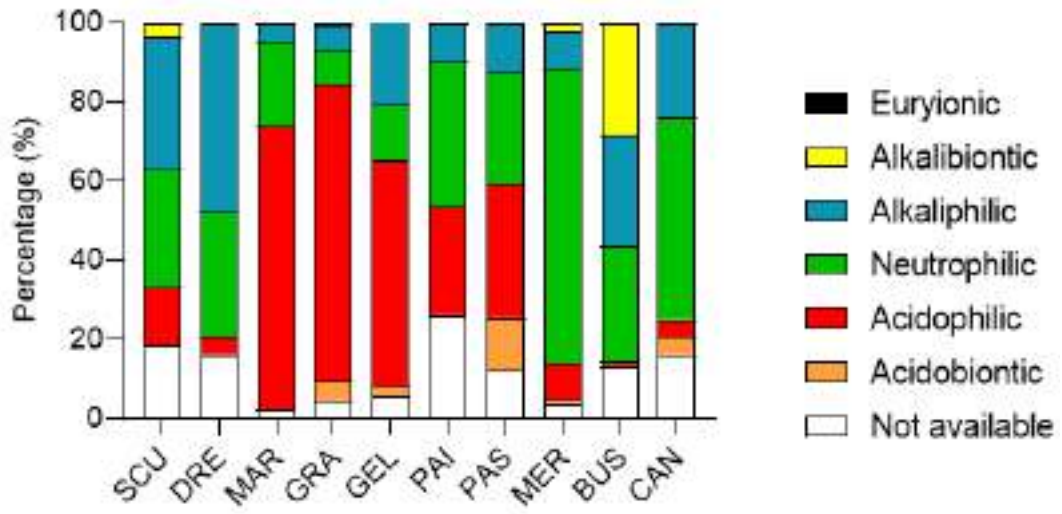

Figure 6.2.7. Diatoms pH requirements according to Van Dam et al., 1994 in the study lakes and rivers.

The Van Dam et al. (1994) classification shows a clear variability in pH preferences among the studied lakes. Acidophilous taxa dominate in several lakes, particularly GRA (75.1%), MAR (71.6%), and GEL (56.8%), indicating strongly acidic conditions in these systems. In contrast, other lakes show a marked prevalence of neutrophilous species, such as MER (74.7%), CAN (51.1%), and PAI (36.9%), suggesting environments close to neutral pH. Alkaliphilous species also play an important role in certain lakes: DRE (47.6%), SCU (33.3%), and BUS (28.1%) display the highest proportions of this group, while BUS is notable for hosting the only significant presence of alkalibiontic species (28.3%), absent or negligible in the other lakes. Acidobiontic taxa are generally rare, with the highest value observed in PAS (13.1%) and very low percentages elsewhere. Indifferent (euryionic) species are practically absent across the dataset. These results indicate that the lakes are not uniform in their response to pH conditions. Some sites, such as GRA, MAR, and GEL, remain dominated by acidophilous assemblages, while others (MER, CAN, PAI) show conditions close to neutrality, and DRE and BUS are characterized by communities with strong alkaliphilous tendencies. The variability observed suggests differences in chemical status and possibly in the degree of recovery from acidification, with some lakes approaching or even surpassing neutral conditions, while others remain clearly acid-sensitive.

Canonical Correspondence Analysis (CCA) was used to analyse the distribution of diatoms and macroinvertebrates in relation to environmental variables (lake/river and catchment characteristics, water chemistry). Square root transformation was applied to macroinvertebrate and diatom relative abundances. Very rare species (abundance lower than 3% in any sample) were excluded from the dataset to avoid any noise effect (Gauch, 1982). Environmental variables to be used in the CCA were selected through Spearman correlation analysis, excluding highly correlated variables. Log-transformation was applied to environmental variables to nearly conform to normality.

To assess the role of environmental features in shaping diatom and macroinvertebrate assemblages, 12 variables were selected (altitude, pH, TP, TN, Si, TOC, SO_4, NO_3, area/length, lake and catchment areas, mean air temperature (Tmean) and precipitation (PCNP) and their associations with biological elements, considered at genus/species taxonomic levels, were assessed by CCA (Figure 6.2.8).

In the CCA applied to the dataset, the first two canonical axes together represented 36.07% of the constrained inertia, with the first axis accounting for 20.32% and the second axis for 15.75%.

The CCA ordination clearly separates sites based on environmental gradients. High-altitude lakes cluster together on the negative side of Axis 1, strongly associated with increasing altitude and consequent lower temperatures. In contrast, lakes such as Mergozzo and Scuro are positioned toward vectors indicating slightly higher nutrient concentrations, particularly TP. River sites form a distinct group, influenced by NO_3 and Si. The position of sites along these gradients highlights the combined effects of altitude, trophic status, and catchment features on diatom assemblages.

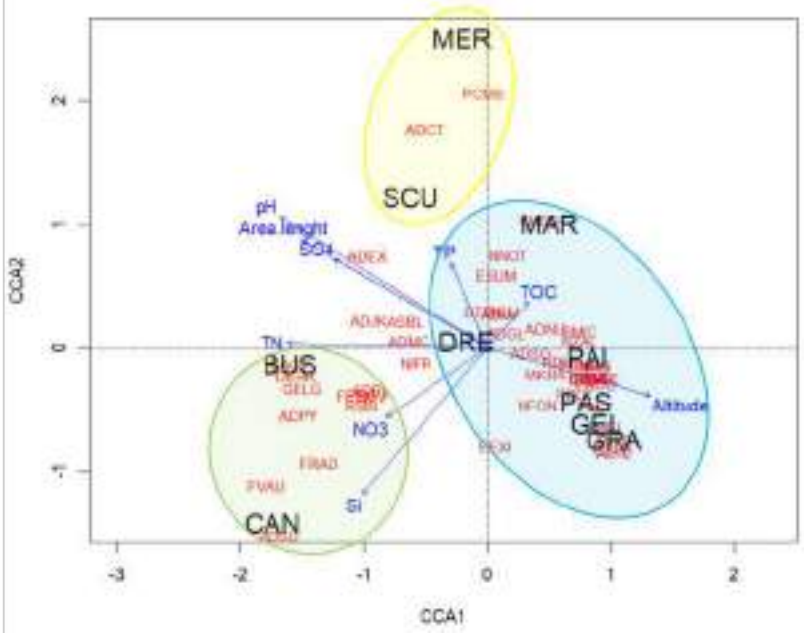

Figure 6.2.8. CCA applied to environmental features and diatoms in the sampling lakes and rivers. Black points: sites, red: taxa, blue arrows: environmental variables. Taxa were shown using four letter OMNIDIA codes (ver. 6.1.7; Lecointe et al., 1993), available in Table X. Distinct groups resulting from the analysis are visually differentiated by color in the corresponding plot: yellow = low-altitude lakes; blue = high-altitude lakes; green = rivers.

6.2.4 Macroinvertebrates and altitude gradients

Based on known environmental gradients, we tested H1) the association between macroinvertebrate diversity and altitude consistent with hypotheses that higher-altitude sites support less diverse or distinctive assemblages, likely due to harsh environmental factors; H2) the association between pH and overall diversity, and between pH and Evenness consistent with pH-related stress shaping the assemblage structure (acidic or highly alkaline conditions reducing taxa richness and altering dominance patterns); H3) the association between diversity and precipitation amount likely promoting macroinvertebrate diversity through enhanced habitat complexity and resource supply. On the other hand, this effect may be mitigated or reversed by disturbance from extreme rainfall.

After the first run, MERo emerged as an outlier, presumably due to its unique ecological constraints: higher temperatures, filamentous algae, slower flow in an artificial canal, flow direction linked to the water levels of the two connected lakes (Maggiore and Mergozzo), and fish presence. Together, these factors likely suppress diversity relative to other sites. To assess robustness, we re-run several analyses excluding MERo.

H1: the correlation between macroinvertebrate diversity and altitude was significantly negative (Fig. 6.15 left: R^2= 0.87) in lakes, only negative (Figure 6.2.9 right: R^2 = 0.42) in rivers. Diversity remains relatively constant across the 2000–2500 m range, after which it declines markedly toward the lowlands. The trend is consistent with altitudinal shifts in meteorological and ecological conditions (e.g. snow cover, ice-free period, light and temperature regime, and food availability) that constrain habitat and resource availability along the gradient. This relationship appears to be altitude-dependent: meteorological drivers more strongly constrains macroinvertebrate distribution and diversity at higher elevations than at lower ones (Fjellheim et al., 2000; Boggero et al., 2019).

H2: a positive correlation (Fig. 6.2.10 left: R^2=0.41, right: R^2=0.54) was found between pH and overall diversity (rivers and lakes) likely because many aquatic habitats harbor greater taxa richness under neutral to slightly alkaline conditions, whereas several taxa are intolerant of low pH (such as molluscs and EPT taxa) (Boggero et al., 2023; Martins et al., 2020). The loss of acid-sensitive groups under acidic conditions can create an uneven community structure, reducing evenness even when total diversity remains relatively high. In other words, pH appears to influence the composition by selectively filtering taxa, which increases overall richness in neutral or alkaline environments. No significant association between pH and evenness was found. This may reflect a restricted pH range or may indicate that pH has a limited influence on evenness relative to other drivers such as habitat complexity, nutrient availability, or disturbance.

H3: a non-significant association was found between overall diversity and precipitation amount (Figure 6.2.11; R^2 = 0.09). This weak relationship suggests that, at the sampled sites, overall diversity does not appear to be related to precipitation alone; rather, other factors may mask its effects (Theodoropoulos et al., 2017; O'Brian 2019; Martins et al., 2020): (1) diversity is indirectly influenced by precipitation via alteration of habitat structure, hydrological connectivity, or nutrient fluxes ; (2) diversity respond to precipitation seasonality or to the intensity or antecedent amount of rainfall preceding the sampling period; (3) diversity is indirectly influenced by precipitation via alteration of habitat size, water depth, or pH that could mask any direct precipitation effect.

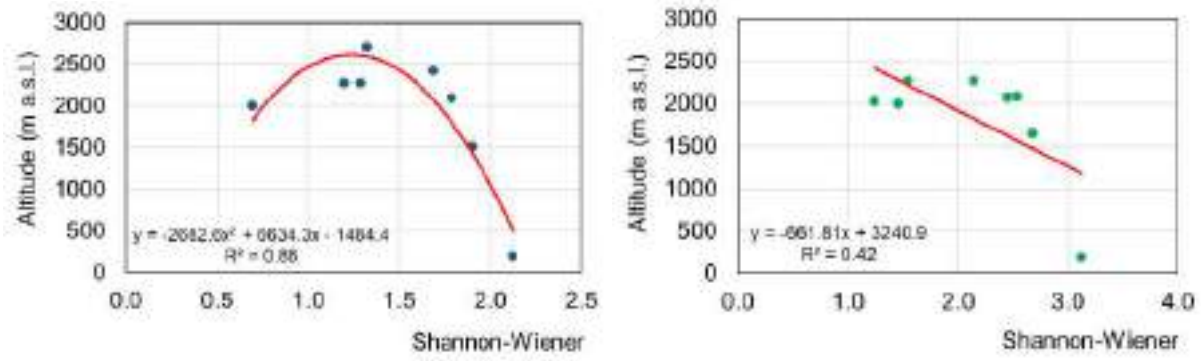

Figure 6.2.9. Relationship between macroinvertebrates Shannon-Wiener diversity and altitude in lakes (left), and in rivers (right: MERo excluded).

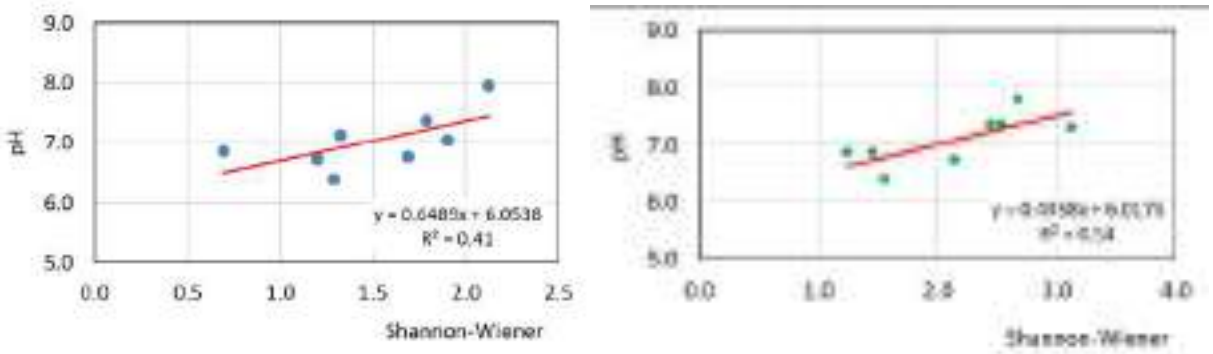

Figure 6.2.10. Relationship between pH and Shannon diversity across lakes and rivers (blue: lakes, green: rivers) (right: MERo excluded).

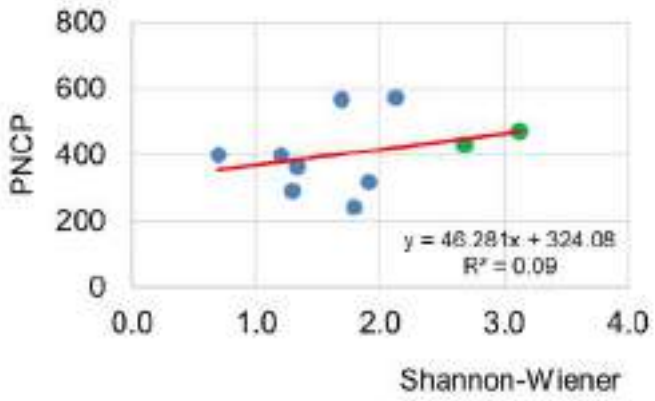

Figure 6.2.11. Relationship between PNCP and Shannon diversity across lakes and rivers (blue: lakes, green: rivers)

Successively, we applied a set of selected acidification indices to the presence/abundance of macroinvertebrate taxa known to be sensitive to acidification. The scoring system was built to reflect how these taxa respond to acidified conditions, with higher scores indicating stronger sensitivity or greater abundance of acid-sensitive taxa under lower pH. For macroinvertebrates, we tested indices that have already been used at the European level, because their effectiveness in assessing lake acidification has been previously evaluated (Schartau et al., 2008). The indices applied were: Raddum Index (Raddum et al., 1988); Raddum Index expanded version (Fjellheim & Raddum, 1990); TL (Hämäläinen & Huttunen, 1990), NIVA (Bækken & Kjellberg, 2004), Braukmann (Braukmann & Biss, 2004), AWICfam (Davy-Bowker et al., 2003, 2005), AWICsp (Davy-Bowker et al., 2003), MILA (Johnson & Goedkoop, 2007), and LAMM (McFarland et al., 2010) (Tab. 5.5). These indices directly target shifts in macroinvertebrate assemblage structure associated with acid stress, and have demonstrated cross-site robustness in European lakes (Poikane et al., 2020). Each index

translates observed taxa presence/abundance patterns into a composite score along an acidification sensitivity gradient. Unfortunately, only three of the eight acidification indices were developed for lacustrine systems, whereas the remaining five were originally designed for river ecosystems and are not directly applicable to lakes. In practice, an index is judged Applicable (A) if at least one acid-sensitive taxon was found in every lake/river and the index value could be calculated for all sites. In our dataset, $AWIC_{fam}$ (family level) and $AWIC_{sp}$ (species level) fall into this category (Tab. 5.6). These indices provide a continuous score across all lakes/rivers and reflect a consistent presence of acid-sensitive taxa.

An index is Partially Applicable if at least one acid-sensitive taxon is found in some but not all lakes/rivers. Examples include Braukmann, and $LAMM_{Sk}$ and $LAMM_{Wk}$ (Tab. 6.2.2). These indices yield site-specific scores only where sensitive taxa occur, and care must be taken when comparing across lakes/rivers with missing taxa. An index is Not Applicable if none of the lakes contain any acid-sensitive taxa, preventing calculation of an index score (Table 6.2.3). In our dataset, this situation is the most common.

Table 6.2.2. List of acidification indices developed at the European level to assess the ecological conditions of lakes and rivers. PA: partially applicable; A: applicable

Index	Author	Country	Result	System type
Raddum 1988	Raddum et al., 1988	Norway	PA	lake
Raddum 1990	Fjellheim & Raddum, 1990	Norway	PA	lake
TL	Hämäläinen & Huttunen, 1990	Finland	PA	river
NIVA	Bækken & Kjellberg, 2004	Norway	PA	river
Braukmann	Braukmann & Biss, 2004	Germany	PA	river
AWICfam	Davy-Bowker et al., 2003, 2005	England and Wales	A	river
AWICsp	Davy-Bowker et al., 2003	England and Wales	A	river
LAMM	McFarland et al., 2010	UK	PA	lake

Table 6.2.3. Application of acidification indices developed at the European level to lakes (blue) and rivers (green). AWICfam: family level; AWICsp: species level; LAMM Sk: acid sensitivity score for taxon k; LAMM Wk: weighted score for taxon k; NA: Not Applicable. Lake/River distribution follows a high to low altitude gradient.

	Raddum 1988	Raddum 1990	NIVA	AWICfam	AWICsp	TL	Braukmann	LAMM Sk	LAMM Wk
MAR	NA	NA	NA	4.36	5.00	NA	4.10	NA	NA
GEL	NA	NA	NA	4.13	5.02	NA	5.69	6.00	0.61
PAS	NA	NA	NA	4.00	5.00	NA	4.45	NA	NA
GRA	0.91	NA	NA	4.29	5.00	NA	3.17	2.00	0.26
DRE	1.00	NA	NA	4.05	5.03	NA	3.36	4.25	0.51
PAI	NA	NA	NA	4.02	5.00	NA	4.29	NA	NA
SOU	1.00	0.50	NA	4.92	5.00	NA	3.25	4.13	0.49
MER	NA	0.00	4.00	3.00	5.00	4.70	4.60	2.00	0.41
GRAo	1.00	NA	NA	4.41	5.00	NA	3.00	NA	NA
PASo	NA	NA	NA	4.00	5.02	NA	5.00	6.00	0.61
DREi	NA	NA	NA	5.60	5.00	NA	NA	NA	NA
DREo	NA	NA	NA	4.00	5.00	NA	NA	NA	NA
PAIi	NA	NA	NA	4.65	5.00	NA	4.18	NA	NA
PAIo	NA	NA	NA	4.00	5.00	NA	NA	NA	NA
BUS	NA	NA	NA	4.10	5.00	NA	4.08	NA	NA
CAN	NA	0.60	4.00	5.35	5.11	4.50	4.12	4.00	0.28
MERo	1.00	1.00	2.00	5.92	5.18	5.10	3.68	7.00	0.30

However, even where the index was applicable or partially applicable, the resulting value exhibits limited variability across lakes, due to the presence of a few sensitive species, limited by geographical barriers and therefore not present in the investigated sites. Furthermore, the indices were developed primarily for Northern European freshwaters and are less applicable to sites south of the Alps, where different species predominate (Boggero et al., 2019, 2023; Steingruber et al., 2013). In summary, with the exception of $AWIC_{fam}$ and $AWIC_{sp}$, none of the tested indices proved fully effective within the study area. A significant limitation of the $AWIC_{fam}$ scoring system was its reduced ability to differentiate based on pH, since acid-sensitive and acid-tolerant species can occur within the same family (Davy-Bowker et al. 2003, 2005). It was hoped that the species level analysis ($AWIC_{sp}$) would reveal more specific pH tolerances and hence a more precise ranking of taxa; however, the absence of many taxa necessary for index calculation undermines its robustness (Cesarini et al., 2025). Although species diversity is generally closely linked to pH, the overall utility of macroinvertebrates as indicators remains limited in this context. This is mainly due to the narrow pH range across the lakes and the absence of truly acidic conditions, which reduces the effectiveness of pH-based assessments.

Lastly, a Canonical Correspondence Analysis (CCA) was used to highlight how macroinvertebrate distributions vary in combination of a set of environmental predictors that characterise both the lake/river systems and their catchments (e.g., size, length, altitude, pluviometry), as well as water chemistry (e.g., pH, conductivity, nutrients). The approach enables visualization of species and sites along canonical axes, revealing key habitat associations and environmental gradients driving community structure.

In the CCA of macroinvertebrate assemblages vs lake variables (Fig. 6.2.12A), the first two canonical axes explained 47.65% of the constrained inertia, with Axis 1 accounting for 25.54% and Axis 2 for 22.11%. Whereas, in the CCA of macroinvertebrates vs river variables (Fig. 6.2.12B), the first two canonical axes represented 48.59% of the constrained inertia, with Axis 1 accounting for 29.18% and Axis 2 for 19.41%.

In both the lake- and river-CCA ordinations, one canonical axis captures a gradient characterized by increasing altitude, lower pH, and nitrogen enrichment, while the second axis captures variations associated with phosphorus enrichment, TOC, and reactive silica.

In the CCA, MERo stands out among rivers for its very simplified assemblage, composed only of Oligochaeta and Chironomidae. This pattern reflects its unique ecological conditions, (higher temperatures, abundant filamentous algae, slower flow in an artificial canal, fish occurrence). Among the other sites, TN consistently emerged as a major determinant of macroinvertebrate distribution in both lakes and rivers. This association may represent multiple interacting mechanisms: higher TN often co-occurs with warmer, low-elevation environments that favor certain taxa, alter primary production, and modify dissolved oxygen dynamics. Svitok et al. (2021) document temperature- and nutrient-driven shifts in flying (or dispersal-capable) macroinvertebrates, supporting the idea that TN-related gradients shape assemblages. Moreover, increasing atmospheric nitrogen deposition is likely to amplify these effects, potentially accelerating changes in assemblage composition and function in freshwater ecosystems (Burpee et al., 2022; Oleksy et al., 2020).

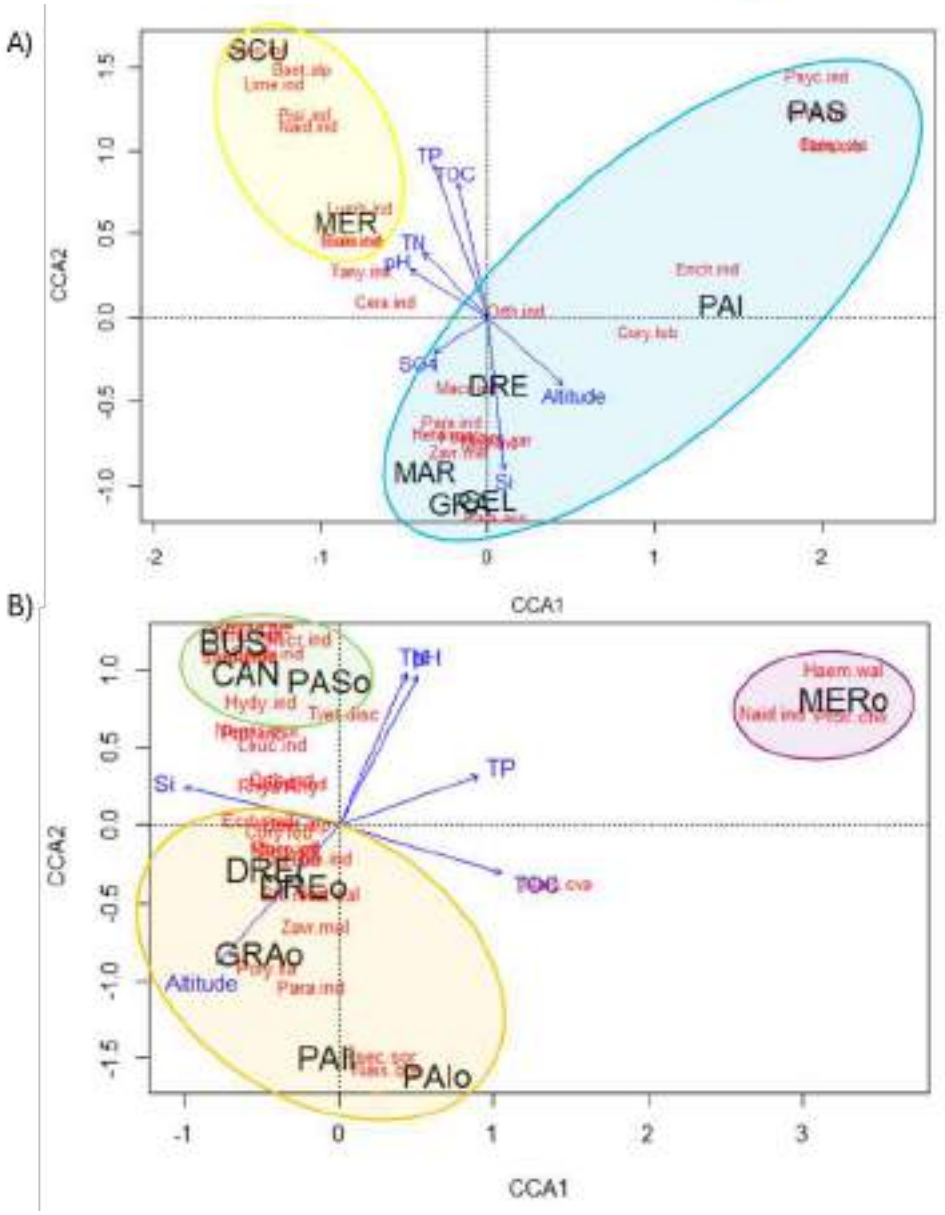

Figure 6.2.12. CCA applied to environmental features and macroinvertebrates in the studied A) lakes; B) rivers. Black uppercase letters: site code, red lowercase letters: taxa code, blue arrows: environmental variables. See Appendix B for macroinvertebrates codes derived from EMERGE project: first four letters of the genus name followed by the first three letters of the species epithet. Color indicates distinct CCA groups: yellow = nutrient-enriched lakes; blue = high-altitude lakes; green = nutrient-enriched rivers; violet = outlier; orange = high-altitude inlets and outlets of lakes.

In conclusion, our analyses collectively reflect the primary environmental shaping assemblage structure in the two freshwater habitats, with potential implications for mitigating nitrogen emissions and deposition to safeguard freshwater biodiversity.

7. Replicability study: preliminary results

In the framework of LIFE MODERn(NEC), replicability is aimed at multiplying the impact of the project, beyond its duration and outside the national partnership, in other EU Member States committed to the NEC Directive. The Replicability Strategy of LIFE MODERn(NEC) was developed by the partners within the second year of the project and firstly put into practice with the cooperation of the Romanian National Institute for Research and Development in Forestry «Marin Dracea» (INCDS), who supported LIFE MODERn(NEC) project proposal and is currently involved in the accomplishment of the NEC Directive in Romania.

Two study visits have been organized to monitor lichen diversity and ground vegetation respectively.

During the week of May 5, 2025, INCDS researchers József Pál Frink and Bodgan Plesca, together with Giorgio Brunialti and Luisa Frati from TerraData, applied the fruticose lichen method for the first time in 4 forests of the ICP Forests Level II Romanian network and 2 forest sites of the RO-LTER network, located in Bucegi Mountains Natural Park (PNB).

During the week of May 26, 2025, INCDS researchers József Pál Frink and Bodgan Plesca, together with Stefano Chelli and Marco Cervellini from the University of Camerino, applied the methods for the sampling of the new indicators related to Functional traits for 4 forests and to Compositional Diversity for 2 forests of the ICP Forests Level II Romanian network.

The study visits allowed to harmonize the methods, thus starting a fruitful collaboration (Fig. 7.1).

Figure 7.1. The replicability survey teams. On the left: INCDS and TerraData members during the lichen diversity survey. On the right: INCDS and UNICAM members during the ground vegetation survey (Mihaesti forest site).

Forest sites

Lichen diversity survey - A total of six among the Romanian ICP Forests (4 Level II plots) and RO-LTER networks (2 plots) have been considered (Fig. 7.2):

- 2 oak forests: Ștefănești (STE) and Mihaesti (MIH)
- 2 beech forests: Fundata (FUN, Fig. 7.3), Poiana Stânii (POI)
- 2 spruce forests: Timeni Grof (TIM), Predeal (PRE)

Ground vegetation - A total of four sites among the Romanian ICP Forests Level II plots (Figure 7.2) have been considered:

- 2 oak forests: Ștefănești (STE, Figure 3) and Mihaesti (MIH)
- 1 beech forest: Fundata (FUN)
- 1 spruce forest: Predeal (PRE)

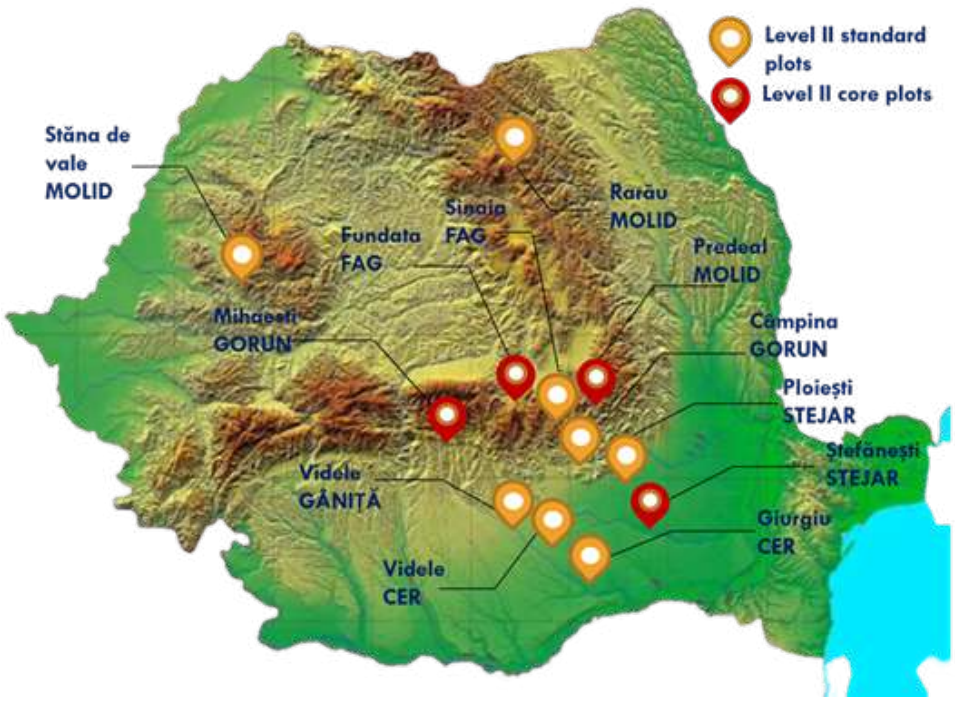

Figure 7.2. Romanian Level II Plots distribution.

Figure 7.3. An example of beech forest (Fundata Level II forest site).

7.1 Epiphytic lichen diversity survey

7.1.1 Fruticose lichens fallen to the ground

Fruticose lichens (Fig. 7.1.1), and especially hair lichens, are particularly sensitive to pollution and climate change, as their large surface area to mass ratios filters moisture and elements from the air (e.g., Knops et al. 1996; Stanton et al. 2014), and they have strongly declined in areas with atmospheric pollution and intensive forestry (see Esseen et al. 2016). This makes this functional group a useful indicator of air pollution and climate change in forest ecosystems.

The simplified method on the assessment of fruticose lichens fallen on the ground has been applied (Fig. 7.1.2). In addition, a list of other lichen species (foliose and crustose) present on the branches fallen to the ground was also drawn up.

Figure 7.1.1. The fruticose lichen Evernia prunastri on a branch fallen to the ground.

Figure 7.1.2. Application of the protocol on fruticose lichens.

Except for the plot of Ștefănești, fruticose lichens were found at the other 5 sites (83%). We found only the two species *Pseudevernia furfuracea* and *Evernia prunastri*. Their abundance is between 10% (FUN) and 100% (POI) of the subplots colonized (Table 7.1.1).

In the plots with fruticose lichens, their cumulated dry biomass ranges from 0,254 g (MIH) to 14,6 g (POI) at the plot level. On average, at the subplot level, the mean weight ranges from 0,025 g (MIH, oak forest) to 1,464 g (Poiana Stânii, beech forest).

Table 7.1.1. Results of the survey on fruticose lichens.

Forest type	Plot code	N species per plot	Lichen species	Abundance (% of subplots)	Weight (g), mean	Weight (g), SD	Weight (g), cumulated
Oak forest	STE	0		0	0,000	0,000	0,000
	MIH	1	*Evernia prunastri*	20	0,025	0,074	0,254
Beech forest	FUN	1	*Pseudevernia furfuracea*	10	0,047	0,147	0,465
	POI	1	*P. furfuracea*	100	1,464	1,532	14,6
Spruce forest	TIM	2	*P. furfuracea, E. prunastri*	90	0,442	0,414	4,42
	PRE	1	*P. furfuracea*	90	0,207	0,263	2,07

7.1.2 Lichen Diversity Value (LDV)

The method of the Lichen Diversity Value (LDV) was applied at 4 forest sites (STE, FUN, PRE, MIH), all core plots within the Romanian Level II network. The protocol follows the ICP Forests Manual (Part VII.2, v.05/206), focusing on the diversity of lower-trunk epiphytic lichens as indicators of the effects of NO_x and SO_2. The occurrence of each lichen species was sampled within a 10 × 50 cm observation grid, placed at each of the four cardinal points of the trunk (N, S, E, W) at a height of 100 cm above the ground (Fig. 7.1.3).

Figure 7.1.3. Application of the protocol on Lichen Diversity Value (LDV).

A total of 24 lichens has been sampled (Tab. 7.1.2): 14 crustose (58%), 9 foliose (38%), 1 fruticose species (4%). 5 nitrophytic species 6 oligotrophic lichens.

The list includes 24 lichen taxa (Tab. 7.1.2), with 10 (42%) easily recognizable macrolichens (i.e. 9 foliose lichens, and 1 fruticose species) and 14 crustose species (58%). Oligotrophyic species represent the 25% of the total (9 lichens: *Buellia griseovirens, Hypogymnia physodes,Lecanora expallens, Pseudoschismatomma rufescens, Pyrenula nitida, Schismatomma pericleum*), while 21% are nitrophytic lichens (5 species: *Candelaria concolor, Candelariella reflexa, Phaeophyscia orbicularis, Physcia adscendens, Physconia grisea subsp. grisea*). Three lichens of the list are species which exclusively occur on old trees in ancient, undisturbed forests or in semi-natural habitats: *Pseudoschismatomma rufescens, Pyrenula nitida, Schismatomma pericleum.*

*Table 7.1.2. List of lichen species found during the survey on Lichen Diversity Value (LDV). Growth form (Gf): C= crustose lichen; F= foliose; FR= fruticose. Eutrophication (Eut): O= oligotrophyc species; N= nitrophytic species. * species which exclusively occur on old trees in ancient, undisturbed forests or in semi-natural habitats.*

Lichen species	
Amandinea punctata (Hoffm.) Coppins & Scheid.	Gf: C
Arthonia radiata (Pers.) Ach.	Gf: C
Buellia griseovirens (Sm.) Almb.	Gf: C; Eut: O
Candelaria concolor (Dicks.) Stein	Gf: F; Eut: N
Candelariella reflexa (Nyl.) Lettau	Gf: C; Eut: N
Candelariella xanthostigma (Ach.) Lettau	Gf: C
Cladonia sp.	Gf: FR
Flavoparmelia caperata (L.) Hale	Gf: F
Hypogymnia physodes (L.) Nyl.	Gf: F; Eut: O
Lecanora carpinea (L.) Vain.	Gf: C
Lecanora chlarotera Nyl. subsp. chlarotera	Gf: C
Lecanora expallens Ach.	Gf: C; Eut: O
Lecidella elaeochroma (Ach.) M. Choisy var. elaeochroma f. elaeochroma	Gf: C
Lepra amara (Ach.) Hafellner	Gf: C
Lepraria sp. 1	Gf: C
Melanelixia subaurifera (Nyl.) O. Blanco, A. Crespo, Divakar, Essl., D. Hawksw. & Lumbsch	Gf: F
Melanohalea elegantula (Zahlbr.) O. Blanco, A. Crespo, Divakar, Essl., D. Hawksw. & Lumbsch	Gf: F
Parmelia sulcata Taylor	Gf: F
Phaeophyscia orbicularis (Neck.) Moberg	Gf: F; Eut: N
Physcia adscendens H. Olivier	Gf: F; Eut: N
Physconia grisea (Lam.) Poelt subsp. grisea	Gf: F; Eut: N
** Pseudoschismatomma rufescens (Pers.) Ertz & Tehler*	Gf: C; Eut: O
** Pyrenula nitida (Weigel) Ach.*	Gf: C; Eut: O
** Schismatomma pericleum (Ach.) Branth & Rostr.*	Gf: C; Eut: O

At the plot level, LDVs are between 38,7 and 65 (mean: 49,3), while at the tree level they range from 24 to 74 (Tab. 7.1.3).

Table 7.1.3. Results of the survey on Lichen Diversity Value (LDV).

	Site			**Number of species per tree**	**LDV per tree**

Plot code		Tree species	Total number of species	mean	min	max	mean	min	max
STE	Ștefănești	*Tilia tomentosa*	9	4,7	2	8	38,7	24	53
FUN	Fundata	*Fagus sylvatica*	7	5,0	4	6	50	41	61
PRE	Predeal	*Abies alba*	9	5	4	6	43,3	42	45
MIH	Mihaesti	*Quercus petraea*	8	6	6	6	65	57	74

7.1.3 Lobaria polmonaria: viability and conservation assessment

The large foliose species *Lobaria pulmonaria* (L.) Hoffm. is very sensitive to air pollution and in large decline throughout Europe. Several studies demonstrated its suitability both as a flagship and as an umbrella species for nature conservation, since it is easy to identify, and it is associated with many other rare or endangered forest dwelling organisms.

We found *Lobaria pulmonaria* only in the forest site of Poiana Stânii (RO-LTER network), where it is present on more than 5 beech trees (Fig. 7.1.4).

The observed specimens showed good vitality and conservation status, with abundant meristematic lobes and well-developed dimensions. Baby thalli (< 2cm) were sporadic. On considering the reproductive strategy, vegetative propagules were abundant while apothecia were absent. However, the rainy weather and the short time prevented us from going into more detail and explore all the trees of the plot.

Figure 7.1.4. A large specimen of the foliose species *Lobaria pulmonaria* colonizing the base of a beech tree in the plot Poiana Stânii.

7.2 Ground vegetation survey

7.2.1 List of species sampled for Leaf Functional traits

We applied the standard protocol produced during the LIFE project to collect and measure leaf traits (i.e., leaf area and specific leaf area) for the five most abundant plant species on each site. Leaves have then been stored, and their area was assessed with a scanner. By the end of the summer 2025 we will dry out the samples to measure also the dry weight, a parameter useful to calculate the specific leaf area.

Here below we report the species measured for each plot (Table 7.2.1).

Leaf traits have been collected and measured also in the summer 2024 and the sampling will be repeated by INCDS during summer 2025. This will enable us to have a certain variability of years and seasons to properly assess how much leaf traits change according to climate.

Table 7.2.1. Species sampled during the campaign.

Year	Season	Date	Biome	Site	Species
2025	Spring	27/05/25	Nemoral oak forest	Mihăiești-gorun (MIH)	*Melica uniflora*
2025	Spring	27/05/25	Nemoral oak forest	Mihăiești-gorun (MIH)	*Fagus sylvatica*
2025	Spring	27/05/25	Nemoral oak forest	Mihăiești-gorun (MIH)	*Cardamine bulbifera*
2025	Spring	27/05/25	Nemoral oak forest	Mihăiești-gorun (MIH)	*Quercus petraea*
2025	Spring	27/05/25	Nemoral oak forest	Mihăiești-gorun (MIH)	*Carex pilosa*
2025	Spring	28/05/25	Nemoral oak forest	Ștefănești-stejar (STE)	*Galium aparine*
2025	Spring	28/05/25	Nemoral oak forest	Ștefănești-stejar (STE)	*Mercurialis perennis*
2025	Spring	28/05/25	Nemoral oak forest	Ștefănești-stejar (STE)	*Carex pilosa*
2025	Spring	28/05/25	Nemoral oak forest	Ștefănești-stejar (STE)	*Lamium maculatum*
2025	Spring	28/05/25	Nemoral oak forest	Ștefănești-stejar (STE)	*Viola suavis*
2025	Spring	29/05/25	Nemoral beech forest	Fundata-fag (FUN)	*Fagus sylvatica*
2025	Spring	29/05/25	Nemoral beech forest	Fundata-fag (FUN)	*Cardamine bulbifera*
2025	Spring	29/05/25	Nemoral beech forest	Fundata-fag (FUN)	*Anemone nemorosa*
2025	Spring	29/05/25	Nemoral beech forest	Fundata-fag (FUN)	*Allium ursinum*
2025	Spring	29/05/25	Nemoral beech forest	Fundata-fag (FUN)	*Cardamine glanduligera*
2025	Spring	29/05/25	Boreal forest	Predeal-molid (PRED)	*Abies alba*
2025	Spring	29/05/25	Boreal forest	Predeal-molid (PRED)	*Rubus hirtus*
2025	Spring	29/05/25	Boreal forest	Predeal-molid (PRED)	*Anemone nemorosa*
2025	Spring	29/05/25	Boreal forest	Predeal-molid (PRED)	*Sanicula europaea*
2025	Spring	29/05/25	Boreal forest	Predeal-molid (PRED)	*Polygonatum verticillatum*

7.2.2 Compositional Diversity

The sampling of Compositional Diversity has been performed in two sites, namely STE and MIH (Figure 7.2.1), since the other two sites (PRE and FUN) have been sampled during 2024 by INCDS. The raw data will be organized by INCDS and then analyzed by UNICAM.

Figure 7.2.1. An example of sampling activity for Compositional Diversity (STE Level II forest site).

8. Annexes

- Annex B3.1. Detailed description of data analysis.
- Annex B3.2. List of species of diatoms and macroinvertebrates.

9. References

Amélie J., Groner E., Menta C., 2016. SOIL MACROFAUNAL DIVERSITY. In ExpeEr Ecosystem Research Program, 2016.

Amoozegar A., Warrick A.W., 1986. "Hydraulic Conductivity of Saturated Soils: Field Methods." In Methods of Soil Analysis, Part 1: Physical and Mineralogical Methods, edited by E. A. Klute, 735- 770. 2nd ed. Madison, WI.: American Society of Agronomy and Soil Science Society of America.

Ancora S., Dei R., Rota E., Mariotti G., Bianchi N., Bargagli R., 2021. Altitudinal variation of trace elements deposition in forest ecosystems along the NW side of Mt. Amiata (central Italy): Evidence from topsoil, mosses and epiphytic lichens. Atmospheric Pollution Research 12: 101200. https://doi.org/10.1016/j.apr.2021.101200

Andersen K., Bird K.L., Rasmussen M., Haile J., Breuning-Madsen H., Kjær K.H., Orlando L., Gilbert M.T.P., Willerslev E., 2012. Meta-barcoding of 'dirt' DNA from soil reflects vertebrate biodiversity. Molecular Ecology, 21: 1966-1979.

Atemasov A., Atemasova T., 2019. Impact of stand variables on characteristics of avian soundscape in common oak (*Quercus robur* L.) forests. Forestry Studies, vol.70, no.1, pp.68-79.

Avenant N.L., 2000. Small mammal community characteristics as indicators of ecological disturbance in the Willem Pretorius Nature Reserve, Free State, South Africa. South African Journal of Wildlife Research 30, 26–33.

Bækken T., Kjellberg G., 2004. Classification of acidity and assessment of acidification in running waters based on the presence of macroinvertebrates. Classification system developed for humic rivers and brooks in Eastern Norway. Report 4923, Norwegian Institute for Water Research (NIVA), Oslo, Norway: 13 pp.

Baker N.J., Pilotto F., Jourdan J., Beudert B., Haase P., 2021. Recovery from air pollution and subsequent acidification masks the effects of climate change on a freshwater macroinvertebrate community. Science of The Total Environment, 758: 143685. https://doi.org/10.1016/j.scitotenv.2020.143685.

Baker N.R., Rosenqvist E., 2004. Applications of chlorophyll fluorescence can improve crop production strategies: examination of future possibilities. Journal of Experimental Botany 55: 1607–1621.

Balčiauskas L., Čepukienė A., Balčiauskienė L., 2017. Small mammal community response to early meadow–forest succession. *For. Ecosyst.* **4**, 11.

Bartha S. and Kertész M., 1998 - The importance of neutral-models in detecting interspecific spatial associations from 'trainsect' data. Tiscia 31: 95-98.

Bartha S., 2008 - Beyond Trivial Relationships: on the hidden aspects of biodiversity. Folia Geobotanica 43: 371–382

Bartha S., 2014 - Understanding vegetation succession process in habitat and vegetation restoration and rehabilitation. In: Mucina L., Price J.N. and Kalwij J.M. (eds.) Biodiversity and vegetation: patterns, processes, conservation: 25-26. Kwongan Foundation, Perth, AU.

Bartha S., Campetella G., Canullo R., Bódis J., Mucina L., 2004 - On the importance of fine-scale spatial complexity in vegetation restoration. International Journal of Ecology and Environmental Sciences 30: 101-116.

Bartha S., Czárán T., Podani J., 1998. Exploring plant community dynamics in abstract coenostate spaces. Abstracta Botanica 22: 49–66.

Battarbee R.W., 1994. Diatoms, lake acidification and the Surface Water Acidification Programme (SWAP): a review. Hydrobiologia 274, 1–7 (1994). https://doi.org/10.1007/BF00014621

Battarbee R.W., Jones V.J., Flower R.J., Cameron N.G., Bennion H., Carvalho L., Juggins S., 2001. Diatoms. In: Smol J, Birks HJ, Last W (eds), Tracking Environmental Change Using Lake Sediments. Volume 3: Terrestrial, Algal, and Siliceous Indicators. Kluwer Academic Publishers, The Netherlands: 155-202.

Benítez Á., Medina J., Vásquez C., Loaiza T., Luzuriaga Y., Calva J., 2019. Lichens and Bromeliads as Bioindicators of Heavy Metal Deposition in Ecuador. Diversity 11: 28. https://doi.org/10.3390/d11020028

Bennion H., Kelly M.G., Juggins S., Yallop M.L., Burgess A., Jamieson J., Krokowski J., 2014. Assessment of ecological status in UK lakes using benthic diatoms. Freshw. Sci. 33 (2): 639-654..

Bird S., Coulson R.N., Crossley D.A., 2000. Impacts of Silvicultural Practices on Soil and Litter Arthropod Diversity in a Texas Pine Plantation. Forest Ecology and Management 131, fasc. 1–3 (June 2000): 65–80. https://doi.org/10.1016/S0378-1127(99)00201-7.

Boelman N.T., Asner G.P., Hart P.J., Martin R.E., 2007. Multi-trophic invasion resistance in Hawaii: Bioacoustics, field surveys, and airborne remote sensing. Ecological Applications, 17(8)

Boggero A., 2018. Macroinvertebrates of Italian mountain lakes: a review. Redia: 35-46. https://doi.org/10.19263/REDIA-101.18.06

Boggero A., Zaupa S., Cesarini G., Ruocco M., Ansaloni I., Prevedelli D., Fornaroli R., 2023. Macroinvertebrate Spatial Diversity Patterns of Shore Habitats in Italian High-Altitude Natural and Permanent Lakes and Ponds. Water, 15(21): 3814. https://doi.org/10.3390/w15213814

Boggero A., Zaupa S., Musazzi S., Rogora M., Dumnicka E., Lami A., 2019. Environmental factors as drivers for macroinvertebrate and diatom diversity in Alpine lakes: New insights from the Stelvio National Park (Italy). Journal of Limnology, 78, 147–162. https://doi.org/10.4081/jlimnol.2019.1863

Boggero A., Zaupa S., Musazzi S., Rogora M., Dumnicka E., Lami A., 2019. Environmental factors as drivers for macroinvertebrate and diatom diversity in Alpine lakes: New insights from the Stelvio National Park (Italy). J. Limnol. 78: 147-162. https://doi.org/10.4081/jlimnol.2019.1863

Bohmann K., Evans A., Gilbert M.T., Carvalho G.R., Creer S., Knapp M., Yu D.W., de Bruyn M., 2014. Environmental DNA for wildlife biology and biodiversity monitoring. Trends Ecol Evol. 29(6):358-67.

Brakke D.F., Baker J.P., Bohmer J., Hartmann A., Havas M., Jenkins A., Kelly C., Ormerod S.J., Paces T., Putz R., Rosseland B.O., Schindler D.W., Segner H., 1994. Group report: Physiological and ecological effects of acidification on aquatic biota. In: Steinberg C.E.W. and Wright R.F. (eds), Acidification of freshwater ecosystems: implication for the future. Chichester, John Wiley & Sons, pp. 275-312.

Braukmann U., Biss R., 2004. Conceptual study - An improved method to assess acidification in German streams by using benthic macroinvertebrates. Limnologica, 34, 433–450. https:// doi. org/ 10. 1016/ S0075-9511(04) 80011-2

Brudvig L.A., 2017. Toward prediction in the restoration of biodiversity. Journal of Applied Ecology, 54, 1013–1017. https://doi.org/10.1111/1365-2664.12940

Brunialti G., Frati L., Ravera S., 2015b. Ecology and conservation of the sensitive lichen *Lobaria pulmonaria* in Mediterranean old-growth forests. In: Old-Growth Forests and Coniferous Forests. Ecology, habitat and conservation, Weber R.P. (Ed.), Nova Publisher, New York. Chapter 1: 1-20.

Brunialti G., Luisa F., Sonia R., 2015a. Structural variables drive the distribution of the sensitive lichen *Lobaria pulmonaria* in Mediterranean old-growth forests. Ecological Indicators 53: 37-42. https://doi.org/10.1016/j.ecolind.2015.01.023

Burpee B.T., Saros J.E., Nanus L., Baron J., Brahney J., Christianson K.R., Ganz T., Heard A., Hundey B., Koinig K.A., Kopáček J., Moser KNydick., K., Oleksy I., Sadro S., Sommaruga R., Vinebrooke R., Williams J., 2022. Identifying factors that affect mountain lake sensitivity to atmospheric nitrogen deposition across multiple scales. Water Research, 209: 117883 https://doi.org/10.1016/j.watres.2021.117883.

Bussotti F., Gerosa G., Digrado A., Pollastrini M., 2020. Selection of chlorophyll fluorescence parameters as indicators of photosynthetic efficiency in large scale plant ecological studies. Ecological Indicators 108, 105686

Bussotti F., Kalaji M.H., Desotgiu R., Pollastrini M., Łoboda T., Bosa K., 2012. Misurare la vitalità delle piante per mezzo della fluorescenza della clorofilla. Strumenti per la Didattica e la Ricerca, 137. Firenze University Press (Firenze, Italia). Pp. 132. ISBN: 978-88-6655-215-4

Bussotti F., Pollastrini M., Cascio C,, Desotgiu R., Gerosa G., Marzuoli R., Nali C., Lorenzini G., Pellegrini E., Carucci M.G., Salvatori E., Fusaro L., Piccotto M., Malaspina P., Manfredi A., Roccotello E., Toscano S., Gottardini E., Cristofori A., Fini A., Weber D., Baldassarre V., Barbanti L., Monti A., Strasser R.J., 2011. Conclusive remarks. Reliability and comparability of chlorophyll fluorescence data from several field teams. Environmental Experimental Botany 73, 116-119.

Cammarano P., Manca M., 1997. Studies on zooplankton in two acidified high mountain lakes in the Alps. *Hydrobiologia* **356**, 97–109 https://doi.org/10.1023/A:1003179314456

Campbell J., Fredeen A.L., 2004. *Lobaria pulmonaria* abundance as an indicator of macrolichen diversity in Interior Cedar-Hemlock forests of east–central British Columbia. Canadian Journal of Botany 82: 970-982. https://doi.org/10.1139/b04-074

Campetella G., Canullo R., Bartha S., 2004. Coenostate descriptors and spatial dependence in vegetation: derived variables in monitoring forest dynamics and assembly rules. Community Ecology 5(1): 105-114.

Campetella G., Canullo R., Bartha S., 1999. Fine-scale spatial pattern analysis of the herb layer of woodland vegetation using information theory. Plant Biosystems 133: 277 - 288.

Campetella G., Canullo R., Allegrini M.C., 2005. Stauts and changes of ground vegetation at the CONECOFOR plots, 1999-2005. In: Ferretti M., Bussotti F., Fabbio G., Petriccione B., (Eds.), 2005 - 2006 - Ecological condition of selected forest ecosystem in Italy. Status and changes 1995 - 2005. Fourth report of the Task Force on Integrated and Combined (I&C) evaluation of the CONECOFOR programme. Annali C.R.A. - Centro di Ricerca per la Selvicoltura, Special Issue, Volume 34, - 2005 - 2006: 120 p.

Campetella G., Canullo R., Mucina L., Kertész M., Ruprecht E., Penksza K., Chelli S., Csathó A.I., Zimmermann Z., Komoly C., Szabó G., Házi J., Besnyői V., Koncz P., Čarni A., Paušić A., Juvan N., Wellstein C., Szépligeti M., Csete S., Kun R., Bartha S., 2014. Solving the conflict between intensive and extensive approaches: transect based sampling design for comparative studies on fine scale

plant community organization. In: Mucina L., Price J.N. and Kalwij J.M. (eds.) Biodiversity and vegetation: patterns, processes, conservation: 76. Kwongan Foundation, Perth, AU.

Cantonati M., Kelly M.G., Lange-Bertalot H., 2017. Freshwater benthic diatoms of central Europe: over 800 common species used in ecological assessment. Koeltz Botanical Book, Oberreifenberg: 942 pp.

Canullo R., Starlinger F., Giordani F., 2013 - Diversity and Composition of Plant and Lichen Species. In Ferretti M. and Fischer R. (eds): Forest Monitoring: Methods for Terrestrial Investigations in Europe with an Overview of North America and Asia. Developments in Environmental Science 12: 237-250. Elsevier, Oxford, UK.

Carr A., Weatherall A., Jones G., 2020. The effects of thinning management on bats and their insect prey in temperate broadleaved woodland. Forest Ecology and Management, Volume 457.

Cecchini G, Andreetta A., Marchetto A., Carnicelli S., 2021. Soil solution fluxes and composition trends reveal risks of nitrate leaching from forest soils of Italy. Catena, 200, 105175

Cecchini G., Andreetta A., Marchetto A., Carnicelli S., 2019. Atmospheric deposition control of soil acidification in central Italy. Catena, 182.

Cecchini G., Andreetta A., Marchetto A., Carnicelli S., 2019. Atmospheric deposition control of soil acidification in central Italy. Catena, 182, 104102

Cecchini G., Andreetta A., Marchetto A., Carnicelli S., 2021. Soil solution fluxes and composition trends reveal risks of nitrate leaching from forest soils of Italy. Catena, 200, art. no. 105175.

Cecconi E., Incerti G., Capozzi F., Adamo P., Bargagli R., Benesperi R., Candotto Carniel F., Favero-Longo S.E., Giordano S., Puntillo D., Ravera S., Spagnuolo V., Tretiach M., 2018. Background element content of the lichen *Pseudevernia furfuracea*: A supra-national state of art implemented by novel field data from Italy. Science of The Total Environment 622-623: 282-292. https://doi.org/10.1016/j.scitotenv.2017.11.276

Cesarini G., Fornaroli R., Boggero A., Musazzi S., Dumnicka E., Zaupa S., Marchetto A., Rogora M., 2025. First Assessment of Freshwater Monitoring Under the Eu National Emission Ceilings Directive: Emerging Issues and Way Forward. Water Air Soil Pollut 236: 181. https://doi.org/10.1007/s11270-025-07804-7

Cistrone L., Altea T., Matteucci G., Posillico M., De Cinti B., Russo, D., 2015. The effect of thinning on bat activity in Italian high forests: The LIFE + "ManFor C. BD" experience. Hystrix It. J. Mamm. 26, 125–131.

Conti M.E., Pino A., Botrè F., Bocca B., Alimonti A., 2009. Lichen Usnea barbata as biomonitor of airborne elements deposition in the Province of Tierra del Fuego (southern Patagonia, Argentina). Ecotoxicology and Environmental Safety 72: 1082-1089. https://doi.org/10.1016/j.ecoenv.2008.12.004

Coulis M., Hättenschwiler S., Fromin N., David J.F., 2013. Macroarthropod-Microorganism Interactions during the Decomposition of Mediterranean Shrub Litter at Different Moisture Levels. Soil Biology and Biochemistry 64 (September 2013): 114–21. https://doi.org/10.1016/j.soilbio.2013.04.012.

Cristina M., Conti F.D., Pinto S., Bodini A., 2018. Soil Biological Quality Index (QBS-Ar): 15 Years of Application at Global Scale. Ecological Indicators 85 (Febbraio 2018): 773–80. https://doi.org/10.1016/j.ecolind.2017.11.030.

Cristina M., Leoni A., Gardi C., Delia Conti F., 2011. Are Grasslands Important Habitats for Soil Microarthropod Conservation? Biodiversity and Conservation 20, fasc. 5 (Maggio 2011): 1073–87. https://doi.org/10.1007/s10531-011-0017-0.

Cristofolini F., Giordani P., Gottardini E., Modenesi P., 2008. The response of epiphytic lichens to air pollution and subsets of ecological predictors: A case study from the Italian Prealps. Environmental Pollution 151: 308-317. https://doi.org/10.1016/j.envpol.2007.06.040

D'Avino L., Bigiotti G., Vitali F., L'Abate G., Jacomini C., 2022. QBS-Ar and QBS-Ar_BF Index Toolbox for Biodiversity Assessment of Microarthropods Community in Soil, 5 Settembre 2022. https://doi.org/10.5281/ZENODO.7041394.

Darras K., Batáry P., Furnas B.J., Grass I., Mulyani Y.A., Tscharntke T., 2019. Autonomous sound recording outperforms human observation for sampling birds: a systematic map and user guide. *Ecological Applications* 29(6): e01954.

Davy-Bowker J., Furse M.T., Murphy J.F., Clarke R.T., Wiggers R., Vincent H.M., 2003. Development of the Acid Water Indicator Community (AWIC) macroinvertebrate family and species level scoring systems. Monitoring acid water Phase I. R&D Technical Report P2–090/TR1. Bristol, UK. Environment Agency.

Davy-Bowker J., Murphy J. F., Rutt G.P., Steel J.E.C., Furse M.T., 2005. The development and testing of a macroinvertebrate biotic index for detecting the impact of acidity on streams. Archiv fur Hydrobiologie, 163, 383–403. https:// doi. org/ 10. 1127/ 0003-9136/ 2005/ 0163- 0383

Degtjarenko P., Matos P., Marmor L., Branquinho C., Randlane T., 2018. Functional traits of epiphytic lichens respond to alkaline dust pollution. Fungal Ecology 36: 81-88. https://doi.org/10.1016/j.funeco.2018.08.006

Deiner K., Bik H.M., Mächler E., et al., 2017. Environmental DNA metabarcoding: Transforming how we survey animal and plant communities. *Mol Ecol*. 26: 5872– 5895.

Descy J.P., Coste M., 1991. A test of methods for assessing water quality based on diatoms. Verh. Int. Ver. Limnol. 24: 2112-2116.

Dettki H., Esseen P.-A., 2003. Modelling long-term effects of forest management on epiphytic lichens in northern Sweden. Forest Ecology and Management 175: 223-238. doi: https://doi.org/10.1016/S0378-1127(02)00131-7

Di Nuzzo L., Giordani P., Benesperi R., Brunialti G., Fačkovcová Z., Frati L., Nascimbene J., Ravera S., Vallese C., Paoli L., Bianchi E., 2022. Microclimatic alteration after logging affects the growth of the endangered lichen *Lobaria pulmonaria*. Plants 11(3). https://doi.org/10.3390/plants11030295

Dobbertin M., 2005. Tree growth as indicator of tree vitality and of tree reaction to environmental stress: a review. European Journal of Forest Research 124: 319-333. - doi: 10.1007/s10342-005-0085-3.

Ellis C.J., Asplund J., Benesperi R., Branquinho C., Di Nuzzo L., Hurtado P., Martínez I., Matos P., Nascimbene J., Pinho P., Prieto M., Rocha B., Rodríguez-Arribas C., Thüs H., Giordani P., 2021. Functional Traits in Lichen Ecology: A Review of Challenge and Opportunity. *Microorganisms 9*: 766. https://doi.org/10.3390/microorganisms9040766

Esseen P.-A., Ekström M., Westerlund B., Palmqvist K., Jonsson B.G., Grafström A., Ståhl G., 2016. Broad-scale distribution of epiphytic hair lichens correlates more with climate and nitrogen deposition than with forest structure. Canadian Journal of Forest Research 46: 1348-1358. doi: https://doi.org/10.1139/cjfr-2016-0113

Federer C.A., 2002. BROOK 90: A simulation model for evaporation, soil water, and streamflow. http://www.ecoshift.net/brook/brook90.htm

Federico R., Settineri G., Sidari M., Mallamaci C., Muscolo A., 2020. Responses of Soil Quality Indicators to Innovative and Traditional Thinning in a Beech (*Fagus sylvatica* L.) Forest. Forest Ecology and Management 465 (June 2020): 118106. https://doi.org/10.1016/j.foreco.2020.118106.

Ferretti M., Marchetto A., Arisci S., Bussotti F., Calderisi M., Carnicelli S., Cecchini G., Fabbio G., Bertini G., Matteucci G., de Cinti B., Salvati L., Pompei E., 2014. On the tracks of Nitrogen deposition effects on temperate forests at their southern European range - an observational study from Italy. Global Change Biology, 20, 3423-3438.

Firbank, Les G., Chiara Bertora, David Blankman, Gemini Delle Vedove, Mark Frenzel, Carlo Grignani, Elli Groner, et al. «Towards the Co-Ordination of Terrestrial Ecosystem Protocols across European Research Infrastructures». Ecology and Evolution 7, fasc. 11 (Giugno 2017): 3967–75. https://doi.org/10.1002/ece3.2997.

Frati L., Santoni S., Nicolardi V., Gaggi C., Brunialti G., Guttova A., Gaudino S., Pati A., Pirintsos S.A., Loppi S., 2007. Lichen biomonitoring of ammonia emission and nitrogen deposition around a pig stockfarm. Environmental Pollution 146: 311-316.

Froidevaux J.S.P., Zellweger F., Bollmann K., Obrist M.K., 2014. Optimizing passive acoustic529sampling of bats in forests. Ecology and Evolution, 4, 4690-4700

Füreder L., Ettinger R., Boggero A. et al., 2006. Macroinvertebrate Diversity in Alpine Lakes: Effects of Altitude and Catchment Properties. Hydrobiologia 562, 123–144. https://doi.org/10.1007/s10750-005-1808-7

Gadsdon S.R., Dagley J.R., Wolseley P.A., Power S.A., 2010. Relationships between lichen community composition and concentrations of NO2 and NH3. Environmental Pollution 158: 2553-2560. https://doi.org/10.1016/j.envpol.2010.05.019

Galli L., Capurro M., Menta C., Rellini I., 2014. Is the QBS-Ar Index a Good Tool to Detect the Soil Quality in Mediterranean Areas? A Cork Tree Quercus Suber L. (Fagaceae) Wood as a Case of Study. Italian Journal of Zoology 81, fasc. 1 (2 Gennaio 2014): 126–35. https://doi.org/10.1080/11250003.2013.875601.

Gardi C., Menta C. Leoni A., 2008. EVALUATION OF THE ENVIRONMENTAL IMPACT OF AGRICULTURAL MANAGEMENT PRACTICES USING SOIL MICROARTHROPODS. Fresenius Environmental Bulletin 17, fasc. 8 (2008).

Gasc A., Sueur J., Jiguet F., Devictor V., Grandcolas P., Burrow C., Depraetere M., Pavoine S., 2013. Assessing biodiversity with sound: do acoustic diversity indices reflect phylogenetic and functional diversities of bird communities? Ecol. Indicat. 25, 279–287.

Geiser L.H., Jovan S.E., Glavich D.A., Fenn M.E., 2014. Predicting Lichen-based Critical Loads for Nitrogen Deposition in Temperate Forests. In: M. A. Sutton et al. (eds.), Nitrogen Deposition, Critical Loads and Biodiversity, Springer Science+Business Media Dordrecht, DOI 10.1007/978-94-007-7939-6_33

Geiser L.H., Nelson P.R., Jovan S.E., Root H.T., Clark C.M., 2019. Assessing Ecological Risks from Atmospheric Deposition of Nitrogen and Sulfur to US Forests Using Epiphytic Macrolichens. Diversity 11: 87. https://doi.org/10.3390/d11060087

Geiser L.H., Root H.T., Smith R.J., Jovan S.E., St Clair L., Dillman K.L., 2021. Lichen-based critical loads for deposition of nitrogen and sulfur in US forests. Environmental Pollution 291: 118187. https://doi.org/10.1016/j.envpol.2021.118187

Gilliam F.S., 2007. The ecological significance of the herbaceouslayer in temperate forest ecosystems. BioScience 57: 845-857. - doi:https://doi.org/10.1641/B571007

Giordani P., Benesperi R., Bianchi E., Brunialti G., Cecconi E., Contardo T., Di Nuzzo L., Fortuna L., Frati L., Loppi S., Monaci F., Munzi S., Nascimbene J., Paoli L., Ravera S., Tretiach M., Vannini A., 2020. Guidelines fo the use of lichens as bioaccumulators. ISPRA Manuali e Linee Guida 189/2019. ISBN 978-88-448-0966-9.

Giordani P., Brunialti G., Bacaro G., Nascimbene J., 2012. Functional traits of epiphytic lichens as potential indicators of environmental conditions in forest ecosystems. Ecological Indicators 18: 413-420. https://doi.org/10.1016/j.ecolind.2011.12.006

Giordani P., Calatayud V., Stofer S., Seidling W., Granke O., Fischer R., 2014. Detecting the nitrogen critical loads on European forests by means of epiphytic lichens. A signal-to-noise evaluation. Forest Ecology and Management 311: 29-40. https://doi.org/10.1016/j.foreco.2013.05.048

Hämäläinen H., Huttunen P., 1990. Estimation of acidity in streams by means of benthic invertebrates: evaluation of two methods. In: Acidification in Finland. Springer, Berlin, Heidelberg: 1051–1070.

Hammel K., Kennel M., 2001. Charakterisierung und Analyse der Wasserverfügbarkeit und des Wasserhaushalts von Waldstandorten in Bayern mit dem Simulationsmodell BROOK90. Forstliche Forschungsberichte München 185.

Hauer F., Resh V., 2007. Macroinvertebrates. In: Methods in Stream Ecology (Second Edition). https://doi.org/10.1016/B978-012332908-0.50028-0.

Hirsch R.M., Slack J.R., 1984. A nonparametric test for seasonal data with serial dependance. Water Resources Research 20: 727-732.

Hotaling S., Tronstad L.M., Cody Bish J., 2017. Macroinvertebrate richness is lower in high-elevation lakes vs nearby streams: evidence from Grand Teton National Park, Wyoming. J. Nat. Hist. 51: 29-30.

Hruška J., Ouhlele F., Šamonil P., Šebesta J., Tahovská K., Hleb R., Houška J., Šikl J., 2012. Long-term forest soil acidification, nutrient leaching and vegetation development: linking modelling and surveys of a primeval spruce forest in the Ukrainian Transcarpathian Mts. Ecol. Model. 24, 28–37.

ICP Waters Programme Manual 2010. ICP Waters Report 105/2010. Report No. 6074-2010.

ICP Waters, 2010. Programme Manual, ICP Waters Report 105/2010. Report No. 6074–2010. https:// niva. brage. unit. no/ niva-xmlui/ bitst ream/ handle/ 11250/ 215220/ ATT36 6BE. pdf? seque nce=1

ICP WATERS, 2025. ICP Waters Programme Manual. ICP Waters Report 158/2025. ISBN 978-82-577-7818-7. NIVA report ISSN 1894-7948: 86 pp. https://drive.google.com/file/d/1I7Ur8YRQEgMzljfNiE6Jk-TivQ1FAJll/view?usp=sharing

Jeran Z., Mrak T., Jaćimović R., Batič F., Kastelec D., Mavsar R., Simončič P., 2007. Epiphytic lichens as biomonitors of atmospheric pollution in Slovenian forests. Environmental Pollution 146: 324-331. https://doi.org/10.1016/j.envpol.2006.03.032

Jones G., Jacobs D.S., Kunz T.H., Willig M.R., Racey P.A., 2009. Carpe noctem: The importance of bats as bioindicators. Endanger. Species Res. 8, 93–115.

Jones K.E., Russ J.A., Bashta A.-T., Bilhari Z., Catto C., Csősz I., Gorbachev A., Győrfi P., Hughes A., Ivashkiv I., Koryagina N., Kurali A., Langton S., Collen A., Margiean G., Pandourski I., Parsons S., Prokofev I., Szodoray-Paradi A., Szodoray-Paradi F., Tilova E., Walters C.L., Weatherill A., Zavarzin O., 2013. Indicator Bats Program: A System for the Global Acoustic Monitoring of Bats. In Biodiversity Monitoring and Conservation (eds B. Collen, N. Pettorelli, J.E.M. Baillie and S.M. Durant)

Jovan S., Riddell J., Padgett P.E., Nash T.H., 2012. Eutrophic lichens respond to multiple forms of N: implications for critical levels and critical loads research. Ecological Applications, 22: 1910-1922. https://doi.org/10.1890/11-2075.1

Juhász-Nagy P., Podani J., 1983 - Information theory methods for the study of spatial processes and succession. Vegetation 51: 129-140.

Kalaji H.M., Schansker G., Brestic M., Bussotti F., Calatayud A., Ferroni L., Goltsev V., Guidi L., Jajoo A., Li P., Losciale P., Mishra V.K., Misra A.N., Nebauer S.G., Pancaldi S., Penella C., Pollastrini M., Suresh K., Tambussi E., Yanniccari M., Zivcak M., Cetner M.D., Samborska I.A., Stirbet A., Olsovska K., Kunderlikova K., Shelonzek H., Rusinowski S., Bąba W., 2017. Frequently asked questions about chlorophyll fluorescence, the sequel. Photosynthesis Research 132:13–66.

Kalaji H.M., Schansker G., Ladle R.J., Goltsev V., Bosa K., Allakhverdiev S.I., Brestic M., Bussotti F., Calatayud A., Dąbrowski P., Elsheery N.I., Ferroni L., Guidi L., Hogewoning S.W., Jajoo A., Misra A.N., Nebauer S.G., Pancaldi S., Penella C., Poli D.B., Pollastrini M., Romanowska-Duda Z.B., Rutkowska B., Serôdio J., Suresh K., Szulc W., Tambussi E., Yanniccari M., Zivcak M., 2014. Frequently Asked Questions about chlorophyll fluorescence: practical issues. Photosynthesis Research. 122:121–158. DOI 10.1007/s11120-014-0024-6.

Karst-Riddoch T.L., Pisaric M.F.J., Smol J.P., 2005. Diatom responses to 20th century climate-related environmental changes in high-elevation mountain lakes of the northern Canadian Cordillera. J Paleolimnol 33, 265–282 (2005). https://doi.org/10.1007/s10933-004-5334-9

Kasten E.P., Gage S.H., Fox J., Joo W., 2012. The remote environmental assessment laboratory's acoustic library: An archive for studying soundscape ecology. Ecological Informatics 12:50-67.

Kelly M.G., Gómez-Rodríguez C., Kahlert M., Almeida S.F.P., Bennett C., Bottin M., Delmas F., Descy J-P., Dörflinger G., Kennedy B., Marvan P., Opatrilova L., Pardo I., Pfister P., Rosebery J., Schneider S., Vilbaste S., 2012. Establishing expectations for pan-European diatom based ecological status assessments. Ecol. Ind. 20: 177-186.

Kłos A., Ziembik Z., Rajfur M., Dołhańczuk-Śródka A., Bochenek Z., Bjerke J.W., Tømmervik H., Zagajewski B., Ziółkowski D., Jerz D., Zielińska M., Krems P., Godyń P., Marciniak M., Świsłowski P., 2018. Using moss and lichens in biomonitoring of heavy-metal contamination of forest areas in southern and north-eastern Poland. Science of The Total Environment 627: 438-449. https://doi.org/10.1016/j.scitotenv.2018.01.211

Knops J.M.H., Nash T.H. III, Schlesinger W.H., 1996. The influence of epiphytic lichens on the nutrient cycling of an oak woodland. Ecological Monographs 66: 159-179. doi: https://doi.org/10.2307/2963473

Kopácek J., Stuchlík E., Wright R.F., 2005. Long-term trends and spatial variability in nitrate leaching from alpine catchment-lake ecosystems in the Tatra Mountains (Slovakia-Poland). Environ Pollut., 136: 89-101 https://doi.org/10.1016/j.envpol.2004.12.012

Krammer K., 2000. The genus Pinnularia. Diatoms of Europe. 1: 1-703. (ISBN 978-3-904144-24-7)

Krammer K., 2002. Cymbella. Diatoms of Europe. 3: 1-584. (ISBN 978-3-904144-84-1)

Krammer K., 2003. Cymbopleura, Delicata, Navicymbula, Gomphocymbellopsis, Afrocymbella Supplements to cymbelloid taxa. 2003. Diatoms of Europe. 4: 1-530. (ISBN 978-3-904144-99-5).

Krammer K., Lange-Bertalot H., 1986–1991. Süßwasserflora von Mitteleuropa. In: E.H.J. Gerloff, H. Heynig and D. Mollenhauer (eds.), 2/1Bacillariophyceae, Naviculaceae; 2/2Bacillariaceae, Epithemiaceae, Surirellaceae, Centrales, 2/3 Fragilariaceae, Eunotiaceae, 2/4 Achnanthaceae. Gustav Fischer Verlag, Stuttgart: 876 pp + 596 pp + 576 pp + 468 pp.

Krause G.H., Weis E., 1991. Chlorophyll fluorescence and photosynthesis. The basics. Annual Review of Plant Physiology and Plant Molecular Biology 42: 313–349.

Krivograd Klemenčič A., Toman M.J., 2010. Influence of environmental variables on benthic algal associations from selected extreme environments in Slovenia in relation to the species identification. Period. Biol. 112: 179-191.

Kroes J.G., Van Dam J.C., Groenendijk P., Hendriks R.F.A., Jacobs C.M.J., 2008. SWAP version 3.2. Theory description and user manual. Alterra Report 1649, Alterra, Wageningen. https://www.swap.alterra.nl/Documents/Alterra%20Report1649%20-%20Swap32%20Theory%20description%20and%20user%20manual.pdf

Lange-Bertalot H, 2001. Navicula sensu stricto. 10 Genera separated from Navicula sensu lato. Frustulia. In Lange-Bertalot, H. (ed.), Diatoms of Europe, 2. Gantner Verlag, Ruggell: 526 pp.

Leempoel K., Hebert T., Hadly E.A., 2020. A comparison of eDNA to camera trapping for assessment of terrestrial mammal diversity. Proc. R. Soc. B 287: 20192353.

Lehmkuhl J.F., 2004. Epiphytic lichen diversity and biomass in low-elevation forests of the eastern Washington Cascade range, USA. Forest Ecology and Management 187: 381-392. doi: https://doi.org/10.1016/j.foreco.2003.07.003

Ling Q., Huang W., Jarvis P., 2011. Use of a SPAD-502 meter to measure leaf chlorophyll concentration in Arabidopsis thaliana. Photosynth Res 107, 209–214 (2011). https://doi.org/10.1007/s11120-010-9606-0

Ling Y., Teng S., Liu C., Dash J., Morris H., Pastor-Guzman J., 2022. Assessing the Accuracy of Forest Phenological Extraction from Sentinel-1 C-Band Backscatter Measurements in Deciduous and Coniferous Forests, Remote Sens., 14, 674. https://doi.org/10.3390/rs14030674, 2022.

Liu M., Bardossy A., Li J., Jiang Y., 2012. Physically-based modeling of topographic effects on spatial evapotranspiration and soil moisture patterns through radiation and wind. Hydrology and Earth System Sciences, 16, 357–373.

Loppi S., Cenni E., Bussotti F., Ferretti M., 1998. Biomonitoring of geothermal air pollution by epiphytic lichens and forest trees. Chemosphere 36: 1079-1082. https://doi.org/10.1016/S0045-6535(97)10175-8

Loppi S., Pirintsos S.A., 2003. Epiphytic lichens as sentinels for heavy metal pollution at forest ecosystems (central Italy). Environmental Pollution 121: 327-332. https://doi.org/10.1016/S0269-7491(02)00269-5

Magurran A.E., 2004. Measuring biological diversity. 2nd ed. Oxford, U.K: Blackwell Science Ltd: 256 pp.

Malm W.C., Sisler J.F., Huffman D., Eldred R.A. and Cahill T.A., 1994. Spatial and seasonal trends in particle concentration and optical extinction in the United States. J. Geophys. Res. 99: 1347–1370.

MalmW.C., 1999. Introduction to Visibility. ISSN 0737-5352-40.

Malusà E., 2009. COMMON GUIDELINES FOR ANALYTICAL METHODS.

Manninen S., 2018. Deriving nitrogen critical levels and loads based on the responses of acidophytic lichen communities on boreal urban Pinus sylvestris trunks. Science of The Total Environment 613–614: 751-762. https://doi.org/10.1016/j.scitotenv.2017.09.150

Marchetto A., Barbieri A., Mosello R., Tartari G.A., 1994a. Acidification and weathering processes in high mountain lakes in Southern Alps. Hydrobiologia, 274, 75-81 https://doi.org/10.1007/BF00014629

Marchetto A., Mosello R., Rogora M., Manca M., Boggero A., Morabito G., Musazzi S., Tartari G.A., Nocentini A.M., Pugnetti A., Bettinetti R., Panzani P., Armiraglio M., Cammarano P., Lami A., 2004. The chemical and biological response of two remote mountain lakes in the Southern Central Alps (Italy) to twenty years of changing physical and chemical climate. J. Limnol. 63: 77-89.

Marchetto A., Rogora M., Boggero A., Musazzi S., Lami A., Lotter A.F., Tolotti M., Thies H., Psenner R., Massaferro J., Barbieri A., 2009. Response of alpine lakes to major environmental gradients, as detected through planktonic, benthic and sedimentary assemblages. Advanc. Limnol., 62: 419-440. https://doi.org/10.1127/advlim/62/2009/419

Markwell J., Osterman J.C., Mitchell J.L., 1995. Calibration of the Minolta SPAD-502 leaf chlorophyll meter. Photosynth Res 46, 467–472 (1995). https://doi.org/10.1007/BF00032301

Marmor L., Tõrra T., Randlane T., 2007. The vertical gradient of bark pH and epiphytic macrolichen biota in relation to alkaline air pollution. Ecological Indicators 10: 1137-1143. https://doi.org/10.1016/j.ecolind.2010.03.013

Martins F.S., Formigo N., Antunes S.C., 2020. Can be the environmental and biotic factors responsible for macroinvertebrate communities' alterations in Portuguese alpine ponds? Limnologica, 83, 2020, https://doi.org/10.1016/j.limno.2020.125782

Maxwell C., Johnson G.N., 2000. Chlorophyll fluorescence – a practical guide. Journal of Experimental Botany 51: 659–668.

McCune B., 1994. Using Epiphyte Litter to Estimate Epiphyte Biomass. The Bryologist 97: 396-401. doi: https://doi.org/10.2307/3243905

McFarland B., Carse F., Sandin L., 2010. Littoral macroinvertebrates as indicators of lake acidification within the UK. Aquat. Conserv.: Mar. Freshw., 20, S105–S116. https://doi.org/10. 1002/aqc.1064

MCPFE 2003 - Improved Pan-European Indicators for Sustainable Forest Management. Liaison Unit, Vienna. [https://www.cbd.int/doc/pa/tools/Improved%20Pan-European%20Indicators%20for%20Sustainable%20Forest%20Management.pdf] (accessed Jan 2023).

Menta C., Conti F.D., Pinto S., Leoni A., Lozano-Fondón C., 2014. Monitoring Soil Restoration in an Open-Pit Mine in Northern Italy». Applied Soil Ecology 83 (November 2014): 22–29. https://doi.org/10.1016/j.apsoil.2013.07.013.

Metcalf, O.C., Barlow, J., Marsden, S., Gomes de Moura, N., Berenguer, E., Ferreira, J. and Lees, A.C. (2022), Optimizing tropical forest bird surveys using passive acoustic monitoring and high temporal resolution sampling. Remote Sens Ecol Conserv, 8: 45-56

Meusburger K., Trotsiuk V., Schmidt-Walter P., Baltensweiler A., Brun P., Bernhard F., Gharun M., Habel R., Hagedorn F., Köchli R., Psomas A., Puhlmann H., Thimonier A., Waldner P., Zimmermann S., Walthert L., 2022. Soil–plant interactions modulated water availability of Swiss forests during the 2015 and 2018 droughts. Global Change Biology; 28, 5928–5944.

Morillas L., Roales J., Cruz C., Munzi S., 2021. Resilience of Epiphytic Lichens to Combined Effects of Increasing Nitrogen and Solar Radiation. Journal of Fungi 7: 333. https://doi.org/10.3390/jof7050333

Murchie E.H., Lawson T., 2013. Chlorophyll fluorescence analysis: a guide to good practice and understanding some new applications. Journal of Experimental Botany 64: 3983–3998.

Murillo-Amador B., Avila-Serrano N.Y., Garcia-Hernandez J.L., Lopez-Aguilar R., Troyo-Dieguez E., Kaya C., 2004. Relationship between a nondestructive and an extraction method for measuring chlorophyll contents in cowpea leaves. J. Plant Nutr. Soil Sc. 167

Murphy J.F., Winterbottom J.H., Orton S., Simpson G.L., Shilland E.M., Hildrew A.G., 2014. Evidence of recovery from acidification in the macroinvertebrate assemblages of UK fresh waters: A 20-year time series. Ecological Indicators 37, Part B, 330–340. https://doi.org/10.1016/j.ecolind.2012.07.009

Nascimbene J., Benesperi R., Giordani P., Grube M., Marini L., Vallese C., Mayrhofer H., 2019. Could Hair-Lichens of High-Elevation Forests Help Detect the Impact of Global Change in the Alps? Diversity 11: 45. doi: https://doi.org/10.3390/d11030045

Nascimbene J., Casazza G., Benesperi R., Catalano I., Cataldo D., Grillo M., Isocrono D., Matteucci E., Ongaro S., Potenza G., et al., 2016. Climate change fosters the decline of epiphytic *Lobaria* species in Italy. Biological Conservation 20: 377-384. https://doi.org/10.1016/j.biocon.2016.08.003

Nascimbene, J., Benesperi, R., Brunialti, G., Catalano, I., Delle Vedove, M., Grillo, M., Isocrono, D., Matteucci, E., Potenza, G., Puntillo, D., Puntillo, M., Ravera, S., Rizzi, G., Giordani, P., 2013. Patterns and drivers of beta-diversity and similarity of *Lobaria pulmonaria* communities in Italian forests. Journal of Ecology 101: 493-505. https://doi.org/10.1111/1365-2745.12050

Nascimbene, J., Brunialti, G., Ravera, S., Frati, L., Caniglia, G., 2010. Testing *Lobaria pulmonaria* (L.) Hoffm as an indicator of lichen conservation importance of Italian forests. Ecological Indicators 10: 353-360. https://doi.org/10.1016/j.ecolind.2009.06.013

Nilsson, S.G., Arup, U., Baranowski, R., Ekman, S., 1995. Tree-dependent lichens and beetles as indicators in conservation forests. Conservation Biology 9: 1208-1215. https://doi.org/10.1046/j.1523-1739.1995.9051199.x-i1

Nimis P.L., 2022. ITALIC - The Information System on Italian Lichens. Version 7.0. University of Trieste, Dept. of Biology, (https://dryades.units.it/italic), accessed on 2022, 12, 16.

O'Briain R., 2019. Climate change and European rivers: An eco-hydromorphological perspective. Ecohydrology, 12.5(2019), e2099. https://doi.org/10.1002/eco.2099

Oleksy I.A., Baron J.S., Leavitt P.R., Spaulding S.A., 2020. Nutrients and warming interact to force mountain lakes into unprecedented ecological states. Proc. R. Soc. B.28720200304 http://doi.org/10.1098/rspb.2020.0304

Orusa T., Viani A., Cammareri D., Borgogno Mondino E., 2023. A Google Earth Engine Algorithm to Map Phenological Metrics in Mountain Areas Worldwide with Landsat Collection and Sentinel-2. Geomatics, 3, 2.

Otnyukova T., 2007. Epiphytic lichen growth abnormalities and element concentrations as early indicators of forest decline. Environmental Pollution 146: 359-365. https://doi.org/10.1016/j.envpol.2006.03.043

Parisi V., Menta C., Gardi C., Jacomini C., Mozzanica E., 2005. Microarthropod Communities as a Tool to Assess Soil Quality and Biodiversity: A New Approach in Italy. Agriculture, Ecosystems & Environment 105, fasc. 1–2 (gennaio 2005): 323–33. https://doi.org/10.1016/j.agee.2004.02.002.

Paul K.I., Polglase P.J., O'Connell A.M., Carlyle J.C., Smethurst P.J., Khanna P.K., Worledge D., 2003. Soil water under forests (SWUF): a model of water flow and soil water content under a range of forest types. Forest Ecology and Management 182, 195–211.

Perez-Harguindeguy N., Diaz S., Garnier E., Lavorel S., Poorter H., Jaureguiberry P., Cornelissen, J.H.C., 2016. Corrigendum to: New handbook for standardised measurement of plant functional traits worldwide. *Australian Journal of botany*, *64*(8), 715-716.

Pieretti N., Farina A., Morri D., 2011. A new methodology to infer the singing activity of an avian community: The Acoustic Complexity Index (ACI). Ecol. Indic., 11: 868-873.

Piksa K., Brzuskowski T., Zwijacz-Kozica T., 2022) Distribution, Dominance Structure, Species Richness, and Diversity of Bats in Disturbed and Undisturbed Temperate Mountain Forests. *Forests*, *13*, 56. https://doi.org/10.3390/f13010056

Pinho P., Bergamini A., Carvalho P., Branquinho C., Stofer S., Scheidegger C., Máguas C., 2012a. Lichen functional groups as ecological indicators of the effects of land-use in Mediterranean ecosystems. Ecological Indicators 15: 36-42. https://doi.org/10.1016/j.ecolind.2011.09.022

Pinho P., Theobald M.R., Dias T., Tang Y.S., Cruz C., Martins-Loução M.A., Máguas C., Sutton M., Branquinho C., 2012b. Critical loads of nitrogen deposition and critical levels of atmospheric ammonia for semi-natural Mediterranean evergreen woodlands. Biogeosciences 9: 1–11. doi:10.5194/bg-9-1-2012

Pollastrini M., Feducci M., Bonal D., Fotelli M., Gessler A., Gossiord C., Guyot V., Jactel H., Nguyen D., Radoglou K., Bussotti F., 2016c. Physiological significance of forest tree defoliation: results from a survey in a mixed forest in Tuscany (central Italy), 361, 170-178. doi.org/10.1016/j.foreco.2015.11.018

Pollastrini M., Holland V., Brüggemann W., Bruelheide H., Dănilă I.C., Jaroszewicz B., Valladares F., Bussotti F. (2016a). Taxonomic and ecological relevance of the chlorophyll a fluorescence signature of tree species in mixed European forests. New Phytologist 212 (1): 51-65.

Pollastrini M., Holland V., Brüggemann W., Bussotti F., 2016b. Chlorophyll a fluorescence analysis in forests. Annali di Botanica (Roma) 6: 23-37. doi: 10.4462/annbotrm-13257

Pollastrini M., Salvatori E., Fusaro L., Manes F., Marzuoli R., Gerosa G., Brüggemann W., Strasser R.J., Bussotti F., 2020. Selection of tree species for forests under climate change: is PSI functioning a better predictor for net photosynthesis and growth than PSII? Tree Physiology 44, 1561–1571

Ponge J-F., Vannier G., Arpin P., David J-F., 1986. Caractérisation des humus et des litières par la faune du sol: intérêt sylvicole. Revue forestière française 38, fasc. 6 (1986): 509. https://doi.org/10.4267/2042/25685.

Puhlmann H., von Wilpert K., 2011. Test und Entwicklung von Pedotransferfunktionen für Wasserretention und hydraulische Leitfähigkeit von Waldböden. Waldökologie, Landschaftsforschung und Naturschutz, 12, 61–71.

Raddum G.G., Fjellheim A., Hesthagen T., 1988. Monitoring of acidification by the use of aquatic organisms. Verh. Int. Ver. Limnol., 23: 2291–2297. https://doi.org/10.1080/03680770.1987.11899 891

Raddum G.G., Skjelkvåle B.L., 1995. Critical limits of acidification to invertebrates in different regions of Europe. Water, Air, and Soil Pollution, 85, 475–480. https://doi.org/10.1007/BF004 76874

Raddum G.G., Skjelkvåle B.L., 2001. Critical Limit of Acidifying Compounds to Invertebrates in Different Regions of Europe. Water Air Soil Pollut., 130, 825-830.

Ranghetti L., "sen2rts: Build and Analyse Sentinel-2 Time Series". https://doi.org/10.5281/zenodo.4682829, 2021.

Rempel R.S., Naylor B.J., Elkie P.C., Baker J., Churcher J., Gluck M.J., 2016. An indicator system to assess ecological integrity of managed forests. Ecological indicators, 60, 860-869.

Richardson A.D., Duigan S.P., Berlyn G.P., 2002. An evaluation of noninvasive methods to estimate foliar chlorophyll content. New Phytologist, 153: 185-194. https://doi.org/10.1046/j.0028-646X.2001.00289.x

Rodgers T.W., Mock K.E., 2015. Drinking water as a source of environmental DNA for the detection of terrestrial wildlife species. Conservation Genet Resour, 7:693–696

Rogora M., Arisci S., Marchetto A., 2012. The role of nitrogen deposition in the recent nitrate decline in lakes and rivers in Northern Italy. Science of the Total Environment 417-418C: 219-228 https://doi.org/10.1016/j.scitotenv.2011.12.067

Rogora M., Colombo L., Lepori F., Marchetto A., Steingruber S., Tornimbeni O., 2013. Thirty years of chemical changes in alpine acid-sensitive lakes in the Alps. Water Air Soil Pollut. 224:1746 https://doi.org/10.1007/s11270-013-1746-3

Rosenberg D.M., Resh V.H., 1993. Introduction to Freshwater Biomonitoring and Benthic Macroinvertebrates. In: Rosenberg DM, Resh VH (eds.), Freshwater Biomonitoring and Benthic Macroinvertebrates. Chapman/Hall, New York: 1-9.

Rosenqvist L., Hansen K., Vesterdal L., van der Salm C., 2010b. Water balance in afforestation chronosequences of common oak and Norway spruce on former arable land in Denmark and southern Sweden. Agricultural and Forest Meteorology 150, 196–207.

Rosenqvist L., Kleja D.B., Johansson M.-B., 2010a. Concentrations and fluxes of dissolved organic carbon and nitrogen in a Picea abies chronosequence on former arable land in Sweden. Forest Ecology and Management 259 275–285.

Rossaro B., Marziali L., Boggero A., 2022. Response of chironomids to key environmental factors: Perspective for biomonitoring. Insects, 13(10), 911. https://doi. org/10.3390/insects13100911

Rühland K.M., Paterson A.M., Smol J.P., 2015. Lake diatom responses to warming reviewing the evidence. J Paleolimnol 54, 1–35. https://doi.org/10.1007/s10933-015-9837-3

Russo D., Salinas-Ramos V.B., Cistrone L., Smeraldo S., Bosso L., Ancillotto L., 2021. Do We Need to Use Bats as Bioindicators? Biology, 10, 693.

Russo D., Voigt C.C., 2016. The use of automated identification of bat echolocation calls in acoustic monitoring: A cautionary note for a sound analysis. Ecological Indicators,Volume 66: 598-602,

Schaap M.G., Leij F.J., van Genuchten M.T., 2001. ROSETTA: A computer program for estimating soil hydraulic parameters with hierarchical pedotransfer functions. Journal of Hydrology 251, 163–176.

Schaap M.G., Nemes A., van Genuchten M.T., 2004. Comparison of Models for Indirect Estimation of Water Retention and Available Water in Surface Soils. Vadose Zone Journal 3(4): 1455-1463.

Schmidt-Walter P., Trotsiuk V., Meusburger K., Zacios M., Meesenburg H., 2020. Advancing simulations of water fluxes, soil moisture and drought stress by using the LWF-Brook90 hydrological model in R. Agricultural and Forest Meteorology 291, 108023.

Sen P.K., 1968. Estimates of the regression coefficient based on Kendall's tau. Journal of the American Statistical Society, 63: 1379-1389.

Shamas A., 2019. Are plant traits a practical indicator for monitoring ecological restoration projects? Master Thesis Degree. http://hdl.handle.net/10012/14547

Shaw T., Hedes R., Sandstrom A., Ruete A., Hiron M., Hedblom M., Eggers S., Mikusiński G., 2021. Hybrid bioacoustic and ecoacoustic analyses provide new links between bird assemblages and habitat quality in a winter boreal forest. *Environmental and Sustainability Indicators* 11:100141.

Solheim A., Globevnik L., Austnes K., Kristensen P., Moe J., Persson J., Phillips G., Poikane S., Bund W., Birk S., 2019. A new broad typology for rivers and lakes in Europe: Development and application for large-scale environmental assessments. Science of The Total Environment. 697. 134043 https://doi.org/10.1016/j.scitotenv.2019.134043

Sommaruga R, 2015. When glaciers and ice sheets melt: consequences for planktonic organisms. J. Plankton Res. 37: 509-518.

Standish, R. J., Hobbs, R. J., Mayfield, M. M., Bestelmeyer, B. T., Suding, K. N., Battaglia, L. , Eviner V., Hawkes C. V., Temperton V. M., Cramer V. A., Harris J.A., Funk J. L., Thomas P. A. (2014). Resilience in ecology: abstraction, distraction, or where the action is? Biological Conservation, 177, 43–51. https://doi.org/10.1016/j.biocon.2014.06.008

Stanton D.E., Huallpa Chávez J., Villegas L., Villasante F., Armesto J., Hedin L.O., Horn H., 2014. Epiphytes improve host plant water plant use by microenvironment modification. Functional Ecology 28: 1274-1283. doi: https://doi.org/10.1111/1365-2435.12249

Steingruber S., Boggero A., Pradella C., Dumnicka E., Colombo L., 2013. Can we use macroinvertebrates as indicators of acidification of high-altitude Alpine lakes? Bollettino della Società ticinese di scienze naturali, 101, 23–34. http://repository.supsi.ch/id/eprint/4667

Stoddard J., 1994. Long-term changes in watershed retention of nitrogen: its causes and aquatic consequences. In: Baker L.A. (Ed). Environmental Chemistry of Lakes and Reservoirs, 237: 223-284. DOI: 10.1021/ba-1994-0237.ch008

Stofer S, Calatayud V, Giordani P, Neville P, 2016: Part VII.2: Assessment of Epiphytic Lichen diversity. In: UNECE ICP Forests Programme Co-ordinating Centre (ed.): Manual on methods and criteria for harmonized sampling, assessment, monitoring and analysis of the effects of air pollution on forests. Thünen Institute of Forest Ecosystems, Eberswalde, Germany, 13 p. + Annex [http://www.icp-forests.org/manual.htm]

Stofer S, Calatayud V, Giordani P, Neville P, 2016: Part VII.2: Assessment of Epiphytic Lichen diversity. In: UNECE ICP Forests Programme Co-ordinating Centre (ed.): Manual on methods and criteria for harmonized sampling, assessment, monitoring and analysis of the effects of air pollution on forests. Thünen Institute of Forest Ecosystems, Eberswalde, Germany, 13 p. + Annex [http://www.icp-forests.org/manual.htm]

Strasser R.J., Srivastava A., Tsimilli-Michael M., 2000. The fluorescence transient as a tool to characterize and screen photosynthetic samples. In: Yunus M, Pathre U, Mohanty P, eds. Probing photosynthesis: mechanisms, regulation and adaptation. London, UK: Taylor & Francis, 445–483.

Strasser R.J., Tsimilli-Michael M., Srivastava A., 2004. Analysis of the fluorescence transient. In: Papageorgiou GC, Govindjee, eds. Advances in photosynthesis and respiration series. Chlorophyll fluorescence: a signature of photosynthesis. Dordrecht, the Netherlands: Springer, 321–362.

Süß A., Danner M., Obster C., Locherer M., Hank T., Richter K., 2015. Measuring Leaf Chlorophyll Content with the Konica Minolta SPAD-502Plus – Theory, Measurement, Problems, Interpretation. EnMAP Field Guides Technical Report, GFZ Data Services. DOI: http://doi.org/10.2312/enmap.2015.010

Svitok M., Kubovčík V., Kopáček J., Bitušík P., 2021. Temporal trends and spatial patterns of chironomid communities in alpine lakes recovering from acidification under accelerating climate change. Freshwater Biology, 66, 2223–2239. https://doi.org/10.1111/fwb.13827

Svitok M., Kubovčík V., Kopáček J., Bitušík P., 2021. Temporal trends and spatial patterns of chironomid communities in alpine lakes recovering from acidification under accelerating climate change. Freshw Biol, 66, 2223– 2239. https://doi.org/10.1111/fwb.13827

Swoczyna T., Kalaji H.M., Bussotti F., Mojski J., Pollastrini M., 2022. Environmental stress - what can we learn from chlorophyll a fluorescence analysis in woody plants? A review. Front. Plant Sci. 13:1048582. doi: 10.3389/fpls.2022.1048582

Theodoropoulos C., Vourka A., Stamou A., Rutschmann P., Skoulikidis N., 2017. Response of freshwater macroinvertebrates to rainfall-induced high flows: A hydroecological approach, Ecological Indicators, 73, Pages 432-442. https://doi.org/10.1016/j.ecolind.2016.10.011.

Thomsen P.F., Willerslev E., 2015. Environmental DNA – An emerging tool in conservation for monitoring past and present biodiversity. Biological Conservation, 183:4-18.

Thrane J.E., H. de Wit, K. Austnes. 2021. Effects of nitrogen on nutrient-limitation in oligotrophic northern surface waters. NIVAs 7680-2021. ICP Waters report 146/2021: 37 pp. https://www.icp-waters.no/2022/01/07/2021-report-effects-of-nitrogen-on-nutrient-limitation-in-oligotrophic-northern-surface-waters/

Tichý L., Axmanová I., Dengler J., Guarino R., Jansen F., Midolo G. et al., 2023. Ellenberg-type indicator values for European vascular plant species. Journal of Vegetation Science, 34, e13168. Available from: https://doi.org/10.1111/jvs.13168

TraitDivNet, 2022. version 24

Tsakalos J.L., Chelli S., Campetella G., Canullo R., Simonetti E., Bartha S., 2022. comspat: an R package to analyze within-community spatial organization using species combinations. Ecography, 2022: e06216. https://doi.org/10.1111/ecog.06216

Tsimilli-Michael M., Strasser R.J., 2008. Experimental resolution and theoretical complexity determine the amount of information extractable from the chlorophyll fluorescence transient OJIP. In: Allen JF, Gantt E, Golbeck JH, Osmond B, eds. Photosynthesis: energy from the Sun. 14th International

Tuneu-Corral C., Puig-Montserrat X., Flaquer C., Mas M., Budinski I., López-Baucells A., 2020. Ecological indices in long-term acoustic bat surveys for assessing and monitoring bats' responses to climatic and land-cover changes. Ecological Indicators, Volume 110, 105849

Uchino H., Watanabe T., Ramu K., Sahrawat K.L., Marimuthu S., Wani S.P., Ito O., 2013. Calibrating chlorophyll meter (SPAD-502) reading by specific leaf areafor estimating leaf nitrogen concentration in sweet sorghum. J. Plant Nutr. 36,1640–1646.

Uddling J., Gelang-Alfredsson J., Piikki K., Pleijel H., 2007. Evaluating the relationship between leaf chlorophyll concentration and SPAD-502 chlorophyll meter readings. Photosynth Res. 2007 Jan;91(1):37-46. doi: 10.1007/s11120-006-9077-5. Epub 2007 Mar 7. PMID: 17342446.

United States Environmental Protection Agency, 1999. Visibility Monitoring Guidance. EPA-454/R-99-003.

Ushio M., Fukuda H., Inoue T. et al., 2017. Environmental DNA enables detection of terrestrial mammals from forest pond water. Mol Ecol Resour, 17: e63–e75.

van der Heyde M., Bunce M., Nevill P., 2022. Key factors to consider in the use of environmental DNA metabarcoding to monitor terrestrial ecological restoration. Science of the Total Environment 848 (2022) 157617.

Villanueva-Rivera L.J., Pijanowski B.C., Doucette J., et al., 2011. A primer of acoustic analysis for landscape ecologists. Landscape Ecol 26, 1233–1246.

Vlaschenko A., Kravchenko K., Yatsiuk Y., Hukov V., Kramer-Schadt S., Radchuk V., 2022. Bat Assemblages Are Shaped by Land Cover Types and Forest Age: A Case Study from Eastern Ukraine. *Forests*, *13*, 1732. https://doi.org/10.3390/f13101732

Wegehenkel M., Wagner A., Amoriello T., Fleck S., Meesenburg H., Raspe S., 2017. Impact of stoniness correction of soil hydraulic parameters on water balance simulations of forest plots. J. Plant Nutr. Soil Sci., 180, 71–86

Wessolek G., Kaupenjohann M., Renger M., 2009. Bodenphysikalische Kennwerte und Berechnungsverfahren für die Praxis.' Bodenökologie und Bodengenese 40

Wessolek G., Schwarzel K., Greiffenhagen A., Stoffregen H., 2008. Percolation characteristics of a water-repellent sandy forest soil. European Journal of Soil Science, 59, 14–23.

Wildi O., Feldmeyer-Christe E., Ghosh S., Zimmermann N.E., 2004 - Comments on vegetation monitoring approaches. Community Ecology 5(1): 1-5.

Zhang Y., Schaap M.G., 2017. Weighted recalibration of the Rosetta pedotransfer model with improved estimates of hydraulic parameter distributions and summary statistics (Rosetta3). Journal of Hydrology 547 39–53.

Zhang, Y., Schaap, M.G., 2017. Weighted Recalibration of the Rosetta Pedotransfer Model with Improved Estimates of Hydraulic Parameter Distributions and Summary Statistics (Rosetta3). Journal of Hydrology 547, 39–53.